Experimental and Computational Investigation of Adhesion Junction Mechanosensation

Fiona E. Griffin B.E. (2011)

A thesis submitted to the National University of Ireland as fulfilment of the requirements for the degree of Doctor of Philosophy

February 2017

Department of Biomedical Engineering
College of Engineering and Informatics
National University of Ireland, Galway

Supervisors of Research: Dr. Laoise M. McNamara
Dr. Patrick J. McGarry

Abstract

Bone is an adaptive tissue that remodels in response to the mechanical loads placed upon it during normal daily activity. This remodelling process is vital to maintaining the mechanical integrity, mass and structure of bone throughout life and is facilitated by the cells which reside within bone, such as mesenchymal stem cells (MSCs) and bone producing osteoblasts. Both of these cell types are widely known to regulate their mechanical properties and gene expression in response to their mechanical environment, a phenomenon known as mechanosensitivity. Adhesion junctions are a class of mechanosensors, which form a direct connection between the cytoskeletons of neighboring cells, and thereby transmit forces generated by cytoskeletal contraction and can transduce mechanical stimulus into a cellular biochemical or mechanical response. The importance of adhesion junctions for mechanosensation and mechanotransduction by osteoblasts remains unclear, in particular it is not known whether adhesion junctions facilitate an osteogenic response under applied loading. The objectives of this Thesis are (a) to investigate the importance of adhesion junctions in transducing FSS stimulation into an osteogenic response in vitro, (b) computationally predicting the forces experienced at cell-cell contacts during FSS stimulation and (c) to investigate the influence of N-cadherin and OB-cadherin adhesion junctions in dictating the viscoelastic properties of MSCs.

The first study of this thesis investigates the role of adhesion junction mechanosensation in the osteogenic response of pre-osteoblast MC3T3-E1 cells to oscillatory and pulsatile FSS. The work presented in this chapter revealed that interference with adhesion junction formation prior to application of oscillatory fluid shear stress results in a significantly reduced biochemical response (PGE_2, Cox-2 and Runx2), but did not significantly reduce stress fibre formation with FSS. Pulsatile fluid flow did not cause significantly higher production of PGE_2, or significantly higher stress fibre formation for control samples.

The second study of this thesis investigates the mechanical response of two contacting cells subjected to FFS in a parallel plate bioreactor. To this end, A) a global

computational fluid dynamics (CFD) model of the entire flow system was constructed to compute the fluid velocity and pressure in the channel region of the bioreactor, and B) fluid shear stress, pressure and cellular contractility were applied to deformable contacting cells in a local fluid structure interaction (FSI) model. Simulations revealed that oscillating FFS within the bioreactor results in alternating tensile and compressive normal contact stress at the cell-cell interface. This work presents a mechanical indication as to why cells respond differently to steady and oscillatory fluid flow regimes in parallel plate bioreactors.

Chapter six of this thesis investigates the role of N-cadherin and OB-cadherin adhesion junctions in dictating the viscoelastic material properties of MSC spheres (mesenspheres) during osteogenesis. This study demonstrated that at day 2, silencing of OB-cadherin adhesion junctions results in significantly higher instantaneous and long term Young's moduli, viscosity and stress fibre formation in comparison to N-cadherin silenced and scrambled siRNA treated mesenspheres. Additionally, there is significantly higher viscosity, instantaneous and long term Young's moduli for scrambled siRNA treated mesenspheres between days 2 and 7, whereas this effect is not observed for either OB-cadherin or N-cadherin silenced groups. These results demonstrate that OB-cadherin and N-cadherin adhesion junctions play different roles in influencing the viscoelastic material properties of mesenchymal stem cells differently and this is likely due to their connectivity to the cytoskeleton.

Taken together, the work presented in this thesis provides a novel insight into the role of adhesion junctions in sensing and dictating the mechanical environment of osteoblasts and mesenchymal stem cells. Mechanical stimulation is vital to the maintenance of healthy bone throughout life and the results of this thesis provide an insight into the adhesion junction related mechanisms through which cells within bone sense external mechanical stimulus but also dictate their mechanical environment.

Acknowledgements

I would like to take the time to extend a heartfelt thank you to all of the people who have helped me during my PhD studies. Firstly, I want to express my gratitude to my supervisors Dr Laoise McNamara and Dr Pat McGarry for their support, advice and patience over the years. The depth of their knowledge in this field and their attention to detail was inspirational, and made the work done in this thesis possible. Laoise and Pat, thank you so much for all of your help.

I would also like to thank three of the past postdocs from the MMDRG group; Muriel, Matt and Ted. I would like to thank Ted for all of his help with the computational work in this thesis. To Muriel and Matt, a big thank you for all of the advice, protocols and teaching me the numerous practical techniques and skills needed to perform the lab work in this thesis.

I'd like to thank all of the past and current members of the McNamara and McGarry research groups for brightening my days and making my time more enjoyable. There are so many to thank, but I'd like to extend a particular thanks to Myles, Mary, Muriel, Conleth and Feihu for their endless supply of tea and chats. The hard work, dedication, skill and humour of all the members of both groups were a constant source of inspiration and strength throughout this process.

Additionally, I would like to say thank you to Professor Todd McDevitt. I had the fantastic opportunity to work in the McDevitt lab in Georgia Institute of Technology during my PhD studies. Todd and his research group welcomed me into their midst and made it a hugely enjoyable, educational experience. Thank you Todd for all of your advice, support and enthusiasm. Particular thanks also go to Marissa, Christian, Elizabeth, Melissa and Josh for their friendship and advice during my time in Atlanta.

I would like to thank my friends for all of their love, support, and general divilment over the years. A huge thank you to Mary, Muriel, Clare, Leanne, Maura, Michael and Shane for being my rocks over the years. Thank you to Ana, Bryan and Mairead for feeding me wine and cake and getting me through the last year, your friendship means a great deal to me.

Last but by no means least; I would like to thank my parents, Brian and May, my brother Mark and my sister Nicola for their endless love, support and encouragement. Finishing this PhD would not have been possible without you.

Publications

The following publications have been generated from this thesis:

1. Griffin, F.E., Voisin, M.C., Haugh M.G., Owens P., McGarry, J.P., McNamara, L.M. 'Adhesion junctions play a role in osteoblast mechanotransduction of oscillatory fluid shear stress'. (In preparation)
2. Griffin, F.E., Vaughan, T.J., McNamara, L.M., McGarry, J.P. 'Computational investigation into the Forces generated at Cell-Cell Adhesion Junctions by Fluid Flow Stimulation'. (in preparation)
3. Griffin, F.E., McGarry, J.P., McDevitt, T.C., McNamara, L.M., 'OB-Cadherin and N-Cadherin Adhesion Junctions Differentially Influence the Mechanical Properties of 3D Osteogenic Mesenchymal Stem Cell Spheroids'. (in preparation)

Conference Presentations:

1. F.E. Griffin, J.P. McGarry, L.M. McNamara. *The Role of Intracellular Forces in the osteogenic differentiation of intramembranous stem cell aggregate.* Proceedings of the Bioengineering in Ireland, the Eighteenth Annual Conference of the Section of Bioengineering of the Royal Academy of Medicine in Ireland, Dublin, Ireland Templepatrick, Ireland, January 2012. (Poster Presentation)
2. F.E. Griffin, J.P. McGarry, L.M. McNamara. *The Role of Intracellular Forces in the osteogenic differentiation of intramembranous stem cell aggregates.* Proceedings of the UL - NUI Galway Alliance Second Annual Research Day - Book of Abstracts, April 2012. (Poster Presentation)
3. F.E. Griffin, M.C. Voisin, M.G. Haugh, J.P. McGarry, L.M. McNamara. (2013) *The Role of Intracellular Forces in the Stimulation of Osteogenesis.* Proceedings of Bioengineering in Ireland, the Nineteenth Annual Conference of the Section of Bioengineering of the Royal Academy of Medicine in Ireland, Dublin, Ireland, Meath, Ireland, p.155, January 2013. (Podium Presentation)
4. F.E. Griffin, M.J. McGarrigle, F.E. Freeman, P. Owens, M.C. Voisin, M.G. Haugh, J.P. McGarry, L.M. McNamara. (2013) *Adhesion Junctions effect the Cytoskeletal*

Response to Fluid Flow. Proceedings of the Anatomical Society Summer Meeting, Dublin, Ireland July 2013. (Poster Presentation)

5. F.E. Griffin, T.J. Vaughan, P. Owens, M.C. Voisin, M.G. Haugh, J.P. McGarry, L.M. McNamara. *The Role of Adhesion Junctions and Fluid Flow in the Stimulation of Osteogenesis.* Proceedings of the 19th Congress of the European Society for Biomechanics, Patras, Greece, August 2013. (Podium Presentation)

6. F.E. Griffin, M.J. McGarrigle, F.E. Freeman, P. Owens, M.C. Voisin, M.G. Haugh, J.P. McGarry, L.M. McNamara. *Adhesion Junctions effect the Cytoskeletal Response to Fluid Flow.* Proceedings of the TERMIS-Americas Conference and Expo, Atlanta, Georgia, U.S.A., November 2013. (Poster Presentation)

7. Griffin, F.E., Owens P., Voisin, M.C., Haugh M.G., McGarry, J.P., McNamara, L.M., 'Adhesion Junctions Regulate the Cytoskeletal Response to Fluid Flow Stimulation', UL - NUI Galway Alliance Fourth Annual Research Day - Book of Abstracts, University of Limerick, May 2014. (Poster Presentation)

8. Griffin, F.E., McGarry, J.P., McDevitt, T.C., McNamara, L.M., 'OB-Cadherin and N-Cadherin Adhesion Junctions Differentially Influence the Mechanical Properties of 3D Osteogenic Mesenchymal Stem Cell Spheroids', Orthopaedic Research Society 2015 Annual Meeting, Las Vegas, March 2015. (Poster Presentation)

Nomenclature

	Roman Letters
C	Coefficient of Contractility
$\boldsymbol{C}_{el}$	4th order elastic moduli tensor
b	Flow channel width
$\boldsymbol{D}$	Rate of deformation tensor
D_h	Hydraulic diameter of the bioreactor chamber
D_o	Initial mesensphere diameter
E	Young's modulus
E_o	Instantaneous Young's modulus
E_∞	Long term Young's modulus
$\boldsymbol{F}$	Force vector
$\boldsymbol{F}_{def}$	Deformation gradient tensor
G	Shear modulus
h	Flow channel height
$\boldsymbol{K}$	Element stiffness matrix
K	Bulk modulus
$\boldsymbol{L}$	Spatial velocity gradient
N	Shape Function
P	Pressure
Q	Flow rate
Re	Reynolds number
σ_0	Nominal stress
t	Time
$u(t)$	Creep displacement at time t
u	Displacement
$\boldsymbol{u}, \boldsymbol{v}$	Velocity vector
v_m	Mean velocity
x,y,z	Deformed point co-ordinates
W	Work Done

Greek Letters

ε	Logarithmic strain tensor
ε^{th}	Thermal strain
ε^{el}	Elastic strain
ρ	Density
μ	Apparent viscosity
σ	Stress tensor
ν	Poisson's ratio
Π	Potential energy
Λ	Strain energy
τ_w	Wall shear stress
Ω	Domain

Acronyms

AFM	Atomic Force Microscopy
AJ	Adhesion Junction
ALP	Alkaline Phosphatase
ANOVA	Analysis of Variance
ATF4	Activating transcription factor 4
ATP	Adenosine triphosphate
BAPTA	1,2-bis-(2-aminophenoxy)ethane-N,N,N',N'-tetraacetic acid
BMP-2	Bone morphogenic protein 2
Ca^{2+}	Calcium
Cbfa1	Core-binding factor alpha 1
cDNA	Complementary DNA
CFD	Computational fluid dynamics
Cox-2	Cyclooxygenase-2
DAPI	4',6-diamidino-2-phenylindole
DNA	Deoxyribonucleic acid
ECM	Extracellular Matrix
EC	Extracellular cadherin
EDTA	Ethylenediaminetetraacetic acid

EGTA	Ethylene glycol-bis (β-aminoethyl) ether
EIA	Enzyme Immunoassay
FBS	Foetal bovine serum
FE	Finite Element
FEM	Finite Element Method
FFS	Fluid Flow Stimulus
FSA	Force sensor array
FSI	Fluid structure interaction
FSS	Fluid shear stress
GSK3	Glycogen synthase kinase 3
GTP	Guanosine-5'-triphosphate
H_20	Hydrogen dioxide
LRP5	Low-density lipoprotein receptor-related protein 5
M-CSF	Macrophage colony stimulating factor
MDCK	Madin-Darby canine kidney
mRNA	Messenger ribonucleic acid
MSC	Mesenchymal stem cell
Mesensphere	Mesenchymal Stem Cell spheroid
-N	N-cadherin siRNA treated MSCs
-OB	OB-cadherin siRNA treated MSCs
OCN	Osteocalcin
OFSS	Oscillatory fluid shear stress
OPG	Osteoprotegrin
OPN	Osteopontin
PA	Polyacrylamide
PBS	Phosphate buffered saline
PFSS	Pulsatile fluid shear stress
PGE_2	Prostaglandin E_2
PI3K	Phosphatidylinositol-4,5-bisphosphate 3-kinase
RANKL	Receptor activator of nuclear factor kappa-B ligand
RhoA	Ras homolog gene family, member A
RNA	Ribonucleic acid

ROCK	Rho-associated protein kinase
RT-PCR	Real time, reverse transcription polymeric chain reaction
Runx2	Runt-related transcription factor 2
Scram	Scrambled siRNA treated MSCs
siRNA	Small interfering RNA
SLS	Standard Linear Solid
TRITC	Tetramethylrhodamine isothiocyanate
α-MEM	Alpha-Modified Eagles Medium
2D	Two dimensional
3D	Three dimensional

Table of Contents

List of Figures

List of Tables

Chapter 1:

Introduction

1.1 Bone Mechanobiology and Mechanosensing

Throughout life, the skeleton protects and supports the organs of the body and facilitates movement in co-ordination with muscles. Bone formation can occur via two different processes; intramembranous ossification forms irregular non-long bones such as the skull, the mandible and the clavicles, or endochondral ossification that forms the long bones of the body, such as the femur, the tibia, the rib cage and the fingers. Bone is an adaptive tissue that remodels in response to the mechanical loads placed on it during normal daily activity. One example of this is the well-known loss of bone mineral density in astronauts after long-duration missions in gravitationally unloaded space stations (Vico et al. 2000; Lang et al. 2004). This remodelling process is vital to maintaining the mechanical integrity, mass and structure of bone throughout life. A number of cells reside within bone, which work in harmony to regulate bone turnover during the bone remodelling process; namely mesenchymal stem cells (MSCs), osteoblasts, osteocytes and bone lining cells. A complex communication system of genes and proteins expressed by these cells act to co-ordinate bone remodelling (Kirkham and Cartmell 2007). In addition to this communication network, MSCs, osteoblasts and osteocytes have been shown to be sensitive to mechanical stimulus in the form of shear stress, strain, hydrostatic pressure or substrate mechanical properties (Mehrotra et al. 2006; Kim et al. 2007; Mullen et al. 2015; Zeng et al. 2015). MSCs can respond to their mechanical environment by differentiating into osteoblasts, while osteoblasts and osteocytes can express factors that influence the formation or resorption of bone. The response of osteogenic cells to mechanical stimulus has led to an emerging area of research, seeking to uncover the mechanisms through which these cells sense and respond to their mechanical environment, known as

mechanobiology. By improving the understanding of the factors that govern the formation and resorption of bone under mechanical loading, such as MSC and osteoblast mechanosensation and mechanotransduction, new and improved osteogenic tissue engineering strategies for treating bone diseases such as osteoporosis could be developed to target these mechanisms.

The production of new bone is governed by bone forming osteoblast cells, which are derived from mesenchymal stem cells (MSCs) of the bone marrow. MSCs are multi-potent, self-renewing progenitor cells that can differentiate into osteogenic cells (Owen 1985). Osteoblasts are characterised by their ability to form bone by secreting new collagenous bone matrix, which they subsequently mineralise. Alkaline phosphatase (ALP) and prostaglandin E_2 (PGE_2) expression are two hallmarks of mature osteoblasts (Hui et al. 1993) and these cells secrete a number of other proteins that facilitate cell binding to the bone matrix, and promote mineralisation.

Osteogenic cells are widely known to be responsive to their mechanical environment and regulate their mechanical properties, and the expression of osteogenic proteins and genes in response to different mechanical stimuli. One example of this is the change in mechanical properties of MSCs and osteoblasts in response to the variation in mechanical properties of the substrate they are adhered to. Bone cells cultured on substrates of high stiffness are known to alter their stiffness and differentiation relative to those cultured on softer substrates (Takai et al. 2005; Leong et al. 2010; Mullen et al. 2015). Externally applied mechanical stimulation such as applied strain, fluid shear stress and hydrostatic pressure also influences the osteogenesis of MSCs and osteoblasts. Such stimulation can alter cellular mechanical properties, induce formation of actin stress fibres and influence stress fibre alignment, influence osteogenic differentiation and up-regulate the expression of osteogenic proteins and genes such as PGE_2 and cyclooxygenase-2 (Cox-2) (Smalt et al. 1997; Chen et al. 2000; Bakker et al. 2003a; Mai et al. 2013). Oscillatory fluid shear stress is thought to imitate the movement of interstitial fluid flow within bone during normal daily activities, as the bone is compressed and decompressed by applied loads. Application of fluid shear stress in vitro has proved to illicit a larger-fold increase in osteogenic responses than the application of strain or hydrostatic pressure alone (Owan et al. 1997; Gardinier et al. 2009).

The phenomenon of cellular mechanical or biochemical responses to mechanical stimuli is known as mechanosensitivity and there are a number of cellular structures thought to translate mechanical stimulus into a cellular response. Specifically, cadherins connect the cytoskeletons of adjacent cells, integrins connect the cell to extra-cellular substrates such as extra-cellular matrix in vivo or cell culture substrates in vitro (e.g. glass, tissue culture plastic), and primary cilia protrude out from the cell membrane. The cytoskeleton forms the backbone of the cell and connects cadherins, integrins and primary cilia to each other and to the nucleus (Ando and Yamamoto 2013). It should also be noted that gap junctions, which facilitate the movement of molecules and ions between the cytoplasm of adjacent cells, are also sensitive to mechanical stimulation (Salameh and Dhein 2013). Each of these mechanisms has been proposed to play a role in the response of osteogenic cells to mechanical stimulus. Indeed, specific osteogenic responses to fluid shear stress stimulation such as significantly higher PGE_2, Cox-2, Runt-related transcription factor 2 (Runx2) or osteopontin expression can be inhibited when integrins (Lee et al. 2008b; Haugh et al. 2015), the cytoskeleton (Arnsdorf et al. 2009b; Higuchi et al. 2009), primary cilia (Malone et al. 2007b; Delaine-Smith et al. 2014) or gap junctions (Saunders et al. 2001; Jekir and Donahue 2009) are down-regulated. However, only limited data is available on the role of adhesion junctions in the response to fluid flow stimulation. One of the most compelling indications that adhesion junctions are important for mechanosensation of fluid shear stress is the significantly higher translocation of β-catenin into the nucleus of osteoblasts and MSCs with stimulation (Norvell et al. 2004a; Arnsdorf et al. 2009a). β-catenin is a canonical Wnt signalling protein that is sequestered at adhesion junctions during static conditions. Canonical Wnt signalling influences the significantly higher Runx2 expression of MSCs in response to fluid shear stress, the levels of Cox-2 in static conditions and mineralisation in vivo (Norvell et al. 2004a; Rodda and McMahon 2006; Arnsdorf et al. 2009a). However, the influence of adhesion junctions on the significantly higher Cox-2, Runx2 and PGE_2 expression with fluid flow stimulation are still unclear.

Cadherins form a complex, known as an adhesion junction (AJ), which mechanically links the cytoskeletons of adjacent cells (Ganz et al. 2006). Adhesion junctions are transmembrane glycoproteins and the cadherin is the extracellular

component of this junction. The intramembranous section of the adhesion junctions links the junction to the cytoskeleton via a network of accessory proteins such as β-catenin and vinculin. Adhesion junctions play important roles in the formation and maintenance of a wide variety of tissues and organs (Yagi and Takeichi 2000), including bone (Castro et al. 2004; Haÿ et al. 2009). MC3T3-E1 cells, seeded at high density to enable adhesion junction formation, had significantly higher expression of osteogenic transcription factors osterix, osteomodulin and osteoglycin in comparison to cells seeded at low density (Guntur et al. 2012). Osterix, osteomodulin and osteoglycin are important genes for bone formation and the expression of osterix was reduced when an N-cadherin blocking antibody was used (Guntur et al. 2012). There are a wide variety of cadherins and the expression of particular cadherins depends on the cell type. N-cadherin and OB-cadherin are the main cadherin types expressed by MSCs and osteoblasts (Cheng et al. 1998a; Haÿ et al. 2000; Kawaguchi et al. 2001). Adhesion junctions influence the osteogenic differentiation of mesenchymal stem cells in a manner dependent on the specific cadherin incorporated in the junction (Kii et al. 2004b). For example, N-cadherin is important for the osteogenic differentiation of osteoblasts (Ferrari et al. 2000) but N-cadherin over-expression results in significantly lower osteogenesis of MSCs and osteoblasts (Haÿ et al. 2009; Xu et al. 2013). It has also been shown that teratomas originating from cells over-expressing OB-cadherin preferentially form bone and cartilage tissue (Kawaguchi et al. 2001). However, MSCs are known to be sensitive to their mechanical environment and it remains unknown what these two cadherin types contribute to the mechanical properties of MSCs during osteogenic differentiation.

Experimental techniques commonly applied to assess the mechanosensing roles of adhesion complexes such as integrins and cadherins can be divided into two main categories; adhesion functions and adhesion mechanics. The first category looks at the role of adhesion complexes in the biological response of osteogenic cells during the application of a mechanical stimulus such as fluid shear stress, strain or changing mechanical environment. As previously discussed, such research has revealed the involvement of integrins, primary cilia, gap junctions and the cytoskeleton in the osteogenic response to fluid shear stress stimulation. However, beyond the translocation of β-catenin into the nucleus with application of fluid flow, (Norvell et al.

2004a; Arnsdorf et al. 2009a), the influence of cadherins on the osteogenic response to fluid flow is still unclear. Therefore, the first research hypothesis of this thesis is "*The osteogenic response of pre-osteoblasts to fluid shear stress is inhibited by a reduction in adhesion junctions*."

Previous computational models have investigated the forces experienced by single cells in parallel plate bioreactors during fluid shear stress stimulation (McGarry et al. 2005a; Vaughan et al. 2013b). These models have demonstrated the importance of the pressure within the chambers for stimulating cells (Vaughan et al. 2013b) and compared the deformation caused by fluid shear stress to that caused by strain (McGarry et al. 2005a). However, computational models of parallel plate chambers have not investigated the forces experienced at cell-cell contacts, or the role of the cytoskeleton in generating these forces. The cytoskeleton is of vital importance to cellular mechanics. This highly dynamic structure is one of the main factors influencing the mechanical properties of cells (Lee et al. 2012). Adhesion junctions require the tension generated by the cytoskeleton in order to form and maintain the structure (Hong et al. 2013), but previous parallel plate models report high levels of pressure within the system that could influence the forces experienced at cell-cell contacts. Therefore, the second research hypothesis of this thesis is "*Fluid shear stress stimulus results in pressure dependent compression and tension of cell-cell contacts*."

Experimental techniques to assess adhesion junction mechanosensing also investigate adhesion mechanics. These studies look at the mechanics of cell adhesion structures by testing how much force is required to break the adhesive bonds (Pittet et al. 2008), or by observing how much force is transmitted through these bonds by various cell types in varying mechanical environments (Ganz et al. 2006; Ladoux et al. 2010; Liu et al. 2010b; Chopra et al. 2011). Experiments of this type have shown that significant forces (300 nN) can be transmitted through cadherins (Chopra et al. 2011). Interestingly, OB-cadherin bonds can resist greater forces (95±20 pN) than N-cadherin bonds (44±19 pN) before rupturing (Pittet et al. 2008). The use of anti-VE-cadherin antibody to reduce cell-cell adhesion caused significantly higher endothelial cell mechanical properties (Stroka and Aranda-Espinoza 2011). Additionally, thicker stress fibres form in myogenic cells adhered to a stiff (95 kPa) N-cadherin coated gel substrate, in comparison to softer gels (10 kPa) (Ladoux et al. 2010). Taken together,

these show that adhesion junctions can transmit significant forces and influence the mechanical properties of cells and stress fibre formation in response to the mechanical environment. However, it is not clear if the removal of adhesion junctions (N-cadherin or OB-cadherin) from osteoblasts or MSCs causes significant changes in the mechanical properties or cytoskeleton stress fibre formation in 3D aggregate culture. Due to the variation in forces transmitted through cadherins, and the altered cadherin expression depending on cell type, the exact contribution of these structures to osteogenic cellular mechanics is still unclear. In culture systems of aggregated MSCs grown in minimal contact with extracellular substrates, cadherins could feasibly be the primary means of mechanosensation. Therefore, the third research hypothesis of this thesis is "*Adhesion junctions can regulate the mechanical properties of mesenchymal stem cell aggregates.*

1.2 Objectives and Hypothesis

The global objective of this thesis is to further the understanding of the importance of adhesion junctions in sensing and responding to, or dictating their mechanical environment, in the context of osteogenic differentiation of pre-osteoblasts and mesenchymal stem cells. The first specific objective of this thesis is to determine the role of adhesion junctions in the osteogenic response of pre-osteoblasts to applied fluid shear stress stimulus. The second specific objective of this thesis is to characterise the mechanical stimulus received by the adhesion junctions during application of fluid shear stress. The third specific objective of this thesis is to investigate the influence of specific adhesion junctions on the mechanical properties of mesenchymal stem cells as they undergo osteogenic differentiation. To address each of these specific objectives, three hypotheses have been defined, each of which will underpin the research of Chapters 4 - 6 of this thesis.

Hypothesis 1: *The osteogenic response of pre-osteoblasts to fluid shear stress is inhibited by a reduction in adhesion junctions.*

Hypothesis 2: *Fluid shear stress stimulus results in pressure dependent compression and tension of cell-cell contacts.*

Hypothesis 3: Adhesion junctions can regulate the mechanical properties of mesenchymal stem cell aggregates.

A parallel plate flow chamber with oscillatory fluid flow parameters applied to induce an osteogenic response will be used in conjunction with in vitro cell culture of the pre-osteoblast cell line MC3T3-E1 to investigate the influence of adhesion junctions in the osteogenic response of these cells to oscillatory fluid shear stress stimulation (Hypothesis 1). Fluid-structure interaction computational modelling will be employed to assess the stress-state generated at cell-cell contacts due to the contractility of the cell body and the application of oscillatory fluid shear stress (Hypothesis 2). Finally, mechanical testing of spherical aggregates of C57BL/6 Mouse MSCs grown in an in vitro suspension cell culture system will be conducted using a parallel plate compression testing system to assess the changing mechanical properties of the aggregates when N-cadherin or OB-cadherin adhesion junctions are down-regulated (Hypothesis 3). An improved understanding of the role of adhesion junctions in sensing, responding to, and dictating their mechanical environment will inform the development of improved strategies in bone tissue engineering, and may also influence the development of novel treatments for osteogenic disease.

1.3 Thesis Structure

This thesis comprises the work completed for the duration of the candidates' PhD studies. Chapter 2 presents a review of relevant literature, detailing an in-depth introduction to the structure and function of bone, bone adaptation, bone porosity and fluid flow, bone cells and mechanosensation, cytoskeleton and adhesion junction mechanobiology, and a summary of computational modelling of cell mechanics in vitro. Chapter 3 details the theory behind the computational fluid-structure interaction modelling used in the work presented in Chapter 5. Chapter 4 investigates the effect of impaired formation of adhesion junctions on the osteogenic response of pre-osteoblast MC3T3-E1 cells to applied fluid shear stress stimulation to test Hypothesis 1. Chapter 5 details the computational fluid-structure interaction simulations of idealised cells exposed to oscillatory fluid shear stress to test Hypothesis 2. Chapter 6

investigates the changing viscoelastic material properties of C57BL/6 Mouse MSC aggregates undergoing osteogenic differentiation when N-cadherin or OB-cadherin adhesion junctions are down-regulated to test Hypothesis 3. Finally, Chapter 7 summarises the main findings of the thesis, placing these findings in the context of the wider field of cell mechanobiology, and discusses recommendations for future research in the field.

Chapter 2:

Literature Review

2.1 Bone

Bone is a unique, mineralised connective tissue that serves a variety of functions in the body. Bone provides shape, mechanical support and protection for the body and is of vital importance in facilitating movement via the contractions of muscles, tendons and ligaments, which form attachments between bones. Throughout life, bone is constantly remodelled in order to withstand the stresses placed on it by everyday activities (Frost 1973). Bone maintenance is an intricate balance between bone formation and resorption, which allows bone to adapt itself to changing forces or to repair itself after damage. An imbalance between bone resorption and formation can lead to a net decrease in bone mass, decreased bone strength and a significantly higher risk of bone fracture that is characteristic of osteoporosis (Lanyon and Skerry 2001).

2.1.1 Structure of Bone

Bone tissue can be divided into two distinct types; known as cortical or trabecular bone (Figure 2.1). Cortical bone forms a dense (470 - 640 mg/cm^3) outer shell of compact, stiff bone that is the main source of mechanical strength for the bone (Lehtinen et al. 2004; Augat and Schorlemmer 2006). A highly porous network is found within the shell of cortical bone, composed of supporting struts that form the mesh-like trabecular bone (density 180 - 290 mg/cm^3) (Goldstein et al. 1993). Bone marrow can be found within the cortical shell and between the trabeculae and is composed of a variety of cells such as mesenchymal stem cells and fat cells.

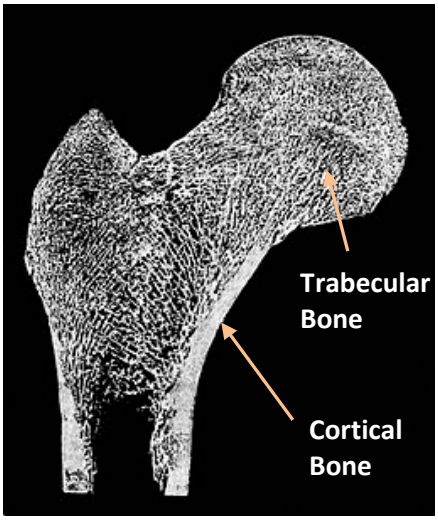

Figure 2.1: Cross section of the proximal femur showing cortical and trabecular bone. Public domain image via Wikimedia Commons (Wikipedia).

Bone is a hierarchical tissue that is organised into functional units of multiple scales (Figure 2.2). Approximately 65% of bone is composed of nano-scale mineral hydroxyapatite crystals (Fratzl et al. 2004), while 35% of bone is composed of organic molecules such as collagen type 1, osteopontin and osteocalcin (Miller and Parker 1984). The mineralised collagen fibrils form lamellae that can organise into either strut-like trabeculae, in trabecular bone, or form a relatively thick shell composed of numerous osteons in cortical bone. In the dense cortical bone, the lamellae form concentrically around a vascular Haversian canal. The Haversian canal contains blood vessels, nerves and lymphatics (Datta et al. 2008) that nourish and maintain the cells of the cortical bone, thus providing a hospitable environment for cells (Pavalko et al. 2003b; Tarbell et al. 2005). Trabeculae have a similar concentric organisation of lamellae but these smaller functional units lack a Haversian canal. The trabeculae are primarily aligned in the direction of applied stress (Waarsing et al. 2006). This hierarchical organisation produces a tissue with a high strength-to-weight ratio, which is optimised to bear the variety of everyday loads (Hart 2001; Currey 2014). Within the lamellae are small cavities called lacunae. Each lacuna contains a single bone cell called an osteocyte that is connected to other osteocytes through a network of small channels in the lamellae known as canaliculi.

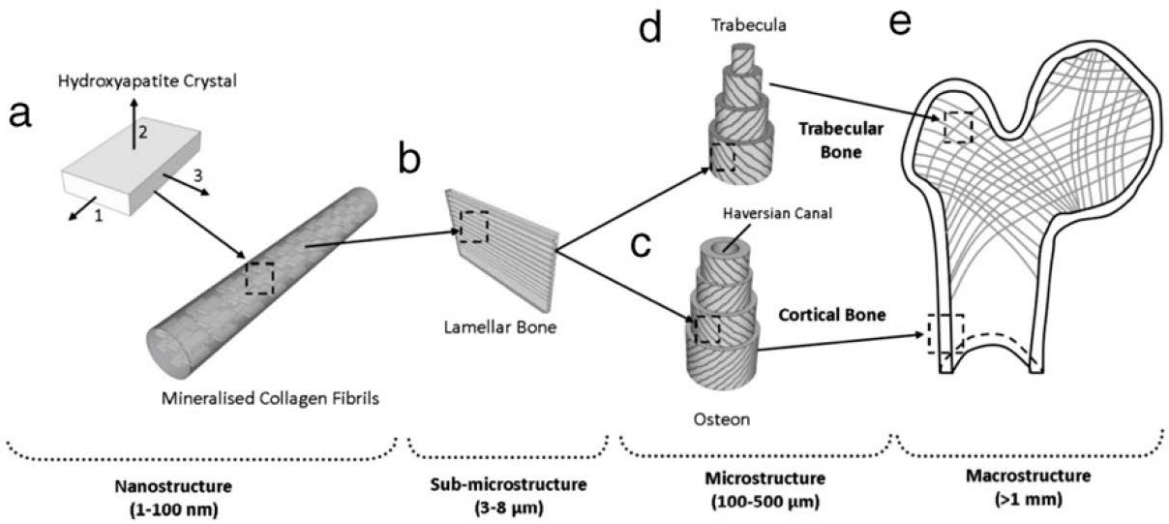

Figure 2.2: Diagram of the hierarchal structure of bone. a) Hydroxyapatite crystals are a component of the mineralised collagen fibrils. b) Collagen fibrils form oriented sheets of lamellar bone. c) Lamellar bone at varying orientations encircles a Haversian canal in osteons and also forms trabeculae. e) Trabeculae and Osteons forms cortical and trabecular bone (Vaughan et al. 2012).

2.1.2 Bone Formation and Remodelling

Bone can form via two different processes; endochondral ossification and intramembranous ossification. Endochondral ossification is the process where long bones of the body are formed, such as the femur, the tibia, the rib cage and the fingers, while intramembranous ossification forms irregular non-long bones such as the skull, the mandible and the clavicles and also plays an important role in bone fracture healing. The primary difference between these two bone formation processes is the formation of a cartilage template that occurs during endochondral ossification (McNamara et al. 2011). The cartilage template is formed when mesenchymal stem cells (MSCs) differentiate into chondroblasts and secrete cartilage. This template is later vascularised and mineralised to form mature bone. During intramembranous ossification, no cartilage template is formed. Instead, pre-osteoblasts differentiate into osteoblasts, which then secrete osteoid, an unmineralised organic matrix primarily consisting of type I collagen fibrils, upon which the osteoblasts adhere and mineralisation of the osteoid occurs. Intramembranous ossification is the predominant bone forming process during primary bone healing. Primary bone healing happens when bone heals without the formation of a fracture callus and occurs at sites of low strain magnitudes, small displacements between bone fragments, and either small gaps or direct contact between bone fragments (Sfeir et al. 2005; Rüedi et al. 2007).

Bone remodelling occurs throughout life and involves the resorption of old bone by osteoclast cells and the secretion of new bone by osteoblast cells (Figure 2.3). The process of bone remodelling requires osteoblast and osteoclast cells to work closely together in a unique, temporary functional grouping, known as a basic multicellular unit (BMU) (Parfitt 1994). In cortical bone, BMUs tunnel through the bone, while in trabecular bone the BMUs travel across the surface of the trabeculae.

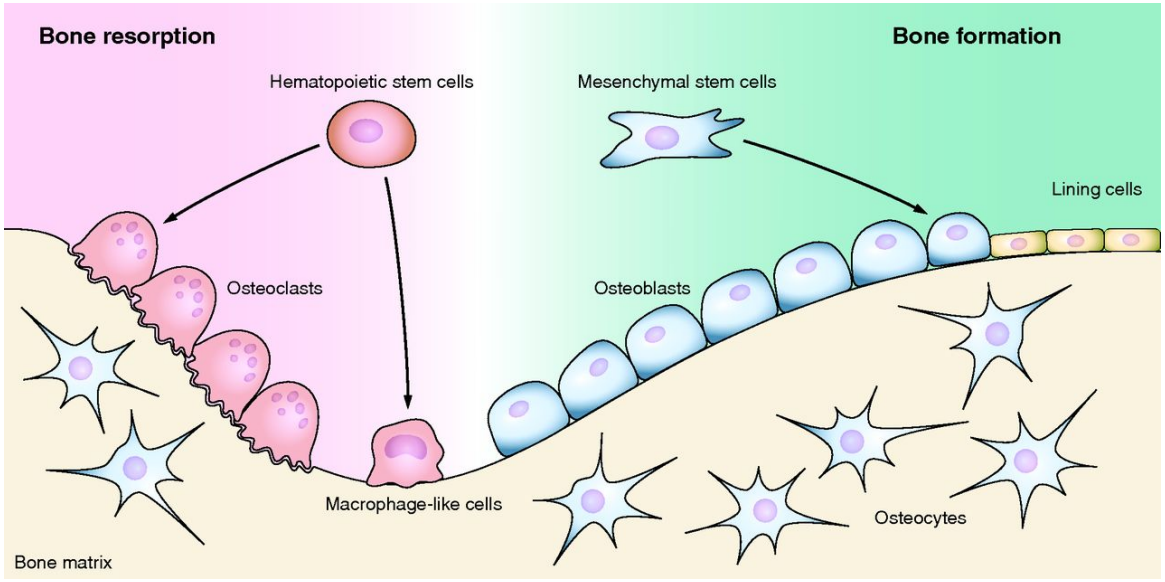

Figure 2.3: The bone remodelling process involves cells of two different lineages, hematopoietic and mesenchymal, differentiating and acting in concert. Osteoclasts resorb old bone and osteoblasts secrete new bone. Image from (Imai et al. 2013)

2.1.3 Bone Porosity and Fluid Flow

In vivo, mechanical stimulation regulates bone mass, with increased stimulation from exercise resulting in increased bone formation (Woo et al. 1981; Rico et al. 1994). The strain induced deformation experienced by bone during mechanical loading leads to the flow of interstitial fluid through the lacuno-canalicular network (Seliger 1970; Burger and Klein-Nulend 1999; Steck et al. 2000; Verbruggen et al. 2014). During normal loading conditions (walking, running etc.), fluid flow in bone is derived from plasma leaking from venous sinusoids in the bone marrow. When the load is applied, plasma is driven radially outward by a relatively steady transmural pressure gradient that exists between the vascular system and the lymphatic drainage system at the periosteal surface (Anderson 1960; Otter et al. 1990). It is thought that this fluid flow

within bone is an important regulator of bone growth as various studies have demonstrated the up-regulation of bone growth (osteogenesis) when cells of the osteogenic lineage are stimulated with fluid flow (Pavalko et al. 2003a; Malone et al. 2007c; Ponik et al. 2007; Haugh et al. 2015). Computational studies have predicted that the magnitude of wall shear stress on surface of osteocyte processes is 0.8 – 3.0 Pa (Weinbaum et al. 1994; Zeng et al. 1994; Verbruggen et al. 2014). Recent experimental studies have shown that there are projections of the extracellular matrix into the pericellular space around the canaliculi (McNamara et al. 2009a). Computational studies have suggested that such ECM projections into the pericellular space amplify the strain stimulus to the osteocyte (Anderson and Tate 2008; Verbruggen et al. 2012) and amplify the wall shear stress on the surface of the osteocyte processes (Joukar et al. 2016). Additionally, theoretical studies have also suggested that ECM projections amplify the strain stimulus (Han et al. 2004; Wang et al. 2008).

2.2 Bone Cells

Bone tissues are populated by numerous cell types that work together to maintain bone throughout life. These cells originate from two stem cell lineages; the mesenchymal lineage and the hematopoietic lineage.

2.2.1 Mesenchymal Stem Cells

Mesenchymal stem cells (MSCs) are self-renewing, multipotent progenitor stem cells that can be found in bone marrow (Dennis et al. 2002; Sarugaser et al. 2009). MSCs are often identified by their ability to adhere to plastic substrates or by expression of surface markers such as CD105, CD34, CD45 and CD14 (Dominici et al. 2006; Kaiser et al. 2007). MSCs can differentiate into osteogenic, chondrogenic or adipogenic cell types (Figure 2.4). Each of these cell types have a specific function; osteogenic cells (osteoblasts and osteocytes) produce bone, chondrogenic cells produce cartilage, while adipogenic cells maintain energy homeostasis by storing or releasing energy as required. When MSCs differentiate osteogenically, they change into osteoblast cells (Owen 1985).

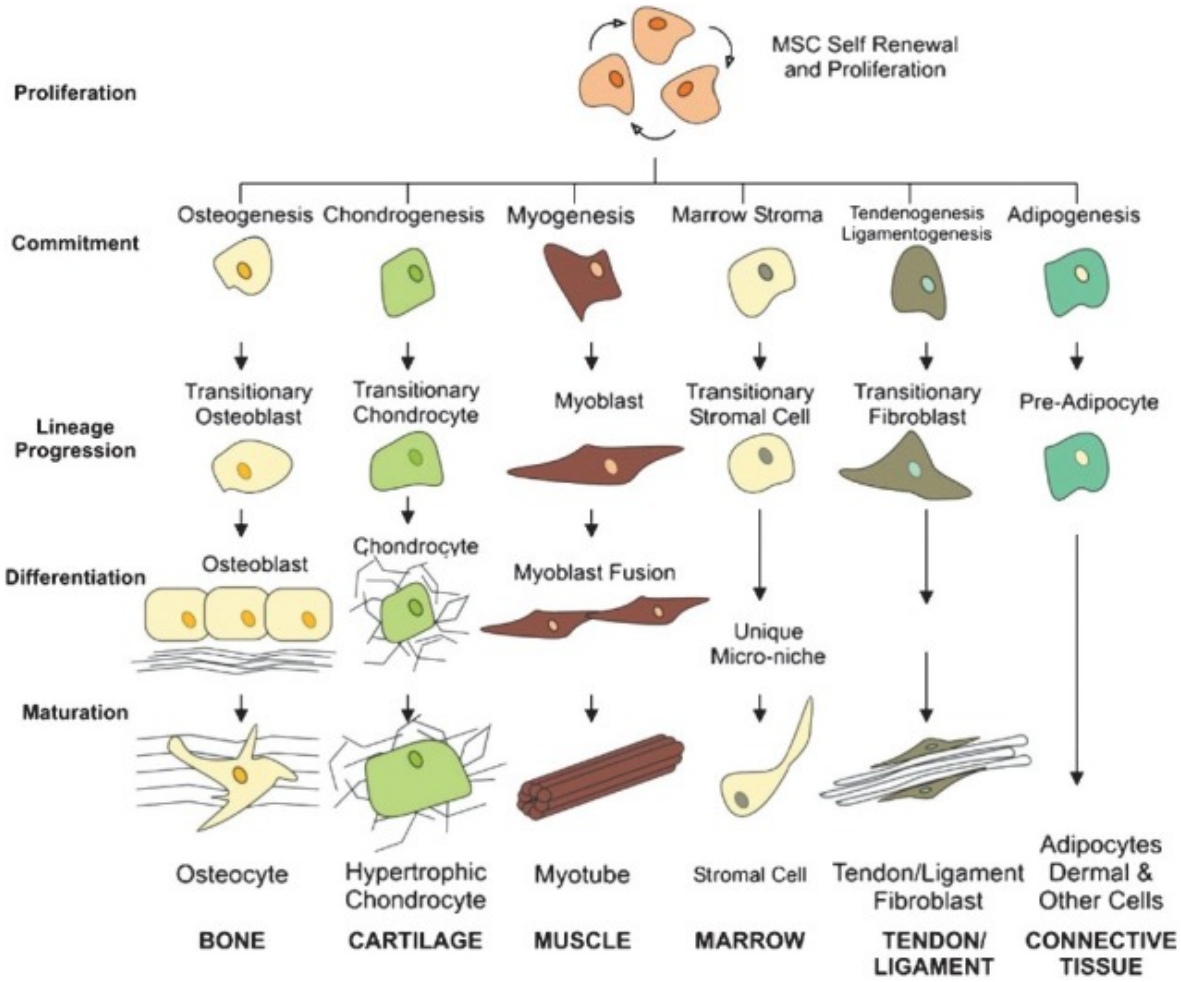

Figure 2.4: Mesenchymal Stem Cells (MSCs) self-renewal, proliferation and potential differentiation pathways that MSCs can undergo to produce cells of various specific lineages (Firth and Yuan 2012).

In vitro, MSC differentiation into osteoblasts is usually induced by addition of β-glycerol, ascorbic acid and dexamethasone (DEX) (Bellows et al. 1987; Jaiswal et al. 1997) to the culture media. The main genes controlling MSC differentiation into osteoblasts are Runt-related transcription factor 2 (Runx2), also known as Core-binding factor alph 1 (Cbfa1), cyclooxygenase-2 (Cox-2), Osterix and activating transcription factor 4 (ATF4) (Ducy et al. 1997; Nakashima et al. 2002; Zhang et al. 2002; Komori 2006; Saito et al. 2011). Runx2/Cbfa1 controls the expression of a variety of osteoblast-associated genes and proteins such as osteocalcin, alkaline phosphatase (ALP), bone sialoprotein and collagen type 1 (Ducy et al. 1997). Cox-2 is known to play a rate limited role in the production of prostaglandin E_2 (PGE_2). Cox-2 negative mice have significantly lower bone mass (Okada et al. 2000) and have also demonstrated

significantly lower levels of Runx2 and osterix than control mice that can be significantly higher with addition of PGE_2 (Zhang et al. 2002).

2.3.2 Osteoblast

Osteoblasts are bone producing cells that are characterised by their ability to form bone, their cuboidal, mononuclear morphology (Aubin et al. 1995; Aubin 1998) and a highly developed actin cytoskeleton (Figure 2.5). The clonal osteoblast-like cell line MC3T3-E1 is derived from new-born mouse calvaria (Sudo et al. 1983).

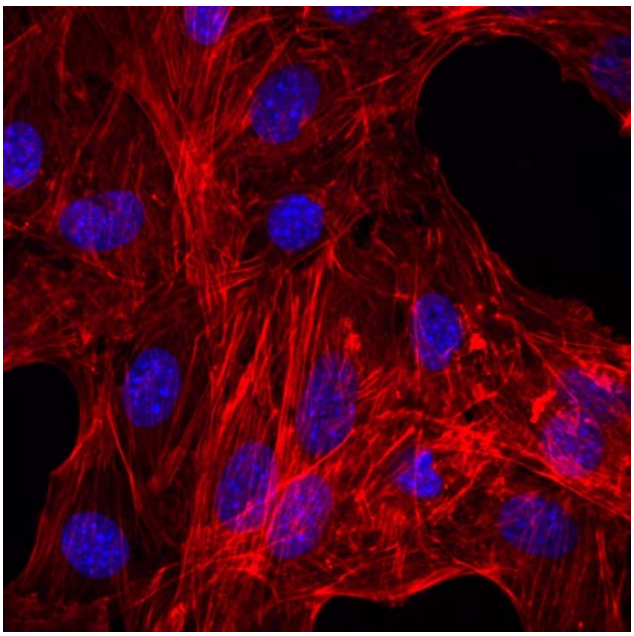

Figure 2.5: MC3T3 pre-osteoblast cells immunofluorescently stained for the nucleus (blue - DAPI), the cytoskeleton (red - TRICT Phalloidin).

Osteoblasts play a multifaceted role in maintaining the mechanical integrity of bone; osteoblasts deposit new bone matrix and play a role in regulating the function of osteoclast cells that resorb bone (Gori et al. 2000). Mature osteoblasts have high ALP and PGE_2 expression (Hui et al. 1993) and secrete proteins including collagen Type 1, osteocalcin and osteonectin that form the vast majority of the bone matrix (Franceschi and Iyer 1992; Crockett et al. 2011). PGE_2 is involved in the regulation of bone remodelling (Igarashi et al. 1994; Thorsen et al. 1996) and ALP promotes mineralisation by binding to pyrophosphate, a mineralisation inhibitor (Golub and Boesze-Battaglia 2007). Other components of the bone matrix secreted by osteoblasts are osteopontin, bone sialoprotein and fibronectin, which facilitate cell attachment to the bone matrix

(Carvalho et al. 1998; Bellows et al. 1999). Subsequent to bone matrix deposition, mature osteoblasts deposit hydroxyapatite to mineralise this matrix (Boskey 1996).

2.3.3 Osteocyte

As osteoblasts secrete bone matrix, some cells become trapped in the matrix. These cells terminally differentiate into osteocyte cells (Frost 1960) and form up to 90% of adult bone cells (Tate et al. 2004). Osteocyte cells are present throughout bone and form a network of interconnected cells by the extension of long thin dendritic processes between cells. Dendrites extend through thin channels within the bone known as canaliculi. The interconnected network of osteocytes has given rise to the thought that osteocytes act as mechanosensors, which signal to osteoblasts and osteoclasts where and when to form or resorb bone (Pavalko et al. 2003b; Tarbell et al. 2005; Burra et al. 2010b).

2.3.4 Osteoclast

Osteoclasts are bone resorbing cells that differentiate from hematopoietic stem cells (Suda et al. 1992). In vivo, mononuclear macrophages of the hematopoietic lineage require contact with osteoblasts to mature into multinucleated osteoclasts (Udagawa et al. 1990). Osteoclastogenesis can be induced in vitro with exposure to macrophage colony stimulating factor (M-CSF) and receptor for activation of nuclear factor kappa B ligand (RANKL) (Lacey et al. 1998). The activity of osteoclast cells is regulated by osteoblasts, who synthesise a decoy protein osteoprotegerin (OPG) that can bind to RANKL and inhibit osteoclast differentiation and activity (Udagawa et al. 2000) (Figure 2.6). Mature osteoclasts form a complex ruffled membrane on the cell surface in contact with the bone to be resorbed. The resorption zone under the ruffled membrane is sealed off from the surrounding tissue by a ring of actin (Silver et al. 1988). To resorb bone, the osteoclasts acidify the isolated extracellular matrix to dissolve the inorganic components (Silver et al. 1988). Subsequently, the organic component of the bone is enzymatically degraded (Li et al. 1999).

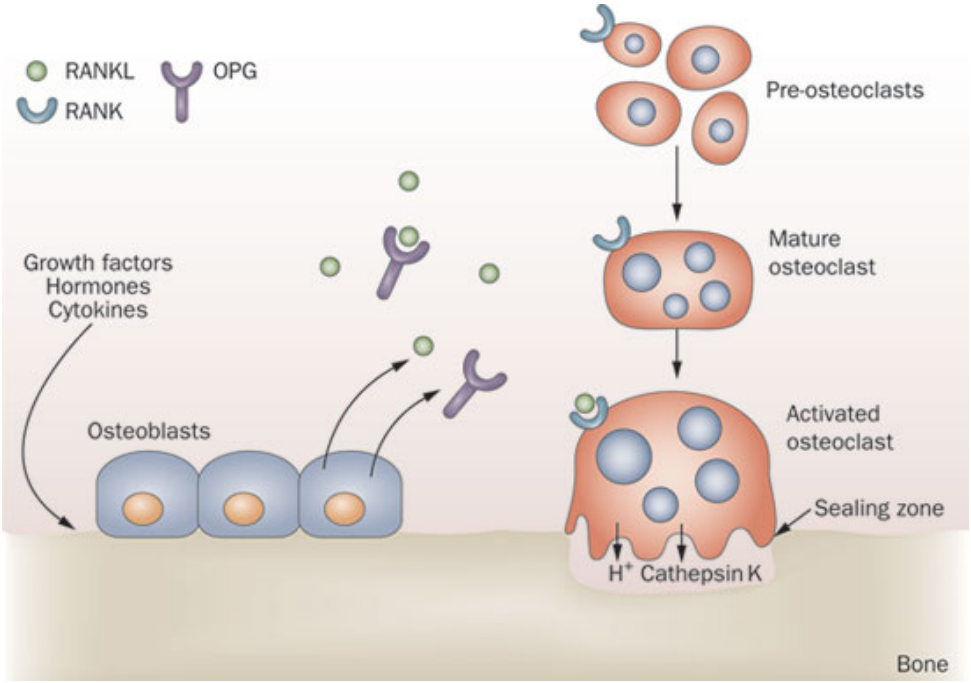

Figure 2.6: RANKL and OPG are both produced by osteoblast cells. RANKL activates osteoclasts and initiates bone resorption, but OPG is a decoy receptor for RANKL that inhibits osteoclast activity. (Lewiecki 2011)

2.3 Cell Mechanics and Mechanobiology

Cells are composed of a variety of substructures which contribute to the mechanical properties of each individual cell. The main components that influence the mechanical properties of cells are the cell membrane, the cytoplasm, the nucleus, and the actin cytoskeleton. The cell membrane encompasses the entire cell and isolates the contents of the cell from the extracellular environment. All vertebrate cells are enclosed by a membrane (Jamieson and Robinson 2014). Within the cell membrane is an aqueous, liquid-like structure with proteins and organelles known as the cytoplasm. The viscous liquid phase of the cytoplasm is the cytosol, and the non-liquid phase is composed of proteins whose total concentration of macromolecules (proteins, lipids, sugars and nucleic acids) has been estimated at up to 400 mg/mL (Guigas et al. 2007) and occupying 5 - 40% of the cytoplasm volume (Ellis and Minton 2003). The cytoplasm influences cellular nano-scale mechanical properties due to the large volume of macromolecules (Guigas et al. 2007). The nucleus is isolated from the rest of the cell by the nuclear membrane (a phospholipid bilayer) (Lodish et al. 2000). The nucleus contains chromatin (DNA and other proteins) and the nucleolus that produces RNA (Van Lommel 2003). The common image of the nucleus is a compartment of densely

packed chromatin (Backman et al. 2000) and this is supported by early studies of differential light scattering from spherical Chinese hamster ovary cells and HeLa cells (Brunsting and Mullaney 1974). However, it must be noted that more recent studies have shown that refractive index (Guigas et al. 2007; Gnutt et al. 2015; Schürmann et al. 2016) and dry mass (Schürmann et al. 2016) of nuclei was lower than that of the cytoplasm. Finally, a dynamic meshwork of proteins known as the cytoskeleton forms a filamentous system of "ropes, cables and poles" in the cell. The cytoskeleton gives rigidity and shape to the cell and determines to a large extent the mechanical properties of the cell (Lee et al. 2012). This structure is discussed in detail in Section 2.4.

Investigations into cell mechanical properties, typically using atomic force microscopy (Takai et al. 2005; Darling et al. 2008; Docheva et al. 2008; Sugawara et al. 2008; Mullen et al. 2014a), micropipette aspiration (Haider and Guilak 2002; Zhao et al. 2009; Yu et al. 2010) or magnetic beads (Bausch et al. 1998), have provided mechanical data (i.e. Young's Modulus, Poisson's Ratio) for the nucleus and cytoplasm. Commonly used techniques to measure the mechanical properties of individual cells can be seen in Figure 2.7. The nucleus has a higher Young's modulus (Tseng et al. 2004) than the cell cytoplasm (3.7 kPa) (Domke et al. 2000).

.

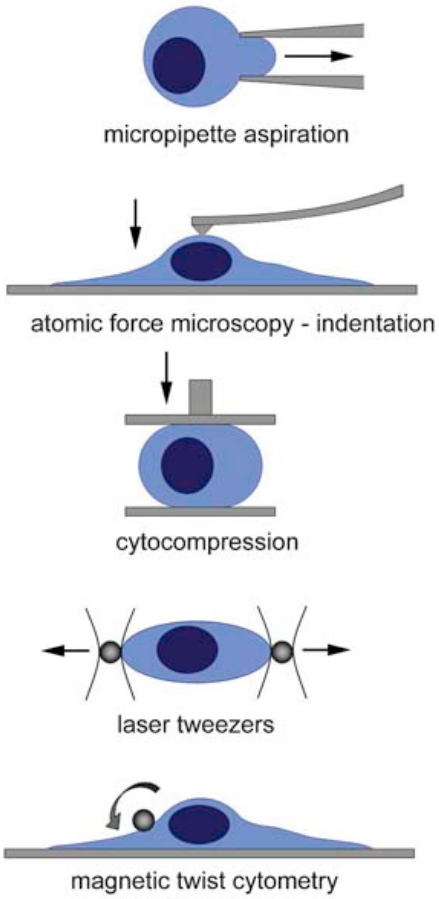

Figure 2.7: Schematics of commonly used techniques to test the mechanical properties of individual cells (Lee et al. 2011).

The reported elastic Young's modulus of the osteoblast cytoplasm measured in the above studies varies from 0.5 to 18 kPa. The Young's modulus of the nucleus has been estimated at between 5.1 kPa and 8 kPa by parallel plate compression testing of the nucleus and then fitting the resulting force and deformation data to a finite element model (Caille et al. 2002). However, other studies have shown that the nucleus is three to four times stiffer in chondrocytes (Guilak et al. 2000) and nine times stiffer in endothelial cells than the cytoplasm (Maniotis et al. 1997). The measured Young's modulus of osteoblasts and MSCs can depend on cell morphology, with spread cells having a higher Young's modulus than spherical cells (Darling et al. 2008).

2.3.1 Mechanosensation

The Young's modulus of the osteoblast cytoplasm is significantly influenced by the substrate that the cell adheres to, with cells on stiffer substrates having a higher Young's modulus than cells on softer substrates (Domke et al. 2000; Takai et al. 2005;

Mullen et al. 2014a). This change in cell mechanical properties with respect to substrate stiffness demonstrates that cells are sensitive to their mechanical environment, a phenomenon known as mechanosensitivity. Osteogenic cells are now widely known to be responsive to mechanical stimuli, including substrate stiffness and fluid flow, and these cells can alter their mechanics, metabolism, gene expression profiles and morphology in response to applied mechanical stimuli. Cell mechanobiology is the study of the response of cells to their mechanical environment. There are a variety of cellular structures that may translate mechanical stimulus into a cellular response; adhesion junctions (Leckband et al. 2011), the cytoskeleton (Arnsdorf et al. 2009b; Higuchi et al. 2009), integrins (Pavalko et al. 1998; Lee et al. 2008b; Haugh et al. 2015), and primary cilia (Malone et al. 2007b; Delaine-Smith et al. 2014) or gap junctions (Saunders et al. 2001; Jekir and Donahue 2009). Adhesion junctions are discussed in detail in Section 2.5, and the cytoskeleton is discussed in detail in Section 2.4.

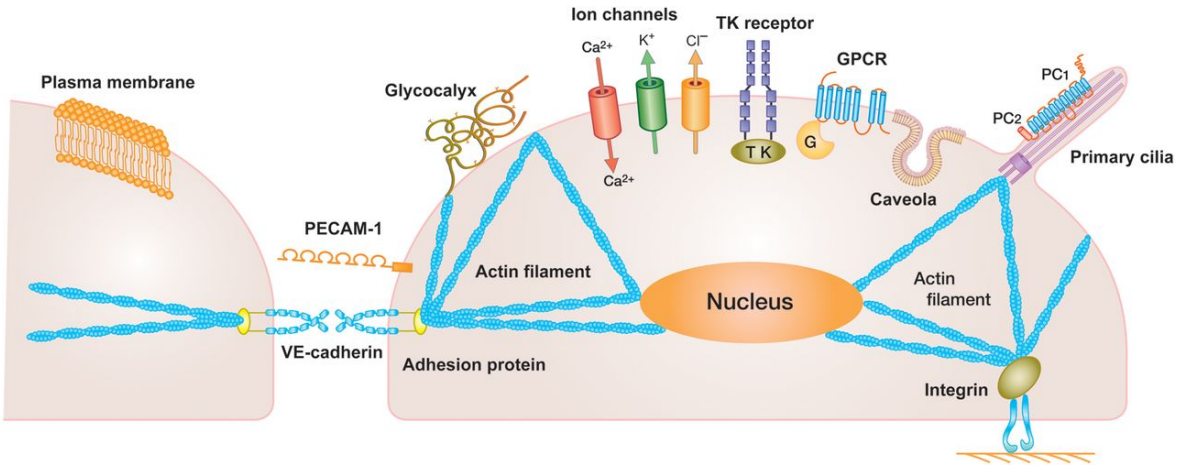

Figure 2.8: Schematic of structures that are involved in mechanosensation (Ando and Yamamoto 2013). Cadherins connect cells to one another. The cytoskeleton may transmit forces experienced at other mechanosensors, or directly sense stimulation itself. Integrins connect cells to extracellular matrix or substrates. Primary cilia extend out from the surface of the cell and the deflection of primary cilia has been implicated in changes in ion concentrations (e.g. Ca^{2+}) within cells.

Integrins are transmembrane proteins, which form focal adhesions that connect the cells to their extracellular environment, and allow cells to adhere to substrates such as extracellular matrix, plastic, glass and even metals. Integrin attachment proteins such as $\alpha_v\beta_3$ are essential for mechanosensation and mechanotransduction in response to fluid flow in osteocytes (Lee et al. 2008a; Haugh

et al. 2015). These focal adhesions function to sense their mechanical environment via the unfolding of specific proteins (e.g. talin, vinculin) in response to physiological loading, thus exposing more binding sites for other focal adhesion associated proteins and initiating signalling cascades that influence gene expression (Sawada et al. 2006; Del Rio et al. 2009; Golji et al. 2011). Vinculin and talin are two of several proteins thought to anchor the cytoskeleton to the cell membrane at points of cell-cell and cell-substrate attachment (Gilmore and Burridge 1996).

Primary cilia are microtubule based structures that originate in the centrisome of the cell, protrude outward from the surface of the cell and can be deflected by fluid flow (Wheatley et al. 1996). MC3T3-E1 osteogenic and bone resorbing responses to dynamic fluid flow require intact primary cilia (Malone et al. 2007b). The influx of Ca^{2+} in response to fluid flow is dependent on primary cilia in kidney epithelial cells (Praetorius and Spring 2001; Praetorius and Spring 2003; Liu et al. 2005), but the dependence on primary cilia is contentious in osteogenic cells. It was first reported as Ca^{2+} independent in MC3T3-E1 osteoblasts and MLO-Y4 osteocytes (Malone et al. 2007b) but more recently it was shown that fluid flow induces Ca^{2+} increases in osteocyte primary cilia which depend on both intracellular Ca^{2+} release and extracellular Ca^{2+} entry (Lee et al. 2015).

The molecular structures that mediate cell-cell adhesion can be divided into three subfamilies; adhesion junctions (AJs), tight junctions and gap junctions (Matter and Balda 2003; Stains and Civitelli 2005; Meşe et al. 2007). Adhesion junctions (AJs) connect the cytoskeletons of adjacent cells via extracellular cadherins, and will be described in further detail in Section 2.5.

2.4 The Cytoskeleton

The cytoskeleton forms the backbone of the eukaryotic cell, providing the mechanical integrity to support cell shape, influences the mechanical properties of the cell (Lee et al. 2012), spatially organises the contents of the cell and has the capacity to generate force that is vital for cell motility and cell-cell and cell-substrate mechanosensitivity. The three main components of the cytoskeleton are microtubules (Ø 25 nm), actin filaments (sometimes called microfilaments or F-actin) (Ø 10 nm) and a group of polymers collectively called intermediate filaments (Ø 7 nm) (Bershadsky and Vasiliev

2012). These components can be classified both by their size and relative flexibility (Figure 2.9). The protein actin is one of the key cytoskeletal filaments in cells (Dos Remedios et al. 2003) and a variety of actin binding proteins work in concert to regulate the kinetics of actin filaments (Vale and Kreis 1999).

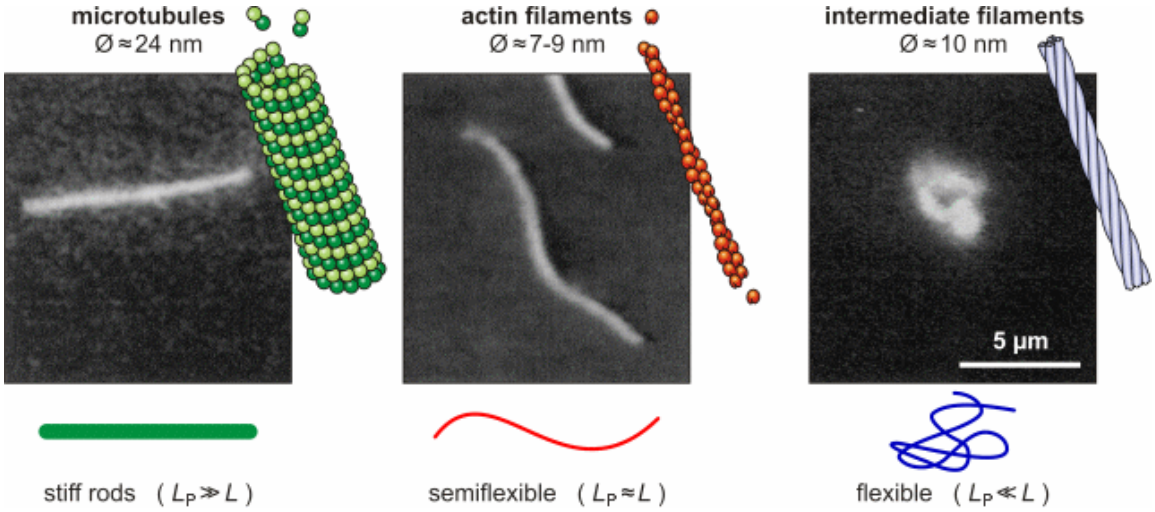

Figure 2.9 Schematic and fluorescent images of the three major components of the cytoskeleton. The flexibility of the three components can be used to identify them and is calculated based on their persistence length (L_P) in comparison to their contour length (L). Image from Steve Pawlizak, Diploma Thesis, 2009 and (Käs et al. 1996). The persistence length is the distance that the polymer is when it is in naturally straight configuration.

The mechanics of the cytoskeleton are not as rigid as their name might suggest due to the highly dynamic, adaptive nature of the cytoskeleton. The main molecular mechanism responsible for the rapid reorganisation of the cytoskeleton fibres is the polymerisation of protein subunits by globular actin monomers (G-actin) to form fibres, and then later depolymerisation of fibres. The RhoA/ROCK and Rac1 signalling pathways play an important role in the development and regulation of contractile stress fibres. Rho-associated protein kinase (ROCK) is activated when Ras homolog gene family, member A (RhoA) binds to it. ROCK indirectly inhibits the depolymerisation of actin filaments (Maekawa et al. 1999), promotes actomyosin contraction (Kimura et al. 1996), is required to form punctate adhesions (Vaezi et al. 2002) and significantly influences the osteogenic differentiation of MSCs (McBeath et al. 2004). Tseng et al. contributed the spontaneous osteogenesis of MSCs to significantly higher in cytoskeletal tension and actomyosin contraction (Tseng et al. 2012). Ras-related C3 botulinum toxin substrate 1 (Rac1), is a small (~21 kDa) member

of the Rac subfamily of the Rho family of GTPases which regulates the cell cycle, cell-cell adhesion and cytoskeletal reorganization and motility (through the actin network) (Chae et al. 2008; Jung et al. 2011; Zheng and Kim 2013) by interacting with downstream proteins to suppress the local formation of contractile actin (Burridge and Wennerberg 2004).

As previously mentioned, the functions of the cytoskeleton are numerous. For example, cytoskeletal function in cell motility can vary from cell contraction to cilia or flagella beating. The interaction of actin filaments with myosin forms the basis of many types of motility. When actin and myosin interact, ATP is consumed and actin filaments can move. The ATP dependent mutual sliding of actin and myosin filaments, which is the cornerstone of cytoskeletal contraction, was first proposed by (Huxley and Niedergerke 1954; Huxley and Hanson 1954) independently. Stress fibres are a specific type of contractile F-actin bundle, which are characterised by repeating units of myosin-II motor proteins and α-actinin (Peterson et al. 2004) (Figure 2.10B). Stress fibres are known to form in response to their mechanical environment and can often be seen in osteogenic cells on stiff substrates like plastic or glass. The mechanical properties of the cytoplasm are greatly influenced by the cytoskeleton and there is a 2.6 - 3.2 fold decrease in Young's Modulus when actin polymerisation is inhibited using Cytochalasin D (Goddette and Frieden 1986; Rotsch and Radmacher 2000). Inhibition of microtubules with Colchicine did not alter the apparent elastic modulus of myocytes measured using atomic force microscopy (Collinsworth et al. 2002). Other studies have shown that inhibition of microtubule formation results in significantly higher actomyosin contractility, traction force magnitude, and cortical elasticity (Danowski 1989; Kolodney and Elson 1995; Ezratty et al. 2005; Rape et al. 2011; Al-Rekabi et al. 2014). The Young's moduli of fibroblasts with and without vimentin intermediate filaments are substrate stiffness dependent, and fibroblasts without vimentin have a lower Young's modulus during AFM indentation than those with vimentin across a range of indentation depths (500 – 1000 nm).

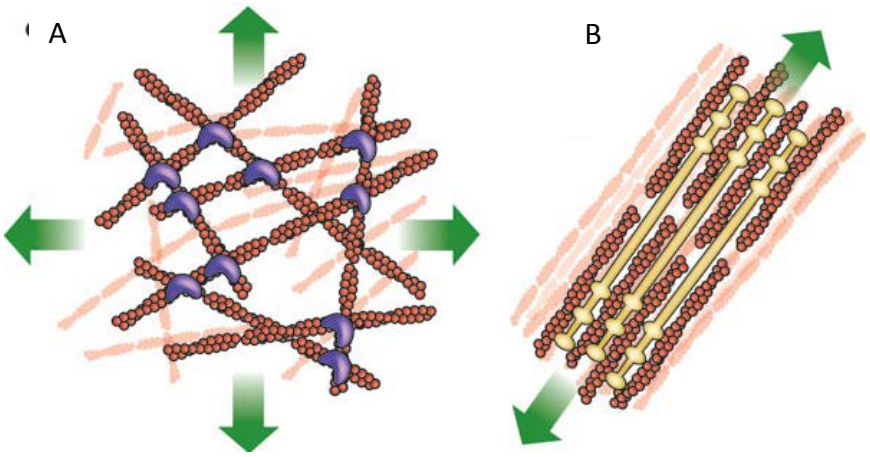

Figure 2.10: (A) Non-aligned Cortical networks form below the plasma membrane and carry tension loads in multiple directions. (B) Stress fibres form from bundled actin filaments, shown here associated with filaments of myosin, and generate tension against cell adhesions to the extracellular matrix (Fletcher and Mullins 2010).

2.5 Adhesion Junctions

Adhesion junctions (AJs) are transmembrane glycoproteins that form a connection between cytoskeletons of adjacent cells (Figure 2.11). They have an extracellular component called a cadherin, a small transmembrane component and an intramembranous (cytoplasmic) section composed of a network of accessory proteins through which the AJ connects to the actin cytoskeleton (Nelson and Nusse 2004). It is believed that these junctions act to transmit forces between cells (Ganz et al. 2006; Ng et al. 2012).

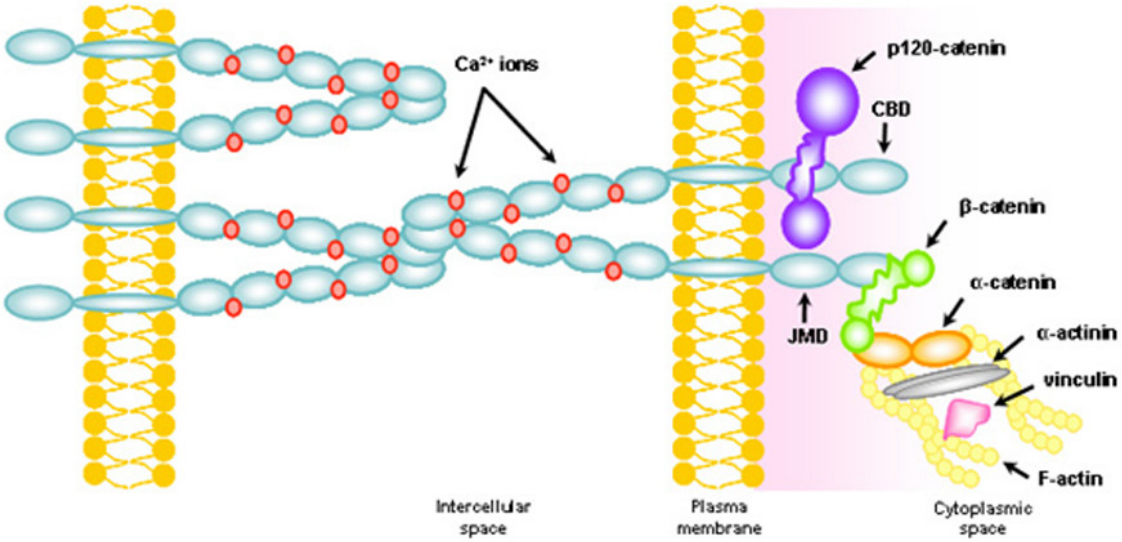

Figure 2.11: The Cadherin Adhesion Complex (Paredes et al. 2007). Classical cadherins (blue), which mediate calcium-dependent (red) intercellular adhesion, are composed of an extracellular domain, a transmembrane domain and a cytoplasmic domain. This last domain is comprised of a juxtamembrane domain (JMD), which binds p120-catenin, and a catenin-binding domain (CBD), which binds β-catenin, which in turn binds α-catenin. Both α-catenin, α-actinin and vinculin establish a direct link between the cadherin-catenin complex and the actin cytoskeleton (yellow).

Interaction between AJs and the cytoskeleton stabilises the AJ and is associated with increased strength of AJ bonds (Pittet et al. 2008; Hong et al. 2013). However, there is debate on the exact mechanisms through which the AJ is connected to the cytoskeleton, and the importance of various intramembranous proteins to this connection. One such protein is vinculin, which is involved in connecting the cytoskeleton to the cell membrane at points of cell-cell and cell-substrate attachment (Geiger et al. 1980). Huveneers et al. recently showed that vinculin is not required for the formation of AJs in primary human umbilical vein endothelial cells (HUVECs) (Huveneers et al. 2012). Initiation of cell-cell contact occurs at the cadherin complex when spatiotemporal activity of Rac1 induces polymerisation of actin filaments (Ehrlich et al. 2002; Yamada and Nelson 2007). Rac1 increases with osteogenic differentiation (Gao et al. 2010). RhoA activity at cell-cell contact sites mediates actomyosin-dependent expansion of the adhesion zone (Yamada and Nelson 2007; Daneshjou et al. 2015). ROCK is activated when RhoA binds to it. ROCK indirectly inhibits the depolymerisation of actin filaments (Maekawa et al. 1999), promotes actomyosin contraction (Kimura et al. 1996), is required to form punctate adhesions (Vaezi et al. 2002).

2.5.1 Cadherins

Adhesion junctions are believed to initiate contact between cells through pairing of cadherins on adjacent cells (Gumbiner 2005). Cadherins are a family of glycoproteins that can be identified by their characteristic extracellular cadherin repeats (EC) (Nollet et al. 2000). Cadherins bond to one another in a homophilic, Ca^{2+}-dependent fashion (Stains and Civitelli 2005), as shown in Figure 2.11. Cadherins can be divided into six subfamilies; type 1 classical cadherins, type 2 atypical cadherins, desmosomal cadherins, flamingo cadherins, proto-cadherins and several ungrouped members. Type 1 and Type 2 cadherins have well established roles in cell-cell adhesion (Takeichi 1990). Cadherins are expressed in almost all tissues (Takeichi 1995) and play important roles in the formation and maintenance of a wide variety of tissues and organs (Yagi and Takeichi 2000). It is because of the diverse roles played by cadherins that altered cadherin expression has been linked to a variety of diseases including metastatic cancer (Van Roy 2014), Crohn's disease (Muise et al. 2009) and diabetes related complications (Navaratna et al. 2007).

There are multiple types of cadherins and these are typically named after the tissue where they were initially first observed (Table 2.1). Most tissues express more than one cadherin (Suzuki et al. 1991; Tanihara et al. 1994). The cadherins expressed on the surface of a cell differ depending on both cell lineage and differentiation stage within a lineage (Kawaguchi et al. 2001). The predominantly homophilic bonding of cadherins means that, for example, N-cadherin will preferentially bond to N-cadherin.

Symbol	Name	Tissue Origin of Name	Cadherin Type
CDH1	E-cadherin	Epithelial	1
CDH2	N-cadherin	Neural	1
CDH3	P-cadherin	Placental	1
CDH4	R-cadherin	Retinal	1
CDH5	VE-cadherin	Vascular Endothelial	2
CDH6	K-cadherin	Kidney	2
CDH11	OB-cadherin	Osteoblast	2
CDH12	N-cadherin 2	-	2
CDH13	T-cadherin H-cadherin	Heart	-
CDH15	M-cadherin	Myotubule	1
CDH17	LI-cadherin	Liver-Intestine	-

Table 2.1: Details of some of the Type 1 and Type 2 Cadherins as documented by HUGO Gene Nomenclature Committee (HGNC), a committee of the Human Genome Organisation.

Mesenchymal and osteoblast stem cells express mainly N-cadherin and OB-cadherin AJs (Cheng et al. 1998a; Haÿ et al. 2000; Kawaguchi et al. 2001). Osteoprogenitor cells also express low levels of P-cadherin, K-cadherin (Kawaguchi et al. 2001) and E-cadherin (Haÿ et al. 2000). N-cadherin has been found in all stages of osteogenic differentiation (Ferrari et al. 2000; Shin et al. 2000). The expression levels of N-cadherin mRNA levels remain constant during osteogenic differentiation of MSCs while the level of OB-cadherin mRNA increases (Shin et al. 2000). This expression of mRNA translates into an increase in both N-cadherin and OB-cadherin proteins with osteogenic differentiation (Shin et al. 2000).

The presence of N-cadherin was linked to significantly higher expression of osteoblast transcription factors osterix, osteomodulin and osteoglycin (Guntur et al. 2012). Osterix is vitally important for bone formation, inhibits the major gene for chondrogenesis (Sox9), and is activated by phosphorylation of p38 MAPK (Nakashima et al. 2002; Nakashima and de Crombrugghe 2003; Ortuño et al. 2010). Mouse models without the osterix gene display a complete lack of ossification (Nakashima et al. 2002; Huang et al. 2004). It is thought that osterix is either independent or downstream of

Runx2 (Lee et al. 2003). Osteomodulin regulates the diameter and alters the shape of collagen fibrils (Tashima et al. 2015). Osteoglycin has been indicated to enhance bone formation in osteoblasts (Tanaka et al. 2012). N-cadherin is important for osteoblast differentiation as it is necessary for the significantly higher ALP expression and mineralisation in response to bone morphogenetic protein (BMP-2) (Ferrari et al. 2000). Additionally blocking of N-cadherin has been linked to deactivation of PI3K signalling (Guntur et al. 2012). Active PI3K signalling leads to osteogenic differentiation of MC3T3-EIs. PI3Ks are intracellular phosphorylating signal transducing enzymes whose absence or down-regulation is linked to tumorigenesis (Cully et al. 2006). Additionally, the presence of OB-cadherin and N-cadherin in teratomas generated bone and cartilage preferentially (Kii et al. 2004b). L cells (gut endocrine which do not express cadherins) double transfected with OB-cadherin and N-cadherin expressed elevated levels of ALP but single transfected (OB-cadherin or N-cadherin) L cells did not illicit a response (Kii et al. 2004b). C2C12 (mouse myoblasts that express N-cadherin) expressed elevated levels of ALP when transfected with OB-cadherin (Kii et al. 2004b). These results demonstrate that OB-cadherin influences the differentiation of mesenchymal stem cells in a different manner than N-cadherin. N-cadherin over-expression in bone marrow MSCs resulted in significantly lower ALP activity, and significantly lower OPN, OCN, Runx2 and BMP-2 expression in comparison to controls (Xu et al. 2013). In addition, N-cadherin over-expression resulted in significantly lower ectopic bone formation. Reducing N-cadherin caused significantly higher ALP expression.

As mentioned previously, the cadherin family of adhesion proteins can be identified by their extracellular cadherin repeats (EC). Cadherins are composed of five connected domains (EC1-5) (Nelson and Nusse 2004) and the most distal EC1 domain of each cadherin is capable of connection to the EC1 domains on cadherins of adjacent cells (a trans-dimer). Additionally, there is emerging evidence that other regions of the cadherin may have a functional role in cadherin adhesion, particularly for cis-dimer formation between the EC3 domains of cadherins on the same cell (Figure 2.12) (Zhu et al. 2003; Stains and Civitelli 2005).

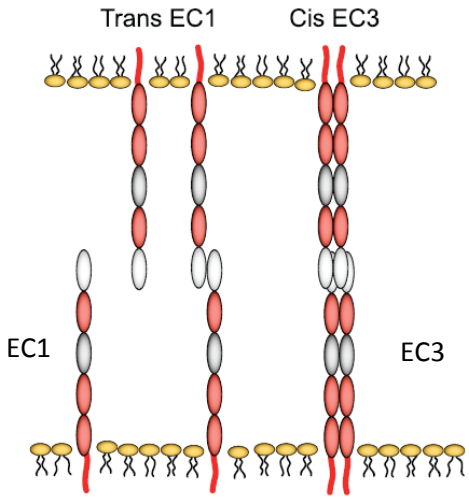

Figure 2.12: Initial cadherin formation occurs between adjacent cells (trans) at the most distal EC1 domain. Subsequently, slower lateral oligomerisation of the EC3 domain occurs with the formation of cis-dimers between cadherins on the same cell. Image adapted from (Niessen et al. 2011).

Cadherin binding is highly transient and in a steady state structure the AJ will continuously gain and lose cadherins (Troyanovsky et al. 2007; Hong et al. 2010). This rapid decoupling of cadherin bonds is thought to occur via reconfiguration of the adhesive bond between cadherins from the principal adhesive 'strand swap' type to an unstable X dimer type (Figure 2.13) (Hong et al. 2011). It is hypothesised that this transition could be controlled by intercellular traction forces (Hong et al. 2011). When AJs have formed, tension pulls the cadherins so that only the most distal section of the EC1 domain can touch but less tension allows more of the EC1 domain to come into contact and the X-dimer to form (Hong et al. 2011).

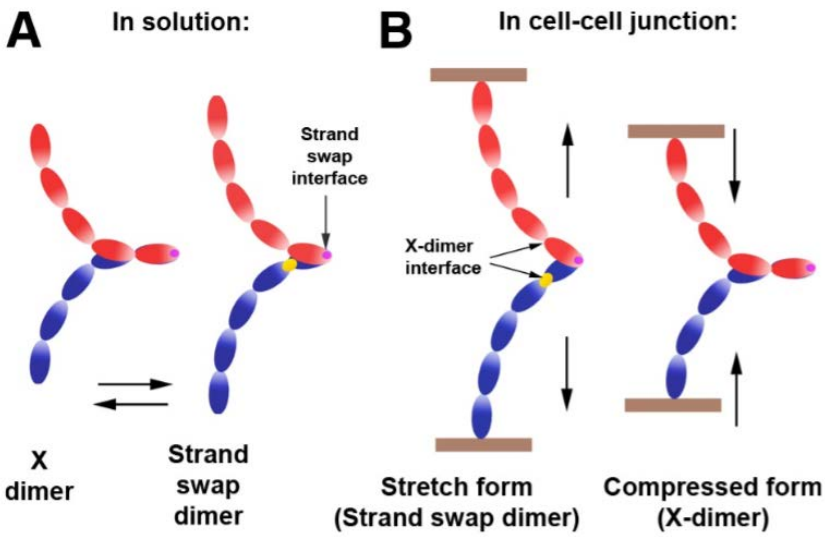

Figure 2.13: Diagram depicting the hypothetical mechano-regulation of the cadherin dimerization states (Hong et al. 2011). A) In solution cadherin dimers are unregulated by traction forces and can switch between unstable x dimers and stable strand swap dimers. B) In cell-cell junctions the binding mode of the dimer is regulated by traction forces.

2.5.2 Intercellular Protein β-catenin

The cytoskeletons of adjacent cells are connected by AJs via a variety of proteins in the intramembranous section of the AJ, some of which bind to the actin cytoskeleton (Overduin et al. 1995; Shapiro et al. 1995; Stains and Civitelli 2005). β-catenin is one such intramembranous protein and was first observed at AJs in osteogenic cell lines (Cheng et al. 1998b) and later observed in the cytoplasm and nucleus of osteoblasts (Monaghan et al. 2001). β-catenin was later discovered to be essential for the osteogenic differentiation of mouse MSCs (Day et al. 2005). However, conflicting data exists with regards to how necessary β-catenin is for the formation of AJs. Studies have shown that cadherins and β-catenin have a 1:1 binding affinity (Miyake et al. 2006; Maki et al. 2015), that the cytoplasmic tail of the cadherin becomes structured on binding to β-catenin (Roura et al. 1999; Huber et al. 2001; Murase et al. 2002) and subsequently recruits α-catenin (Bajpai et al. 2008). α-catenin is one of the intramembranous proteins that binds to the actin cytoskeleton. Other studies have shown that β-catenin may only be necessary to recruit α-catenin by demonstrating that a cadherin-α-catenin fusion protein can form a junction without β-catenin (Pacquelet and Rørth 2005). Interesting, plakoglobin (also called γ-catenin - another intercellular protein linking the AJ to the cytoskeleton) can functionally compensate for

the loss of β-catenin, as E-cadherin expression was only significantly lower when both β-catenin and plakoglobin were depleted (Fukunaga et al. 2005; Lyashenko et al. 2011).

β-catenin is an important component of the canonical Wnt signalling pathway (Westendorf et al. 2004). Canonical Wnt signalling heavily influences the maintenance and development of bone by effecting cell differentiation, proliferation, migration, polarity and gene expression (Moon et al. 2002). Canonical Wnt signalling influences Cox-2 and Runx2 gene expression, and osteoblast mineralisation (Norvell et al. 2004a; Rodda and McMahon 2006; Arnsdorf et al. 2009a). Down-regulation of canonical Wnt signalling encourages MSC renewal, while an up-regulation of canonical Wnt signalling encourages osteogenic differentiation of MSCs (Bennett et al. 2005; Gregory et al. 2005; Jackson et al. 2005). The canonical Wnt signalling pathway has multiple regulatory mechanisms, including adhesion junction sequestering of β-catenin, degradation of cytoplasmic β-catenin when canonical Wnt signalling is not active, and conformation changes in β-catenin and other receptors during active canonical Wnt signalling (Nusse 2012). These steps all act in concert to regulate canonical Wnt signalling. This pathway can be divided into two different states (Nusse 2012); inactive signalling and active signalling (Figure 2.14).

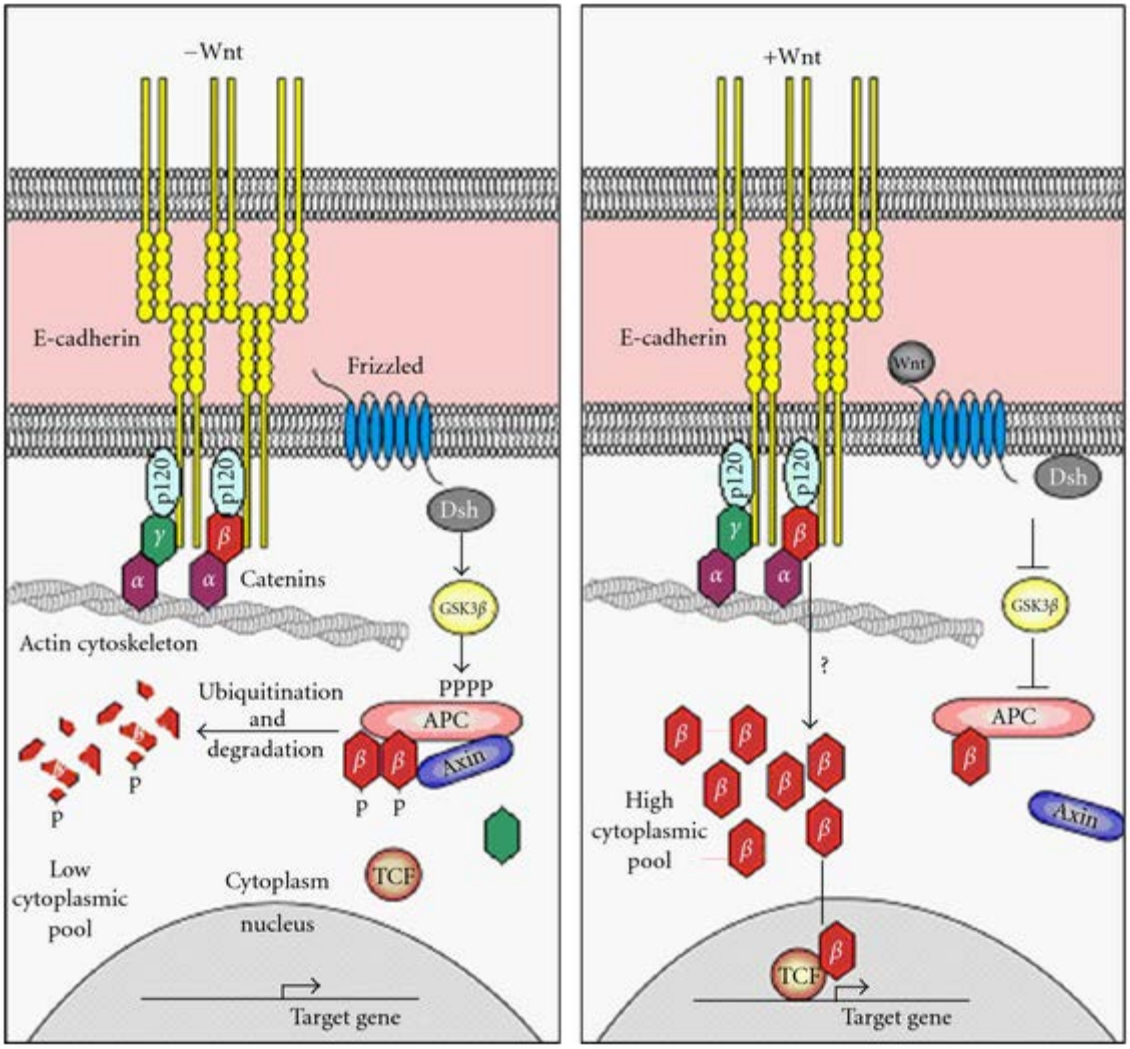

Figure 2.14: Canonical Wnt signalling pathway showing E-Cadherin/β-catenin/plakoglobin interactions (Tian et al. 2011).

This pathway is in the inactive state when Wnt signalling is absent (Figure 2.14 Left Panel). In the absence of Wnt signalling, Wnt target genes are repressed (Cavallo et al. 1998; Roose et al. 1998). Wnt target genes are numerous but some of the most relevant targets are Runx2/Cbfa1 (Dong et al. 2006), RANK ligand (RANKL) (Spencer et al. 2006), osteoprotegerin (OPG) (Glass Ii et al. 2005) and Cox-2 (Haertel-Wiesmann et al. 2000). Osteoblasts synthesise both OPG and RANKL. RANKL binds to osteoclasts and is a key factor in osteoclast activation. OPG is a decoy protein that can bind to RANKL and inhibit osteoclast differentiation and activity (Udagawa et al. 2000). β-catenin levels in the cytoplasm are kept low via phosphorylation by the protein kinases glycogen synthase kinase 3 (GSK3) and CK1 (Aberle et al. 1997; Zeng et al. 2005).

Active state Wnt signalling rearranges these complexes (Figure 2.14-Right Panel). Wnt ligands bind to a complex that includes GSK3 (Fiedler et al. 2011). This sequestering of GSK3 leads to significantly lower phosphorylation of β-catenin. Stable, unphosphorylated β-catenin can translocate into the nucleus, where it targets genes such as Runx2/Cbfa1, RANKL and OPG (Behrens et al. 1996; Molenaar et al. 1996).

Cell-cell adhesion and canonical Wnt signalling are not mutually exclusive pathways and can affect each other. The quantity of AJs formed on the cell membrane influences the levels of free β-catenin in the cytoplasm that can become involved in canonical Wnt signalling (Fagotto and Gumbiner 1994; Tufan and Tuan 2001). Additionally, the presence of OB-cadherin coincides with significantly lower phosphorylated β-catenin in the cytoplasm (Di Benedetto et al. 2010) and significantly higher binding of β-catenin to N-cadherin (Kii et al. 2004a). Interestingly, MC3T3-E1 cells over-expressing N-cadherin after stable transfection with a flag-tagged N-cadherin siRNA were found to have significantly lower ALP production and significantly lower Runx2 and Cox-2 expression (Haÿ et al. 2009). This inhibitory function of over-expressed N-cadherin was attributed to N-cadherin forming a complex with Axin and low-density lipoprotein receptor-related protein 5 (LRP5) that increased β-catenin degradation.

2.5.3 Adhesion Junction Mechanosensation

Adhesion junctions are sensitive to their mechanical environment and respond to it by altering their junction size or cell mechanical properties via the cytoskeleton (Ladoux et al. 2010; Liu et al. 2010b; Chopra et al. 2011). Investigations into AJ mechanosensation, using polyacrylamide gels coated with N-cadherin particles, showed that myogenic C2 cells on stiff substrates (95 kPa) form an actin cytoskeleton network, and β-catenin was recruited at the cell-substrate interface (Ladoux et al. 2010). However in softer substrates (10 kPa), no actin cytoskeleton network formed, and β-catenin was not recruited at the cell-substrate interface (Ladoux et al. 2010). Another study used traction force microscopy to track beads within polyacrylamide gels of varying stiffness, with an N-cadherin particle coating on the surface of the gel. For gels of 5 and 10 kPa stiffness, neonatal ventricular rat myocytes formed actin stress fibres and the traction force exerted on N-cadherin coated gels was approximately 300

nN (Chopra et al. 2011). The myocyte elastic modulus measured using atomic force microscopy (AFM) testing significantly increased (2000 Pa, 8000 Pa, and 1600 Pa) as gel stiffness increased (0.3 kPa, 10 kPa, 30 kPa) (Chopra et al. 2011).

Similar to the behaviour of cell-substrate contacts (focal adhesion), the size of cell-cell adhesion junctions is influenced by the tugging force applied to the junction (Liu et al. 2010b). The rate of cadherin turnover during steady state is influenced by the local tension acting on the junction and that higher tension leads to quicker cadherin-cadherin bond turnover (de Beco et al. 2015).

Adhesion junction mechanosensation may be facilitated through the intramembranous accessory proteins such as β-catenin, α-catenin and vinculin that connect adhesion junctions to the cytoskeleton (Yonemura et al. 2010; Huveneers et al. 2012). However, it should be noted that most investigations into adhesion junction mechanosensation have been limited to one or two cells interacting with one another or extracellular constructs.

2.5.4 Adhesion Junctions and Cell Mechanics

The formation of AJs requires tension generated by the cytoskeleton (Miyake et al. 2006; Hong et al. 2011; Hong et al. 2013). The ability of an AJ to resist rupture due to tension depends on the specific cadherin in the AJ. Mechanical testing using atomic force microscopy with cadherin coated cantilever tips has shown that OB-cadherin can resist approximately two-fold higher tensile forces (95±20 pN) than N-cadherin AJs (44±19 pN) in fibroblast cells before rupture (Pittet et al. 2008).

Cadherins have been observed to influence the Young's modulus of endothelial cells. When monolayers of human umbilical vein endothelial cells (HUVECs) are treated with VE-cadherin antibody, the Young's modulus is significantly higher both at the cell body (approximately, control 750 Pa and treated 900 Pa), and at the cell periphery (approximately, control 1000 Pa, treated 1200 Pa) (Stroka and Aranda-Espinoza 2011). As previously mentioned the mechanics of different cadherin types vary, therefore it is feasible that the contribution of different cadherins to different cell types will also vary but this has not yet been established.

2.5.5 Mechanical Relationship between Adhesion Junction and Integrins

Early studies investigating MC3T3-E1 AJs found that the cadherin levels were significantly higher with confluency (Luegmayr et al. 2000). The significantly higher cadherin levels were visualised via immunofluorescent staining of OB-cadherin, N-cadherin and Pan-cadherin in MC3T3-E1 cells. Additional studies have shown using flow cytometry that N-cadherin expression is higher in confluent cells than non-confluent cells (Ko et al. 2001). Further study has been carried out to assess if cadherin expression levels are related to cell-substrate binding. Integrins are transmembrane structures that mediate cell-substrate adhesion (Hynes 2004). Emerging evidence indicates cross-talk between integrins and cadherins during cell adhesion, cell contraction and motility (Figure 2.15 and Figure 2.16) (Weber et al. 2011).

Traction force microscopy has been used to compare the forces transduced through cell-cell (cadherin) and cell-ECM (integrin) adhesions using single cells (Ganz et al. 2006) or cell pairs (Maruthamuthu et al. 2011). The average C2 myogenic cell traction forces exerted by cadherins (0-50 nN) on N-cadherin coated micro-force sensor array (μFSA) were seen to be approximately half of that exerted by cell-ECM (0-100 nN) contacts on μFSA coated with fibronectin (Ganz et al. 2006). An alternative study looked at the traction forces generated by two Madin-Darby canine kidney (MDCK) cells in contact on a collagen-coated polyacrylamide gel (Maruthamuthu et al. 2011). For a cell pair to remain stationary, the sum of the traction forces exerted by the cell in any particular direction must sum to zero. This study saw that, when each cell in a cell pair was considered separately, there was an imbalance in the traction forces exerted on the gel. It was deduced that this imbalance reflects the force exerted at the cell-cell contact between the neighbouring cells. Individual cells in a cell pair had approximately equal unbalanced traction forces. Total cell-cell tugging forces varied from approximately 25 to 200 nN, while total cell-ECM traction forces varied from approximately 60 to 400 nN.

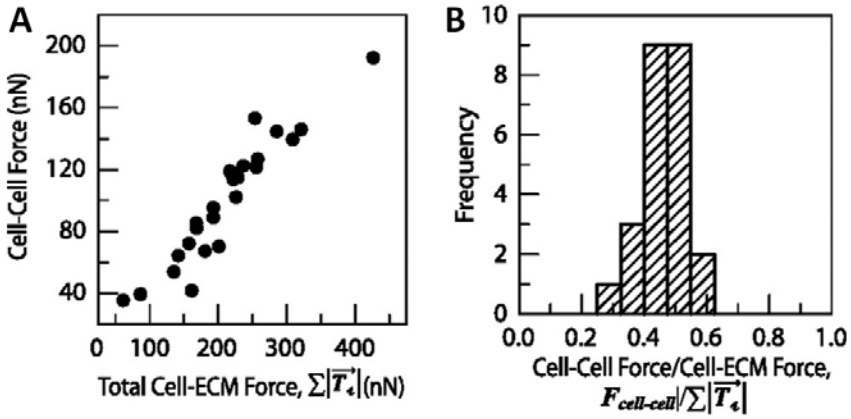

Figure 2.15: (A) Cell–cell force as a function of the total traction force exerted per cell. (B) Histogram of the ratio of the cell–cell force to the total traction force exerted per cell, mean ± SD = 0.47 ± 0.07 (Maruthamuthu et al. 2011).

Attachment of human hepatocellular carcinoma (HCC) cell line, KYN-2, to a substrate results in significantly lower immunofluorescent signal of E-cadherin and β-catenin at the cell membrane (Genda et al. 2000). De Rooij showed that during HGF induced cell scattering of MDCK cells (de Rooij et al. 2005). Time lapse imaging of HGF treated cells suggest that increased integrin adhesion causes increased cell-cell tension and pulls cells apart, resulting in cell scattering (de Rooij et al. 2005). Similar findings emerged in a more recent study, which found that as integrin binding area to micro-printed fibronectin patterns increased (<150 µm to >300 µm), a corresponding decrease in the Young's modulus (2 min incubation, 450 Pa for <150 µm, 100 Pa for >300 µm) of the bond between the cell and an E-cadherin coated microbead was observed for a S180 mouse sarcoma clone stably transfected to produce E-cadherin (Al-Kilani et al. 2011). However, this cross-talk may not yet be fully understood as another study showed that during dual-micropipette aspiration, the separation force (approx. 40nN) of S180 clones stably transfected to produce E-cadherin increase when the cells were cultured with fibronectin coated micro-beads before testing (approx. 70 nN) (Martinez-Rico et al. 2010). This increase was dependent on the size of the cell-fibronectin attachment area, with larger beads (15 µm) or increased number of smaller beads (1, 2 or 3 10 µm beads) resulting in greater cell-cell separation force during micropipette testing.

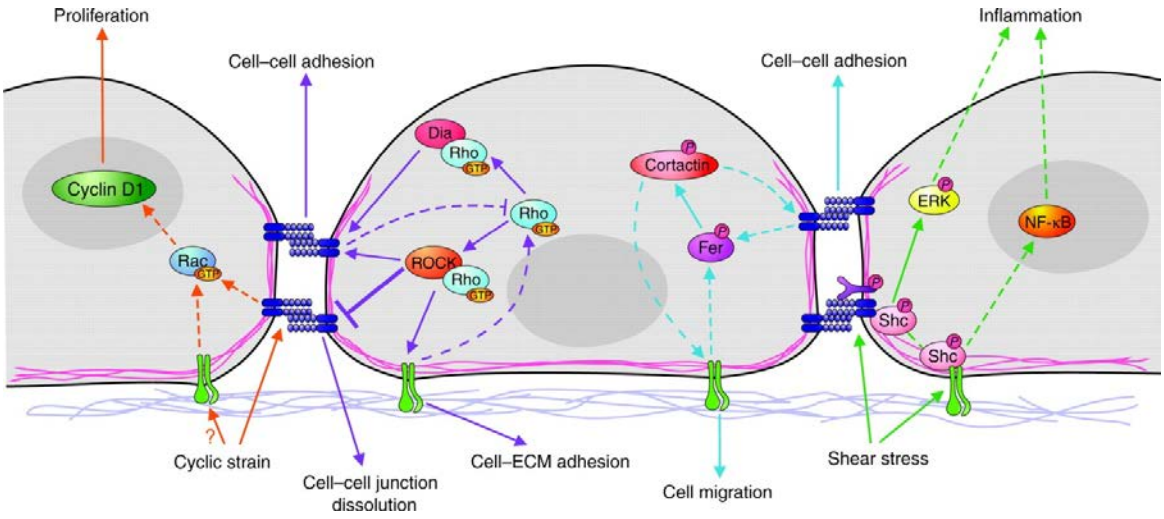

Figure 2.16: Diagram of signalling molecules integrating signalling between cell-cell adhesions (Cadherins) and cell-ECM adhesion (Integrins) (Weber et al. 2011).

2.5.6 Adhesion Junctions in 3D Tissues

Adhesion junctions serve a variety of functions in 3D tissues, such as cell sorting, cell-cell communication, collective cell migration and transmission of mechanical forces between cells. Adhesion junctions provide a mechanism for cells to recognise neighbouring cells and organise themselves within tissues and organs (Niessen et al. 2011). Cell-cell recognition plays an important role during embryonic development when cells are moving, differentiating and grouping into homogenous cell structures (Townes and Holtfreter 1955; Schäfer et al. 2014). The variation in cadherin expression, depending on the specific differentiation pathway, has been observed to help the cells sort into homogenous groups (Figure 2.17) (Gumbiner 1996; Dady et al. 2012).

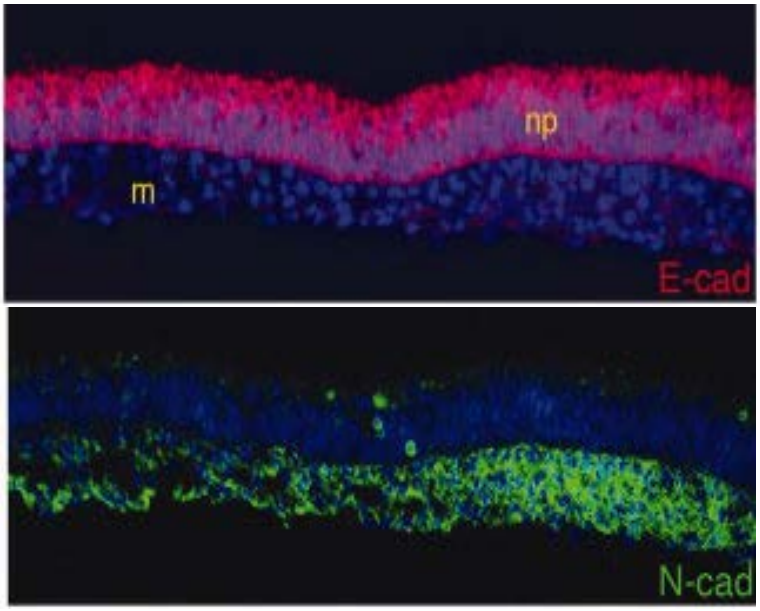

Figure 2.17: Immunostaining for E-cadherin (E-cad), N-cadherin (N-cad) on cross-sections through the neural plate of stage-HH4 chick embryo. Cell nuclei (blue) are stained with DAPI, m: mesoderm, np: neural plate (Dady et al. 2012).

It has been demonstrated that cells expressing the same cadherins are able to form aggregates in vitro (Nose et al. 1988; Steinberg and Takeichi 1994). However, it is not just the type of cadherin that is expressed that influences cell sorting. It has been shown that cells will sort into groups of cells expressing similar quantities of a particular cadherin (Figure 2.18) (Steinberg and Takeichi 1994; Duguay et al. 2003). Further to this, adhesion junctions may contribute to the sorting of osteogenic precursors by providing them with molecular targets in the form of cadherins for migration towards the bone surface (Tsutsumimoto et al. 1999; Luegmayr et al. 2000; Lemonnier et al. 2001).

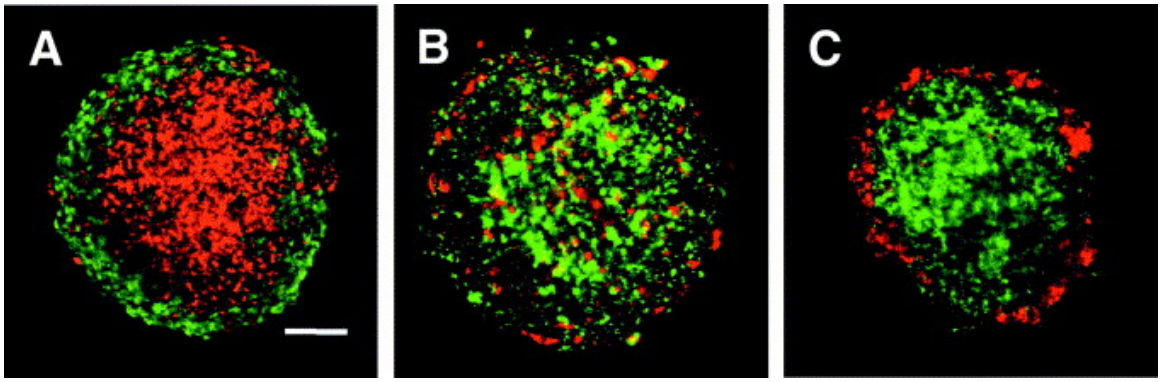

Figure 2.18: L cells expressing E- (green) or P- (red) cadherin sort out according to cadherin expression levels. A) P-cadherin expressing L cells expressing more cadherins than E-cadherin cells organise so that the P-cadherin cells segregate internally. B) Expression levels of P-cadherin or E-cadherin were the same and cells do not segregate. C) E-cadherin cells induced to have greater cadherin expression than P-cadherin expressing cells. E-cadherin cells segregate internally (Duguay et al. 2003).

In addition to providing molecular targets for migration, AJs play an important role in the collective migration of cells as groups, sheets or strands (Li et al. 2012a; Ng et al. 2012). This is evident in embryogenesis, during the process of intercalation when cells in a sheet rearrange themselves so as to elongate in one direction and narrow in the perpendicular direction (Keller 2002; Kim et al. 2010).

AJs facilitate cell-cell communication in a manner closely linked with the formation of gap junctions between embryonic myocytes (Luo and Radice 2003). N-cadherin down-regulation results in significantly lower movement of a fluorescent dye between neighbouring NIH3T3 fibroblasts (Wei et al. 2005) and significantly less AJ binding proteins β-catenin and plakoglobin leads to gap junction remodelling in mouse myocytes (Swope et al. 2012). Formation of AJs can also lead to the assembly of tight junctions, which forms a gateway for the select passage of ions and solutes (Tunggal et al. 2005; Taddei et al. 2008). Together, these studies indicate that AJs play a role beyond their own mechanical and biochemical roles and aid in intercellular movement of molecules.

Despite the knowledge that AJs are important for cell grouping and biochemical communication, there is very limited data to date on the role that AJs play in the mechanics of groups of cells. Previously discussed traction force and laser-tweezer experiments show that AJs can transmit forces between cells, but the implication of

this in terms of dictating the mechanical environment within cell aggregates and the specific influence of different cadherin types on this environment remain unclear.

2.5.7 Adhesion Junctions and Cytoskeleton Relationship

Increasing evidence is emerging indicating a close relationship between AJ formation and actin stress fibres formation. These structures have a reciprocal relationship both mechanically and biochemically. The formation of AJs is influenced mechanically by the cytoskeleton. The cytoskeleton stabilises the junctions by generating intracellular tension through actin stress fibre formation and aids clustering by limiting the degrees of freedom of movement of individual cadherin bonds (Hong et al. 2013).

AJ formation has been shown to be important for stress fibre formation both biochemically and by forming a structural basis for fibre formation. Sites of active polymerisation, identified by free barbed ends of actin filaments, can be found at adhesion junctions (Vasioukhin et al. 2000; Tao et al. 2007). However, cell confluency, cadherin engagement and cytoskeletal interaction with AJ intracellular proteins has been shown to cause a marked reduction in the activity of RhoA molecules that bind to ROCK (Maekawa et al. 1999; Anastasiadis et al. 2000; Noren et al. 2001; Noren et al. 2003). As mentioned in Section 2.4, ROCK indirectly inhibits the depolymerisation of actin filaments. The regulatory mechanisms surrounding the AJ-cytoskeleton interface are complex and also include regulation of Rac1 activity by cadherin engagement (Nakagawa et al. 2001; Ehrlich et al. 2002; Liu et al. 2006) and by cell adhesion (Wozniak et al. 2003; Pattabiraman and Rao 2010). Rac1 suppresses formation of stress fibres and is an important gene for cytoskeleton remodelling (Castets et al. 2005). Additionally, it has been shown that Rac1 activity can downregulate Rho activity (Sander et al. 1999a).

2.6 The role of Mechanical stimulation in Osteogenesis

Bone is a mechanically sensitive structure that responds to a variety of mechanical stimuli, such as substrate strain, extracellular matrix (ECM) stiffness, hydraulic pressure and fluid shear stress. Substrate strain experiments mimic the deformation that occurs in bone in vivo, during normal loading conditions. This stimulus increases ECM production and induces osteoblast differentiation (Guo et al. 2012; Zeng et al. 2015).

ECM stiffness has been shown to have a significant influence on the differentiation of osteoblasts (Mullen et al. 2015). However, it has been found that fluid shear stress has a greater effect on osteoblast osteopontin expression than substrate strain (Owan et al. 1997). Osteopontin is a secreted adhesive glycophosphoprotein, which plays a role in cell adhesion, migration and survival (Standal et al. 2004; Kirkham and Cartmell 2007). Similarly, it has been found that fluid shear stress produces larger fold increases in ATP release and Cox-2 expression than cyclic hydraulic pressure (Gardinier et al. 2009). ATP release mediates the release of intracellular stores of calcium (Chen et al. 2000; Katz et al. 2006). Cox-2 plays a role in early bone formation in response to mechanical stimulus, particularly by contributing to prostaglandin production (Wadhwa et al. 2002; Bakker et al. 2003a).

2.6.1 Fluid Flow

One of the most widely used methods to investigate osteogenic cell mechanobiology is the application of fluid shear stress (FSS). This method provides clinical relevance as it imitates the flow of fluid within the bone laculo-canalicular network (Weinbaum et al. 1994). FSS is the tangential force generated by the velocity gradient in laminar fluid flow (Figure 2.19).

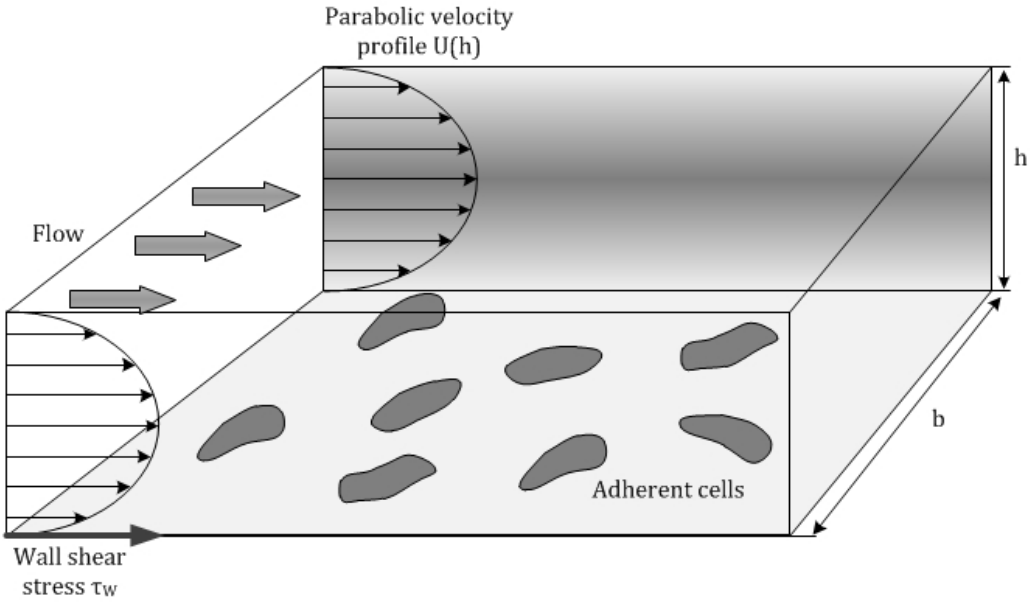

Figure 2.19 Diagram showing wall shear stress acting on cells adhered to a substrate. (h: chamber height, b: chamber width) (Eibl et al. 2008).

In general, application of fluid flow stimulation to MSCs, osteoblasts or osteocytes has a positive effect on the osteogenesis of these cells. Fluid flow stimulation can increase markers for early osteogenesis like ALP and PGE_2 expression (Kapur et al. 2003; Vance et al. 2005; Delaine-Smith et al. 2012), significantly higher expression of genes associated with osteogenesis like Cox-2 (Wadhwa et al. 2002; Bakker et al. 2003a), Runx2 (Mehrotra et al. 2006) and bone morphogenetic protein-2 (BMP-2) (Yourek et al. 2010), as well as influencing the formation of actin stress fibres and alignment of these fibres to the direction of fluid flow. As discussed in Section 2.2, PGE_2 is involved in the regulation of bone remodelling (Igarashi et al. 1994; Thorsen et al. 1996), ALP promotes mineralisation (Golub and Boesze-Battaglia 2007), Runx2 controls the expression of a variety of osteoblast-associated genes and proteins (Ducy et al. 1997) and Cox-2 is known to play a rate-limited role in the production of prostaglandin (Kirkham and Cartmell 2007).

FSS is applied to cells using a variety of methods. The most commonly used methods are parallel plate bioreactors, spinning disk bioreactors, stirring flasks and 3D perfusion bioreactors (Jossen et al. 2014). Each of these bioreactors has different fluid or mechanical motion that imparts a defined stimulus on the cells within each system. Parallel plate bioreactors are often used to investigate osteogenesis in response to applied fluid shear stress as this mode of stimulation mimics fluid flow within bone (Weinbaum et al. 1994). Parallel plate bioreactors function by forcing a fluid between two parallel plates that are very close together. Fluid flow through the chamber applies a controllable wall shear stress to the cells located on one plate of the bioreactor. Parallel plate bioreactors are flexible in terms of the flow regime which they can apply to the cells, as the exact flow regime and wall shear stress imparted on the cells can be controlled by the pumping system.

The most studied fluid flow regimes used to investigate the role of FSS for MSC and osteoblast osteogenesis are steady state laminar, pulsatile fluid flow and oscillatory fluid flow (Jacobs et al. 1998; Malone et al. 2007c; Arnsdorf et al. 2009a; Kamel et al. 2010; Liu et al. 2010a). The specific flow regime used can influence the responses elicited from the cells and this is explained in more detail below.

Oscillatory fluid flow is of particular clinical relevance as this modality of stimulation imitates the dynamic oscillatory fluid flow that occurs in the lacuno-

canalicular network during walking (Weinbaum et al. 1994). During walking, the spatially varying deformation of bone occurs due to applied loads. This deformation results in pressure gradients within the bone that are resolved via the movement of fluid within the Haversian canals and lacuno-canalicular network. When the load is removed, the fluid movement is reversed due to the reversal of the pressure gradient. This dynamically changing pressure gradient within loaded bone produces an oscillatory fluid flow pattern (Knothe Tate et al. 1998).

An array of studies have demonstrated that PGE_2 expression is significantly higher when pre-osteoblast cells are stimulated with oscillatory fluid flow (Saunders et al. 2001; Donahue et al. 2003; Saunders et al. 2003; Malone et al. 2007b). Additionally, the expression of osteopontin and Cox-2 mRNA by pre-osteoblasts is significantly higher with oscillatory fluid flow stimulation (Chen et al. 2000; You et al. 2001). Pulsatile fluid flow (PFSS) can also produce significantly higher PGE_2 expression, but in a more limited capacity depending on cell type and shear stress applied (Klein-Nulend et al. 1995; McGarry et al. 2005b; Kamel et al. 2010). Some studies show that PGE_2 expression cumulatively increased in FSS media under the application of 0.7 Pa shear stress using PFSS (Klein-Nulend et al. 1995), whereas other work showed that pre-osteoblasts can only increase PGE_2 expression in response to high shear stress (1.6 - 2.4 Pa) PFSS and not low shear stress (0.2 - 0.8 Pa) (Figure 2.20) (Kamel et al. 2010). Additionally, some studies have reported no significantly higher PGE_2 expression with PFSS application (McGarry et al. 2005b). Laminar fluid flow has been shown to increase the formation of actin stress fibres, induce alignment of the cytoskeleton with the direction of flow, increase MC3T3 PGE_2 production and expression of Runx2 and Cox-2 (Smalt et al. 1997; Norvell et al. 2004b; Mehrotra et al. 2006; Malone et al. 2007c).

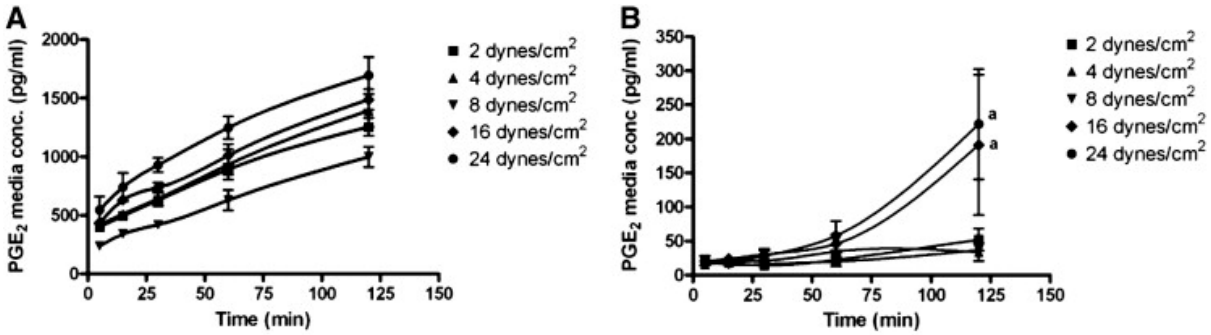

Figure 2.20: PGE_2 accumulation in the fluid flow media during the application of various levels of pulsatile fluid flow shear stress to MLO-Y4 osteocyte cells (Panel A) and to 2T3 osteoblastic cells (Panel B). All time points in the MLO-Y4 are significantly different compared to static controls at $p < 0.05$ (Kamel et al. 2010).

2.6.2 Cytoskeleton Response to Fluid Flow

MC3T3-E1 pre-osteoblast cells in static conditions display a cytoskeleton with actin filaments orientated at random (Figure 2.21). Fluid shear stress application can cause the actin cytoskeleton to remodel in a manner that is dependent on the stimulus applied. Steady, unidirectional fluid flow induces shear stresses that cause the actin filaments to bundle into thicker fibres, and these can orientate with the long axis of the cell (Jaasma et al. 2007; Malone et al. 2007c) or aligned in the direction of flow (Ponik et al. 2007). However, oscillatory fluid flow causes less mature stress fibres to form without strong alignment in the direction of fluid flow (Ponik et al. 2007). Cells exposed to oscillatory fluid flow gradually form more mature stress fibres when stimulated for longer periods (24 hrs).

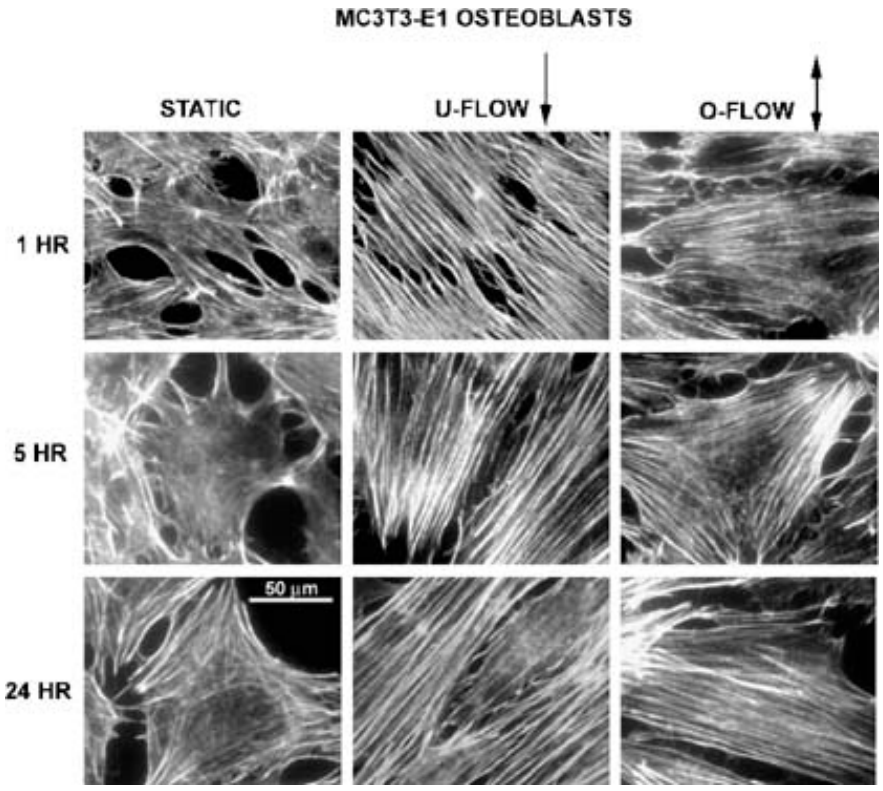

Figure 2.21: Stress fibre organisation visualised by rhodamine phalloidin staining of F-actin. MC3T3-E1 osteoblasts were subjected to static or flow conditions for 1, 5, or 24 hr. (U-flow: unidirectional flow. O-Flow: oscillatory flow) Arrows indicate the direction of fluid flow relative to the images. Cells in static culture formed fewer stress fibres. U-flow induced formation of organised stress fibres at all time points. Actin reorganised into a few stress fibres in response to 1 and 5 hr of O-flow. 24 hr of O-flow induced formation of organised stress fibres in MC3T3-E1 osteoblasts. (Ponik et al. 2007)

It has been shown that intracellular calcium has a significant effect on stress fibre formation and Cox-2 production in response to FSS (Chen et al. 2000). When FSS is applied, calcium production is upregulated and the cytoskeletal response depends on this calcium (Chen et al. 2000). Chen et al. (2000) also demonstrated by blocking membrane calcium ion channels that the cytoskeletal response requires the release of intracellular calcium, but not the transport of calcium into the cell. However, extracellular Ca^{2+} influx during FSS is seen to be important for F-actin cytoskeleton realignment and morphological changes in response to fluid flow (Liu et al. 2010a) in a system where 1.6 - 1.9 Pa of FSS was applied and the controls were seen to align to the flow direction. Calcium (both extracellular and intracellular) appears to play a role in ERK1/2 activation (Liu et al. 2008), which is important for Runx2 phosphorylation.

Studies have looked at the role of various components of the actin cytoskeleton in the FSS-induced osteogenic differentiation of MSCs. It was found that destruction of

microtubules for 5 days had no effect on the ALP activity of MSCs (Pablo Rodríguez et al. 2004) but the inhibition of actin filaments using Cytochalasin D caused an increase in ALP activity (Higuchi et al. 2009).

2.6.3 Adhesion Junction Response to Fluid Flow

The quantity of N-cadherin and OB-cadherin adhesion junctions does not change with application of FSS to MC3T3-E1 pre-osteoblasts (Norvell et al. 2004a), as seen by immunoblot analysis. However, the location of adhesion junctions can change when FSS is applied as the cell remodels to the changing mechanical environment (Noria et al. 1999). Immunofluorescent observations have shown that when porcine aortic endothelial cells are stimulated with FSS, cytoskeletal stress fibres form and punctate adhesion junctions can be seen at the end of fibres where they insert into the cell membrane. This is in contrast to the presentation of predominantly linear arrays of adhesion junctions along the cell-cell contact boundaries of static endothelial cells (Noria et al. 1999). In vitro experimentation has shown that osteoblast adhesion junctions respond biochemically to FSS by decreasing β-catenin sequestration at the AJs (Ferraro et al. 2004; Norvell et al. 2004a). β-catenin is an important osteogenic signalling molecule in the Wnt signalling pathway (Moon et al. 2002; Westendorf et al. 2004). Application of FSS causes a significantly lower presence of β-catenin at the AJs and significantly higher β-catenin translocation into the nucleus (Norvell et al. 2004a) and this is likely responsible for some of the osteoblast osteogenic responses to FSS. However, it has not yet been established if the presence of AJs in osteoblasts influences osteogenic responses to fluid flow stimulation such as significantly higher in Cox-2, PGE_2 and Runx2.

2.7 Finite Element Analysis of Osteogenic Cells under Fluid Flow

Finite Element (FE) analysis is a mathematical method that divides a 2D or 3D structure into a finite number of elements and nodes and can be used to calculate a variety of parameters including stresses and strains of the structure. FE analysis methods have recently advanced significantly and are increasingly being applied to the study of cell biomechanics and fluid dynamics. Advances in commercially available FE analysis software have made it possible to model complex 3D cells in addition to modelling cell

substructures and a wide variety of solid and fluid mechanical environments influencing the cells. Computational modelling of cells exposed to fluid shear stress provides empirical data detailing the stresses imparted to the cells by the stimulus, thus giving detailed information about stress location and magnitude. Chapter 3 of this thesis provides further detail on FE analysis.

2.7.1 Structural Modelling of Osteogenic Cells

Cells are highly complex units with irregular, dynamic morphologies and numerous substructures. Usually, most cell substructures are excluded due to their negligible influence on cell mechanical properties and high computational expense. Cells have been modelled with complexities varying from simple isotropic linear elastic solids (Mijailovich et al. 2002; Ladjal et al. 2009) to complex viscoelastic solids with actively remodelling cytoskeletons (Reynolds et al. 2014) and mechanically sensitive adhesive structures (Ronan et al. 2015). Many models of cells use approximate, idealised morphologies, often based on brightfield or immunofluorescent imaging of cells (McGarry and Prendergast 2004). However, recent advances in this field include modelling of highly detailed realistic models of in vitro and ex vivo cells (Slomka and Gefen 2010; Verbruggen et al. 2012).

Linear elastic, isotropic material models of cells have been applied to compute the stresses and strains generated in cells undergoing various stimuli (atomic force microscopy (AFM) indentation, fluid shear stress, substrate strain) to help understand the deformations and stresses caused by each modality of stimulation (Charras and Horton 2002; McGarry et al. 2005a; Dailey et al. 2009; Ladjal et al. 2009). By modelling AFM experiments using linear elastic material properties, factors contributing to the mechanical properties of the cell, such as cell contractility and cell spread area, can be investigated (Vichare et al. 2012). More recently, linear elastic material models have been used to ascertain the stress distributions within cells resulting from interaction with extracellular structures or stimulus both in 2D in vitro simulations (Figure 2.22) (Mullen et al. 2014a), in idealised 2D simulations (Khayyeri et al. 2015) and in realistic 3D simulations (Verbruggen et al. 2012).

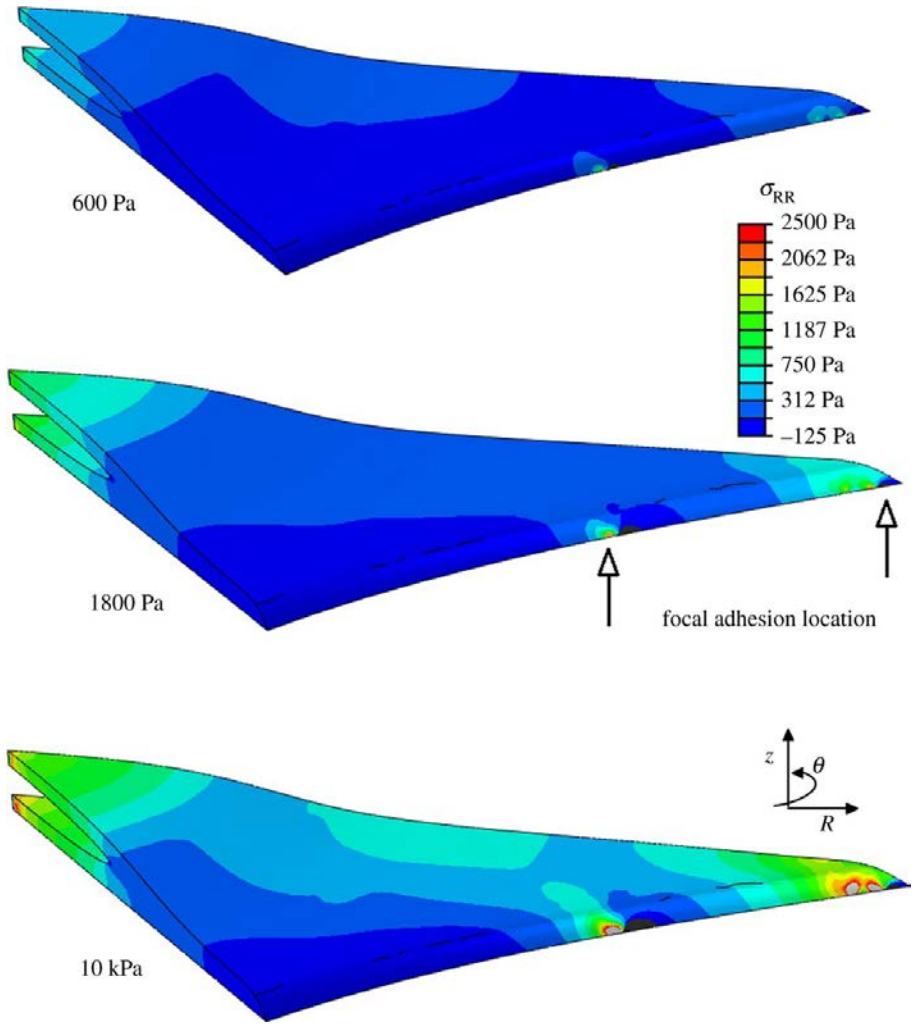

Figure 2.22: A spread cell attached to substrates of Young's modulus 600, 1800 or 10,000 Pa through realistic focal adhesion location. Stress concentrations were observed at the adhesion sites. (Mullen et al. 2014a)

However, the response of cells to mechanical stimuli is time dependant (A-Hassan et al. 1998; Darling et al. 2008; Pravincumar et al. 2012) and non-linear (Wang et al. 1993; Ohashi et al. 2001; Ohayon et al. 2004) and cells can change their mechanical properties as they differentiate (Bongiorno et al. 2014). Viscoelastic Maxwell material models have been used to determine the stress and strain induced in a single cell or a cell monolayer by the pulling of a magnetised microbead (Karcher et al. 2003). Viscoelastic material models have been used to investigate the mechanical properties of chondrocytes (Nguyen et al. 2010) and osteocytes (Qiu et al. 2014). The changing mechanical properties of chondrocytes and endothelial cells during cell spreading has been investigated using viscoelastic material models (McGarry 2009). In some circumstances, when they are undergoing large deformations, it is also accurate

to model cells as hyperelastic structures. Hyperelastic material models have been applied to capture the deformation during micropipette aspiration or parallel plate compression, when cells undergo non-linear large deformations (Caille et al. 2002; Sen et al. 2009; Jafari Bidhendi and Korhonen 2012). Neo-Hookean viscoelastic models have also been used to characterise the erythrocyte cytoskeleton during modelling of laser tweezer induced cell deformation (Klöppel and Wall 2011).

The viscoelastic material model for cells does not completely capture the response of cells to mechanical stimuli (Reynolds et al. 2014), as the cytoskeleton has a dynamic influence on cell mechanical properties. A variety of methods have been used to model the cytoskeleton to attempt to accurately account for the contribution of this structure. The least computationally expensive method is the use of thermal contraction to generate a pre-stress within the cytoplasm of the cell and this has been used to investigate whole-cell stress and strain in response to applied deformation (AFM testing, scaffold strain) (Stops et al. 2008; Vichare et al. 2012) or mechanical environment (substrate stiffness) (Mullen et al. 2014a). Pre-positioned stress fibres have been modelled as linearly elastic cables supporting only tensile loads and discretised using non-compression bearing truss elements. The stress fibres had different mechanical properties to the rest of the cytoplasm (Milner et al. 2012) and were pre-strained so as to put the fibres in tension (Mohrdieck et al. 2005). Milner et al. (2012) assigned localised cytoplasmic mechanical properties, based on measurements taken at an array of locations and used this model to investigate localised increases in cell stress in response to cyclic strain. This method has also been used to investigate cell rounding (Jean et al. 2005). Models using pre-positioned stress fibres have revealed the importance of cytoskeleton interaction with cell adhesion sites for stress propagation through the cytoskeleton network (Paul et al. 2008). A further improvement to this method was the inclusion of both tensile and compressive 'cytoskeleton' elements to represent the compressive microtubule and tensile actin components of the cytoskeleton (McGarry et al. 2005a).

In recent years, modelling of the cytoskeleton has developed greatly with the introduction of active cytoskeleton material models (Deshpande et al. 2006; Besser and Schwarz 2007; Vernerey and Farsad 2011). The 3D model developed by Deshpande is entirely predictive; the distribution, formation and contractility of the

stress fibres are dynamically governed by cell signalling and tension. Implementation of this material model has accurately modelled the generation of cell traction forces on micropillars due to cell contractility (McGarry et al. 2009). Further advances to this model have been implemented in 3D to investigate the role of the cytoskeleton during cell spreading and parallel plate compression (Ronan et al. 2012), during AFM compression (Weafer et al. 2013; Reynolds and McGarry 2015), during cyclic strain application (Dowling et al. 2013), during shear force application (Dowling et al. 2012) and during micropipette aspiration (Reynolds et al. 2014). The interplay between the cytoskeleton and cell-substrate and cell-cell interactions is now also being investigated using this active cytoskeleton model (Ronan et al. 2014; Ronan et al. 2015). The work of (Besser and Safran 2006) has developed a predictive model for force-induced growth of focal adhesions, and another study by this research group predicted using a mechanosensitive material model that focal adhesion size can be tuned by the mechanical properties of substrate matrix (Nicolas and Safran 2006). Another predictive model by (Kaunas and Hsu 2009) assumed that when stress fibres were stretched beyond a critical length, they would dissociate. A 2D model developed by Vernerey and Farsad is a mechano-sensitive multiphasic predictive model, incorporating a mixture fluid, solute and solvent, and the transport of fluid and momomers within the cell via convection/diffusion (Vernerey and Farsad 2011). This model can capture the dependency of cell contractility, facilitated by stress fibres, on the mechanical environment of the cell (Vernerey and Farsad 2011). Obbink-Huizer developed a model that predicted the orientation of stress fibres to the direction of substrate strain and have a dependence on substrate material properties (Obbink-Huizer et al. 2014). In vitro studies of actin cytoskeleton remodelling have shown that strains of 15% are required for widespread actin re-organisation to occur, therefore, for applications with small strains it may not be necessary to include an active cytoskeleton model (Costa et al. 2002).

2.7.2 Parallel Plate Bioreactor Fluid Flow Analysis

Computational investigations into the stresses experienced by cells in parallel plate flow chambers require analysis of the flow regime within the bioreactor system. It has been shown that the stimulus applied to cells within parallel plate flow chambers

varies with chamber design and varies spatially within each chamber (Anderson et al. 2006; Vaughan et al. 2013b). The works of Anderson (2006) and Vaughan (2013) have demonstrated that for any study investigating the forces imparted to cells within a bioreactor, it is necessary to investigate the flow patterns and pressure fluctuations specific to each bioreactor system, to ascertain the forces being imparted on the cells. To date, the fluid pressure and velocity generated within an entire bioreactor system (parallel plate flow chamber and tubing) during oscillatory fluid flow has not been computationally modelled.

2.7.3 Fluid-Structure Interaction Modelling of In Vitro Experiments

During stimulation of cells in a parallel plate flow chambers, the mechanical stimulus is applied to the cells via movement of a fluid. This movement creates a force vector in the direction of flow, tangential to the surface of the cells. As such, fluid-structure interaction (FSI) modelling is the most appropriate form of analysis to capture the forces generated by the fluid and apply these forces to the solid cells. The theory behind this type of modelling is described in detail in Chapter 3. Fluid-structure interaction models have shown that the strains experienced by idealised single Neo-Hookean hyperelastic cells within parallel plate flow chambers have a greater dependence on the pressure within the system than the applied shear stress (Vaughan et al. 2013b). Other studies have investigated the stress and deformation generated in a single linear elastic cell incorporating a constitutive cytoskeleton model under laminar FSS stimulation (McGarry et al. 2005a). FSI models have more recently also been used to determine osteocyte viscoelastic properties by recording cell deformation during steady laminar FSS and then assigning cell viscoelastic properties to accurately model the observed in vitro cellular deformation (Qiu et al. 2014). However, these models have all investigated single cells and have not accounted for intercellular forces in cell morphology and mechanics.

FSI computational investigations into the stresses experienced by mechanosensitive structures such as integrins and primary cilia during FSS have demonstrated the heightened stress-states of these structures during stimulation (Rydholm et al. 2010; Verbruggen et al. 2012; Vaughan et al. 2013a; Vaughan et al. 2014; Khayyeri et al. 2015), which correlates with in vitro osteogenic responses to FSS.

Additionally, a recently published study using a realistic 3D model of an individual MSC found that peak stresses localised at the interface between the nucleus and the cytoplasm (Vaez Ghaemi et al. 2015) for low levels of FSS (0.006 - 0.03 Pa). However, the stresses generated at cell-cell contacts during fluid shear stress stimulated in a parallel plate flow chamber have yet to be modelled.

2.8 Summary

A detailed overview of the structure of bone including its hierarchical composition and function has been presented here in Chapter 2. Particular attention has been given to the osteogenic cells that form and remodel bone and detail has been provided on mechanisms of interest, specifically adhesion junctions and the cytoskeleton, that are involved in the activities of these cells. To summarise, the adaptive response of bone is mediated by the osteogenic cells that live in the marrow cavity (mesenchymal stem cells), on the surface of the bone (osteoblasts), or within the bone (osteocytes). These cells sense the forces placed on the bone via the flow of fluid within the bone cavities and can respond to this stimulus by signalling for new bone to be produced or old bone to be resorbed. Currently, only limited data is available on the role of adhesion junctions and the cytoskeleton in osteogenic cell mechanosensation of mechanical stimuli. An increased understanding of these processes is important to the development of improved medical techniques to repair or replace damaged bone. Literature referenced in this chapter details the influence of fluid flow on osteogenic cells and explores the limited available data on the role of cell-cell adhesion junctions and the cytoskeleton in sensing mechanical stimulus.

In Chapter 4, the influence of adhesion junctions on the osteogenic response of pre-osteoblast MC3T3-E1 cells to fluid shear stress stimulation is investigated using a parallel plate bioreactor. Chapter 5 uses a combination of fluid-structure interaction modelling and cell culture techniques to investigate the forces experienced at cell-cell contacts between osteoblasts during oscillatory fluid shear stress stimulation, and relates these forces to the in vitro cytoskeletal and biochemical response. Chapter 6 investigates the mechanical role of N-cadherin and OB-cadherin adhesion junctions

during the osteogenic differentiation of 3D aggregates of C57BL/6 MSCs by down-regulating specific cadherins.

Chapter 3:

Theory

3.1 Introduction

This chapter presents the theoretical basis for the computational modelling techniques used in Chapter 5, in addition to presenting an overview of constitutive models used in later chapters. Firstly, in Section 3.2 an overview of continuum mechanics is provided. This is followed by the theoretical framework and governing equations for the finite element method. Section 3.3 presents an overview of computational fluid dynamics techniques. Section 3.4 outlines a standard methodology for coupling of finite element and fluid dynamics computational techniques in the form of fluid-solid interaction modelling. This technique is used in Chapter 5 to investigate the deformation of cells due to applied fluid flow in a parallel plate bioreactor.

3.2 Finite Element Analysis

3.2.1 Fundamental Theory of Continuum Mechanics

Finite element analysis of biological cells subjected to external loading requires the consideration of large deformation kinematics. This describes the deformation of a body from a reference configuration into a deformed or current configuration, as shown in Figure 3.23. The locations of a point on a 2D body in the reference and deformed configurations are represented with position vectors $\boldsymbol{x}$ and $\boldsymbol{y}$ respectively. Equation 3.1 gives the displacement vector, $\boldsymbol{u}$, and equation 3.2 gives the velocity vector, $\boldsymbol{v}$.

$$\boldsymbol{u}(x,t) = \boldsymbol{y}(x,t) - \boldsymbol{x} \tag{3.1}$$

$$\boldsymbol{v}(\boldsymbol{x},t) = \frac{\partial \boldsymbol{u}}{\partial t} \tag{3.2}$$

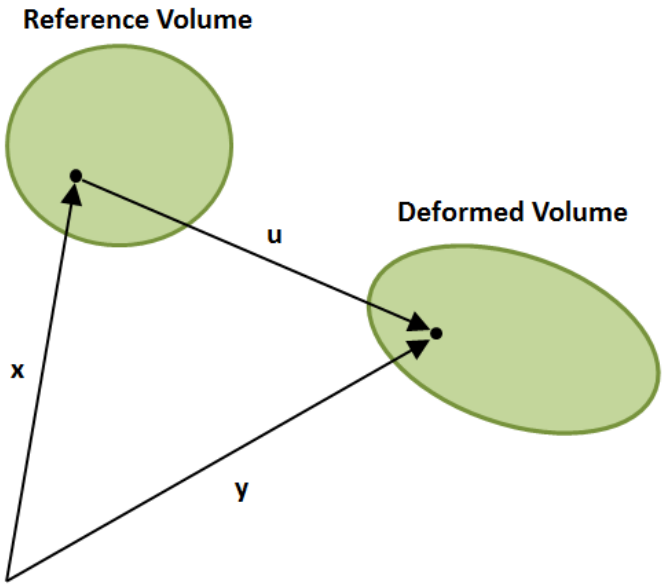

Figure 3.23 Diagram of finite deformation kinematics, showing the displacement and deformation of a reference configuration where ***u*** is the displacement vector of a point defined by vectors ***x*** and ***y***.

The deformation occurring between the reference and current configurations is calculated by relating the distance between a point in the deformed volume and a point in the reference volume (Figure 3.23) according to equation 3.3:

$$\boldsymbol{F_{def}} = \frac{d\boldsymbol{y}}{d\boldsymbol{x}} \tag{3.3}$$

where $\boldsymbol{F_{def}}$ is the deformation gradient tensor and $d\boldsymbol{x}$ and $d\boldsymbol{y}$ are the distance between the points in the reference and deformed configurations respectively. The spatial velocity gradient ($\boldsymbol{L}$) is calculated by equation 3.4:

$$\boldsymbol{L} = \frac{d\boldsymbol{v}}{d\boldsymbol{y}} = d\boldsymbol{F_{def}}.\boldsymbol{F_{def}}^{-1} \tag{3.4}$$

The symmetric rate of deformation tensor ($\boldsymbol{D}$) can be calculated from the spatial velocity gradient ($\boldsymbol{L}$) according to equation 3.5.

$$\boldsymbol{D} = sym(\boldsymbol{L}) = \frac{1}{2}(\boldsymbol{L} + \boldsymbol{L}^T) \tag{3.5}$$

Lastly, the symmetric rate of deformation tensor ($\boldsymbol{D}$) can be integrated with respect to time to give the logarithmic strain tensor ($\boldsymbol{\varepsilon}$) according to equation 3.6.

$$\boldsymbol{\varepsilon}(t) = \int_0^t \boldsymbol{D} dt \tag{3.6}$$

3.1.1.2 Material Constitutive Theory - Elasticity

The linear elastic constitutive model is given as:

$$\boldsymbol{\sigma} = \boldsymbol{C}^{el}\boldsymbol{\varepsilon} \tag{3.7}$$

where $\boldsymbol{\sigma}$ is the 3D Cauchy stress tensor, $\boldsymbol{C}^{el}$ is a fourth order stiffness tensor and $\boldsymbol{\varepsilon}$ is the strain tensor. Equation 3.8 shows the 3D Cauchy stress tensor and equation 3.9 shows the three dimensional strain tensor.

$$\sigma_{ij} = \begin{bmatrix} \sigma_{11} & \sigma_{12} & \sigma_{13} \\ \sigma_{21} & \sigma_{22} & \sigma_{23} \\ \sigma_{31} & \sigma_{32} & \sigma_{33} \end{bmatrix} \tag{3.8}$$

$$\varepsilon_{ij} = \begin{bmatrix} \varepsilon_{11} & \varepsilon_{12} & \varepsilon_{13} \\ \varepsilon_{21} & \varepsilon_{22} & \varepsilon_{23} \\ \varepsilon_{31} & \varepsilon_{32} & \varepsilon_{33} \end{bmatrix} \tag{3.9}$$

The elastic material model utilised in Chapter 5 considers the material to be isotropic and linear. Therefore, the deformation can be defined in terms of just two constants; the bulk modulus (K) and the shear modulus (G). These can be calculated using the Young's modulus (E) and the Poisson's ratio (υ) according to equations 3.10 and 3.11.

$$K = \frac{E}{3(1 - 2\upsilon)} \tag{3.10}$$

$$G = \frac{E}{2(1+\upsilon)} \tag{3.11}$$

3.2.2 Finite Element Method

The finite element method (FEM) is applied in commercially available FE codes such as the ANSYS Structural software package used in this thesis. The first step in finite element (FE) analysis is the division of the structure of interest into subdivisions, known as elements. The elements are interconnected to adjacent element at nodes. The number and type of elements in the mesh are chosen so that the variable distribution throughout the whole structure can be adequately approximated. The distribution across each element can be predefined by a polynomial (e.g. linear or quadratic) or a trigonometric function. The element type used in the structural analysis in this thesis is three dimensional quadratic tetrahedral elements (Figure 3.24).

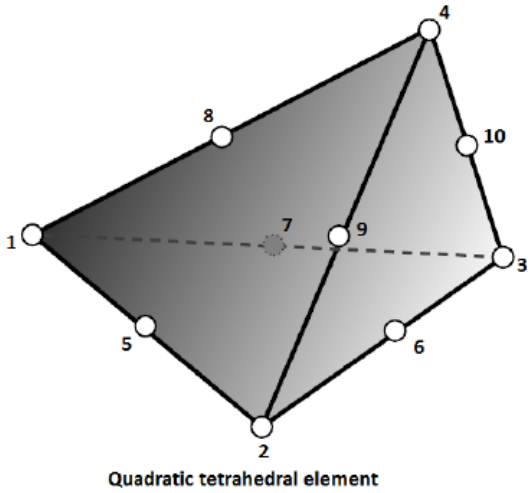

Figure 3.24 A 10 node quadratic tetrahedral element.

The shape functions (N_i) for this element are listed below (Equation 3.12). The choice of the shape function (N_i) is important as this function is used to interpolate the solution between the discrete values obtained at the mesh nodes (1 → i). Shape functions must satisfy the criteria that N_i = 1 at node i and N_i = 0 at all other nodes.

$$N_1 = \xi_1(2\xi_1 - 1) \tag{3.12 a}$$

$$N_2 = \xi_2(2\xi_2 - 1) \tag{3.12 b}$$

$$N_3 = \xi_3(2\xi_3 - 1) \quad (3.12\text{ c})$$

$$N_4 = \xi_4(2\xi_4 - 1) \quad (3.12\text{ d})$$

$$N_5 = 4\xi_1\xi_2 \quad (3.12\text{ e})$$

$$N_6 = 4\xi_2\xi_3 \quad (3.12\text{ f})$$

$$N_7 = 4\xi_1\xi_3 \quad (3.12\text{ g})$$

$$N_8 = 4\xi_1\xi_4 \quad (3.12\text{ h})$$

$$N_9 = 4\xi_2\xi_4 \quad (3.12\text{ i})$$

$$N_{10} = 4\xi_3\xi_4 \quad (3.12\text{ j})$$

where ξ_1, ξ_2, ξ_3, and ξ_4 are the transformation co-ordinates. Considering the tetrahedral element shown in Figure 3.24, the element geometry is described by 3.13, and the displacement interpolation is defined by 3.14. These equations describe the position (x, y, z) and displacement (u_x, u_y, u_z) of any point within the element with respect to the nodes (1 – 10).

$$\begin{bmatrix} x \\ y \\ z \end{bmatrix} = \begin{bmatrix} x_1 & \dots & x_{10} \\ y_1 & \dots & y_{10} \\ z_1 & \dots & z_{10} \end{bmatrix} \begin{bmatrix} N_1 \\ \dots \\ N_{10} \end{bmatrix} \quad (3.13)$$

$$\begin{bmatrix} u_x \\ u_y \\ u_z \end{bmatrix} = \begin{bmatrix} u_{x1} & \dots & u_{x10} \\ u_{y1} & \dots & u_{y10} \\ u_{z1} & \dots & u_{z10} \end{bmatrix} \begin{bmatrix} N_1 \\ \dots \\ N_{10} \end{bmatrix} \quad (3.14)$$

Once a structure has been discretised, the governing equations for each element in the mesh are calculated and then assembled to give the system equations (Fagan 1992). Quantities such as the strain tensor $\boldsymbol{\varepsilon}$ can be expressed as**:**

$$\boldsymbol{\varepsilon} = \boldsymbol{B}\boldsymbol{u} \quad (3.15)$$

where $\boldsymbol{B}$ is a 3D matrix of spatial gradient of the shape function (N_i) as calculated in Equation 3.16, and $\boldsymbol{u}$ is a nodal displacement vector.

$$\boldsymbol{\varepsilon} = \begin{bmatrix} N_{x1} & 0 & 0 & \cdots & N_{xi} & 0 & 0 \\ 0 & N_{y1} & 0 & \cdots & 0 & N_{yi} & 0 \\ 0 & 0 & N_{z1} & \cdots & 0 & 0 & N_{zi} \\ N_{x1} & N_{y1} & 0 & \cdots & N_{xi} & N_{yi} & 0 \\ 0 & N_{y1} & N_{z1} & \cdots & 0 & N_{yi} & N_{zi} \\ N_{x1} & 0 & N_{z1} & \cdots & N_{xi} & 0 & N_{zi} \end{bmatrix} \begin{bmatrix} u_{x1} \\ u_{y1} \\ u_{z1} \\ \vdots \\ u_{xi} \\ u_{yi} \\ u_{zi} \end{bmatrix} = \boldsymbol{Bu} \tag{3.16}$$

N_{xi}, N_{yi} and N_{zi} are the derivatives of the shape function N_i with respect to x, y and z. These are calculated as:

$$\frac{\partial \mathrm{N}_i}{\partial \mathrm{x}} = \frac{\partial \mathrm{N}_i}{\partial \xi}\frac{\partial \xi}{\partial \mathrm{x}} + \frac{\partial \mathrm{N}_i}{\partial \eta}\frac{\partial \eta}{\partial \mathrm{x}} + \frac{\partial \mathrm{N}_i}{\partial \mu}\frac{\partial \mu}{\partial \mathrm{x}} \tag{3.17 a}$$

$$\frac{\partial \mathrm{N}_i}{\partial \mathrm{y}} = \frac{\partial \mathrm{N}_i}{\partial \xi}\frac{\partial \xi}{\partial \mathrm{y}} + \frac{\partial \mathrm{N}_i}{\partial \eta}\frac{\partial \eta}{\partial \mathrm{y}} + \frac{\partial \mathrm{N}_i}{\partial \mu}\frac{\partial \mu}{\partial \mathrm{y}} \tag{3.17 b}$$

$$\frac{\partial \mathrm{N}_i}{\partial \mathrm{z}} = \frac{\partial \mathrm{N}_i}{\partial \xi}\frac{\partial \xi}{\partial \mathrm{z}} + \frac{\partial \mathrm{N}_i}{\partial \eta}\frac{\partial \eta}{\partial \mathrm{z}} + \frac{\partial \mathrm{N}_i}{\partial \mu}\frac{\partial \mu}{\partial \mathrm{z}} \tag{3.17 c}$$

where ξ, η and μ are the local co-ordinates of the reference element. The stress generated in an element is given by:

$$\boldsymbol{\sigma} = \boldsymbol{D\varepsilon} = \boldsymbol{DBu} \tag{3.18}$$

Where $\boldsymbol{D}$ is the stiffness matrix relating element stress to element strain. The potential energy (Π) for the entire system can be calculated as:

$$\Pi = \Lambda - W = \frac{1}{2}\int_V \boldsymbol{\sigma}^T \boldsymbol{\varepsilon}\, dV - \int_V \boldsymbol{U}^T \boldsymbol{F}\, dV \tag{3.19}$$

where Λ is the strain energy and W is the work done by external loads. Introducing shape function transformation (equations 3.16 and 3.18) to equation 3.19 gives:

$$\Pi = \Lambda - W = \frac{1}{2}\int_V (\boldsymbol{DBu})^T \boldsymbol{Bu}\, dV - \int_V (\boldsymbol{Nu})^T \boldsymbol{F}\, dV \tag{3.20}$$

This can be rearranged as:

$$\Pi = \frac{1}{2}\boldsymbol{U}^{T}\boldsymbol{K}\boldsymbol{U} - \boldsymbol{U}^{\boldsymbol{T}}\boldsymbol{F} \tag{3.21}$$

where the element stiffness matrix, **K**, and element force vector, **F** are defined according to Equations 3.22 and 3.23.

$$\boldsymbol{K} = \int_{\boldsymbol{V}} \boldsymbol{B}^{\boldsymbol{T}}\boldsymbol{D}\boldsymbol{B}\, dV \tag{3.22}$$

$$\boldsymbol{F} = \int_{\boldsymbol{V}} \boldsymbol{N}^{\boldsymbol{T}}\boldsymbol{F}\, dV \tag{3.23}$$

Finally, equation 3.24 is derived from the principle of minimum potential energy.

$$\frac{\partial \Pi}{\partial \mathrm{u}} = 0 = \boldsymbol{K}\boldsymbol{U} - \boldsymbol{F} \tag{3.24}$$

To provide information of the behaviour of a discretized structure, the individual stiffness matrices of each element are computationally combined.

3.2.3 Cell Contraction

Cytoskeletal actin-myosin contraction of cells cultured in vitro has been demonstrated to apply stresses to deformable substrates (Ganz et al. 2006; Maruthamuthu et al. 2011). The resistance of the substrate to deformation caused by the cell contraction generates isometric stress within the cell. The cellular stress generated by contraction was modelled in Chapter 5 of this thesis so as to better understand the change in stress at cell-cell contacts when fluid shear stress is applied.

To simulate cell contraction, a thermal contraction coefficient (C) was assigned to the cytoplasm material properties. C is the percentage change in volume relative to a change in temperature and is defined in Equation 3.25,

$$C = \frac{1}{V}\frac{\delta V}{\delta T} \tag{3.25}$$

where $\boldsymbol{C}$ is the volumetric coefficient of thermal expansion, V is the undeformed volume and T is temperature. For a linear elastic isotropic material, the material has a single co-efficient of thermal expansion and the shear components of $\boldsymbol{C}$ are zero. The thermal strain tensor ($\boldsymbol{\varepsilon}^{\text{th}}$) generated by cell contraction relates to the total strain tensor ($\boldsymbol{\varepsilon}$) in Section 3.2 and the linear elastic strain tensor ($\boldsymbol{\varepsilon}^{\text{el}}$) as follows:

$$\boldsymbol{\varepsilon} = \boldsymbol{\varepsilon}^{el} + \boldsymbol{\varepsilon}^{th} = \boldsymbol{C}^{el^{-1}}\boldsymbol{\sigma} + \boldsymbol{C}\Delta\mathrm{T} \tag{3.26}$$

where $\boldsymbol{C}^{el}$ is a fourth order stiffness tensor as in equation 3.7.

3.3 Computational Fluid Dynamics

The computational simulations in Chapter 5 are based on the fluid-structure interaction (FSI) framework. The FSI framework is a two-way coupling of the structural and fluid dynamics solvers. This section elaborates on the theoretical background of computational fluid dynamics (CFD), as a basis for the FSI analysis discussed in Section 3.4.

3.3.1 Mass Conservation Principle and Continuity Equation

Fluid flow is governed by four basic conservation laws that describe the conservation of mass, linear momentum, angular momentum and energy. These conservation laws result in a set of partial differential equations called the governing equations of the fluid. The mass conservation principle states that the rate of increase of mass in a fluid element is equal to the net rate of flow of mass into a fluid element. Figure 3.25 shows a control volume (*dx*, *dy*, *dz*) in which flow through each side of the element is approximately one dimensional, where *ρ* denotes density and *t* denotes a point in time and *u* denotes velocity. Since the control volume is infinitesimally small, one can assume that the fluid properties are uniform and constant within the control volume.

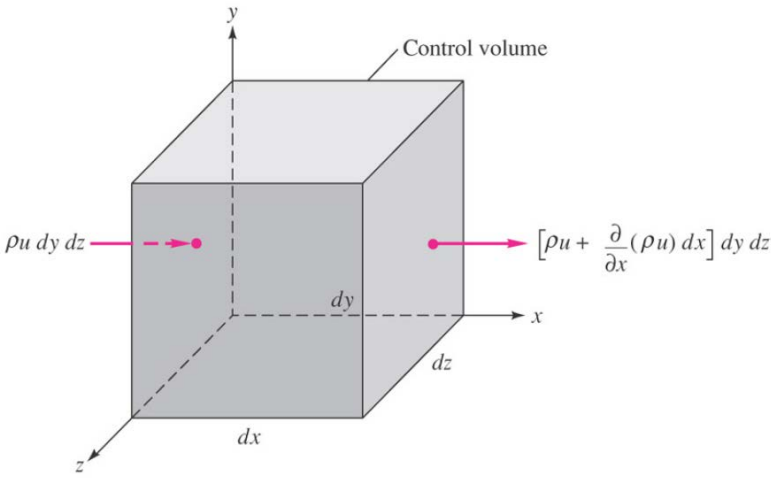

Figure 3.25 Element Cartesian fixed control volume showing the inlet and outlet mass flows on the x faces (White 2008).

Figure 3.25 shows the mass flows on the faces with normals parallel to the x-axis, but mass flow terms occur on all six faces. According to the continuum concept, where all fluid properties are considered to be uniformly varying functions of time and position, then if ρ*u* is the mass flow on the left face of the element, the right face will have a slightly different mass flow denoted by ρ*u* + (δρ*u*/δ*x)*dx. When this is applied to all six faces, the following equation is obtained:

$$-\frac{\delta\rho}{\delta t}dx\,dy\,dz = \frac{\delta}{\delta x}(\rho u)\,dx\,dy\,dz + \frac{\delta}{\delta y}(\rho v)\,dx\,dy\,dz + \frac{\delta}{\delta z}(\rho w)\,dx\,dy\,dz \quad (3.27)$$

where *dx/dt = u*, *dy/dt = v* and *dz/dt = w*, where *u*, *v* and *w* are velocities. The continuity equation is therefore given as:

$$\frac{\delta\rho}{\delta t} + \frac{\delta}{\delta x}(\rho u) + \frac{\delta}{\delta y}(\rho v) + \frac{\delta}{\delta z}(\rho w) = 0 \tag{3.28}$$

The continuity equation can also be expressed as:

$$\frac{\delta\rho}{\delta t} + \nabla \cdot \rho \boldsymbol{V} = 0 \tag{3.29}$$

where $\boldsymbol{V}$ is the velocity vector and ∇ is the vector gradient operator:

$$\nabla = \boldsymbol{i}\frac{\delta}{\delta x} + \boldsymbol{j}\frac{\delta}{\delta y} + \boldsymbol{k}\frac{\delta}{\delta z} \tag{3.30}$$

The analysis done in this thesis involved liquids that are modelled as incompressible fluids, which negates the first term of equations 3.28 and 3.29 as there is no change of density with respect to time. Thus, the continuity equation becomes:

$$\frac{\delta u}{\delta x} + \frac{\delta v}{\delta y} + \frac{\delta w}{\delta z} = \nabla \cdot \boldsymbol{V} = 0 \tag{3.31}$$

3.3.2 Newton's Second Law and Momentum Equation

Newton's second law states that the rate of change of momentum of a fluid particle is equal to the sum of the forces acting on a particle. Using the same infinitesimally small control volume as in Section 3.3.1, the net force on the control volume can be calculated using:

$$\sum F = \frac{\delta}{\delta t}(\rho \boldsymbol{V}) dx dy dz + \sum (\dot{m}_i V_i)_{out} - \sum (\dot{m}_i V_i)_{in} \tag{3.32}$$

where $\dot{m}$ is mass flow. The inlet moment flux on the x face is ρ*u***V** dydz, and the outlet moment flux is [ρ*u***V** + (δρ*u***V**/δx)]dydz, where **V** is the velocity vector field. Summing these terms for all 6 faces, gives:

$$\sum F = dx\ dy\ dz\ \left[\frac{\delta}{\delta t}(\rho \boldsymbol{V}) + \frac{\delta}{\delta x}(\rho u \mathbf{V})\ + \frac{\delta}{\delta y}(\rho v \mathbf{V}) + \frac{\delta}{\delta z}(\rho w \mathbf{V})\right] \tag{3.33}$$

The term in brackets can be split up as follows:

$$\begin{aligned}\frac{\delta}{\delta t}(\rho \boldsymbol{V}) + \frac{\delta}{\delta x}(\rho u \mathbf{V})\ + \frac{\delta}{\delta y}(\rho v \mathbf{V}) + \frac{\delta}{\delta z}(\rho w \mathbf{V}) \\ = \boldsymbol{V}\left[\frac{\delta \rho}{\delta t} + \nabla \cdot (\rho \boldsymbol{V})\right] + \rho\left(\frac{\delta \mathbf{V}}{\delta t} + u\frac{\delta \mathbf{V}}{\delta x} + v\frac{\delta \mathbf{V}}{\delta y} + w\frac{\delta \mathbf{V}}{\delta z}\right)\end{aligned} \tag{3.34}$$

The term in square brackets is the equation of continuity and this vanished. The term in round brackets is ***dV/dt,*** the total acceleration of a particle that instantaneously occupies the control volume:

$$\frac{\delta \mathbf{V}}{\delta t} + \left(u\frac{\delta \mathbf{V}}{\delta x} + v\frac{\delta \mathbf{V}}{\delta y} + w\frac{\delta \mathbf{V}}{\delta z}\right) = \frac{d\boldsymbol{V}}{dt} \tag{3.35}$$

The term $\delta \mathbf{V}/\ \delta t$ is the local acceleration and this term vanished if the flow is steady, i.e. independent of time. The three terms in brackets are called the convective acceleration. Convective acceleration arises when a particle moves through regions of spatially varying velocity. Thus, equation 3.33 can be simplified to:

$$\sum F = \rho\ \frac{d\mathbf{V}}{dt} dx\ dy\ dz \tag{3.36}$$

The net forces are of two types, body forces such as gravity, and surface forces. The surface forces (σ_{ij}) (Figure 3.26 and equation 3.37) are due to stresses on the sides of the control volume in the form of hydrostatic pressure p or shear stresses τ_{ij} that arise from motion with velocity gradients.

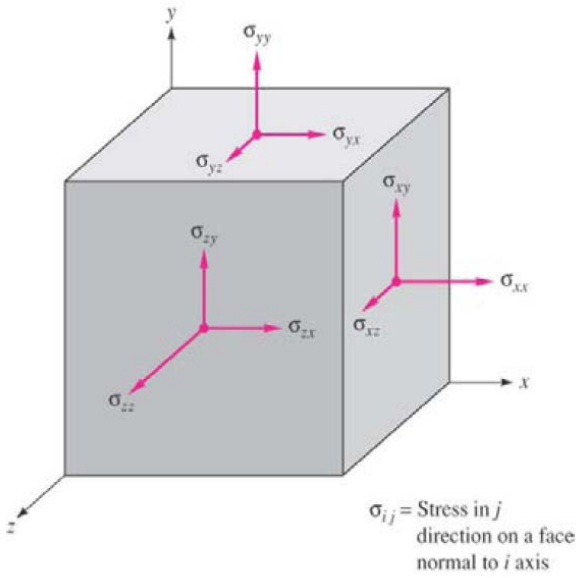

Figure 3.26 Notation for stresses on a volume element (White 2008).

$$\sigma_{ij} = \begin{bmatrix} -p + \tau_{xx} & \tau_{yx} & \tau_{zx} \\ \tau_{xy} & -p + \tau_{yy} & \tau_{zy} \\ \tau_{xz} & \tau_{yz} & -p + \tau_{zz} \end{bmatrix} \tag{3.37}$$

It is not these forces, but their gradients that cause a net force on the differential control surface. Using the x-faces as an example once more, the leftward forces on the left face are balanced by the rightward forces on the right face, leaving only the net rightward force ($\delta\sigma_{xx}/\delta x$) on the right face. Summing the forces in the x-direction for all six faces gives:

$$dF_{x,surf} = \left[\frac{\delta}{\delta x}(\sigma_{xx}) + \frac{\delta}{\delta y}(\sigma_{yx}) + \frac{\delta}{\delta z}(\sigma_{zx})\right] dx\, dy\, dz \tag{3.38}$$

Using equation 3.49, and splitting up the equation into pressure plus viscous stresses, gives:

$$\frac{dF_x}{dV} = -\frac{\delta p}{\delta x} + \frac{\delta}{\delta x}(\tau_{xx}) + \frac{\delta}{\delta y}(\tau_{yx}) + \frac{\delta}{\delta z}(\tau_{zx}) \tag{3.39}$$

where $dV = dx\, dy\, dz$. The forces on the y and z directions on the control volume surface can be derived in a similar manner. By multiplying the x, y and z forces by

Cartesian vectors **i**, **j** and **k** respectively, and then summing these forces, one can obtain the following expression for the net vector surface force:

$$\left(\frac{d\boldsymbol{F}}{dV}\right)_{surf} = -\nabla \mathrm{p} + \left(\frac{d\boldsymbol{F}}{dV}\right)_{viscous} = -\nabla \mathrm{p} + \nabla \cdot \tau_{ij} \tag{3.40}$$

where the viscous stress tensor (τ_{ij}) is:

$$\tau_{ij} = \begin{bmatrix} \tau_{xx} & \tau_{yx} & \tau_{zx} \\ \tau_{xy} & \tau_{yy} & \tau_{zy} \\ \tau_{xz} & \tau_{yz} & \tau_{zz} \end{bmatrix} \tag{3.41}$$

Body forces are due to external fields. In this thesis, the only body force considered is the force of gravity. The gravity force on the differential mass within the control volume is:

$$d\boldsymbol{F}_{grav} = \rho \boldsymbol{g}\, dx\, dy\, dz \tag{3.42}$$

where **g** has an orientation with respect to the coordinate system. Substituting the surface forces (Eq. 3.40) and body forces (Eq. 3.42) back into equation 3.36, the basic momentum equation for an infinitesimal element is obtained:

$$\rho \boldsymbol{g} - \nabla \mathrm{p} + \nabla \cdot \tau_{ij} = \rho \frac{d\boldsymbol{V}}{dt} \tag{3.43}$$

3.3.3 Finite Volume Method

Commercially available software packages, such as ANSYS 2011 used in this thesis, use the finite volume method to solve the governing equations of the fluid under various boundary conditions. The fundamental and first step of this method is to discretise the fluid domain using a mesh that divides the domain of interest into smaller regions called control volumes. All solution variables and fluid properties, such as mass and momentum, are stored at the node at the centre of each control volume. The control

volume (Figure 3.27) is defined by lines joining the centres of the element rims and the element centres on the node of interest.

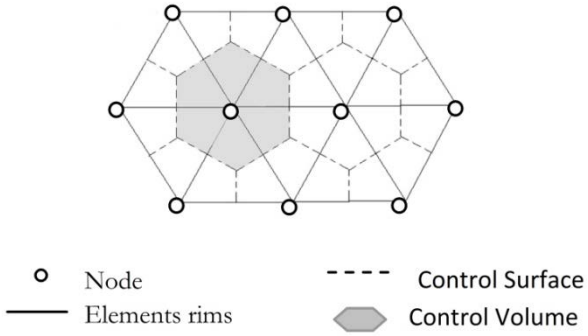

Figure 3.27 Control volume definition. A control volume (grey shaded area) is constructed around each node (white circle) by defining lines that join the centres of the element rims and the element centres. The borders of the control volume are the control surface (Samir et al. 2012).

The governing equations for fluid flow can be described with the general transport equation as follows (Versteeg and Malalasekera 2007):

$$\frac{d}{dt}(\rho\phi) + \nabla \cdot (\rho\phi u) = \nabla \cdot (\Gamma \nabla\phi) + S_\phi \tag{3.44}$$

where the variable ϕ can be replaced by any scalar quantity, Γ is the diffusion coefficient and S_ϕ is the source term of ϕ per unit volume per unit time. This last term serves to include the overall effect of body forces on the unit volume. The left-hand side of the equation contains the rate of change term and the convective term, while the diffusive term and source term are on the right-hand side of the equation. This equation can be integrated over the control volume and Gauss' divergence theorem is applied to give:

$$\frac{d}{dt}\int_{CV} \rho\phi dV + \int_A n\,(\rho\phi u) dA = \int_A n\,(\Gamma \nabla\phi) dA + \int_{CV} S_\phi dV \tag{3.45}$$

where *n* is the outward pointing unit vector of the volume boundary surface (A). The volume integrals represent source or accumulated terms, while the surface integrals represent the summation of the fluxes. Equation 3.40 is the general transport equation

converted into a system of algebraic equations which can be solved iteratively (Versteeg and Malalasekera 2007).

3.4 Fluid-Structure Interaction Modelling

Chapter 5 of this thesis investigates the stresses and strains experienced by idealised biological cells during stimulation with fluid shear stress in a parallel plate bioreactor. Computational fluid dynamics simulations typically analyse fluid flow in domains defined by rigid undeformable boundaries. However, in this thesis the interaction of solid deformable cells with the surrounding fluid (media) requires fluid-structure interaction (FSI) modelling whereby a coupling between the deformable solid domain and the contacting fluid domain is implemented. Commercially available FSI solvers use either a monolithic approach or a partitioned approach. The FSI simulations detailed in this thesis used the partitioned approach, as described below.

3.4.1 Partitioned FSI Approach

In the partitioned FSI approach, the fluid and solid problems are solved separately: the fluid flow does not change while the structural solution is calculated, and vice versa. With this approach, the FSI modelling software alternates between two distinct solvers that solve the governing equations for the fluid or the solid. The partitioned approach is described in Figure 3.28 where S^f and S^S denote the solutions of the fluid and solid domains respectively, at times t_n and t_{n+1}.

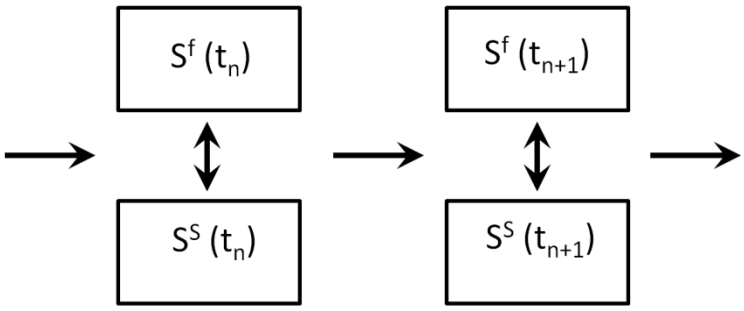

Figure 3.28 The partitioned approach flow process diagram, where S^f and S^S denote the solutions of the fluid and solid domains respectively, at times t_n and t_{n+1}.

The partitioned approach allows for transmission of forces from a fluid domain onto the solid domain as boundary conditions, and then transmits force and deformation data from the solid domain back to the fluid domain as updated boundary conditions. These forces are transmitted through a designated interface surface (a boundary between the fluid and solid). The transmission of forces between domains via the interface surface continues in an iterative fashion until the entire model reaches convergence. The interface between the two solvers is defined as the coupling, and can be implemented as a one-way or two-way coupling. Two-way coupling was used in the FSI simulations in this thesis and is described in Section 3.4.2.

3.4.2 Two-way Coupling

Two-way coupling is necessary for problems wherein the motion of the fluid influences the solid, and the reaction of the solid influence the fluid flow (Benra et al. 2011). The flow process diagram for a strong two-way coupling is shown in Figure 3.29. Within one time step of a transient simulation, the solution for the flow field reaches convergence and then the forces from the fluid mesh are interpolated onto the surface mesh of the structure. Then, the structural solver computes the structural solution, including displacement of the solid. These displacements are then interpolated back onto the fluid mesh, leading to deformation of this mesh. For a strong two-way coupling, these stages are repeated until the normalized change in forces at the fluid-solid interface between successive iterations fall below a pre-defined convergence amount, set to 1% of the final value in the simulations in this thesis, and the time step ends. For weak two-way coupling, the convergence at the interface surface is not considered and a new time step is launched automatically. Strong two-way coupling is applied in the fluid-structure interaction modelling performed in Chapter 5 of this thesis.

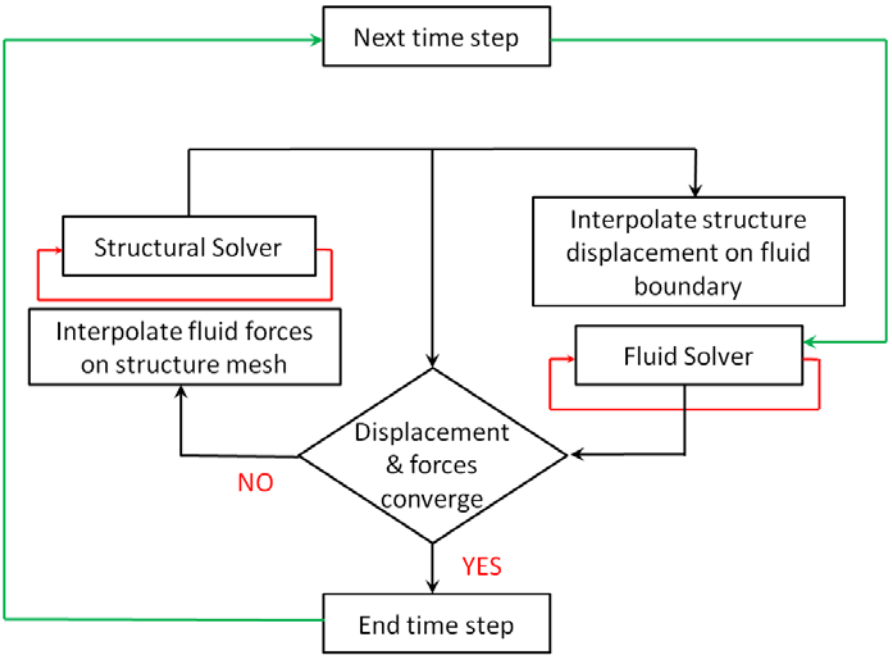

Figure 3.29 Flow process diagram of the two-way coupling procedure (Benra et al. 2011). Red lines indicate iterations within a solver, green lines indicate a change in time-step.

3.5 Parallel Plate Compression Testing

Chapter 6 of this thesis required the measurement of viscoelastic material properties of mesenchymal stem cell spheroids (mesenspheres) with or without N-cadherin or OB-cadherin adhesion junctions. To this end, creep testing was performed using a parallel plate compression testing system (Microsquisher). The basic principle of creep testing is that the material is subjected to a constant tensile or compressive load, at a constant temperature, for a prolonged period of time, and deformation of the material is measured in real time. The force-displacement data from the compressive creep test was then fitted to a standard linear solid (SLS) material model to ascertain the material instantaneous Young's modulus (E_0), relaxed Young's modulus (E_∞) and viscosity (μ).

3.5.1 The Standard Linear Solid (SLS) material model

The SLS material model (Figure 3.30) consists of a spring element and a dashpot element in series, and in parallel with another spring element (Crawford and Crawford 1998; Athanasiou and Natoli 2008). The spring elements allow for an instantaneous response to applied stress, while the dashpot element allows for a time-dependent response to applied stress.

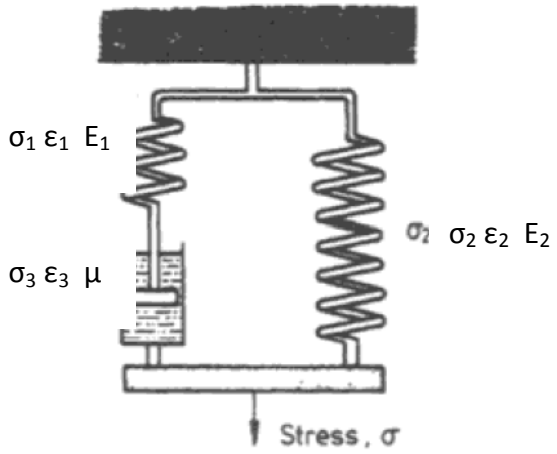

Figure 3.30 Diagram of the Standard Linear Solid (SLS) material model showing the arrangement of the spring and dashpot elements of this configuration of the model (Crawford and Crawford 1998).

Equilibrium of forces in this model yields:

$$\sigma_1 = \sigma_3 \tag{3.46 a}$$

$$\sigma = \sigma_1 + \sigma_2 \tag{3.46 b}$$

$$\varepsilon = \varepsilon_2 = \varepsilon_1 + \varepsilon_3 \tag{3.46 c}$$

Where σ is total stress and ε is total deformation. Based on these relations, the governing equation for the SLS model can be derived and written as follows:

$$\mu(E_1 + E_2)\dot{\varepsilon} + E_1E_2\varepsilon - E_1 + \mu\dot{\sigma} = 0 \tag{3.47}$$

For a creep test, the applied stress is kept constant. Therefore, $\dot{\sigma}$ = 0. Equation 3.47 becomes:

$$\mu(E_1 + E_2)\dot{\varepsilon} + E_1E_2\varepsilon - E_1 = 0 \tag{3.48}$$

The solution (equation 3.49) for this differential equation is obtained when strain is defined according to equation 3.410.

$$\varepsilon(t) = \frac{\sigma_0}{E_2} - \frac{\sigma_0 E_1}{E_2(E_1 + E_2)} e^{-tE_1E_2/\mu(E_1+E_2)} \tag{3.49}$$

$$\varepsilon = \frac{\sigma_0}{(E_1 + E_2)} \tag{3.50}$$

Using the correspondence principal, the general elastic and viscoelastic solutions can be combined in the Laplace domain to obtain an equation describing the modulus of rigidity (G) (Equation 3.51), as described by (Darling et al. 2006).

$$\bar{G}(s) = \frac{1}{2}\frac{E_\infty(1 + \tau_\sigma S)}{(1 + \tau_\varepsilon S)} \tag{3.51}$$

The modulus of rigidity is related to the Young's modulus (E_Y) through:

$$G = \frac{E_Y}{2(1 + \upsilon)} \tag{3.52}$$

Combining these, the Young's modulus can be written as (3.53 a) in the Laplace domain, and (3.53 b) in the time domain for an incompressible material ($\upsilon = 0.5$).

$$\bar{E}(s) = 2(1 + \upsilon)\bar{G}(s) = (1 + \upsilon)\left[\frac{E_\infty(1 + \tau_\sigma S)}{(1 + \tau_\varepsilon S)}\right] \tag{3.53 a}$$

$$E_Y = E_2 = (1 + \upsilon)E_R = \frac{3}{2}E_\infty \tag{3.53 b}$$

For the SLS model, instantaneous Young's modulus (E_0) and relaxed Young's modulus (E_∞) are defined according to the following equations:

$$E_0 = E_1 + E_2, \ \ and \ \ E_\infty = \frac{2}{3}E_2 \tag{3.54}$$

Rearranging, equation 3.49 becomes equation 3.52 wherein τ_σ is the creep time constant. Viscosity (μ) can then be calculated according to equation 3.56.

$$\varepsilon(t) = \frac{2\sigma_0}{3E_\infty}\left[1 + \left(\frac{E_\infty}{E_0} - 1\right)e^{-t/\tau_\sigma}\right] \tag{3.55}$$

$$\mu = \tau_\sigma \frac{E_\infty}{E_0}(E_0 - E_\infty) \tag{3.56}$$

In order to fit the force-displacement data to the SLS model, equation 3.49 can also be written as:

$$u(t) = \frac{2\sigma_0 D_0}{3E_\infty}\left[1 + \left(\frac{E_\infty}{E_0} - 1\right)e^{-t/\tau_\sigma}\right] \tag{3.57}$$

Whereby u(t) is displacement at time t, and D_0 is initial mesensphere horizontal diameter and σ_0 is the nominal stress, calculated as force normalised to initial mesensphere cross section area.

3.6 Summary

The theory outlined in sections 3.2, 3.3 and 3.4 of this chapter formed the basis of the computational simulations of the stress and strains experienced by osteoblasts in a parallel plate bioreactor during oscillatory fluid flow using an FSI approach in Chapter 5. The theory developed in section 3.5 was used in Chapter 6 to experimentally investigate the viscoelastic material properties of mesenchymal stem cells with and without N-cadherin or OB-cadherin adhesion junctions.

Chapter 4:

Adhesion junctions play a role in osteoblast mechanotransduction of oscillatory fluid shear stress

---

4.1 Introduction

The growth and development of bone from birth provides an adult skeleton that is mechanically adapted for the activities of daily life. Bone remodelling replaces aged or damaged bone tissue in order to maintain bone strength throughout life. Bone mass and size are also adapted in response to changes in the mechanical loads placed on our bones. Osteocytes are widely accepted to play an important role in sensing mechanical stresses in bone (Carter and Caler 1985; Cowin et al. 1991; Lanyon 1993; Mullender et al. 1994; Mullender and Huiskes 1995; Prendergast and Huiskes 1996; Mullender and Huiskes 1997; Huiskes et al. 2000; Smit and Burger 2000; Burger et al. 2003), along with bone-lining cells and osteoblasts at the bone surface (Chambers et al. 1993; Mullender and Huiskes 1997) and thereby govern bone remodelling and adaptation processes. Bone cell protein complexes, known as mechanosensors, act to monitor the mechanical environment and communicate the need for adaptation by producing specific biochemical signals to initiate an adaptive response when the mechanical environment is not favourable, a process known as mechanotransduction. Certain mechanosensory organelles have been identified in bone tissue and cells, in particular integrin receptors, primary cilia, adhesion junctions and gap junctions (Thi et al. 2003; Malone et al. 2007a; Wang et al. 2007; McNamara et al. 2009b; Burra et al. 2010a; Litzenberger et al. 2010; Haugh et al. 2015), and have thus been proposed to facilitate mechanosensation in bone tissue. Recent in vitro studies have provided an understanding of the role of integrins (Martinez-Rico et al. 2010; Haugh et al. 2015) and primary cilia (Malone et al. 2007b; Kwon et al. 2010; Hoey et al. 2012a; Delaine-Smith et al. 2014) for mechanosensation during osteogenesis of bone cells. It has also

been demonstrated that gap junctions play a pivotal role in osteogenic signalling between osteocyte and osteoblast cells (Jeansonne et al. 1979; Doty 1981; Zhang et al. 1997; Huo et al. 2008; Nakahama 2010). However, the role of cell-cell contact via adhesion junctions during osteogenesis is still unclear.

Adhesion junctions are transmembrane junctions that allow cell-cell adhesion via extracellular glycoproteins known as cadherins. Cadherins form a connection between the cytoskeleton of adjacent cells by bonding with cadherins on the adjacent cells in a homophilic, calcium dependant manner (Overduin et al. 1995; Shapiro et al. 1995; Stains and Civitelli 2005). N-cadherin adhesion junctions have been found in all stages of osteogenic differentiation (Ferrari et al. 2000; Shin et al. 2000) and are one of the most prevalent cadherins expressed in bone (Cheng et al. 1998a; Haÿ et al. 2000). In static conditions the presence of N-cadherin adhesion junctions in osteoblasts (MC3T3-E1s) has been linked to significantly higher expression of important osteogenic transcription factors Osterix, Osteomodulin and Osteoglycin (Guntur et al. 2012). Additionally, blocking of N-cadherin in osteoblasts during static conditions results in a significantly lower Runt-related transcription factor 2 (Runx2) gene expression (Haÿ et al. 2000). Runx2, also known as Core-binding factor alpha 1 (Cbfa1), controls the expression of osteoblast-associated genes and proteins such as collagen I (Kern et al. 2001), osteocalcin (Ducy et al. 1997), osteopontin (Harada et al. 1999) and bone sialoprotein (Javed et al. 2001; Otto et al. 2003).

It is only in the past decade that the active mechanosensing role of adhesion junctions has begun to come to light (Leckband et al. 2011). Adhesion junction mechanosensation is evident by the cell stiffening when shear forces are applied directly to E-cadherin (Liu and McGrath 2007) and in the failure of the endothelial cell cytoskeleton to align to the direction of fluid flow after 16 hrs when VE-cadherin is silenced (Tzima et al. 2005). More recent studies have even measured the traction forces exerted at intercellular junctions using traction force microscopy on deformable gels and pillars (Ganz et al. 2006; Liu et al. 2010b; Maruthamuthu et al. 2011). The intracellular domain of the adhesion junction is connected to the cytoskeleton through a series of intracellular accessory proteins (Nelson and Nusse 2004), in particular β-catenin, which is an important osteogenic signalling molecule due to its pivotal role in

the canonical Wnt signalling process (Moon et al. 2002; He et al. 2004; Logan and Nusse 2004; Westendorf et al. 2004). Canonical Wnt signalling influences cyclooxygenase 2 (Cox-2) and Runx2 gene expression and osteoblast mineralisation (Norvell et al. 2004a; Rodda and McMahon 2006; Arnsdorf et al. 2009a). Cox-2 plays a role in early bone formation in response to mechanical stimulus by contributing to prostaglandin production (Wadhwa et al. 2002; Bakker et al. 2003a). The application of fluid shear stress (FSS) stimulation to osteoblasts has been shown to result in significantly lower N-cadherin associated β-catenin and significantly higher β-catenin nuclear translocation but there was no change in overall levels of N-cadherin or β-catenin (Norvell et al. 2004a). The significantly lower association of N-cadherin and β-catenin with FSS stimulation demonstrates the mechanotransduction role of adhesion junctions. Moreover the molecular composition of adhesion junctions and the mechanical connection of adhesion junctions to the actin cytoskeleton give these junctions a unique platform from which to greatly influence osteogenesis (Yonemura et al. 2010; Huveneers and de Rooij 2013).

Osteoblasts are commonly known to upregulate their expression of Cox-2, Runx2 and prostaglandin E_2 (PGE_2) in response to FSS (Wadhwa et al. 2002; Bakker et al. 2003a; Kapur et al. 2003; Mehrotra et al. 2006; Malone et al. 2007b; Jaasma and O'Brien 2008; Gardinier et al. 2009). PGE_2 is involved in a variety of processes, including the regulation of bone remodelling (Igarashi et al. 1994; Thorsen et al. 1996), the regulation of mucosal protection of the gut, gastrointestinal secretion and motility (Dey et al. 2006), regulating inflammatory responses (Portanova et al. 1996), and in immunology (Yao et al. 2009). Studies investigating the response of osetoblasts to FSS have used a variety of fluid flow regimes, including steady, pulsatile and oscillatory fluid flow (OFSS). Comparison of all three regimes revealed that pulsatile and oscillatory fluid shear stress stimulation yielded higher Cox-2 and PGE2 responses than steady fluid flow (Jaasma and O'Brien 2008). Oscillatory fluid shear stress (OFSS) is of particular clinical relevance as this flow regime imitates the dynamic oscillatory fluid flow that occurs in the lacuno-canalicular network during walking (Weinbaum et al. 1994). However it is not yet known whether adhesion junctions influence the Cox-2, Runx2 or PGE_2 response to OFSS or PFSS stimulation in pre-osteoblast (MC3T3-E1) cells.

This study seeks to enhance understanding of the role of N-cadherin adhesion junctions in the mechanotransduction of fluid shear stress in osteogenic cells. The specific objectives are to quantify and compare PGE_2 production, Runx2 and Cox-2 mRNA expression and cytoskeletal organisation in response to fluid shear stress when adhesion junction formation is inhibited. Additionally, the effect of oscillatory and pulsatile fluid shear stress stimulation on PGE_2 production and stress fibre formation are compared, with and without adhesion junctions. This knowledge will increase our understanding of the mechanism by which osteoblasts respond to FSS and specifically elucidate whether adhesion junctions play a role in cytoskeleton reorganisation in osteoblast like cells under applied mechanical stimulation.

4.2 Materials and Methods

4.2.1 Cell Culture and Treatment

MC3T3-EIs were cultured in expansion media consisting of α-minimum essential medium (α-MEM) supplemented with 10 % FBS, 2 mM L-glutamine, 100 U/mL penicillin and 100 µg/mL streptomycin (all Sigma-Aldrich). Cells were maintained in a humidified atmosphere at 37°C and 5 % CO_2. Cells were subcultured onto glass slides at a seeding density of 15,000 cells/cm^2 48 hrs prior to fluid flow application so that they were 80-90% confluent during stimulation. Adhesion Junction Inhibited groups were treated with expansion media supplemented with 0.25mg/ml EGTA (Sigma-Aldrich) for three hours to chelate extracellular Ca^{2+} (Guntur et al. 2012), which prevents the formation of AJs (Figure 4.30B). Control groups were fed with expansion media three hours prior to stimulation.

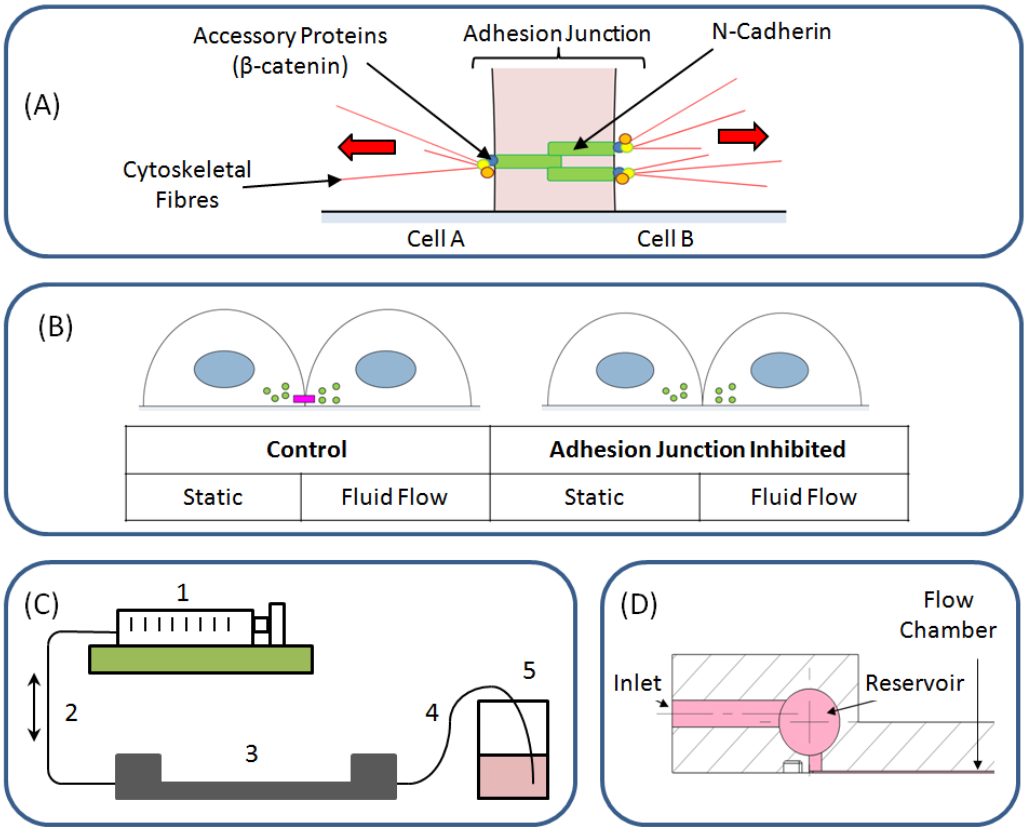

Figure 4.31: (A) Schematic of the adhesion junction complex. Red arrows indicate the direction of the forces generated by the cytoskeletal fibres (B) Schematic of the experimental groups comprised of two treatment groups with either no mechanical stimulation (static) or mechanically stimulated by fluid shear stress. (C) Parallel plate bioreactor configurations. 1) Syringe Pump, 2) inlet tubing, 3) Parallel Plate flow chamber, 4) Outlet tubing, 5) Fluid Reservoir. (D) Schematic of the fluid flow field within the parallel plate bioreactor.

4.2.2 Fluid Shear Stress Stimulation

Oscillatory fluid shear stress (OFSS) of maximum ±1 Pa at 0.5 Hz, or pulsatile fluid shear stress (PFSS) of maximum 1 Pa were applied for one hour directly after treatment. A frequency of 0.5 Hz was chosen as bending of rat tibia at frequencies below 0.5 Hz had no effect on bone formation in the tibia (Turner et al. 1994), and higher frequencies of 1.0 or 2.0 Hz produced a significantly lower in the calcium responsiveness of osteoblasts (Jacobs et al. 1998). Fluid shear stress (FSS) of 1 Pa is estimated to be representative of physiological loading conditions in bone (Weinbaum et al. 1994). OFSS was applied using a NE-1600 Syringe Pump (New Era Pump Systems, Farmingdale, NY) and 50 mL syringe (BD) in series with peristaltic pump tubing and a parallel plate flow chamber (Figure 4.30C), which was custom built (Appendix 1) based on the design of (Lane et al. 2012) (Figure 4.30). The NE-1600 syringe pump with a 50 mL syringe used in this experiment has been validated for application of oscillatory fluid flows as low as 0.5-2.0 mL/min at a range of frequencies (0.5 to 2.0 Hz) by laser Doppler velocimetry (Jaasma and O'Brien 2008). PFSS was applied using a Masterflex peristaltic pump in series with peristaltic pump tubing and a parallel plate flow chamber. The fluid in the bioreactor systems was MC3T3-E1 expansion media described above. Static samples were placed in the bioreactor incubator in 5mL of fresh media for the duration of FSS stimulation. Samples for biochemical assays were incubated in 1 ml of expansion media for two hours after FSS stimulation and then media samples and cell lysate were collected. Samples for immunofluorescent staining were fixed directly after one hour FSS stimulation (or static control) using 4% Paraformaldehyde.

4.2.3 Immunofluorescent Staining and Confocal Microscopy

Subsequent to fixation, cell membranes were permeabilised using 0.1% Triton-X (Sigma X100) in PBS and blocked using 1% Goat serum (Sigma) in PBS. Subsequent to blocking, all washes and fluorescent dye dilutions were carried out using 0.1% Goat serum in PBS. For immunofluorescent staining, samples were incubated in 1:200 polyclonal N-cadherin rabbit anti-mouse primary antibody (Santa Cruz, sc-7939), 1:200 Alexa Fluor 488 goat anti-rabbit secondary antibody (Jackson Immuno), 1:1000 TRITC Phalloidin (Sigma) and Fluoroshield mounting media with DAPI (Sigma).

4.2.4 Image Analysis

Two samples from each group and ten images from each sample were analysed. Fluorescent N-cadherin staining (488 nm wavelength) was isolated and thresholded using Image-J software. To quantify membrane-associated N-cadherin, cytoplasmic and nuclear staining were manually removed and images were analysed to identify membrane associated N-cadherin clusters (Figure 4.31). This was necessary and appropriate because N-cadherin is produced and transported in these areas but it is not functioning, i.e. not yet connected to the cytoskeleton or to cadherins on neighbouring cells. For analysis of cadherin in the entire cell body, cytoplasmic and nuclear staining were not removed. N-cadherin clusters were counted using the Particle analysis function for particles > 0.5 μm^2. Cytoskeletal stress fibres were identified in the 564 nm wavelength channel using the threshold function. The area of the resulting particles were quantified using the analyse particles function. Total cell area per image was found by reducing the image threshold of the 564nm channel to visualise total cell body and using the analyse particles function.

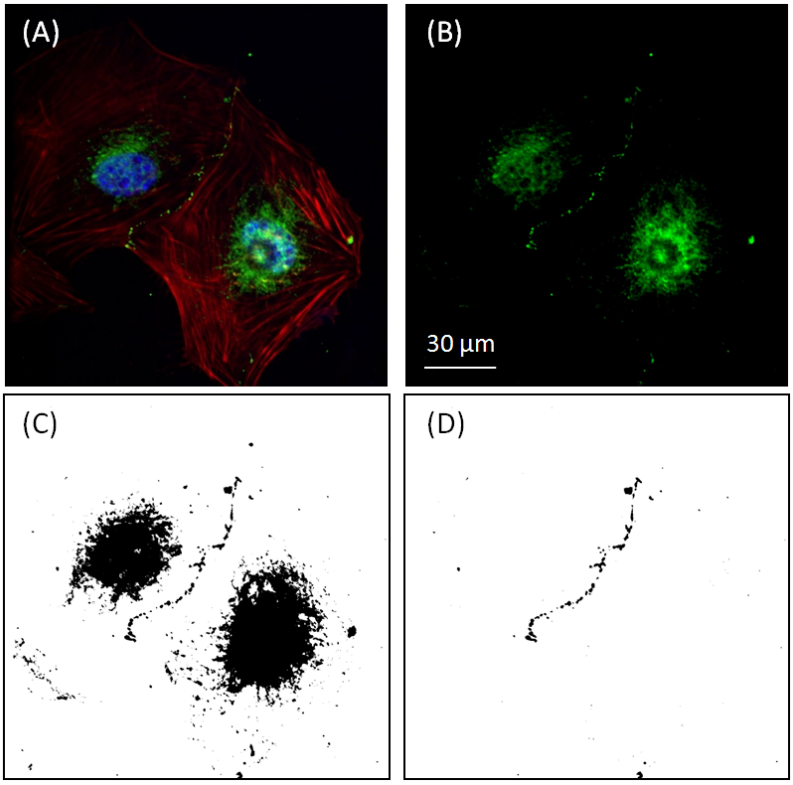

Figure 4.32: Immunofluorescent image analysis methodology. (A) 3 colour immunofluorescent image of the cytoskeleton (red), N-cadherin (green) and the nucleus (blue) for a control static

sample. (B) N-cadherin immunofluorescent staining alone. (C) N-cadherin immunofluorescent staining was thresholded to removed background noise. (D) N-cadherin staining at the cell-cell contacts was judged by eye based on 3-colour immunofluorescent images. Staining not on this contact border was manually removed.

4.2.5 PGE_2 Assay

PGE_2 production was analysed using a Prostaglandin E_2 Enzyme Immunoassay (EIA) Monoclonal kit (Cayman Biosciences). 50 µL of the samples/standards were added to appropriate wells in a 96 well plate. 100 µL of EIA buffer/media was added to wells assigned for non-specific binding (NSB) controls. 50 µL of EIA buffer was added to the maximum binding (B_0) wells. 50 µL of Prostaglandin E_2 AchE Tracer was added to each well, except the total activity (TA) and blank (Blk) wells and 50 µL of Prostaglandin E_2 Monoclonal Antibody was added to each well, except the NSB, TA and Blk wells. The plate was covered with an adhesive plate seal and stored at 4°C for 18 hours. Each well was washed 5 times with 200 µL Wash Buffer. 200 µL of Ellman's Reagent was added to each well, and 5 µL of Prostaglandin E_2 AchE Tracer was added to the TA wells. The plate was incubated at room temperature for 90 mins. Absorbance was measured at room temperature using a BioTek Synergy HT at absorbance 405 nm. Specific PGE_2 activity was quantified against a standard curve of 1000 - 7.8 pg/ml

4.2.6 DNA Content

DNA content was analysed using a Quant-iT$^{(TM)}$ PicoGreen$^{(R)}$ dsDNA Assay Kit (Life Technologies P11496) according to the manufacturer's instructions in a black 96 well plate. Briefly, samples were subjected to three cycles of freeze-lysis in deionized water (ddH_2O). Each cycle involved freezing at - 80^{o}C for 1 hr and thawing at room temperature for 1 hr. After the first thaw, cells were scraped from the slides and place in 1.5ml Eppendorf tubes before the second freeze. After freeze-thaw lysis samples were vortexed and spun briefly using a desktop centrifuge. DNA content was measured at an emission of 520 nm and excitation of 480 nm using a BioTek Synergy HT. Specific DNA content was quantified against a standard curve of 0 - 300 ng DNA/well.

4.2.7 RNA isolation and RT-PCR

RT-PCR was used to analyse the relative expression of Cox-2 and Runx2, with glyceraldehyde-3-phosphate dehydrogenase (GAPDH) as the house-keeping reference gene. Stimulated and static control samples were harvested directly after the one hour FSS application. RNA was extracted from the samples by lysing in 1 mL of Tri-reagent reagent (Sigma-Aldrich), followed by chloroform extraction. RNA was purified using Qiagen RNeasy columns following the manufacturer's instructions (Qiagen). RNA yield and purity were assessed using a nanodrop spectrophotometer (ND-1000, Thermo Scientific), with 260/280 ratios of > 1.8 for all samples. cDNA was synthesised using an ENZA RNA isolation kit (Omega Bio-tek). RT-PCR was then carried out on the resultant cDNA using a Taqman RT-PCR master mix kit (Applied Biosystems) and a StepOnePlus^{TM} RT-PCR system (Applied Biosystems). Taqman primers for Cox-2 (Mm00478374_m1), Runx2 (Mm00501584_m1), and GAPDH (Mm99999915_g1) were obtained from Applied Biosystems. RT-PCR data was analysed using the comparative $2^{-\Delta\Delta Ct}$ method as described previously (Livak and Schmittgen 2001), with the static untreated control samples used as the calibrator.

4.2.8 Statistical Analysis

The results are presented as mean ± standard deviation. Statistical analysis of acquired data was carried out using a two-way analysis of variance (ANOVA) with treatment group and stimulation as the two independent variables, to test if there is an interaction between these two independent variables. This was followed by pairwise multiple comparison procedures (Tukey test). Significance for all analysis is declared at $p \leq 0.05$.

4.3 Results

4.3.1 EGTA treatment reduces membrane associated N-cadherin immunofluorescence

Immunofluorescent image analysis revealed that EGTA treatment, to inhibit AJ formation on the membrane, resulted in significantly lower ($p<0.001$) membrane associated N-cadherin fluorescence in AJ inhibited static samples in comparison to control static samples (Figure 4.32, Figure 4.33B). EGTA treatment did not cause significantly lower N-cadherin fluorescence for the entire cell body, demonstrating that N-cadherin was still present but was not forming functional adhesion junctions on the contacting membranes of adjacent cells (Figure 4.33A).

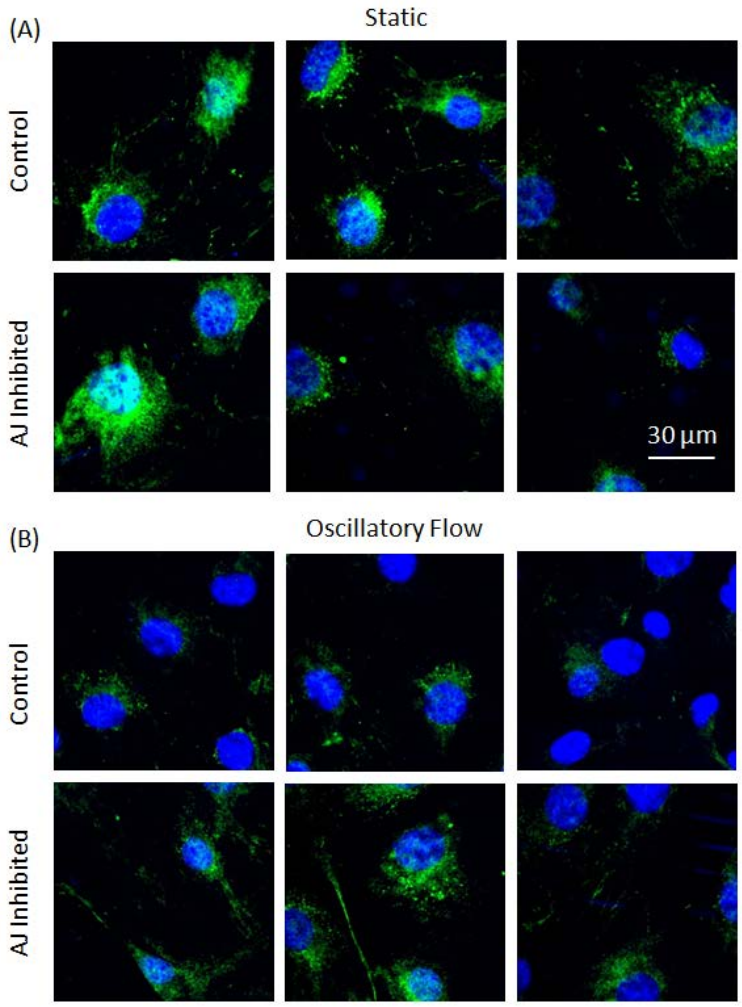

Figure 4.33: Representative images of N-cadherin (green) and the nucleus (blue) for Control and adhesion junction (AJ) inhibited samples directly after 1 hr static (A) or oscillatory fluid flow stimulated (B) conditions. Two slides from separate experiments, and 10 images from each slide were analysed yielding n=20.

4.3.2 N-cadherin adhesion junction immunofluorescence is lower with FSS

When control samples were exposed to OFSS, total N-cadherin (Figure 4.33A) was 5-fold lower ($p<0.001$) and membrane associated N-cadherin was 6-fold lower ($p<0.001$) than control static samples (Figure 4.33B). For AJ inhibited samples, OFSS stimulation caused 2-fold lower fluorescence ($p<0.001$) of total N-cadherin in comparison to AJ inhibited static samples (Figure 4.33A). Membrane associated N-cadherin was not significantly different between static and OFSS stimulated for AJ inhibited samples. Due to AJ inhibition, membrane associated N-cadherin in static AJ inhibited samples was already significantly lower in comparison to control static levels. Thus, because there is less membrane associate N-cadherin before OFSS application, AJ inhibition abrogated the normal decrease in N-cadherin adhesion junction immunofluorescence associated with OFSS.

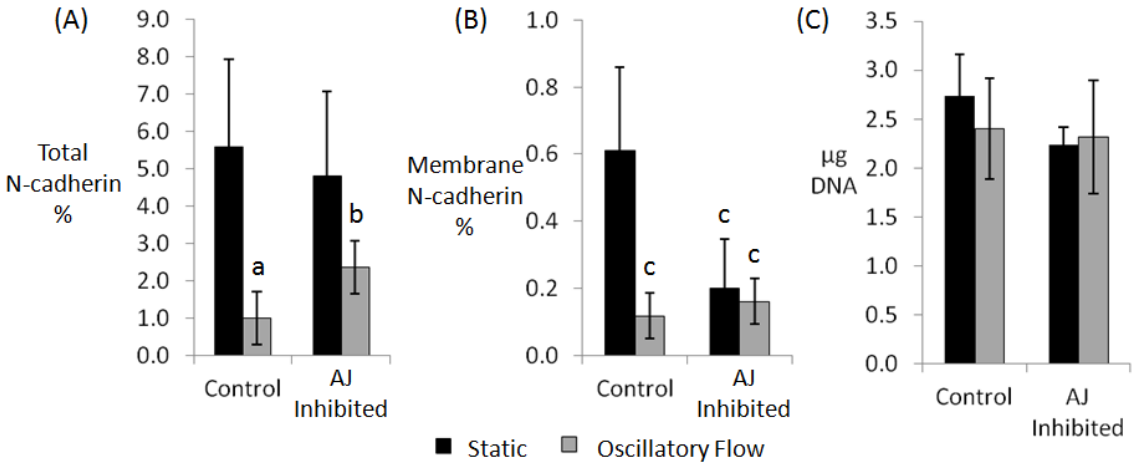

Figure 4.34: (A) Total N-cadherin quantification quantified a percentage of total cell area, divided by the number of nuclei per image. a, b: $p<0.001$ indicates significantly lower than Control and AJ Inhibited static groups. (B) Membrane associated N-cadherin particle quantification from immunofluorescent images. Membrane associated particles are quantified a percentage of total cell area, divided by the number of nuclei per image. c: $p<0.001$ indicates significantly lower than Control static. (C) Total DNA (µg) per sample for control and AJ Inhibited samples under static and oscillatory fluid flow stimulated conditions. Significance is declared at $p<0.05$. 10 images were analysed per slide, and two slides per group, yielding n=20.

4.3.3 AJ Inhibition does not prevent greater stress fibre formation in response to OFSS

Immunofluorescent image quantification of the cytoskeleton for control samples revealed significantly greater ($p<0.001$) stress fibre formation with OFSS stimulation in comparison to control static samples (Figure 4.34A, B). AJ inhibition did not cause a

significant change in stress fibre formation for static samples in comparison to control static samples (Figure 4.34B). AJ inhibited samples also showed significantly greater ($p<0.02$) stress fibre formation with application of OFSS in comparison to static control and static AJ inhibited samples.

PFSS stimulation of control samples caused significantly lower stress fibre formation ($p=0.014$) in comparison to control static samples. AJ inhibition for static samples did not cause a significant difference in stress fibre formation in comparison to control static samples ($p=0.185$) or AJ inhibited PFSS samples ($p=0.317$). However, AJ inhibited PFSS samples showed significantly more stress fibre formation than control PFSS ($p=0.032$).

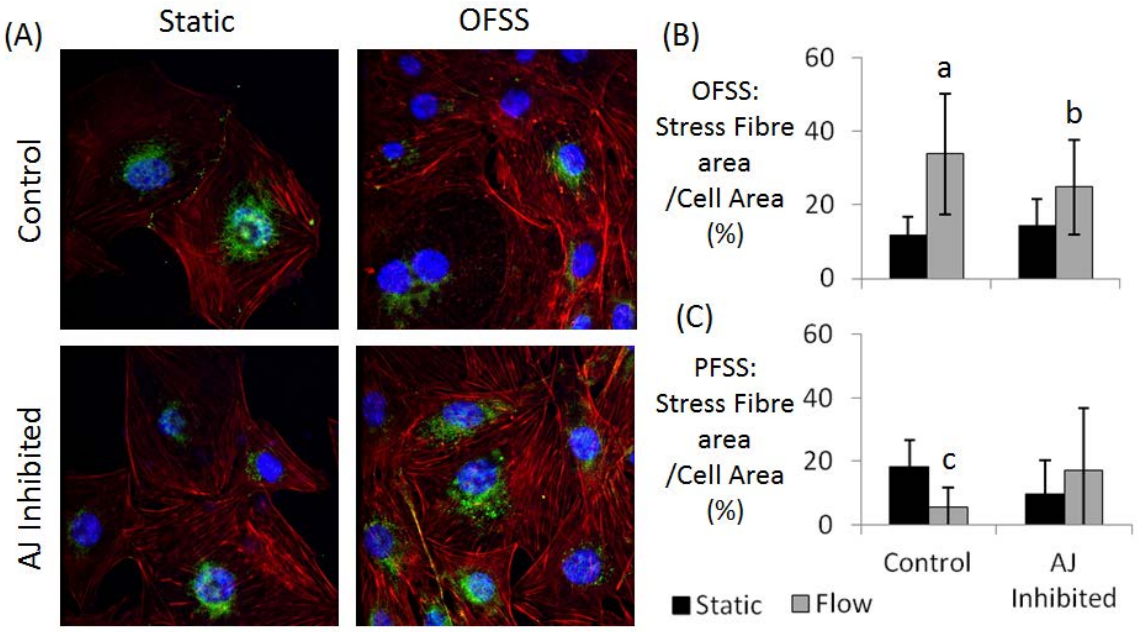

Figure 4.35: (A) Immunofluorescent staining of the cytoskeleton (red), nucleus (blue) and N-cadherin (green) for control and AJ inhibited samples directly after 1 hr static or oscillatory fluid shear stress (OFSS) stimulated conditions. (B) Percentage condensed actin fibre area (μm^2) per total cell area (μm^2) for static and oscillatory fluid shear stress (OFSS) stimulated samples. a: $p<0.001$ vs. control and AJ inhibited static groups, b: $p<0.02$ vs. control and AJ inhibited static groups. (C) Percentage condensed actin fibre area (μm^2) per total cell area (μm^2) for static and pulsatile fluid shear stress (PFSS) stimulated samples. c: $p<0.03$ vs. control static and AJ inhibited flow. Significance is declared at $p<0.05$. 10 images were analysed per slide, and two slides per group, yielding n=20.

4.3.4 Effect of AJs on Osteogenesis

Prostaglandin E_2 (PGE_2) production was significantly higher ($p=0.014$) in samples stimulated with OFSS (Figure 4.35A), but not PFSS (Figure 4.35B), than control static

samples. For AJ inhibited samples, there was no significant difference in PGE_2 production for OFSS or PFSS stimulated samples in comparison to AJ inhibited static samples (Figure 4.35A, B).

Cox-2 gene expression in control samples was also significantly upregulated (p=0.009) after OFSS stimulation in comparison to control static samples (Figure 4.36A). However, AJ inhibited static samples did not exhibit any difference in Cox-2 expression in comparison to control static samples. The higher expression of Cox-2 in AJ inhibited samples with OFSS stimulation was not statistically significant (p=0.213).

OFSS stimulation of control samples caused significant higher (p<0.015) Runx2 expression in comparison to static control samples (Figure 4.36B). For static conditions, AJ inhibition did not significantly change Runx2 expression in comparison to control samples. However, AJ Inhibition rendered the Runx2 response to OFSS insignificant in comparison to control (p=0.442) and AJ inhibited (p=0.386) static samples.

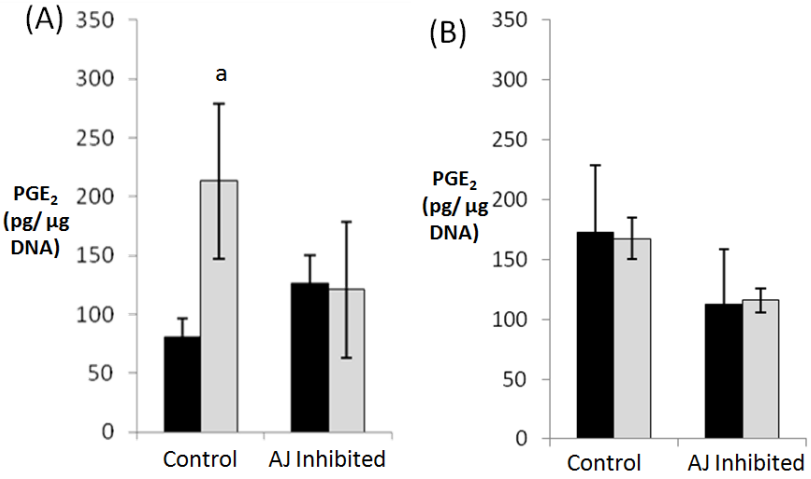

Figure 4.36: Adhesion junction inhibition removes PGE_2 the response of MC3T3-E1 cells to fluid shear stress. (A) PGE_2 release normalised to µg DNA content for cells stimulated with oscillatory fluid shear stress (OFSS). a: p=0.031 vs. control static (B) PGE_2 release normalised to µg DNA content for cells stimulated with pulsatile fluid shear stress (PFSS).

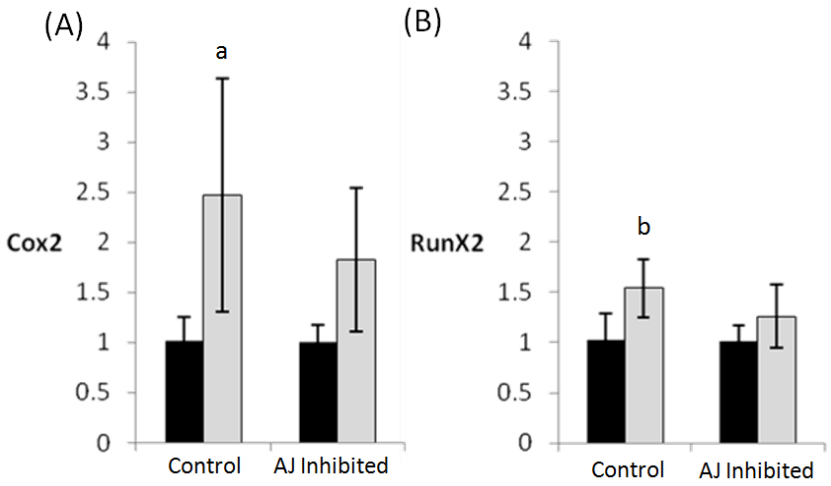

Figure 4.37: Adhesion junction inhibition inhibits the Cox-2 and Runx2 gene expression responses of MC3T3-E1 cells to oscillatory fluid shear stress (OFSS). Fold change in Cox-2 (A) and Runx2 (B) expression normalised to GapDH expression and Control Static levels. a: $p<0.009$ vs. Control and AJ Inhibited static. b: $p<0.015$ vs. Control and AJ Inhibited static. Statistical significance is declared at $p\leq0.05$, with n=6 samples per group.

4.4 Discussion

This study demonstrates the important mechanotransduction role that Adhesion Junctions (AJs) play in the response of MC3T3-E1 pre-osteoblasts to the application of oscillatory fluid shear stress (OFSS) in a parallel plate bioreactor. The results presented in this chapter show that inhibition of AJ formation disrupted the expression of PGE_2, Cox-2 and Runx2, but not stress fibre formation, in response to the application of OFSS. Pulsatile fluid shear stress (PFSS) did not cause higher PGE_2 expression or stress fibre formation in control samples in comparison to static samples. These results indicate that adhesion junctions play an important role in the biochemical response of MC3T3-E1 pre-osteoblast cells to OFSS, but do not significantly influence stress fibre formation.

A limitation of this study is the use of EGTA, an extracellular calcium and magnesium chelator, to hinder the formation of adhesion junctions. Previous studies have used EGTA to demonstrate that E-cadherin (Pece et al. 1999) and N-cadherin (Guntur et al. 2012) can regulate PI3-K and Akt survival pathways, and also to study how p35–Cdk5 regulates N-cadherin AJ formation (Kwon et al. 2000), and how OB-cadherin AJ formation induces VEGF-D expression (Orlandini and Oliviero 2001). However, extracellular calcium is not restricted in governing cell behaviour through adhesion junctions alone, as gap junction and primary cilia mediated communication are also governed by extracellular Ca^{2+} (Quist et al. 2000; Ebihara et al. 2003; Nauli et al. 2003). However, the concentration of EGTA used here (0.25 mg/ml) lowers the extracellular Ca^{2+} concentration from 1.64 mM to 1.58 mM (Keramidas et al. 1999), but a larger decreased of 1.8 mM to 1.6 mM is required to open the epithelial gap junctions (Quist et al. 2000; Ebihara et al. 2003). Moreover, extracellular Ca^{2+} governs primary cilia communication in kidney epithelial cells (Nauli et al. 2003), but not in osteoblasts or osteocytes (Malone et al. 2007b). Extracellular calcium can also be chelated using 1,2-bis-(2-aminophenoxy)ethane-N,N,N',N'-tetraacetic acid (BAPTA). 1 mM of EGTA or BAPTA chelates 1 mM of Ca^{2+}. Cytoskeleton remodelling in response to fluid shear stress (FSS) can occur without influx of extracellular Ca^{2+} and is prevented by blockers of intracellular Ca^{2+} release (Chen et al. 2000). However, large decreases in extracellular Ca^{2+} (e.g. 0.55mM Ca^{2+} media treated with 1.5 mM EGTA (Liu et al. 2010a)) could prevent cytoskeletal remodelling, while smaller decreased (e.g. 1.64 mM

Ca^{2+} media treated with 90 μM of BAPTA (Malone et al. 2007b),) did not. In light of this, calcium containing media was used during FSS stimulation to prevent potential EGTA interference with the cytoskeleton remodelling process. Osteoblast adhesion to glass substrates does not involve Ca^{2+} (Curties 1964) but does involve Mg^{2+} (Zreiqat et al. 2002). EGTA was chosen as a calcium chelating agent as it has a lower affinity for Mg^{2+} than EDTA (Sanui and Pace 1967). The parallel plate flow chamber is an experimental set-up that simplifies the complex 3D environment of fluid movement within bone and could limit the extrapolation of in vitro results to in vivo conditions. This commonly used methodology reduces the number of experimental variables and allows investigation of the response of any adherent cell type to specific, controllable fluid flow regimes. The fluid flow regime was chosen to apply 1 Pa shear stress, as is estimated to be representative of physiological loading conditions in bone (Weinbaum et al. 1994), in an oscillatory or pulsatile pattern to imitate fluid flow caused by cyclic loading of bone due to everyday movement, such as walking. It has been shown that during short (90s) exposure to pulsatile FSS resulted in a higher Ca^{2+} response in a heterogeneous population of primary bone cells treated with 2% FBS in HEPES-buffered Hanks' balanced salt solution (HBSS) than cells treated with 10% FBS in HBSS . Additionally, in static conditions, FBS levels (0-10%) resulted in higher PGE_2 expression in a dose dependent manner (Noguchi et al. 2001). 5-10% FBS causes significantly higher PGE2 expression than 0-1% FBS in epithelial cells (Noguchi et al. 2001).

MC3T3-E1s are a well-established model of pre-osteoblasts that have been used extensively in the study of osteoblast mechanobiology (Chen et al. 2000; Saunders et al. 2003; Malone et al. 2007c; Young et al. 2009). Osteoblast monolayers are known to respond to the application of FSS applied using this method, with higher PGE_2 expression, Runx2 and Cox-2 mRNA expression in comparison to static samples all reported (Norvell et al. 2004b; Ponik et al. 2007; Kamel et al. 2010; Mai et al. 2013). PGE_2 is critical to bone anabolic response to loading, and is upregulated during in vivo bone loading (Thorsen et al.). PGE_2 is synthesised via Cox-2 enzymes (Berenbaum 2000; Funk 2001). Runx2 gene expression influences the production of collagen I (Kern et al. 2001), osteocalcin (Ducy et al. 1997), osteopontin (Harada et al. 1999) and bone sialoprotein (Javed et al. 2001; Otto et al. 2003). Similar to previous studies (Norvell et al. 2004b; Ponik et al. 2007; Kamel et al. 2010; Mai et al. 2013), higher PGE_2 expression

for oscillatory FSS stimulated control samples was observed in comparison to static samples. However, PGE_2 expression was not higher in PFSS stimulated samples in comparison to static samples, suggesting that PFSS is not as stimulatory as OFSS. In this study, PFSS applied a range of 0 to +1 Pa WSS, while OFSS applied a range of ±1 Pa WSS. Although the WSS range is larger for OFSS, the absolute value of WSS is 0-1 Pa, and the sign (±) indicates direction of fluid flow resulting from the change in pressure gradient within the chamber. The work presented here compared OFSS and PFSS which have different mean and amplitude of WSS. Another study compared OFSS (2 ± 4 Pa) to PFSS (4 ± 2 Pa) stimulation of bovine aortic endothelial cells and found that OFSS, with it's lower mean WSS and larger pulse amplitude, resulted in a higher average intracellular free Ca^{2+} concentration than PFSS (Helmlinger et al. 1995). Previous studies have demonstrated that a larger amplitude (0.7 Pa) of the pulses around the same mean (0.7 Pa) during PFSS results in significantly higher nitric oxide expression than lower amplitude pulses (0.31) (Bacabac et al. 2005). This is not surprising as others have shown that PFSS stimulation of osteoblasts either does not cause significantly higher PGE_2 production, or requires high shear stress (1.6 Pa as opposed to 0.8 Pa) for two hours to cause significant higher in PGE_2 (McGarry et al. 2005b; Kamel et al. 2010). The work of Jacobs et al. showed that PFSS (0 - 2 Pa, 0.5 – 2 Hz) resulted in higher intracellular Ca^{2+} ions than OFSS (±2 Pa, 0.5 – 2 Hz), but it should be noted that this experiment was performed in PBS buffer with 2% FBS (Jacobs et al. 1998). Other work showing higher osteoblast PGE_2 production in response to PFSS used a pulse frequency of 5 Hz (WSS of 0.6 ± 0.3 Pa) (Bakker et al. 2003a; Bakker et al. 2003b) or 3 Hz (WSS of 0.6 ± 0.5 Pa) (Nauman et al. 2001). The work presented here did not investigate pulse amplitude as a factor and such investigation could help explain the differences in osteoblast PGE_2 response to PFSS. Additionally, for control samples Cox-2 and Runx2 mRNA expression was higher with OFSS in comparison to static samples, which has also been shown by (You et al. 2001; Xu et al. 2012) although some studies note that Runx2 expression in pre-osteoblasts was not higher with OFSS in comparison to static samples (Barron et al. 2010; Case et al. 2011).

Previous studies have provided an advanced understanding of the role of other mechanosensing mechanisms such as integrins, primary cilia and gap junctions in facilitating this response (Saunders et al. 2001; Malone et al. 2007b). Integrin inhibition

caused significantly lower Cox-2 gene expression, and PGE_2 production in osteocytes in comparison to non-inhibited samples (Haugh et al. 2015) and primary cilia inhibition caused significantly lower Cox-2 gene expression in comparison to non-inhibited samples (Malone et al. 2007b). However the role of AJs for sensing and transducing extracellular mechanical signals into a cellular response remained unclear. The work presented in this chapter shows that adhesion junctions play a role in the ability of osteoblasts to sense and respond to OFSS. When AJ formation was inhibited, Cox-2 was no longer significantly higher in comparison to control or AJ inhibited static levels. Downstream from Cox-2, PGE_2 production was no longer higher in comparison to control or AJ inhibited static samples. Runx2 gene expression also followed this trend; AJ inhibited samples did not have significantly higher Runx2 expression in response to oscillatory FSS, when compared to control and AJ inhibited static samples. This finding is supported by previous work with mesenchymal stem cells, which has shown that silencing of β-catenin inhibited the normal elevated expression of Runx2 in response to OFSS in comparison to static samples (Arnsdorf et al. 2009a). Together these results reveal that AJs play an important role in the mechanosensation of FSS by osteoblastic cells in vitro.

AJs are dynamic structures that can disassemble and reassemble at another location on the cell membrane. It has recently been elegantly demonstrated that adhesion junction intercellular binding to F-actin stabilises the extracellular clusters of cadherins, limits the movement of cadherins and enhances AJ cluster formation (Adams et al. 1998; Mège et al. 2006; Thoumine et al. 2006; Hong et al. 2013). Previous work has demonstrated that interference with cytoskeleton microtubules and microfilaments and integrins inhibits the stress fibre formation response of MC3T3-E1s to FSS stimulation (Pavalko et al. 1998; Norvell et al. 2004b). The results presented in this chapter show that AJ inhibition of a monolayer of MC3T3-E1s did not cause a significant change in stress fibre formation in static conditions, indicating that AJs are not a dominant factor in stress fibre formation on glass substrates. Stress fibre formation was higher ($p<0.001$) in control OFSS stimulated samples in comparison to control static samples. However, the cells had the opposite response to pulsatile FSS, with stress fibre formation decreasing between static and stimulated control groups ($p=0.014$). Other studies have also demonstrated significantly more stress fibre

formation with OFSS (Ponik et al. 2007; Yang et al. 2010). In contrast to the results presented in this chapter, other studies have shown significantly more stress fibre formation in response to PFSS (McGarry et al. 2005b; Li et al. 2012b). The work of Li et al. used a higher shear stress of 1.2 Pa (1.25 Hz) for time points up to 120 mins, and the work of McGarry et al. used a lower PFSS of 0.39 Pa (3 Hz) or 0.64 Pa (5 Hz) for 10 min. The difference in cytoskeletal response to pulsatile or oscillatory FSS could be due to differences in calcium influx with FSS; the significantly higher calcium concentration within osteoblasts during stimulation is greater for OFSS than PFSS or steady FSS (Roy et al. 2014). This is in part due to the opening of a stretch activated ion channel, transient receptor potential (TRP) cation channel, subfamily M, member 7 (TRPM7) (Roy et al. 2014). FSS caused local and transient increases in Ca^{2+} of 3 - 3.5 fold (oscillatory) or 2.25 - 2.75 fold (pulsatile) higher than baseline, unstimulated levels (Roy et al. 2014). Computational modelling of OFSS in this bioreactor system also revealed that due to the fluctuation between positive and negative hydrostatic pressure within the bioreactor flow chamber, cell-cell contacts alternate between compressed and stretched (Chapter 5). Unidirectional flow generates a positive hydrostatic pressure, and so only compresses the cell-cell contacts.

This study has important implications for our understanding of the role of AJs in MC3T3-E1 osteogenesis and mechanosensing. Genome wide association studies have identified β-catenin, an intracellular component of AJs, as a Wnt related gene likely associated with osteoporosis (Estrada et al. 2012). Indeed, OB-cadherin gene expression in primary marrow stromal cells and osteoblastic cells was 9-fold higher in mature rabbits than in old rabbits (Goomer et al. 1998). Treatment with oestrogen, a critical hormone for the maintenance of bone formation, for four months led to higher N-cadherin gene expression in postmenopausal women in comparison to women not treated with oestrogen (Mödder et al. 2011). The results presented in this chapter show that AJs, particularly N-cadherin AJs, are important for transducing mechanosensation into a cellular response and these structures could be a promising target in the treatment of osteoporosis.

4.5 Conclusions

Mechanical loading is a key regulator of bone formation. It is believed that the movement of fluid within the bone is one of the main modalities of force application to osteoblasts. These cells respond to fluid shear stress by up-regulating the production of osteogenic proteins and genes. The results presented in this chapter demonstrate that interference with adhesion junction formation prior to application of oscillatory fluid shear stress results in a significantly reduced biochemical response (PGE_2, Cox-2 and Runx2) but did not significantly reduce stress fibre formation with FSS. Pulsatile fluid flow stimulation of control samples did not cause significantly higher production of PGE_2, or higher stress fibre formation in comparison to static samples. A better understanding of mechanotransduction in osteoblasts may lead to the development of novel treatments for bone diseases where bone production is decreased due to compromised osteoblast mechanosensitivity.

Chapter 5:

Computational Investigation into the Forces generated at Cell-Cell Adhesion Junctions by Fluid Shear Stress and Hydrostatic Pressure

---

5.1. Introduction

Mechanical forces play an important role in the growth, organisation, differentiation and function of living cells and tissues. It is well established that mechanical loading is critical for the maintenance of structural integrity of bone (MacKelvie et al. 2003). The current challenge is to understand the mechanisms by which bone cells sense and respond to applied loads. A hypothesis was proposed by Cowin et al. (1991) wherein macro-scale physiological loading of bone will result in fluid flow within the canalicular network, resulting in application of a wall shear stress on osteocytes. Several studies have been performed in which bone producing cells (osteoblasts) are subjected to fluid flow stimulus (FFS) in a parallel plate bioreactor (Liu et al. 2008; Kamel et al. 2010). A parallel plate bioreactor is a piece of equipment designed with a flow chamber of height of the order of 100 - 500 µm. Typically, cells are seeded onto a glass slide that sits flush with the bottom plate and a laminar flow of cell culture media is induced over the plate (and cells) at a flow rate, calculated to apply a specific wall shear stress to the adherent cells (Malone et al. 2007c). Several studies report significantly higher expression of osteogenic proteins and genes as a result of such FFS. Specifically, higher expression of osteogenic genes (Cox-2 (Norvell et al. 2004b), Runx2, (Case et al. 2011) and osteopontin (You et al. 2001)) are reported. Additionally, osteoblasts respond to FFS with higher expression of osteogenic protein markers such as Prostaglandin E_2 (Smalt et al. 1997), and with translocation of β-catenin, an important osteogenic signalling molecule, into the nucleus (Norvell et al. 2004a). However, the detailed mechanisms underlying such mechanotransduction are not yet fully understood.

A variety of fluid flow regimes are commonly applied to cells in vitro (Malone et al. 2007c; Arnsdorf et al. 2009a; Kamel et al. 2010; Liu et al. 2010a). These include oscillatory (Malone et al. 2007c; Arnsdorf et al. 2009a), pulsatile (Kamel et al. 2010; Liu et al. 2010a) and steady (Jacobs et al. 1998; Jaasma and O'Brien 2008; Case et al. 2011) state fluid flow regimes. A range of applied wall shear stress has been reported in the literature ranging from 0.2 to 2.4 Pa for parallel plate bioreactors (Donahue et al. 2003; Lee et al. 2008b; Kamel et al. 2010) and 0.029 to 0.22 Pa for rocker systems (Delaine-Smith et al. 2014; Tucker et al. 2014). To generate fluid flow within the bioreactor, a pressure gradient is generated and fluid flows from the area of high pressure to the area of low pressure. However, oscillatory fluid flow is an unsteady flow regime wherein the pressure gradient within the bioreactor changes over time. Of particular interest to this work is the changing pressure gradient within the chamber, as the implications of this on the stresses generated in cells has not been previously investigated. Fluid-structure interaction models of single cells in a parallel-plate flow system have decoupled hydrostatic pressure and wall shear stress and demonstrated that increasing hydrostatic pressure (81 – 243 Pa) caused increased cellular equivalent elastic strain, but increased wall shear stress (0.5 – 2 Pa) did not (Vaughan et al. 2013b). However, previous fluid-structure interaction modelling of cells in parallel plate systems have only investigated steady, unidirectional fluid flow (Anderson et al. 2005; McGarry et al. 2005a; Vaughan et al. 2013b; Qiu et al. 2014).

The ability of osteoblasts to sense mechanical stimulus and respond by transducing the mechanical stimulus into biochemical responses is known as mechanosensation (Papachroni et al. 2009). It has been proposed that mechanosensation is mediated by three main mechanisms; integrins, primary cilia and adhesions junctions. Each of these three mechanisms has an emerging body of in vitro evidence indicating their individual importance and contribution to osteogenesis in response to the application of FFS in a parallel-plate bioreactor (Ferraro et al. 2004; Norvell et al. 2004a; Lee et al. 2008a; Leckband et al. 2011; Hoey et al. 2012b) or rocker systems (Delaine-Smith et al. 2014). Computational investigations into the stresses experienced by integrins and primary cilia during FFS have demonstrated the heightened stress-states of these structures (Rydholm et al. 2010; Verbruggen et al. 2012; Vaughan et al. 2013a) that correlates with osteogenic responses to FFS.

However, computational modelling has not yet shown if adhesion junctions experience a heightened stress state during application of FFS.

Adhesion junctions are transmembrane structures that facilitate cell-cell contact and connect the cytoskeletons of adjacent cells. The cytoskeleton plays an important role in the formation and stability of cell-cell junctions by generating intercellular tension through actin stress fibre formation (Hong et al. 2013; Buckley et al. 2014). Experimentation using cyclic strain has shown that a strain of 0.01 results in higher intracellular Ca^{2+} (Harell et al. 1976; You et al. 2000) and higher prostaglandin E2 synthesis (Somjen et al. 1980; Binderman et al. 1984; Binderman et al. 1988), both responses indicative of osteogenesis. Given that intercellular tension is needed for stable adhesion junction formation, a computational model examining the stresses and strains experienced at cell-cell contacts during FFS, when contractility is incorporated in the cell, could give helpful insight into the forces experienced at adhesion junctions that correlate with an osteogenic response. The specific objective of this study is to determine the role of FFS in the development of intercellular forces at cell-cell contacts using fluid-structure interaction models.

5.2. Methods

5.2.1 Static Structural Analysis: Cell Parametric Studies

Cells are assumed to behave as homogenous, isotropic solids. The cell cytoplasm has a Young's Modulus of 3.7 kPa (Domke et al. 2000) and a Poisson's ratio of 0.4. To model the pre-strain generated by the cytoskeleton the cell cytoplasm undergoes volumetric contraction via an instantaneous volumetric coefficient of contractility (C) applied using an arbitrary negative temperature change of 1^{o}C. Chapter 3: Theory, Section 3.2.3 details the theory behind C, and the following equation is used to calculate the thermal strain.

$$\boldsymbol{\varepsilon}^{th} = \boldsymbol{C}\Delta\mathrm{T} \tag{5.1}$$

This method has been used in previous methodology to computationally simulate active cellular contractility (Stops et al. 2008; Mullen et al. 2014b). C was determined as described below. The nucleus has a Young's Modulus of four times that of the cytoplasm, as the nucleus has been shown to be significantly stiffer than the cytoplasm and modelled as such previously (Tseng et al. 2004; Vaughan et al. 2013b) and a Poisson's ratio of 0.4. The cell geometries have ellipsoidal nuclei (major axis 20 µm, minor axis 10 µm), cell base length of 100 µm, width of 80 µm and maximum height of 16.1 µm, based on cell dimensions observed in vitro and as shown in Figure 5.37.

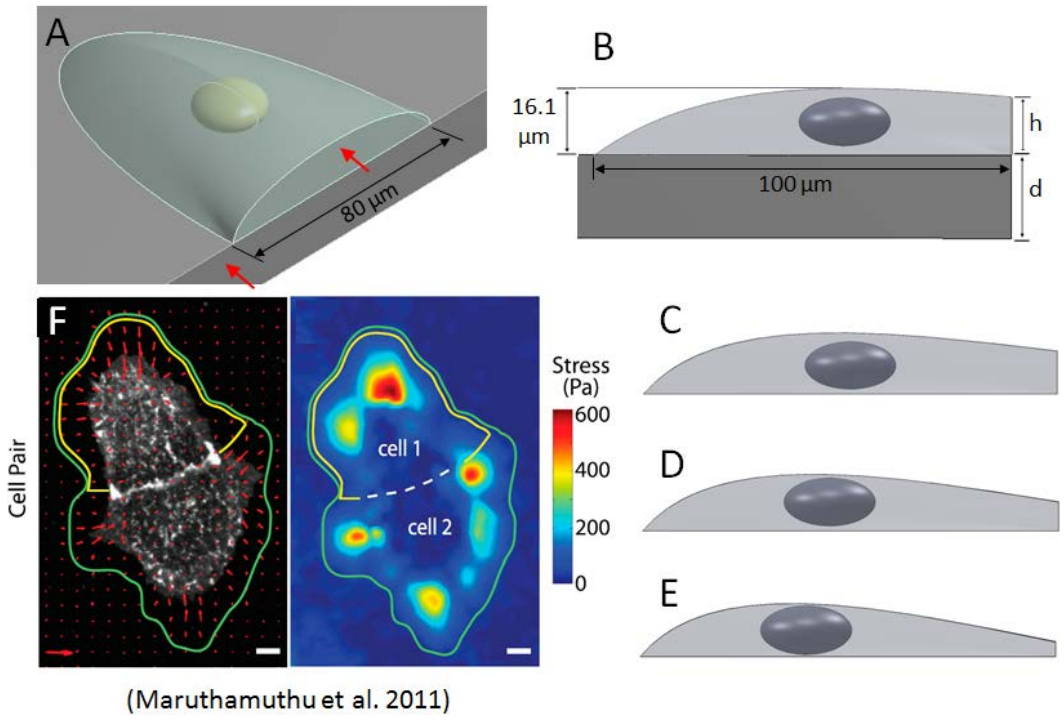

Figure 5.38: Side profiles of idealised cell geometries used to parametrically test the influence of cell-cell contact height on substrate stresses during cell contraction. A) 3D View of a cell and nucleus on a PA gel substrate. The red arrows denote planes of symmetry to model a cell pair. B) Side profile of a cell on PA gel substrate. h denotes cell-cell contact height; d denotes gel depth. Cells with sequentially decreasing h values of B) 14.4 C) 10.5 µm, D) 7 µm and E) 3.5 µm were analysed. F) Stress vectors (left) and heat map of traction stress (right) results of Madin-Darby canine kidney cell pairs from the work of (Maruthamuthu et al. 2011).

To ascertain an estimate of cellular contractility, the previously described cell geometry with varying cell-cell contact height (h) is modelled on polyacrylamide (PA) gel substrates of varying depth (d). These models systematically analyse the effects of cell-cell contact height, PA gel depth and cell contractility on the stress patterns generated in the gel. Four idealised cells were considered (Figure 5.37, B-E) wherein the height (h) of the cell-cell contacting surface of paired cells was decreased sequentially (h = 14.4, 10.5, 7 and 3.5 µm). The PA gel depth (d) was varied as indicated in Figure 5.37B. To find the most suitable magnitude of contractility, the coefficient of contractility is varied (C=0.01, 0.02, 0.025, 0.03) and computed PA gel deformation is compared to the traction forces generated by Madin–Darby canine kidney (MDCK) G II cells on a PA gel during in vitro experiments (Maruthamuthu et al. 2011). The PA gel has a Young's Modulus of 8400 Pa and Poisson's ratio of 0.4

(Maruthamuthu et al. 2011). A model of two adhered cells is constructed, as shown in Figure 5.37. The cells are rigidly adhered to one another through a contact surface (marked 's' in Figure 5.37A) in the YZ plane in the undeformed configuration. The base of each cell is assumed to be rigidly adhered to the PA gel substrate.

5.2.2 Multi-scale Bioreactor Model

A multilevel methodology () is used to (i) simulate the fluid flow within the bioreactor and (ii) simulate the localised cellular deformation as a result of such fluid flow. A global Computational Fluid Dynamics (CFD) model is developed to characterise the fluid velocities and pressures within the entire parallel-plate system. Subsequently, a local Fluid-Solid Interaction (FSI) model, with fluid flow boundary conditions informed directly by the global CFD simulations, is used to compute the stress state in the two contacting cells. The height of the cell-cell contact of the cell pair, and the cell contractility, are informed by the static structural simulations.

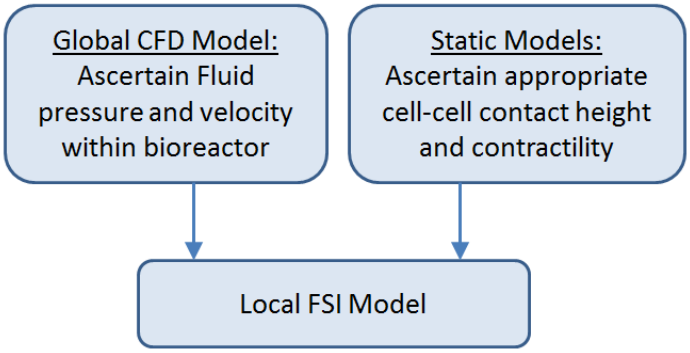

Figure 5.39 Flow chart detailing multilevel methodology used in this chapter.

5.2.2.1 Global CFD Parallel Plate Flow Chamber Model

A global CFD model of the parallel plate bioreactor designed by (Lane et al. 2012) and used in Chapter 4 of this thesis (Figure 5.39) is developed. The tubing has an internal diameter of 3.5 mm and the flow chamber has a height of 200 µm, width of 17.46 mm and length of 144.09 mm. The inlet and outlet tubing are 17 mm long each. The flow field (Figure 5.39C) within the bioreactor is designated as all areas through which the fluid flows from the tubing inlet, through the flow chamber and through the tubing

leading to the outlet. For steady, laminar, fully developed fluid flow between two parallel plates the wall shear stress on the bottom plate of the channel can be expressed in terms of the volumetric flow rate using the following relationship (Chung et al. 2003; Bacabac et al. 2005):

$$\tau_w = \frac{6Q\mu}{bh^2} \qquad (5.2)$$

where τ_w is wall shear stress, Q is flow rate, μ is fluid viscosity, b is chamber width and h is chamber height. Pressure of 1 atm is applied at the outlet. A 1 Hz oscillatory fluid velocity of 0.01714 m/s is assigned as an inlet condition. These inlet and outlet conditions are assigned to generate an oscillatory flow within the chamber with a maximum wall shear stress of 1 Pa. No slip boundary conditions are applied to the walls of the bioreactor and cell culture media is modelled as a Newtonian fluid and assigned the density of water (998 kgm^{-3}) and a dynamic viscosity of $\mu = 8.99 \times 10^{-4}$ kg/ms. The Reynolds number for the flow system is calculated as follows:

$$Re = \frac{\rho v_m D_h}{\mu} \qquad (5.3)$$

where ρ is density, v_m is mean velocity and D_h is hydraulic diameter of the chamber where $D_h=2h$ (White 2008). A Reynolds number of 16.46 computed using Equation. 5.3 indicates that flow within the chamber falls well within the laminar region (Re<1400). The commercially available software ANSYS CFX is used to compute pressures and velocities within the system. Local pressures and velocities in the fluid domain were resolved using a convergence criteria of 1×10^{-4}. The fluid domain is discretised into 6.5×10^6 tetrahedral elements. Due to the relatively small height of the flow chamber, significant refinement of the mesh is required in this region to adequately resolve the fluid velocities near the boundaries walls.

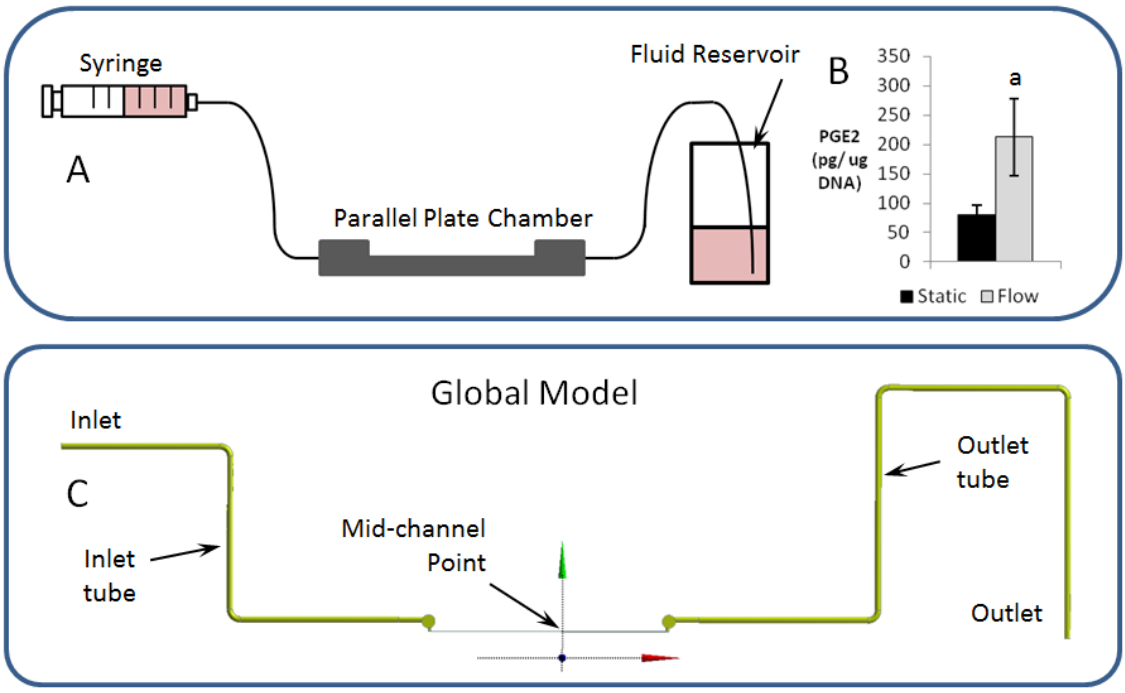

Figure 5.40: A) Parallel plate bioreactor set-up. B) PGE_2 results showing higher PGE_2 expression from MC3T3-E1 cells after 1 hr exposure to 1 Pa Oscillatory fluid shear stress from Chapter 4. Statistical significance is declared at $p \leq 0.05$. a=0.014. C) Global model fluid domain detailing the location of the central point in the parallel plate channel where fluid velocity and pressure are recorded for use in the Local models.

5.2.2.2 Local Fluid-Solid Interaction Model

The local fluid structure interaction (FSI) model (Figure 5.40 A) is used to determine the stress state in two contacting cells due to fluid flow in the bioreactor. A two-way FSI is implemented through bi-directional coupling of the ANSYS CFX solver to the ANSYS Structural finite element solver (Figure 5.40 B) (Vaughan et al. 2013b). To facilitate this coupled two-way analysis, a fluid-solid interface boundary between the fluid and the solid domain is assigned on the upper cell membrane of both cells. This functions by first solving the fluid domain Navier-Stokes equations of momentum and continuity and then mapping the resulting fluid stress tensor to the solid domain as a boundary condition on the fluid-solid interface. The resulting deformation of the solid domain is then relayed back to the fluid domain as boundary conditions for the next iteration until a converged solution is achieved.

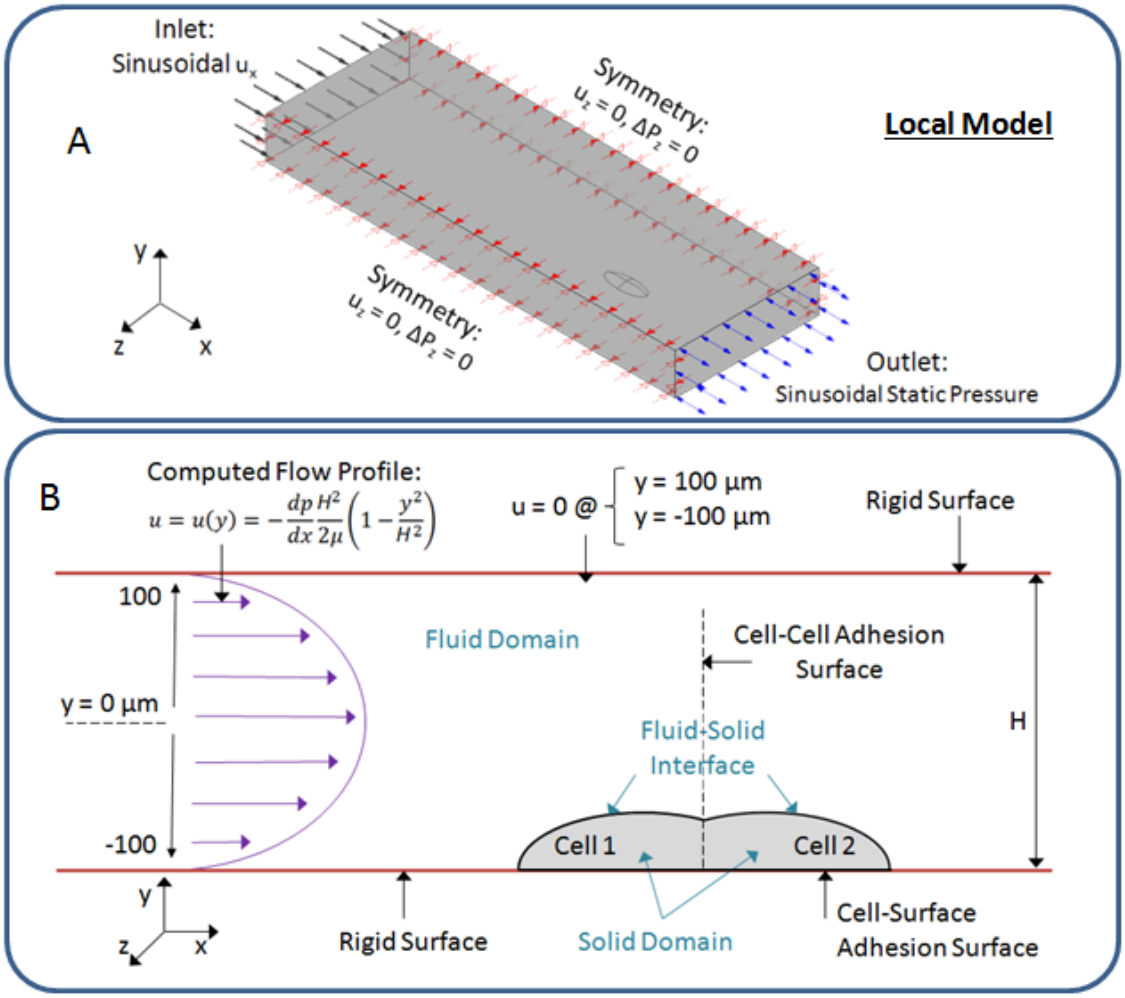

Figure 5.41: A) Schematic of local model boundary conditions with two contacting cells in the flow field. U is fluid velocity and P is fluid pressure. B) Schematic of Fluid-Solid interaction models. The cell bodies formed the Solid Domain and were fixed to a rigid surface via a cell-surface adhesion surface. The top surface of the cells was designated as the Fluid-Solid interface where forces were transmitted between the Fluid and Solid domains. The contact plane between the two cells formed the cell-cell adhesion surface. Fluid flow between the two rigid surfaces forms a parabolic flow profile with fluid velocity (u) at a maximum in the centre of the fluid domain (y = 0) and at zero against the walls due to the no-slip boundary condition applied here. Chamber height (H), fluid viscosity (µ) and fluid pressure (P) influence the flow profile.

5.2.2.2.1 Fluid Domain

The local model fluid domain consists of a flow field of dimensions 2000 x 700 x 200 µm (Figure 5.40 A). Boundary conditions are prescribed using flow conditions computed at the centre of the flow chamber by the global model. A transient (oscillatory) flow velocity boundary condition is applied uniformly on the inlet

boundary surface. An entrance length (L_e) of 307 µm is required for the flow to become fully developed, as calculated via Equation. 5.4 (White 2008).

$$L_e = D_h \, x \, 0.06 \, x \, Re \qquad (5.4)$$

A transient (oscillatory) hydrostatic pressure is applied at the outlet boundary surface. A maximum wall shear stress of 1 Pa is computed under such boundary conditions. In addition to the aforementioned transient boundary conditions (determined by the global model), a steady fluid flow regime is also considered by implementing the maximum pressure and maximum velocity from the global model at the local outlet and inlet boundary surfaces, respectively. No-slip boundary conditions are applied at all surfaces (with the exception of the inlet and outlet surfaces) (Figure 5.40). The model is discretised into 390 x 10^3 tetrahedral elements with a higher mesh density near the fluid-cell interface so as to more accurately calculate stresses and deformations in this area.

5.2.2.2.2 Solid Domain

Cell geometries and dimensions are shown in Figure 5.37. Each cell geometry contains an ellipsoidal nucleus (major axis 20 µm, minor axis 10 µm). Cell material properties were the same as described in Section 5.2.1 with a thermal contractility coefficient of 0.025. The contact surfaces between adjoining cells are either fully bonded (representing cell-cell bonding via adhesion junctions), or set as a frictionless contact (representing impaired cell-cell bonding). For FSI models, cell pairs are rigidly adhered to a substrate rather than the PA gel (Figure 5.40 B) while upper cell surfaces are assigned as an interface area between the static structural analysis and the fluid dynamics analysis as is described in Section 5.2.2.2. The combined cell pairs are discretised into 44,200 tetrahedral elements.

5.3. Results

5.3.1 Parametric Studies: Determination of cell-cell contact height and cell contractility co-efficient

The 14.4 µm cell-cell contact height produces the lowest maximum principal stress in the PA gel adjacent to the cell-cell contact (Figure 5.41). Lower cell-cell contact heights of 3, 7.5 and 10.5 µm produce larger maximum principal stresses in this region of the PA gel. Lower stress in the PA gel adjacent to the cell-cell contact gives the best approximation of the stresses generated by a cell pair, while higher stress in this area produce stress patterns more representative of single cells observed in vitro (Maruthamuthu et al. 2011). An appropriate value for cell contractility is found to be 0.025 (Figure 5.42) as this value generated maximum principle stresses in the PA gel that were in the same range as the traction forces exerted by cell pairs on a PA gel *in vitro* (Maruthamuthu et al. 2011). The thickness of the PA gels investigated (10, 20 and 40 µm) does not significantly affect the stresses experienced in the cells or the gels.

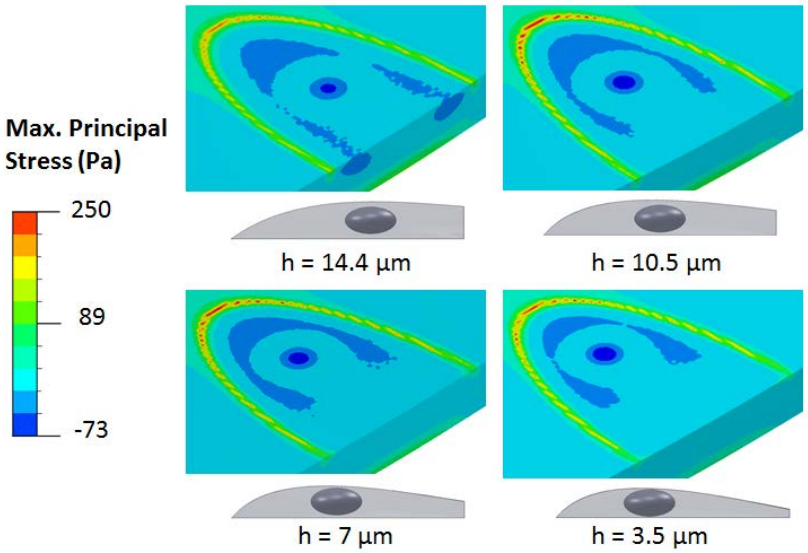

Figure 5.42: The height of the cell-cell contact height has negligible influence on maximum principal stress in the PA gel, and relates linearly to the cell-cell tugging force. (A) Contour plots of maximum principal stress in the PA gel with cells of varying cell-cell contact height (h) when a value of 0.025 is used for cellular contractility.

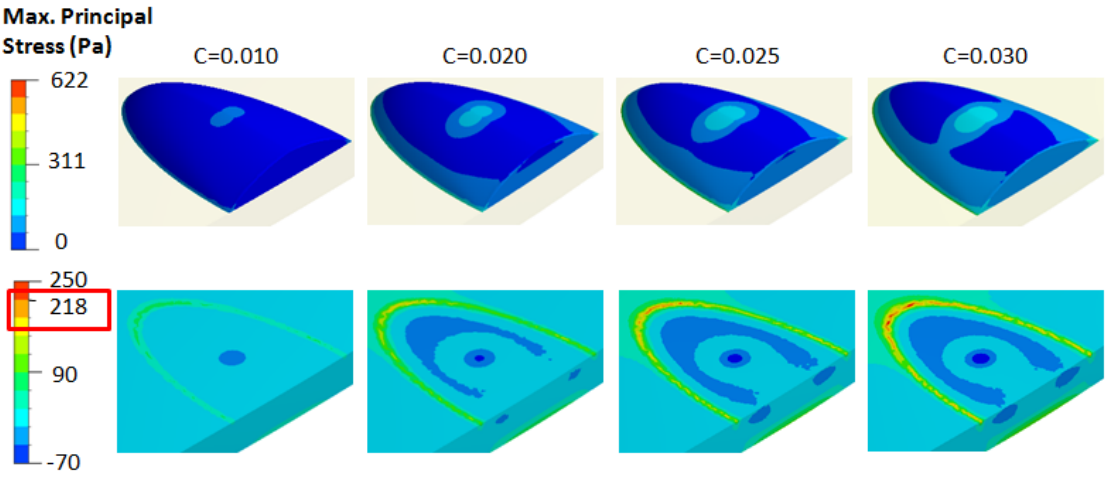

Figure 5.43: Contour plots of maximum principal stress used to investigate different values of contractility coefficient C. C=0.025 gives the best approximation of the in vitro stresses generated by the contracting cell in the work of (Maruthamuthu et al. 2011).

5.3.2 Global model CFD analysis of flow field within bioreactor

A pressure drop of 970 Pa is computed over the distance from the chamber inlet to the chamber outlet (L=144.09 mm) resulting in a pressure gradient of 6.7 Pa/mm. The wall shear stress on the upper and lower walls of the fluid flow chamber is the same along the length of the chamber at any given time point. Pressure in the in vitro bioreactor system was measured, during application of the flow rate calculated to apply 1 Pa of WSS was applied. The measured pressure varied from 600 – 800 Pa, with the higher pressure experienced when the screws holding the parallel plates together were tightened. The transient hydrodynamic pressure and fluid velocity computed at a point in the centre of the flow chamber (shown in Figure 5.43A and 5.6C) are used as boundary conditions for the inlet and outlet of the local models, respectively.

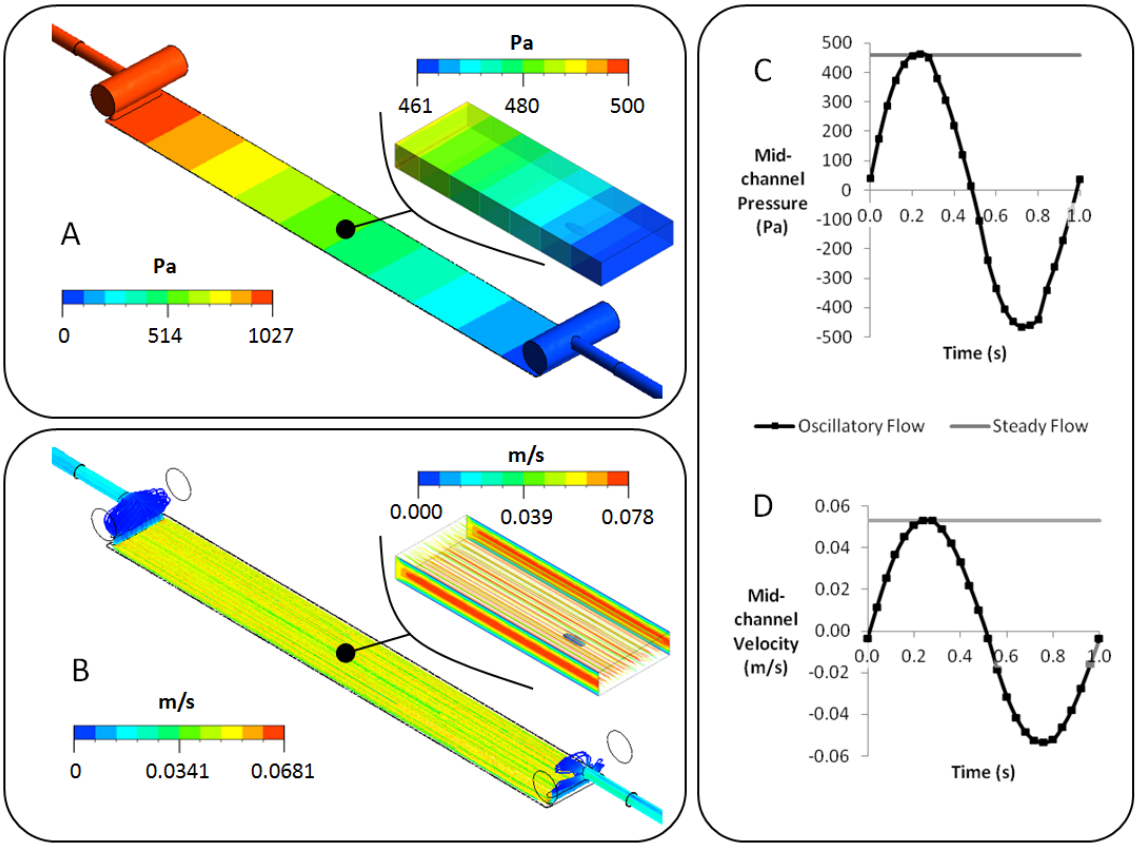

Figure 5.44: Contour plots of A) the pressure and B) the fluid velocity in the Global model for oscillatory fluid flow at t=0.24 s. Inset for each Global model is the Local model pressure or velocity at t=0.24 s. The local model outlet and inlet boundary conditions are prescribed by the pressure (C) and the velocity (D) values respectively, taken from the centre of the Global model channel during oscillatory fluid flow. The maximum pressure and velocity during the forward oscillation are used to prescribe steady fluid flow.

5.3.3 Tensile and compressive stresses at cell-cell contact area during FSI simulations

Figure 5.44A shows the maximum principal stress (σ_{max}) at the cell-cell contact surface (CS) and Figure 5.44B shows the volume averaged maximum principal strain over the whole cell body in the local cell model during one full fluid flow oscillation, with (C=0.025) or without (C=0.000) cell contractility. When the fluid is at rest (t=0.00, 0.50, 1.00: v = 0.000 m/s, P = 0 Pa), peak values of $\sigma_{max} = 140\ Pa$ occur when a contractility of C=0.025 is implemented. In one full oscillation, the CS for C=0.000 cells experience a change in σ_{max} that oscillates from -315 to +480 Pa while C=0.025 cells experience an oscillation in σ_{max} from -170 to +480 Pa.

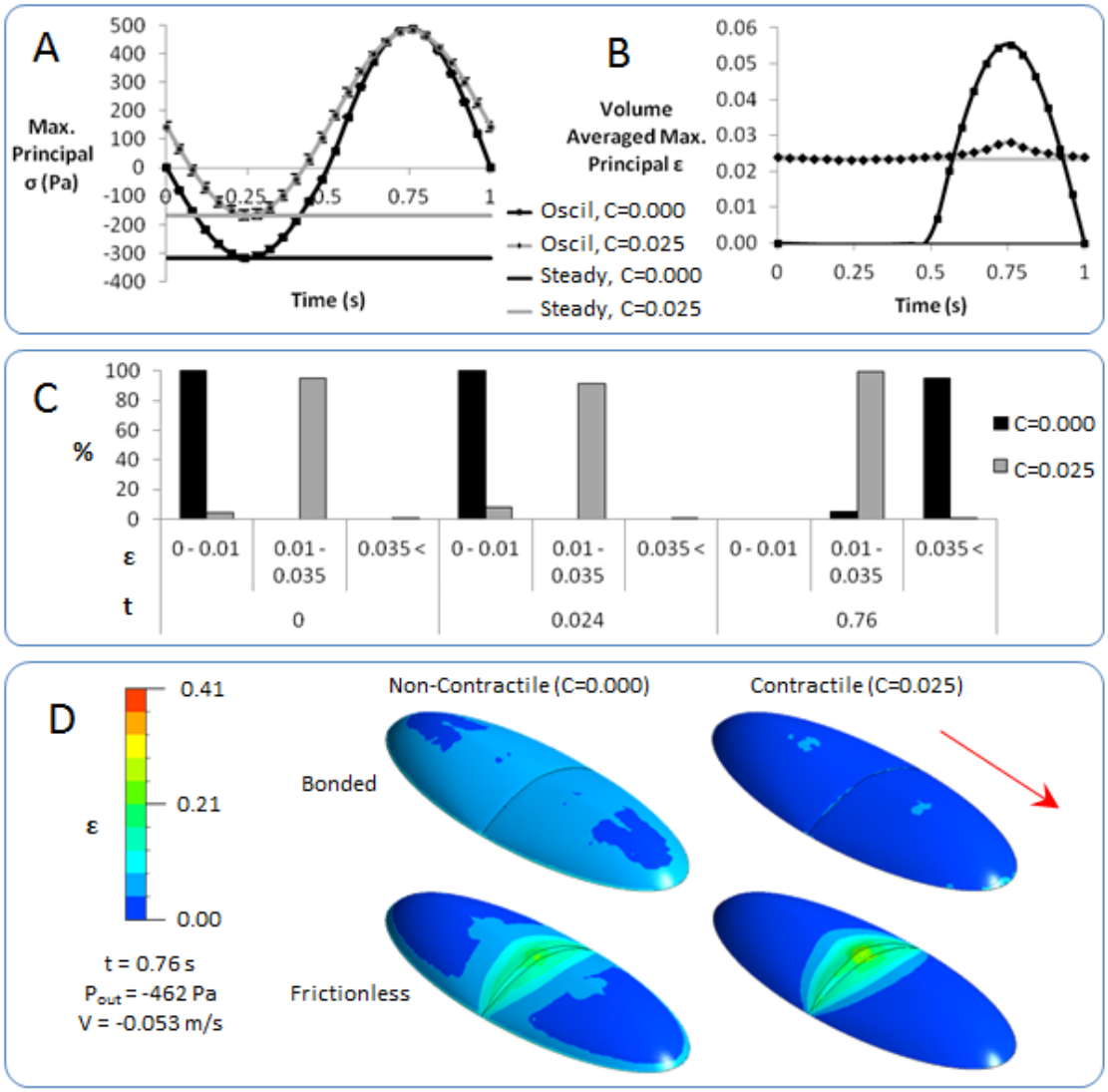

Figure 5.45: Oscillatory fluid velocity and pressure cause large changes in (A) maximum principal stress (σ) at the cell-cell contact surface. Cell contractility results in less compressive stress at t=0.24s, but the tensile stress at t=0.76 is similar with (C=0.025) or without (C=0.000) contractility. Also shown is σ due to steady fluid flow at max forward pressure and velocity. The (B) volume averaged maximum principal strain (ε)across the entire cell remains relatively stable for contractile cells but fluctuates from near zero to highs of 0.06 for non-contractile cells. Also shown is ε due to steady fluid flow at max forward pressure and velocity. (C) Graph of % volume fraction within specific strain (ε) thresholds at approximately zero (t=0.00), minimum (t=0.24) and maximum (t=0.76) flow chamber pressures. (D) Contour plots showing that bonding of the cell-cell contact surfaces prevents these surfaces from separating during the reverse half of the fluid oscillation, resulting in lower strains. The red arrow indicates fluid flow direction.

During the first half of each oscillating flow cycle, fluid is being pushed into the chamber and a compressive maximum principal stress is computed at the contact surfaces ($\sigma_{max} < 0$). The inclusion of contractility partly counteracts the compressive stresses generated by fluid flow (the contractility tends to pull the surfaces apart whereas the fluid tends to compress the surfaces together). Figure 5.44C shows the percentage volume fraction of computed maximum principal strains in the cell cytoplasm. With contractility, the volume averaged maximum principal strain in the cell due to negative hydrostatic pressure is 0.028. As expected, an applied contractility of C=0.025 to the cytoplasm results in a volume averaged strain of 0.024 over the entire cell. Recalling that this level of contractility has been calibrated using experimental traction force microscopy data (Figure 5.42), this result suggests that the negative hydrostatic pressure loading in the bioreactor contributes only ~14.3% of the total cell strain. The volume averaged maximum principal strain in the non-contractile cell body due to negative hydrostatic pressure is 0.055. Due to the implementation of contractility, greater than 92% of the contractile osteoblast volumes (all time points) were above ε=0.01 (Figure 5.44C) the strain value thought to elicit an osteogenic response (Harell et al. 1976; Somjen et al. 1980; Binderman et al. 1984; Binderman et al. 1988; You et al. 2000). In contrast, computed strains due to fluid flow in non-contractile cells are only above this threshold during negative hydrostatic pressure application.

During the second half of the oscillation, when fluid is being pulled from the chamber, a tensile stress ($\sigma_{max} > 0$) is computed at the CS. In consideration of strains in the entire cell body at t=0.76, 100% of the cell volume experienced >0.01 (C=0.025 and C=0.000) and the maximum principal strain (ε) experienced by the cells was 0.07 (C=0.025) and 0.12 (C=0.000). When the CS was assigned as a frictionless contact rather than a bonded surface to assess the influence of the CS on strains in the cell body (Figure 5.44D), maximum ε at t=0.76 increased to 0.41 (C=0.025) and 0.32 (C=0.000), and 91% (C=0.025) and 90% (C=0.000) of the cell volume experienced ε >0.01. The strains experienced in the first half of the cycle due to positive pressure remain the same as in bonded cell pairs, but with application of positive pressure, the cell surfaces assigned as frictionless contact are pulled apart.

As discussed, contractility of C=0.025 applies a volume averaged strain of 0.024 to the cell body before any externally applied mechanical stimulus was implemented. To ascertain if the FFS applied additional strain that could be considered to stimulate an osteogenic response (ε=0.01), strain over a threshold of ε=0.035 was also investigated (Figure 5.44C). At all time-points, 0.4 - 0.5 % of the total cell volume is above ε=0.035 for $C_{0.025}$ cells, while 0% and 95 % of $C_{0.000}$ total cell volume is above ε=0.035 at t=0.24 and t=0.76, respectively.

5.4. Discussion

Adhesion junctions (AJs) at cell-cell contact surfaces have been shown to play a role in osteoblast sensing and response to fluid flow stimulation (FFS) (Norvell et al. 2004a). However, the magnitude of contact stress/traction at the cell-cell interface during FFS has not previously been analysed. The current study considers the mechanical response of two contacting cells subjected to FFS in a parallel plate bioreactor. To this end, A) a global computational fluid dynamics (CFD) model of the entire flow system was constructed to compute the fluid velocity and pressure in the channel region of the bioreactor, and B) fluid shear stress, pressure and cellular contractility were applied to deformable contacting cells in a local fluid structure interaction (FSI) model. Simulations reveal that oscillating FFS within the bioreactor results in alternating tensile and compressive normal contact stress at the cell-cell interface. This work presents a mechanical indication as to why cells respond differently to steady and oscillatory fluid flow regimes (Jaasma et al. 2007; Jaasma and O'Brien 2008; Case et al. 2011) in parallel plate bioreactors.

Previous studies have used thermal contraction to model cytoskeletal contraction (Stops et al. 2008; Mullen et al. 2014a) but the implemented coefficient of contractility was not calibrated based on in vitro experimental results as it is in the work presented here. However, the use of a coefficient of thermal expansion to model cell contractility is a limitation of this study. This method is a non-physiological based model for contractility as it (i) does not capture strain rate effects (e.g. the Hill curve), (ii) does not capture the anisotropic, direction dependent contractility due to alignment of stress fibres within cells and (iii) does not capture stress fibre remodelling due to changes in the local stress state of the cell due to applied FFS. A more refined

method of modelling the contractile actin cytoskeleton is to use the active cytoskeleton model developed by (Deshpande et al. 2006; Deshpande et al. 2008). This active model was utilised (Ronan et al. 2015) to explain the in vitro experimental observations (Liu et al. 2010b) that cell-cell junction tugging forces increase with cell-cell junction size but that traction forces exerted on micro-post arrays are independent of junction size. The coefficient of thermal contractility used in the work presented here did not produce a linear relationship between junction size and tugging force (Figure 5.41). An additional limitation of this study is the idealised cell models used. The idealised cell geometries used were based on cell geometries observed in vitro and the results of the contact height analysis informed the cell geometry used for the FSI analysis. The idealised cell models employed linear elastic material properties. However, the implementation of a homogeneous isotropic material model is a limitation of this work as previous studies have demonstrated that cell behaviour cannot be captured by elastic, hyperelastic or viscoelastic material laws (McGarry and McHugh 2008; Dowling et al. 2012; Reynolds et al. 2014; Reynolds and McGarry 2015). Such passive material models are capable of simulating non-contractile cells in which the actin cytoskeleton is disrupted (Reynolds and McGarry 2015).

The values found for fluid pressure are in the same range as those measured by (Huesa et al. 2010) in a similar parallel plate bioreactor experimental study. A key point of the work presented here is that the method used to generate the pressure gradient that drives the fluid flow within the chamber has a significant influence on the stress and strain state of the cells. When fluid is pushed into the chamber, as happens during the first half of the oscillation, or during unidirectional steady or pulsatile fluid flow, the cells within the chamber experience compressive hydrostatic pressure. When fluid is pulled from the chamber, as occurs during the second half of the fluid oscillation, cells experience a negative pressure, effectively resulting in an increase in maximum principal strain throughout the cell cytoplasm, and an increase in tension in the adhesion junctions between the cells. This work shows that cell location within the bioreactor is an important contributing factor to the hydrostatic pressure experienced; a cell situated at the end of the chamber nearest the syringe is predicted to experience a ±1000 Pa pressure fluctuation, while a cell situated at the end of the chamber near the reservoir is predicted to experience ±0 Pa pressure fluctuation. Therefore, in an

oscillating flow parallel plate bioreactor, the ratio of cell stress or cell-cell tension as a direct result of fluid pressure to that as a result of wall shear stress generated by fluid flow is highly dependent on the position of the cell in the bioreactor and also on the time-point during the oscillatory flow cycle. In vitro experimentation has shown the significant influence of pressure on osteogenesis; oscillating pressure (1 ± 0.1 kPa) with no fluid flow can elicit the same translocation of β-catenin into the nucleus as oscillatory or pulsatile FFS (Huesa et al. 2010). β-catenin is an important part of the canonical Wnt signalling process that regulates osteogenic genes. In vitro measurements of hydrostatic pressure in this bioreactor showed values varying from 600 – 800 Pa when a flow rate calculated to impart 1 Pa of WSS was applied. The variation in pressure had a dependence on the tightness of the screws holding the parallel plates together, as pressure increased when the screws were tightened. In the experimental set-up in Chapter 4, o-rings are used to seal the bioreactor flow chamber. Tightening the screws would further compresses the o-rings and reduce the height of the bioreactor flow chamber. The screws in the in vitro work presented in Chapter 4 were tightened by hand and so the tightness of the screws was not regulated. Better regulation of screw tightness could reduce variation in maximum hydrostatic pressure and improve repeatability of in vitro experiments, such as PGE_2 expression in response to oscillatory FSS (Figure 5.39 B).

Substrate unidirectional normal strains greater than 0.01 produce higher Prostaglandin E2 (PGE_2) or calcium influx, both positive osteogenic responses (Harell et al. 1976; Binderman et al. 1984; Binderman et al. 1988; You et al. 2000) but applied unidirectional strain at lower levels (ε: 0.0005 - 0.005) does not produce higher PGE_2 production (Smalt et al. 1997). In the work presented here, the cell volume averaged maximum principal strain is primarily due to internal cell contractility (calibrated using the experimental data of (Maruthamuthu et al. 2011), with hydrostatic pressure and fluid flow providing secondary effects (up to ~14.3% of the total maximum principal strain. When contractility is not implemented however, the cell volume experiences a volume averaged maximum principal strain of approximately ε=0.000 for the first 0.5s, and then a heightened strain of ε=0.055 (t=0.076 s). Taken together, these two results indicate that the contractile pre-strain applies a strain above the ε=0.01 threshold, but shields the cells from experiencing higher strain, or indeed any notable fluctuations in

strain due to the fluid flow. In vitro osteocyte deformation during steady FFS was computationally modelled using a viscoelastic material model (Qiu et al. 2014) and found instantaneous strains in the cell body of up to 0.107, similar to the maximum strain found in the work presented here of ε=0.12 (C=0.000 at t=0.76). However, it should be noted that the work presented by Qiu et al. (2014) did not model the nucleus and cytoplasm with separate material properties, instead modelling the cell body as one continuous material. Previous computational studies of confocal image-derived osteocytes (Verbruggen et al. 2012) have shown that 1% of the osteocyte volume experienced strains greater than 0.01 when a 3D cube of extracellular matrix surrounding the cells is loaded with ε=0.003. ε=0.003 was assigned to simulate forces experienced during vigorous physiological activity (Burr et al. 1996). The FFS examined in the work presented here caused over 95% of the contractile or non-contractile cell volume to be over ε=0.01 at t=0.76.

Applied tension, usually from contractility of the cytoskeleton, helps AJs to form and strengthen (Peng et al. 2010; Buckley et al. 2014; Leerberg et al. 2014). This research has computationally demonstrated that hydrostatic pressure fluctuation during oscillating fluid flow in a parallel plate bioreactor causes a change in the cell-cell normal contact stress from tensile to compressive. Previous in vitro studies have observed contradictory results on the influence of FFS on intercellular force; the application of steady laminar FFS reduced (Conway et al. 2013; Steward et al. 2015) or hightened (Ting et al. 2012) the intercellular tension in endothelial cells. These differences could be due to differences in method used to calculate intercellular force as Conway et al. used FRET measurement to calculate tension at cell-cell contacts, Steward used gel displacements to calculate gel stress and intracellular tension and Ting used micro-post deflection to calculate intercellular forces, or due to differences in cell types (Steward et al. 2015). The analysis presented in this chapter suggests that steady, laminar fluid flow in a parallel plate system generates a compressive pressure in the flow chamber. This pressure competes with the stress at the cell-cell contact surface (CS) resulting in a net decrease, in agreement with the observations of (Conway et al. 2013; Steward et al. 2015). This work also shows that the presence of cell-cell contacts reduces the maximum strains experienced in the cell. When the CS is assigned as a frictionless contact, rather than as a bonded surface, the cells separated

when exposed to negative pressures and experienced two-fold higher strains in the cell body. This is in agreement with in vitro observations of cell-separation when the formation of adhesion junctions is inhibited by chelating extracellular calcium (Schnittler et al. 1997).

It is well established that cytoskeleton stress fibres will re-orientate first to the long access of the cell, and then to the direction of fluid flow in osteoblasts and endothelial cell monolayers, (Levesque and Nerem 1985; Girard and Nerem 1995; Malek and Izumo 1996; Jaasma et al. 2007). This realignment happens within 1 hr when steady, unidirectional fluid flow is applied, but it takes longer for this to occur with oscillatory fluid flow (Malone et al. 2007c; Ponik et al. 2007). It has also been observed that a reduction in intracellular tension in osteoblasts can induce the disassembly of actin stress fibres (Sato et al. 2006). The work presented here shows the differences in mechanical stimulation applied to cells by steady or oscillatory FFS, but an active material model (Deshpande et al. 2006; Deshpande et al. 2008) is required to investigate the influence of these forces on the cytoskeleton stress fibres.

5.5. Conclusions

The results of the current study provide insight into the stimulus imparted on cells within a parallel plate bioreactor during oscillatory fluid flow. Oscillatory fluid flow causes fluctuations in chamber pressure of ±1000 Pa, and imparts either compressive or tensile stresses on cells in the chamber, depending on the time-point of the oscillating flow cycle. Cell contractility applies a tension at cell-cell contacts which competes with the compressive hydrostatic pressure and shields the cell-cell contacts from more extreme compression, but does not alter the maximum tensile stress experienced at the cell-cell contact.

Chapter 6:

The Role of Adhesion Junctions in the Biomechanical Behaviour and Osteogenic Differentiation of 3D MSC spheroids

---

6.1 Introduction

Mesenchymal stem cells (MSCs) have emerged as an attractive cell source for osteogenic tissue engineering and regenerative medicine treatments for bone defects resulting from disease or trauma. The exploitation of MSCs for treatment of bone disease requires further study of regulating factors, such as the biochemical and mechanical environment, which influence the osteogenic differentiation of MSCs. In vitro, MSCs are commonly cultured in monolayers or on biomaterial scaffolds for the purposes of large scale expansion, to study their biology and investigate how they respond to extracellular biochemical and mechanical stimulation (Simmons et al. 2003; Luu et al. 2007; Mani et al. 2008; Wang et al. 2010; Fujita et al. 2014). Both of these culture methods rely on cell-substrate interactions, which strongly influence the biology and mechanics of the MSCs (Engler et al. 2006; Huebsch et al. 2010). Suspension culture approaches, such as scaffold-free MSC spheroids (mesenspheres) (Wang et al. 2009; Baraniak and McDevitt 2012; Cook et al. 2012; Kabiri et al. 2012) offer an environment dominated by the biophysical behaviour of the cells rather than extracellular substrates. These studies have demonstrated that MSCs grown in mesenspheres have preserved multi-lineage potential (Baraniak and McDevitt 2012), improved differentiation efficiency (Wang et al. 2009), and exhibit enhanced osteogenic gene expression and matrix composition in comparison to MSCs grown in 2D culture (Kabiri et al. 2012).

Stem cell differentiation in vivo is strongly regulated by both intrinsic and extrinsic signalling within the stem cell microenvironment, including cell-cell

interactions, factors secreted by cells, and cellular interactions with extracellular structures (Watt and Hogan 2000; Yin and Li 2006). During intramembranous ossification, one of the two essential processes by which bone is formed during foetal development, MSCs condense into areas of closely contacting cells (Thompson et al. 1989). These MSCs are connected via transmembrane adhesion junctions, comprised of extracellular glycoproteins known as cadherins, which facilitate cell-cell adhesion (Oberlender and Tuan 1994). Cadherins form a connection between the cytoskeleton of adjacent cells by bonding with cadherins on neighbouring cells (Overduin et al. 1995; Shapiro et al. 1995; Stains and Civitelli 2005). The condensed cell aggregates then begin to differentiate, form a membrane known as the periosteum and begin to produce a rudimentary bone matrix within this membrane (Gilbert 2000; Hall and Miyake 2000; Karaplis 2002; Kanczler and Oreffo 2008). In light of the close-contact established during MSC condensation, which initiates intramembranous ossification, mesenspheres offer a comparable environment to elicit osteogenic differentiation of MSCs along the intramembranous pathway.

The mechanical behaviour of MSCs is dictated by the cytoskeleton and is significantly influenced by cytoskeletal realignment and stress fibre formation (Titushkin and Cho 2007). Adhesion junctions are mechanosensitive structures that play an important role in the biomechanical behaviour of cells due to their involvement in the transmission of forces generated by the cytoskeleton (Ganz et al. 2006; Ladoux et al. 2010; Yonemura et al. 2010; Chopra et al. 2011; Maruthamuthu et al. 2011; Huveneers et al. 2012). Adhesion junctions also regulate the expression of osteogenic transcription factors in a manner related to the mechanical environment of the cells (Nelson and Nusse 2004; Guntur et al. 2012). However the mechanisms by which MSCs cultured as 3D mesenspheres sense and respond to their environment are still unclear as investigations into cell mechanosensation have typically been carried out in 2D culture systems (Ladoux et al. 2010; Chopra et al. 2011; Maruthamuthu et al. 2011).

N-cadherin and OB-cadherin are the main cadherins expressed by MSCs and osteoblasts (Kawaguchi et al. 2001; Hsu and Huang 2013). N-cadherin expression significantly lowers with osteogenic differentiation of MSCs whereas OB-cadherin expression increases (Kawaguchi et al. 2001; Hsu and Huang 2013). During in vitro

culture, the expression level of N-cadherin is higher in MSCs grown in 3D spheroids in comparison to those grown in 2D (Hsu and Huang 2013). The extracellular mechanical environment and exogenous stimulation can induce a phenotypic shift towards osteogenic differentiation (Engler et al. 2004; Mullen et al. 2013; Tan et al. 2014). Within 3D spheroids, mechanical cues are primarily in the form of cell-cell contraction, mediated by adhesion junctions, and as such adhesion junctions are likely to play an important role in the osteogenic differentiation of mesenspheres. However the precise role of N- and OB-cadherin on the biomechanical behaviour of mesenspheres remains unknown.

This study tested the hypothesis that adhesion junctions play an important role in dictating the mesensphere mechanical environment. The primary objective was to investigate the influence of N-cadherin and OB-cadherin adhesion junctions and stress fibre formation in the mechanical behaviour of mesenspheres during osteogenesis. The suspension culture system used provides a useful method to investigate cadherin mechanobiology in the absence of the confounding factor of cell-substrate interaction. This investigation was carried out by silencing N-cadherin or OB-cadherin adhesion junctions with siRNA and measuring mesensphere viscoelastic properties using a parallel plate micro-cantilever system. Additionally changes in cell morphology were examined to ascertain the role of N-cadherin, OB-cadherin and the cytoskeleton on mesensphere biomechanics.

6.2 Methods

6.2.1 Mesensphere Formation and Culture

C57BL/6 mouse mesenchymal stem cell (MSC) monolayers (CliniSciences) were expanded in MSC expansion media (IMDM (Gibco, Grand Island, NY) supplemented with 10% foetal bovine serum (Hyclone, South Logan, UT), 10% horse serum (Hyclone) and 2 mM L-glutamine (Corning, Oneonta, NY)). Cells were maintained in a humidified incubator at 37^{o}C and 5 % CO_2. MSCs were dissociated from adherent culture with 0.25% Trypsin (Corning). MSC spheroids (Mesenspheres) were formed using a forced aggregation technique (Zimmermann and McDevitt 2014) whereby cells are centrifuged (200 rcf) into 400 µm diameter 3% agarose (Fisher, Grand Island, NY) microwells (Aggrewell™ StemCell Technologies INC, Tukwila, WA). MSCs were seeded

(3 x 10^6) into 6000 microwells, yielding mesenspheres of approximately 500 cells (Figure 6.45A). After 12 hrs of spheroid formation in microwells, mesenspheres were transferred to 100 mm bacteriological grade petri dishes (approximately 1500 mesenspheres per petri dish) and cultured in suspension in 10 mL osteogenic supplemented media (MSC expansion media without FBS, supplemented with 100 nM Dexamethasone, 50 µg/ml Ascorbic Acid, 10 mM β-glycerol Phosphate (all Sigma, St. Louis, MO)) on a rotary orbital shaker platform at 65 rpm, similar to previously described methods for culture of embryonic stem cell spheroids (Kinney et al. 2012). Media was exchanged every 3-4 days.

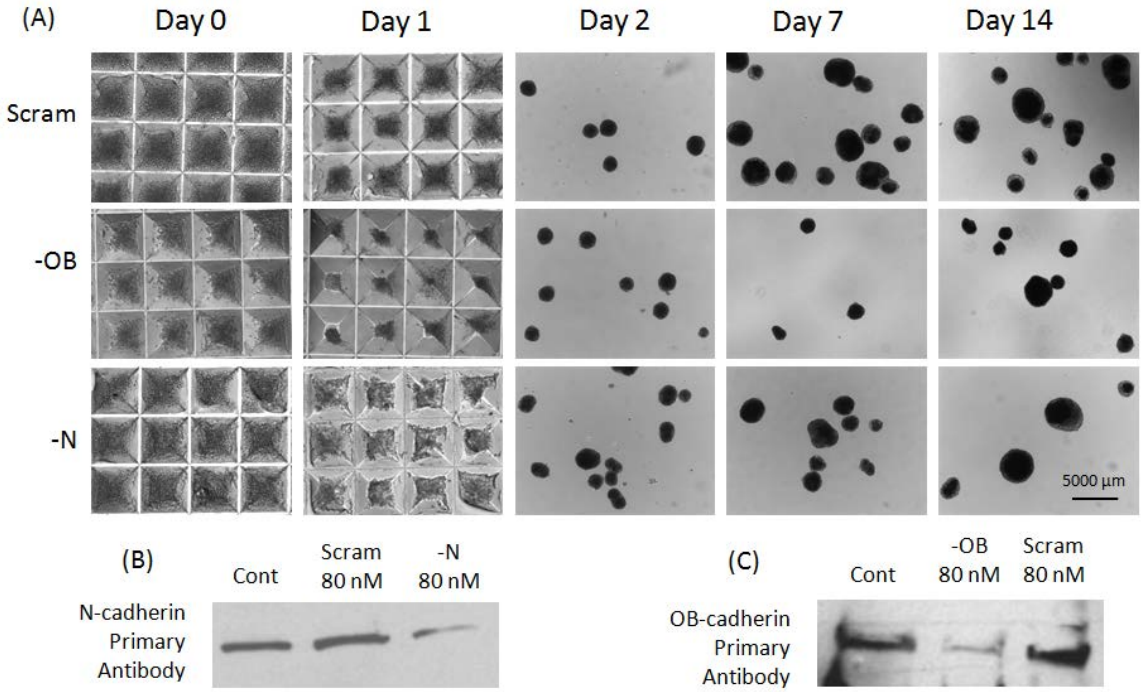

Figure 6.46: (A) Bright field images of mesensphere formation and at days 1, 2, 7 and 14. Mesensphere of approximately 500 cells is formed in each microwell. (B) Western Blot of untreated control MSCs, scrambled siRNA (80 nM) and N-cadherin siRNA (80 nM). (C) Western Blot of untreated control MSCs, OB-cadherin siRNA (80 nM), and scrambled siRNA (80 nM). Western blots shown are representative of western blots of mesenspheres from two separate experiments. Groups: Cont: untreated control, Scram : scrambled siRNA, -N : N-cadherin siRNA, -OB : OB-cadherin siRNA.

6.2.2 siRNA Treatment

The small interfering RNA (siRNA) oligonucleotides for N-cadherin (sc-35999), OB-cadherin (sc-36114) and a scrambled control (sc-37007) were obtained from Santa

Cruz, Dallas, TX. MSC monolayers at 80-90 % confluency in 150 mm bacteriological petri dishes were washed three times with 10 mL PBS and then treated with 80 nM siRNA and 128 µL Lipofectamine 2000 (Invitrogen, Grand Island, NY) in 8 mL of Opti-MEM (Gibco) for 20 hrs prior to mesensphere formation. Knockdown efficiency of siRNA for cadherin protein expression was assessed by Western Blot and compared to untreated cells and cells treated with non-specific scrambled siRNA (Figure 6.45B, C).

6.2.3 Western Blot

Mesenspheres were lysed using CelLytic™ M cell lysis reagent (Sigma) for 15 minutes at room temperature and then centrifuged (12000 g) for 15 minutes to pellet cell debris. Supernatant was transferred to chilled microcentrifuge tubes and stored at -20 ^{0}C. A Coommassie Plus protein assay (Thermo Scientific) was performed to quantify total protein. 50 µg of protein was diluted with 20% 5X loading buffer (1.25 mL 0.5M Tris-HCl, pH 6.8, 1 g SDS (Fisher), 5 mL glycerol (VWR), 5 mg Bromophenol Blue (Sigma), 1.25 mL βME (Sigma), deionised water) and heated to 95 ^{0}C for 5 minutes. Cell lysates were run on 12 % Mini-PROTEAN® TGX™ gels (Bio-Rad) with 5 µL SeeBlue® Plus2 Prestain (Invitrogen), blotted, and proteins were probed with 1:1000 N-cadherin (sc-7939, Santa Cruz) or 1:1000 OB-cadherin (ab151302, Abcam, Cambridge, MA) primary antibody, and a horseradish peroxide (HRP) conjugated secondary antibody (1:1000) (Santa Cruz) and then detected by chemiluminescent (ECL) substrate.

6.2.4 Mesensphere Mechanical Testing Methods

A parallel plate testing system (Microsquisher, CellScale) was used to measure the micro-scale mechanical properties of mesenspheres from non-siRNA treated (control) groups and N-cadherin (-N), OB-cadherin (-OB) and a scrambled control (Scram) siRNA treatment groups at days 2, 7 and 14. This system calculates force via the measurement of beam deflection in response to user defined displacements. All samples were tested in a phosphate buffered saline (PBS) (Corning) fluid bath. Mesenspheres were loaded onto a glass platform and compressed by cantilever beams made of Tungsten (Young's Modulus = 411 GPa). The diameter of the cantilever beams varied from 152.4 µm to 304.8 µm, depending on the relative stiffness of the mesenspheres.

Creep tests were performed to determine the viscoelastic properties of mesenspheres, with the time dependent deformation of the sample being measured under a constant applied force (Figure 6.46). The magnitude of force for the creep test was chosen as the average force corresponding to approximately 40% decrease in mesensphere height. This was determined based on constant strain rate analysis of stress versus vertical strain in n = 6 samples for each time point and condition before commencing creep testing. Steady state deformed configuration was identified from creep test results (Kinney et al. 2014). A minimum of 19 distinct, randomly chosen mesenspheres were creep tested for each time point and condition. The mesensphere is assumed to behave as a homogeneous, isotropic, incompressible standard linear solid (SLS) viscoelastic material. The theory behind the SLS material model is outlined in the Theory chapter. The nominal axial creep strain at time *t*, is given as $\varepsilon(t) = u(t)/H_0$, where $u(t)$ is the change in height of the mesensphere and H_0, the initial undeformed mesensphere height (diameter). σ_o is the applied stress, and was normalised to D_0, the initial mesensphere horizontal diameter. The instantaneous modulus, E_o, the long term modulus, E_∞, and viscosity, μ, are determined by fitting Eqn. 1 to experimental creep curves for each individual sample using the nonlinear least squares fit procedure.

$$\varepsilon(t) = \frac{2\sigma_0}{3E_\infty}\left[1 + \left(\frac{E_\infty}{E_0} - 1\right)\exp\left(-tE_\infty(E_0 - E_\infty)/\mu E_0\right)\right] \quad \text{(Eqn. 1)}$$

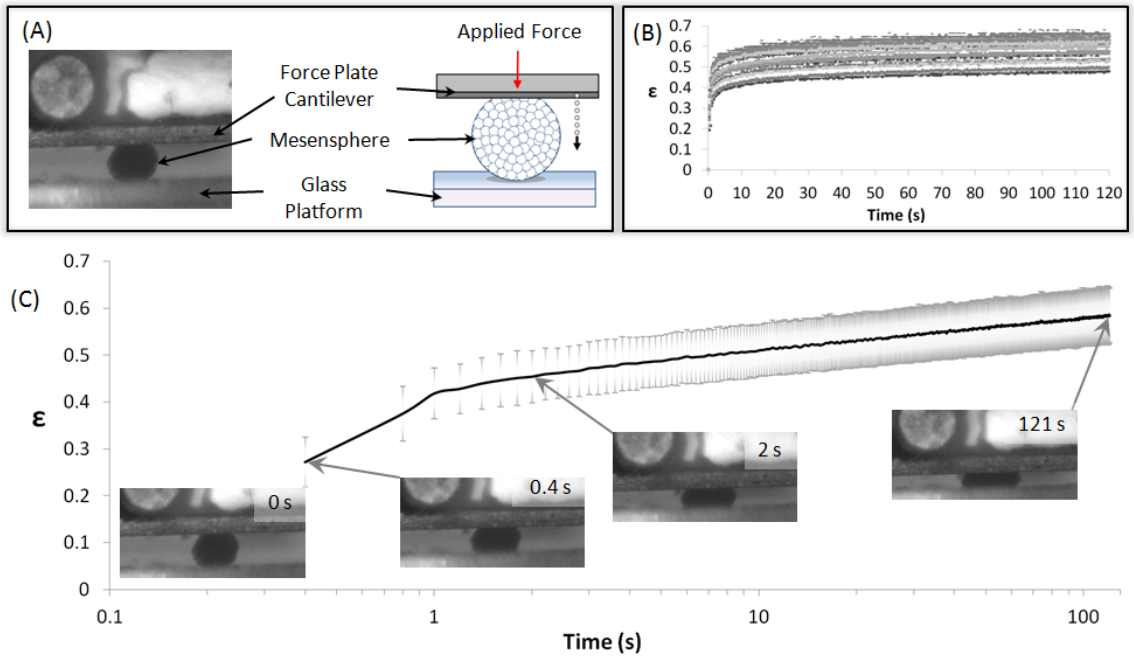

Figure 6.47: (A) Schematic of testing equipment including cantilever for force application (red arrow) and measurement, mesensphere and glass prism. Dotted arrow indicates motion tracking of cantilever displacement during compression of mesensphere. The mesensphere is placed on a glass prism and then a constant force is applied for the duration of the test. (B) Nominal creep strain (ε) calculated as tip displacement normalised to initial mesensphere height. Data from testing of n=19 samples of day 2 Scrambled siRNA treated mesenspheres. (C) Nominal creep strain (ε) for n=19 day 2 Scrambled siRNA treated mesenspheres. The grey borders denote standard deviation of the data. Inset are representative brightfield images showing the initial compression of the mesensphere by the cantilever at 0, 0.4, 2 seconds and the mesensphere in compression at the end of the test (121 seconds).

6.2.5 Histological and Immunofluorescent Staining

4% paraformaldehyde was used to fix mesenspheres at room temperature for 30 minutes. Mesenspheres were rinsed with PBS, embedded within Histogel (Thermo Scientific), and then processed through a series of ethanol and xylene rinses before paraffin embedding. Mesenspheres embedded within paraffin were sectioned at a thickness of 10 µm and then mounted on SuperFrost Plus slides (Fisher). Prior to staining, mesensphere sections were deparaffinised using a series of ethanol and

xylene rinses. Histological staining was done using Gills' III Modified Hemotoxylin and 1% Eosin Y, Alcoholic Solution (Harleco, Cork, Ireland). For immunofluorescent staining, cell membranes were first permeabilised using 0.1% Triton-X (Sigma) in PBS and blocked using 1% Donkey serum (Sigma) in PBS. For immunofluorescent staining, samples were incubated 1:1000 Phalloidin TRITC (P1951, Sigma) and Fluoroshield mounting media with DAPI (F6057, Sigma).

6.2.6 Immunofluorescent Image Analysis

ImageJ software (Fiji) was used to quantify the variation in the actin cytoskeleton between treatment groups (n = 6 aggregates per group). To analyse the cytoskeleton fluorescence, the raw Phalloidin TRITC channel was separated from the nucleur staining channel (DAPI), and then thresholded to remove nonspecific background staining. The percentage of the mesensphere cross-sectional area that was above the threshold was recorded.

6.2.7 Statistical Analysis

For creep testing results, statistics were performed using Minitab on n = 19 individual mesenspheres for each group. Statistical tests between treatment group and time point were carried out using Kruskal-Wallis non-parametric test between individual groups when data was non-normally distributed or had unequal variance. A Levene's test for equal variance was conducted on each group to test for variance. Statistical significance was declared at $p \leq 0.05$. To analyse the correlation between mesensphere diameter and viscosity or Young's moduli, a Pearson's Correlation coefficient (r) for each treatment group and time point was calculated. r ranges from -1 for a perfect negative linear relationship to +1 for a perfect positive linear relationship between two variables. Correlation was considered significant if $r \leq -0.6$ or $r \geq 0.6$ and if $p \leq 0.05$. The band in each box plot represents the data median, and the cross represents the mean. Boxplot whiskers extend to data points that are less than 1.5 x Interquartile Range from the 1st/3rd quartile.

6.3 Results

6.3.1 Osteogenic differentiation causes higher mesensphere viscosity and long term Young's modulus

The maximum force applied during constant strain rate compression of mesenspheres until 40% reduction in mesensphere height is shown in Figure 6.47. The viscosity (μ), instantaneous Young's modulus (E_0) and long term Young's modulus (E_∞) of non-siRNA treated mesenspheres (Cont) was higher with osteogenic differentiation between days 2, 7 and 14 (Figure 6.48). This was demonstrated by significantly higher viscous resistance to deformation at day 14 in comparison to day 2 and day 7 ($p<0.001$). Significantly higher E_∞ at day 14 in comparison to days 2 and 7 ($p<0.001$) was observed (Figure 6.48). Significantly higher E_0 at day 14 in comparison to days 2 and 7 ($p<0.001$) was also observed (Figure 6.48).

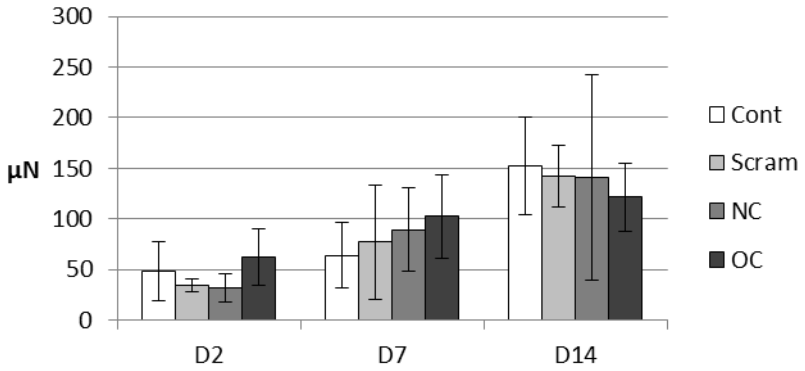

Figure 6.48 Compression force required to decrease mesensphere height by 40% during constant strain rate tests.

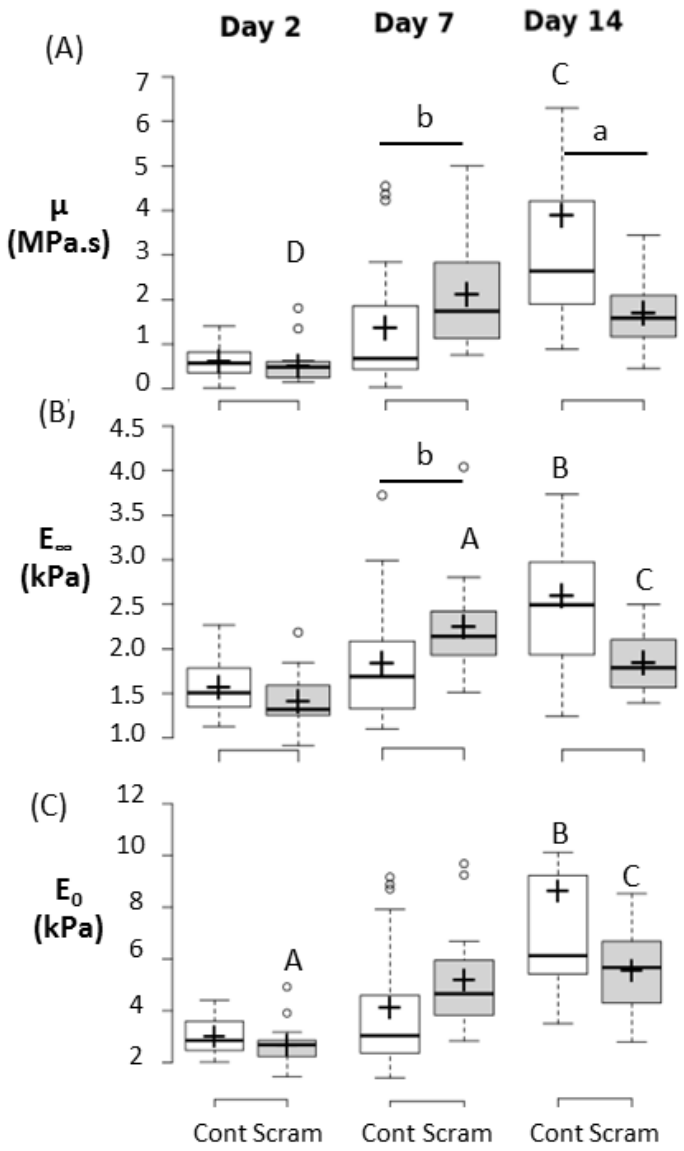

Figure 6.49**:** Scrambled siRNA treatment causes reduced mesensphere viscosity (μ), long term Young's modulus (E_∞) and instantaneous Young's modulus (E_0). Box Plots of (A) Viscosity (μ), (B) Long Term Young's Modulus (E_∞), and (C) instantaneous Young's modulus (E_0) for untreated cells (Cont) and scrambled siRNA treated cells (Scram). For each group/timepoint, n=19 from at least two experiments. Significance is declared at $p < 0.05$. For comparison between time points: For (A) C: a vs. days 2 & 7 Cont, D: a vs. days 7 & 14 Scram. (B) A: a vs. days 2 Scram, B: a vs. days 2 & 7 Cont & day 14 Scram, C: a vs. days 2 & 7 Scram. (C) A: a vs. days 7 & 14 Scram, B: b vs. days 2 & 7 Cont, C: c vs. day 7 Cont. Groups: Scram : scrambled siRNA, -OB : OB-cadherin siRNA, -N : N-cadherin siRNA.

6.3.2 Scrambled siRNA treatment lowers mesensphere viscosity and long term Young's modulus

Control mesenspheres had significantly higher μ and E_∞ than scrambled siRNA treated mesenspheres (Scram) at day 14 ($p=0.001$, $p<0.001$ respectively) (Figure 6.48). Scrambled mesenspheres had significantly higher μ, E_0 and E_∞ than Control at day 7 ($p=0.006$, $p=0.016$, $p=0.006$ respectively). Together, these results indicate a significant effect of siRNA treatment on the mesensphere viscoelastic behaviour. Mean and standard deviation values of μ, E_0 and E_∞ are detailed in Table 6.2.

Table 6.2: Summary table of viscoelastic material constants for Osteogenic control (Control), scrambled siRNA (Scram), OB-cadherin siRNA (-OB), N-cadherin siRNA (-N) treatment groups at days 2, 7 and 14.

		Short term Young's Modulus (E_0) (Pa)		Long term Young's Modulus (E_∞) (Pa)		Viscosity (μ) (MPa.s)	
	Day	**Mean**	**St. Dev.**	**Mean**	**St. Dev.**	**Mean**	**St. Dev.**
Cont	**2**	3060	664	1576	312	6.03E+05	3.29E+05
Scram		2690	789	1422	315	5.32E+05	4.12E+05
-OB		3910	576	1839	346	1.09E+06	4.17E+05
-N		2610	845	1518	364	5.22E+05	4.62E+05
Cont	**7**	3870	2300	1801	715	1.33E+06	1.48E+06
Scram		5130	1920	2198	556	2.04E+06	1.17E+06
-OB		5090	3730	2116	671	2.03E+06	2.52E+06
-N		3140	1380	1555	444	8.12E+05	8.59E+05
Cont	**14**	8640	8860	2552	851	3.76E+06	4.49E+06
Scram		5320	1750	1817	313	1.63E+06	7.99E+05
-OB		5790	1450	2046	257	1.80E+06	5.29E+05
-N		5300	1680	1978	417	1.69E+06	1.09E+06

6.3.3 Mesensphere viscosity and long term Young's modulus are higher with OB-cadherin siRNA treatment

The effects of the siRNA silencing of N-cadherin (-N) and OB-cadherin (-OB) on mesensphere μ, E_0 and E_∞ were most apparent at day 2. At day 2 the μ, E_0 and E_∞ (Figure 6.49) of -OB mesenspheres were significantly higher in comparison to scrambled ($p<0.001$, $p<0.001$, $p<0.001$ respectively) and -N mesenspheres ($p<0.001$, $p<0.001$, $p<0.01$ respectively). -N showed significantly lower μ, E_0 and E_∞ than scrambled and -OB mesenspheres at day 7 ($p<0.012$, $p<0.01$, $p<0.002$ respectively). By day 14, there was no significant difference between μ, E_0 and E_∞ for Scram, -N and -OB mesenspheres.

Mesenspheres from all groups displayed significantly higher μ (all $p<0.001$), E_0 (all $p<0.001$) and E_∞ (all $p<0.004$) between days 2 and 14 (Figure 6.48, Figure 6.49).

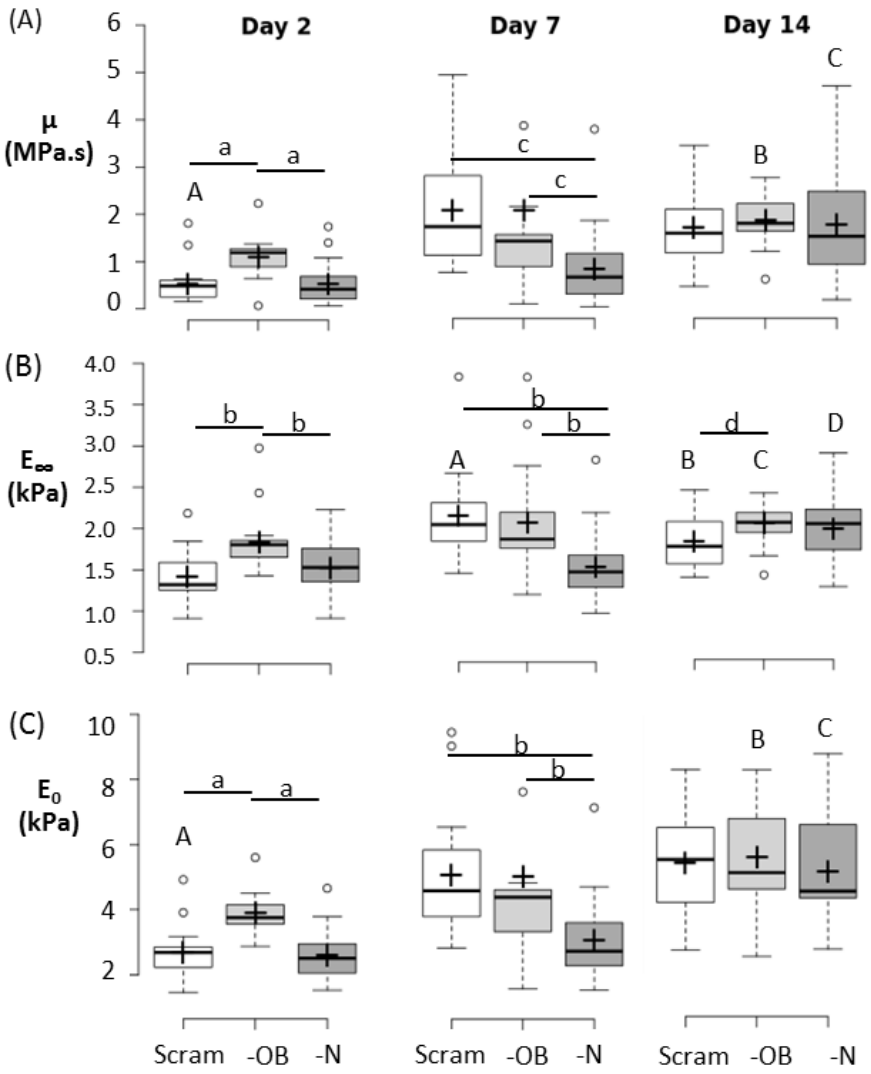

Figure 6.50: -OB mesensphere viscosity (μ), instantaneous Young's modulus (E_0) and long term Young's modulus (E_∞) are higher than Scram and -N at day 2. Box-plots of (A) μ, (B) E_∞, and (C) E_0 comparing between treatment groups during each time point or comparing between time points within each group for day 2, day 7, and day 14. For each group/timepoint, n=19 from at least two experiments. Significance is declared at $p < 0.05$. a: $p<0.001$, b: $p<0.01$, c: $p<0.02$, d: $p<0.05$. For comparison between time points: (A) A: a vs. days 7 & 14 Scram, B: d vs. day 2 & 7 –OB, C: b vs. days 2 & 7 –N. (B) A: a vs days 2 Scram, B: d vs day 2 & 7 Scram, C: d vs day 2 –OB, D: b vs days 2 & 7 –N. (C) A: a vs days 7 & 14 Scram, B: b vs days 2 & 7 –OB, C: a vs days 2 & 7 –N. Groups: Scram : scrambled siRNA, -OB : OB-cadherin siRNA, -N : N-cadherin siRNA.

6.3.4 OB-cadherin silencing causes higher stress fibre formation

Silencing of OB-cadherin resulted in significantly higher immunofluorescent intensity of the cytoskeletal network of mesenspheres in comparison to scrambled (-OB vs. Scram, day 2: $p<0.0001$, day 7: $p=0.003$) and -N (-OB vs. -N, day 2: $p=0.017$, day 14: $p=0.020$) mesenspheres (Figure 6.50A, C). At all time points, -N stress fibre formation did not significantly differ from Scram. This indicates that OB-cadherin may have more influence on stress fibre formation than N-cadherin adhesion junctions. H & E staining demonstrated no discernible difference in cellular morphology between mesenspheres of different groups or time points at days 2, 7 or 14 (Figure 6.50B).

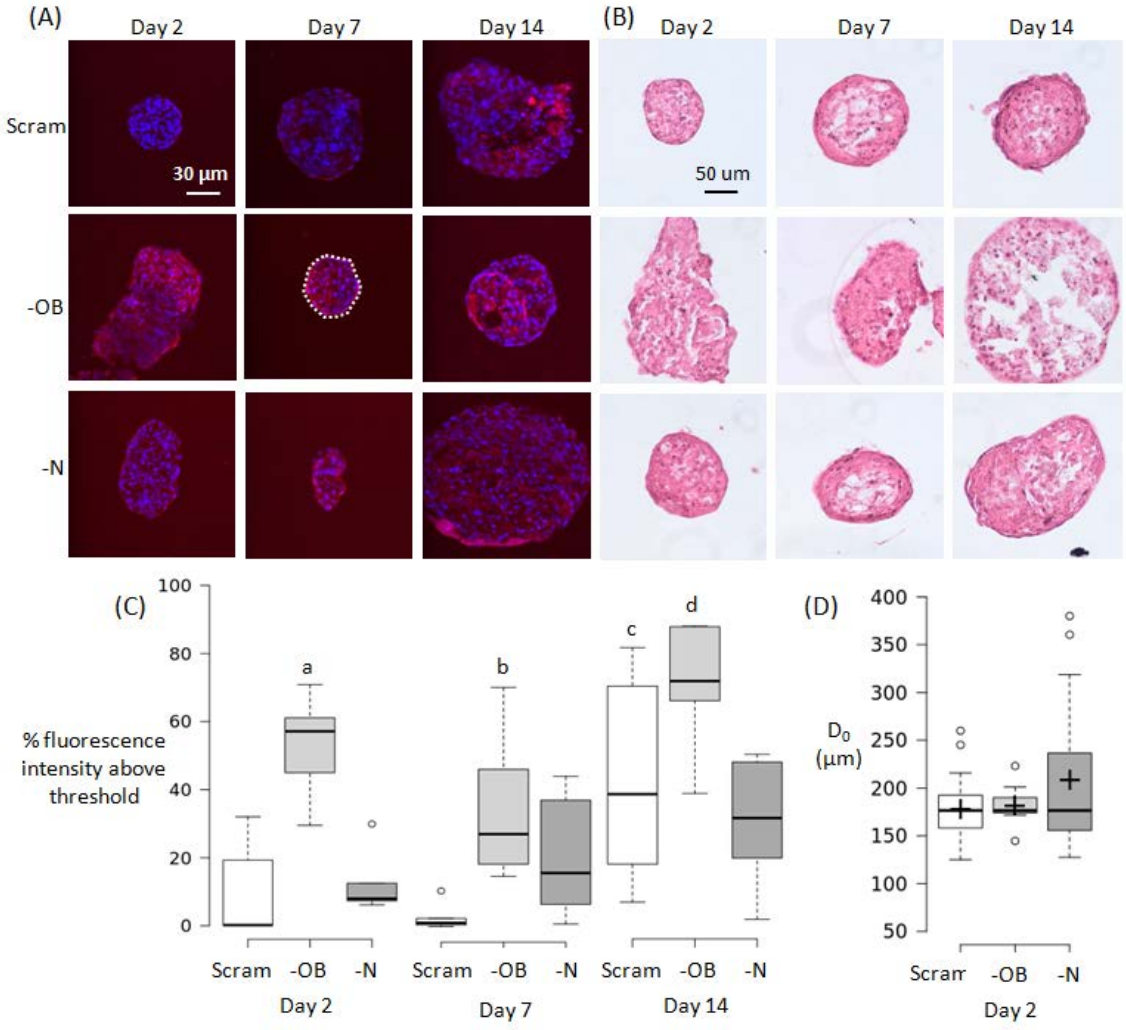

Figure 6.51: (A) Immunofluorescent images of mesenspheres at day 2, 7 and 14. The nucleus (blue) is stained with DAPI and the cytoskeleton (red) is stained with TRITC Phalloidin. The white dashed line in the central panel encloses the mesensphere area analysed for fluorescence intensity in that image. (B) H&E staining of mesenspheres at day 2, 7 and 14. (C) Boxplots of Day 2 cytoskeletal fluorescence showing % intensity above the threshold value. n=6 samples for each group and time point. (D) Horizontal diameter of mesenspheres at day 2 measured before mechanical testing. Groups: scrambled siRNA (Scram), OB-cadherin siRNA (-OB), N-cadherin siRNA (-N). Kruskal-Wallis non-parametric tests were performed and significance is declared at $p < 0.05$. For (C) a<0.002 vs. day 2 (Scram, –N). b=0.003 vs. day 7 Scram. c=0.023 vs. days 2 & 7 Scram. d<0.02 vs. 7 (-OB) and day 14 (-N).

6.3.5 Mesensphere size effects of siRNA treatment

Treatment of MSCs with siRNA resulted in a larger maximum diameter (D_0) of -N mesenspheres (D_0 = 380 µm) than -OB (D_0 = 223 µm) and Scram (D_0 = 259 µm) at day 2 (Figure 6.50D). Larger -N mesenspheres could be indicative of impaired initial

compaction of the cells, suggesting a role for N-cadherin in initial mesensphere formation. At days 2, 7 and 14, there was a strong negative correlation between mesensphere horizontal diameter and μ, E_0 or E_∞ for Scram mesenspheres (Table 6.3), i.e., larger mesenspheres showed less viscous resistance to deformation. -OB mesenspheres had a significant negative correlation at day 2 for μ and E_∞ and day 7 E_0 and E_∞, Untreated mesenspheres had a negative correlation between horizontal diameter and μ, E_0 or E_∞ at day 7. -N mesenspheres displayed a positive correlation between horizontal diameter and μ but a negative correlation with μ, E_0 or E_∞ at day 14. .

Table 6.3: Pearson's Correlation Coefficient (r) and correlation significance (p) for the correlation between mesensphere diameter and viscosity (μ), Long term Young's Modulus (E_∞), and instantaneous Young's Modulus (E_0). Groups: Osteogenic control (Control), scrambled siRNA (Scram), OB-cadherin siRNA (-OB), N-cadherin siRNA (-N).

		Viscosity (μ) (Pa.s)			**Long term Young's Modulus (E_∞) (Pa)**			**Short term Young's Modulus (E_0) (Pa)**		
		D2	**D7**	**D14**	**D2**	**D7**	**D14**	**D2**	**D7**	**D14**
Control	**r**	-0.582	-0.717	-0.484	-0.514	-0.605	-0.581	-0.699	-0.776	-0.464
	p	0.009	0.001	0.036	0.024	0.006	0.009	0.001	0.000	0.046
Scram	**r**	-0.710	-0.788	-0.933	-0.860	-0.707	-0.940	-0.880	-0.786	-0.938
	P	0.001	0.001	0.001	0.001	0.001	0.001	0.001	0.001	0.001
-OB	**r**	-0.666	-0.576	-0.221	-0.563	-0.713	-0.097	-0.829	-0.626	-0.226
	P	0.002	0.010	0.363	0.012	0.001	0.693	0.001	0.004	0.353
-N	**r**	0.633	0.040	-0.907	0.230	0.020	-0.811	0.445	-0.085	-0.916
	P	0.004	0.872	0.001	0.343	0.936	0.001	0.056	0.728	0.001

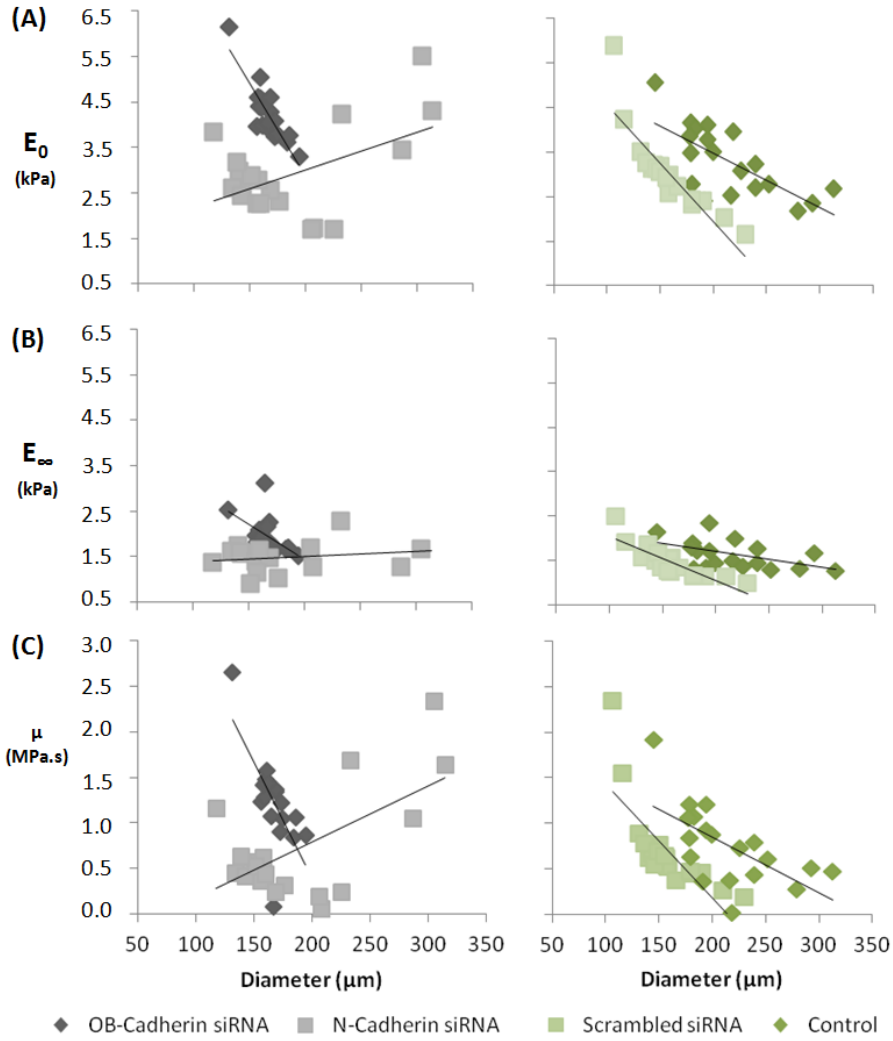

Figure 52 Graphs showing the relationship between Day 2 mesensphere diameter and mesensphere A) short term modulus (E_0), B) long term modulus (E_∞) and C) viscosity (μ).

6.4 Discussion

The overall goal of this study was to investigate the role of adhesion junctions and cytoskeleton stress fibre formation in the mechanical behaviour of mesenspheres undergoing osteogenic differentiation. Mesensphere mechanical behaviour and morphology were analysed at days 2, 7 and 14 to investigate the contribution of N-cadherin or OB-cadherin adhesion junctions and the cytoskeleton to the mechanics of the mesensphere. It was found that silencing of N-cadherin (-N) or OB-cadherin (-OB) expression yielded different effects on the mesenspheres. When OB-cadherin was silenced, the viscosity (μ), initial Young's modulus (E_0), long term Young's modulus (E_∞) and actin stress fibre formation of the mesenspheres was higher in comparison to -N mesenspheres and mesenspheres treated with a scrambled siRNA (Scram) at day 2. Additionally, μ, E_0 and E_∞ were higher for Scram mesenspheres between days 2 and 7, whereas this effect was not observed in -OB and -N treated groups. Taken together, these results indicate that N-cadherin and OB-cadherin both influence mesensphere biomechanics but play different roles and this is likely due to their connectivity to the cytoskeleton.

A potential limitation of this study is the compacted arrangement of cells in a mesensphere, which might lead to diffusion difficulties for nutrients and molecules through 3D constructs due the size of the construct (Sachlos and Auguste 2008). However mesenspheres of 300, 600 or 1000 cells grown in a similar orbital suspension system did not exhibit evidence of necrotic core formation through 14 days of culture (Baraniak and McDevitt 2012). Secondly, the results presented here demonstrate that mesenspheres treated with scrambled siRNA had a higher μ, E_0 and E_∞ than untreated cells at day 7, and lower at day 14. However, previous work using a scrambled siRNA on fibroblasts demonstrated a lower Young's modulus than control cells (Lee et al. 2012). In the work presented here mesenspheres treated with N-cadherin or OB-cadherin siRNA were compared to those treated with scrambled siRNA, rather than untreated cells, so as to account for any change in μ, E_0 and E_∞ resulting from siRNA treatment alone. The assumption of small deformations used in the Standard Linear Solid (SLS) material model used to calculate the material properties of the mesenspheres creates a possible limitation. Mesenspheres experienced strains up to approximately 70%. However, previous studies have demonstrated that the

infinitesimal strain assumption may still be accurate for a viscoelastic halfspace model under micropipette aspiration (cellular strains of greater than 30% were generated) (Haider and Guilak 2002). The parallel plate compression testing system used here is advantageous as it allows for the measurement of the creep strain of a composite material consisting of >500 cells. In comparison, testing of single cells (e.g. Atomic Force Microscopy (AFM)) will result in a high level of variability between samples, and the assumption of a homogeneous isotropic material cannot be justified when choosing a model to interpret single cell data (Reynolds and McGarry 2015; Weafer et al. 2015).

Creep testing of spherical aggregates of embryonic stem cells (EBs) has been performed using the same parallel plate compression testing system (Kinney et al. 2014). The long term Young's modulus of EBs was 0.21 kPa after 14 days of mesenchymal differentiation (Kinney et al. 2014). The results presented in the current paper for control mesenspheres at day 2 reveal that the E_∞ (1.58 ± 0.31 kPa) is approximately three-fold higher than the E_∞ for spherical, unspread MSCs (0.47 ± 0.52 kPa) as measured using AFM testing of single cells (Darling et al. 2008). Interestingly, the control mesensphere E_∞ was approximately 0.7 that of spread MSCs (2.27 ± 1.9 kPa). In contrast to unspread cells, spread cells exhibit highly developed stress fibres. A previous study by (Ronan et al. 2012) demonstrates that the compression resistance of the cell is heightened by the contractile stress fibre network. While cells in mesenspheres do not exhibit the extensive stress fibre network reported for cells spread on stiff substrates, mesenspheres do possess some stress fibres due to the mechanical stimulus generated between neighbouring cells that is transmitted via cell-cell adhesions.

Previous work has shown that the elastic modulus of MSCs is significantly influenced by the cytoskeleton (Titushkin and Cho 2007). Adhesion junctions transmit mechanical forces such as cytoskeletal tension between cells (Ganz et al. 2006; Maruthamuthu et al. 2011) and are strengthened and stabilised by interaction with the cytoskeleton (Pittet et al. 2008; Liu et al. 2010b; Hong et al. 2013; Ronan et al. 2015). The results presented in this chapter demonstrate that the cytoskeleton/adhesion junction relationship is reciprocal; adhesion junctions also influence stress fibre formation and mesensphere mechanical behaviour. Specifically, the results presented

in this chapter show for the first time that higher stress fibre formation, μ, E_0 and E_∞ occur when OB-cadherin expression is inhibited in mesenspheres. Interestingly, the higher μ, E_0 and E_∞ between days 2 and 7 for Scram mesenspheres does not coincide with higher stress fibre formation, perhaps suggesting that the gradual increase in μ, E_0 and E_∞ from Day 2 to Day 14 for mesenspheres within each treatment group is not generated by more cytoskeleton stress fibres. The higher μ, E_0 and E_∞ could be due to the gradual secretion of collagen and osteogenic proteins and minerals as the cells undergo osteogenic differentiation. Scram and -OB mesenspheres showed a trend of less stress fibre formation between days 2 and 7, but significant higher formation only occurred between days 7 and 14. -N mesenspheres showed gradually higher stress fibre formation, but no significant difference between time points. The different influences on stress fibre formation, μ, E_0 and E_∞ could indicate that N-cadherin interacts differently than OB-cadherin, either via biochemical or mechanosensory means, with stress fibre regulatory pathways. Alternatively, the higher stress fibre formation in OB-cadherin inhibited mesenspheres may compensate for less passive tension previously facilitated through OB-cadherin.

Chapter 7:

Discussion

7.1. Introduction

This chapter summarises the main findings of this PhD thesis, drawing together the insight obtained from the computational and experimental studies performed to provide a greater understanding of the role of adhesion junctions in mechanobiology, with a particular focus on osteogenesis of osteoblast and mesenchymal stem cells. The results of the individual research chapters of this thesis are summarised in Section 7.2, and are graphically represented in Figure 7.1. Section 7.3 discusses how the results presented in this thesis build upon the current understanding of this topic from studies conducted by other researchers prior to this thesis. The key results of this thesis are discussed in the context of other relevant publications, and the implications of these findings for the field of cell mechanobiology and adhesion junction mechanosensation and bone diseases such as osteoporosis and metastatic cancer are explored. Section 7.4 details recommendations for future work and Section 7.5 contains concluding remarks.

7.2. Main Findings of the Thesis

The research described in this thesis has focused on deriving an understanding of the role of adhesion junctions for (1) osteogenic mechanotransduction of fluid shear stress stimulation of bone cells and (2) dictating material properties of mesenchymal stem cells undergoing osteogenic differentiation. In particular, the results of this thesis sought to determine whether adhesion junction mechanosensation is a contributing factor to fluid shear stress stimulated osteogenesis, and whether adhesion junctions influence the mechanical properties of 3D cellular aggregates undergoing osteogenesis. A combination of computational work and in vitro experimentation was used to (1) ascertain the stimulus applied to osteoblasts during fluid shear stress stimulation, and (2) understand the contribution of adhesion junctions to the resulting biochemical response, particularly focused on osteogenic differentiation. Moreover, a

3D, spherical cellular aggregate culture system was used to investigate the influence of adhesion junctions on the viscoelastic mechanical properties of mesenchymal stem cells undergoing osteogenesis. The key contributions of each hypothesis are summarised below.

Hypothesis 1: The osteogenic response of pre-osteoblasts to fluid shear stress is inhibited by a reduction in adhesion junctions..

The first study of this thesis, presented in Chapter 4, used in vitro cell culture methods to demonstrate that adhesion junction mechanotransduction is required for the osteogenic response of osteoblasts to oscillatory fluid shear stress (OFSS) in a parallel plate flow chamber. The normal response of osteoblasts to OFSS is higher PGE_2 production and upregulate Cox-2 gene expression (Chen et al. 2000; Saunders et al. 2001; Donahue et al. 2003; Saunders et al. 2003; Malone et al. 2007b), as is reported in this thesis. Higher Runx2 gene expression was also observed in response to OFSS. Chapter 4 of this thesis demonstrated that MC3T3-E1 respond differently to oscillatory (OFSS) or pulsatile (PFSS) fluid shear stress with regard to their stress fibre formation and PGE_2 expression. The results of this study showed that upon inhibition of adhesion junction formation in MC3T3-E1 cells, using EGTA as a pre-treatment before FSS application, there was not significantly higher PGE_2 production, or upregulation of Cox-2 or Runx2 expression following 1 Pa of oscillatory FSS stimulation for 1 hour. This study also showed using immunofluorescent image analysis that OFSS caused significantly more stress fibre formation for control samples, and this heightened stress fibre formation with OFSS stimulation was not inhibited by AJ inhibition. As such, the results of this study provide evidence to support Hypothesis 1; "*The osteogenic response of pre-osteoblasts to fluid shear stress is inhibited by a reduction in adhesion junctions.*".

Hypothesis 2: Fluid shear stress stimulus results in pressure dependent compression and tension of cell-cell contacts.

The second study of this thesis, presented in Chapter 5, employed fluid-structure interaction (FSI) modelling to determine the contributions of hydrostatic pressure and cell contractility to the stresses experienced at cell-cell contacts between adjacent cells

during application of oscillatory FSS or steady FSS in a parallel plate bioreactor. A global computational fluid dynamics (CFD) model was developed to characterise the oscillating fluid flow within the entire bioreactor system, and the fluctuations in pressure and fluid velocity at a central point in the FSS chamber were predicted. The velocity and pressure results were then used as inlet and outlet boundary condition, respectively, for a local FSI model of cells pairs within a parallel plate bioreactor, and the stresses experienced at the cell-cell contact surface of osteoblasts within this complex multiphysics system were determined. The results of this study predicted that oscillatory FSS resulted in sinusoidal oscillations in hydrostatic pressure within the flow chamber from a positive to a negative pressure (±1000 Pa) with each oscillation of the fluid flow. The positive pressure compresses cell-cell contacts (approx. -300 Pa), while the negative pressure applies tension to the cell-cell contacts (approx. 450 Pa). Thermal contractility that was calibrated against in vitro stress patterns generated by contractile canine kidney cells on a PA gel (Maruthamuthu et al. 2011), was used to represent the contractile cell cytoskeleton. Cell contractility produced tensile stress (approx. 140 Pa) at the cell-cell contacts. With application of oscillatory FSS, the compressive stress arising from the negative hydrostatic pressure competed with the tensile stress caused by cell contraction and put the cell-cell contact into net compressive stress (approximately -170 Pa). Application of steady FSS generated only a positive pressure (1000 Pa) within the bioreactor chamber and applied only compressive stress to the cell-cell contacts. Tension is required to maintain adhesion junction stability (Hong et al. 2011; Hong et al. 2013) so the change from tension to compression due to hydrostatic pressure creates an unfavourable mechanical environment for adhesion junction formation or maintenance. The PFSS profile used to stimulate cells in Chapter 4, as well as steady FSS, both employ a positive hydrostatic pressure at one end of the fluid flow chamber, and atmospheric pressure is at the other end to create unidirectional flow. Positive hydrostatic pressure only results in compression at the cell-cell contact area. Together, these two studies show the in vitro difference in cellular response to different FSS regimes (Chapter 4), and the difference in cell stress and strain in response to different FSS regimes (Chapter 5). The results of this study provide evidence to support Hypothesis 2; “Fluid shear stress stimulus

results in pressure dependent compression and tension of cell-cell contacts." and shed light on the different stimulus applied by different fluid flow regimes.

Hypothesis 3: Adhesion junctions can regulate the mechanical properties of mesenchymal stem cell aggregates.

The third study of this thesis, presented in Chapter 6, used a 3D suspension culture technique to investigate cell biomechanics without the confounding factor of cell-substrate interaction. Specific adhesion junctions, namely OB-cadherin or N-cadherin, were silenced and their individual contributions to MSC viscoelastic properties were investigated by performing creep testing. The results of the study demonstrated that OB-cadherin and N-cadherin play different roles on the viscoelastic material properties of mesenchymal stem cells (MSCs) undergoing osteogenic differentiation. Specifically it was shown that viscoelastic material properties (viscosity, instantaneous and long term Young's moduli) were higher with culture in osteogenic differentiation media up to 14 days when no cadherins were silence in MSCs. However, at day 2 OB-cadherin silencing resulted in significantly higher instantaneous and long term Young's moduli, and viscosity of the MSC aggregates, in comparison to MSC aggregates treated with a scrambled control, or N-cadherin silenced MSCs. By day 14, there was no significant difference in the viscoelastic material properties between any treatment groups. Furthermore, immunofluorescent image analysis revealed that OB-cadherin silencing resulted in significantly more stress fibre formation at all time points in comparison to control MSCs and this likely contributes to the differences in viscoelastic material properties between these groups. The results presented in this study provide evidence to support Hypothesis 3; "Adhesion junctions can regulate the mechanical properties of mesenchymal stem cell aggregates", and illustrate the different mechanical and structural responses to removal of OB-cadherin or N-cadherin.

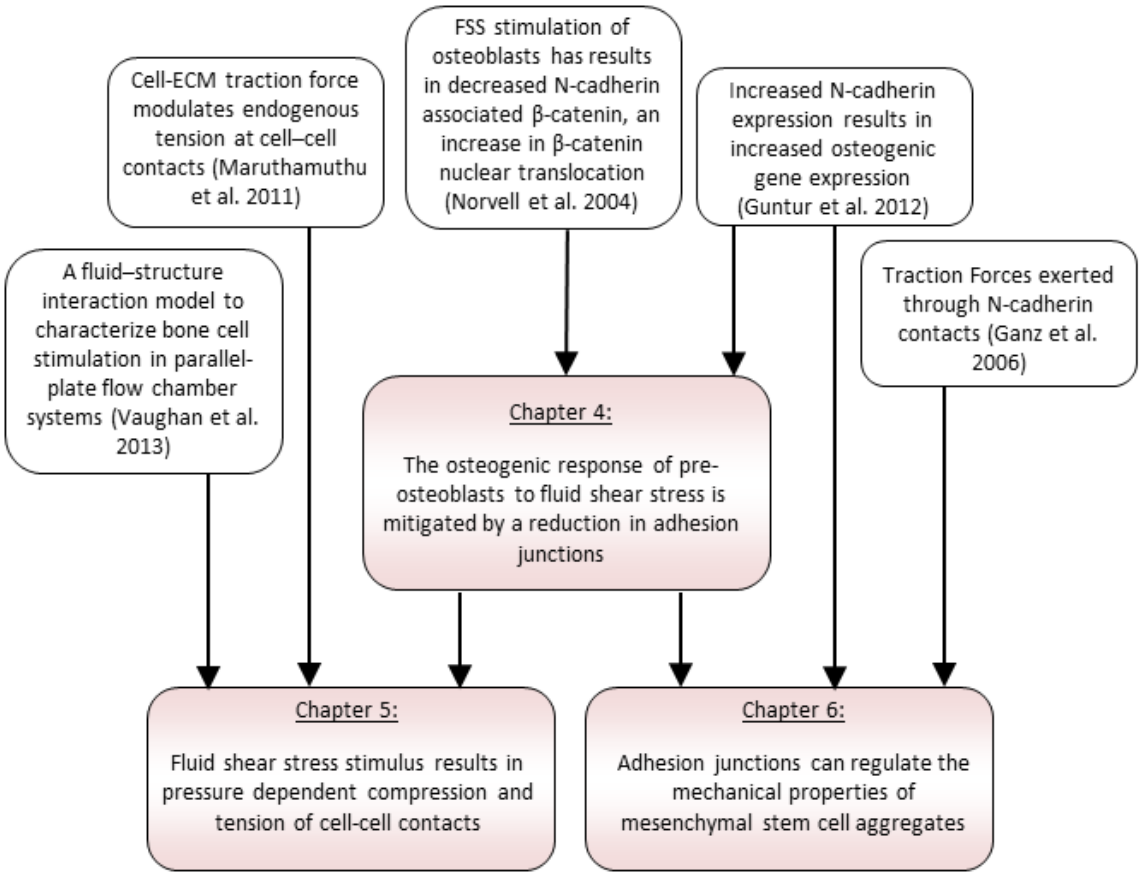

Figure 7.53 Graphical Representation of the work done as part of this PhD thesis, in the context of previous studies.

7.2.1 Thesis Summary

The unifying theme of this thesis is to understand the role of adhesion junctions in sensing or generating the mechanical environment of osteogenic stem cells. Chapter 4 explores pre-osteoblast adhesion junction mechanosensation of fluid shear stress, Chapter 5 characterises the stimulus imparted to the cells during the experiments of Chapter 4, and Chapter 6 explores the influence of adhesion junctions of the viscoelastic material properties of mesenchymal stem cells during osteogenesis.

7.3. Insight into adhesion junction mechanobiology

As discussed in Chapters 2, 4 and 5 of this thesis, the phenomenon of osteoblast mechanosensitivity to FSS is well documented and the cellular responses following FSS stimulation include significantly higher transcription of osteogenic genes (e.g. Cox-2,

Runx2) (Wadhwa et al. 2002; Bakker et al. 2003a; Mehrotra et al. 2006) and significantly higher expression of proteins associated with osteogenesis (PGE_2) (Kapur et al. 2003; Vance et al. 2005). Previous studies in the area of osteoblast mechanosensation have investigated the potential mechanosensing mechanisms responsible for the transcription of mechanical stimulus into a cellular response. It has been previously demonstrated that integrins are important mechanosensors of FSS in osteoblasts (Pavalko et al. 1998; Lee et al. 2008a) and osteocytes (Litzenberger et al. 2010; Haugh et al. 2015). These studies have shown that integrin mechanosensation is a contributing factor to Cox-2 gene expression (Lee et al. 2008a) and of production of PGE_2 (Litzenberger et al. 2010; Haugh et al. 2015). Similarly, primary cilia are important mechanosensors of FSS in osteoblasts (Malone et al. 2007b; Delaine-Smith et al. 2014), osteocytes (Wheatley et al. 1996; Malone et al. 2007b; Kwon et al. 2010) and MSCs (Hoey et al. 2012b). It was demonstrated that primary cilia mechanotransduction promotes bone production in vivo in response to mechanical loading (Chen et al. 2016), is independent of Ca^{2+} flux in osteocytes (Malone et al. 2007b) and contributes to the higher Cox-2 gene expression in response to FSS (Kwon et al. 2010; Hoey et al. 2012b). Additionally, it has been shown that FSS activates gap junction hemichannels (Cheng et al. 2001a; Genetos et al. 2007; Huo et al. 2008; Ishihara et al. 2013). These studies have documented the importance of these structures in sensing the mechanical environment and transducing this into a cellular response. In particular, it has been shown that inhibition of integrins caused a reduction in Cox-2 (Pavalko et al. 1998; Haugh et al. 2015) gene expression and PGE_2 production (Ponik and Pavalko 2004; Haugh et al. 2015) in response to FSS stimulation, indicating that integrins play an important role in mechanosensation for osteogenesis. Similarly, the removal of primary cilia caused significantly lower Cox-2 and bone morphogenetic protein 2 (BMP2) gene expression (Malone et al. 2007b; Hoey et al. 2012b) in response to FSS.

7.3.1. Adhesion Junction Mechanotransduction of Oscillatory FSS

The ability of adhesion junctions to transduce FSS stimulation, within a parallel plate bioreactor, into canonical Wnt signalling has been previously documented (Norvell et al. 2004a; Arnsdorf et al. 2009a). Recent experiments have established the importance

of AJs in osteogenesis of osteoblast and MSC cells grown under static conditions. Specifically, when AJs are decreased in static conditions using either EGTA, N-cadherin antibody or decreased confluency, the expression of osteogenic genes osterix, osteomodulin and osteoglycin is significantly lower than control samples (Guntur et al. 2012). In static conditions, adhesion junctions sequester β-catenin in the junction (Norvell et al. 2004a; Arnsdorf et al. 2009a). β-catenin is an important signalling molecule in the canonical Wnt signalling pathway (Moon et al. 2002; Westendorf et al. 2004) as free β-catenin in the cytosol can translocate into the nucleus and upregulate osteogenic gene expression. Initial investigations into the role of AJs in the mechanotransduction of FSS demonstrated that β-catenin is released from the adhesion junction when FSS is applied to osteoblasts (Norvell et al. 2004a) and MSCs (Arnsdorf et al. 2009a). When adhesion junction formation is inhibited, there are reduced stores of sequestered β-catenin that can be released in response to FSS (Fagotto and Gumbiner 1994; Tufan and Tuan 2001). However, whether adhesion junctions play a role in osteogenic differentiation of pre-osteoblasts under mechanical stimulation had not previously been investigated. Adding to previous work showing that adhesion junctions sequester β-catenin and release this β-catenin in response to FSS, the work presented here showed that inhibition of adhesion junction formation resulted in no significantly higher PGE_2 production, or Cox-2 and Runx2 gene expression in response to oscillatory FSS.

7.3.2. Cytoskeletal response to FSS

Stress fibres form in response to their mechanical environment and, in static conditions, stress fibres can be seen orientated at random when cells such as osteoblasts and osteocytes adhere to glass substrates (Jaasma et al. 2007; Malone et al. 2007c; Ponik et al. 2007). A variety of previous studies have shown that under fluid flow stimulus the cytoskeleton reorganises and forms thick stress fibres that align to the long axes of the cell or with the direction of flow (Jaasma et al. 2007; Malone et al. 2007c; Ponik et al. 2007). In the work presented in Chapter 4, it was shown that a reduction in adhesion junction, by means of EGTA treatment, did not inhibit stress fibre formation in response to OFSS stimulation. A previous study demonstrated using

immunofluorescent staining that adhesion junctions and cytoskeletal stress fibres in endothelial cells re-organise in response to steady FSS; in static conditions both junctions and fibres are mainly dispersed along the cell-cell boundary but the adhesion junctions reorganise into punctate clusters of adhesion junctions at which stress fibres (now spanning the length of the cell) are seen to terminate when steady 1.5 Pa FSS is applied (Noria et al. 1999).

7.3.3. Computational Insights into stimulation of cells using FSS

Previous studies and have shown that adhesion junctions play a role in osteoblast sensing and responding to FSS stimulation, and Chapter 4 furthered the understanding of how adhesion junctions direct osteogenic differentiation of osteoblast-like cells under mechanical stimulation. However, the precise mechanical stimulation (forces, stresses) exerted on these junctions during FSS stimulation remained poorly understood. In vitro studies have shown that the Cox-2 gene expression, PGE_2 production and cytoskeletal response of osteoblasts and osteocytes exposed to FSS is dependent on the fluid flow regime (Ponik et al. 2007; Jaasma and O'Brien 2008; Kamel et al. 2010). However, the difference in the mechanical forces applied to cell-cell contacts exposed to different FSS regimes had not previously been investigated. To address this, Chapter 5 of this thesis characterised the fluid pressures and velocities generated by oscillatory or steady FSS, within the specific bioreactor design used in Chapter 4 of this thesis. Bioreactor design and location of a cell within the chamber significantly influences the stresses applied to cells by steady FSS (Anderson et al. 2006; Vaughan et al. 2013b). Previous computational investigations into the stresses experienced by cells in a fluid flow regime have primarily focused on deriving the mechanical stimulation under the application of steady fluid flow (Anderson et al. 2005; McGarry et al. 2005a; Vaughan et al. 2013b; Qiu et al. 2014). Such models have captured important considerations for bioreactor design, such as revealing that hydrostatic pressure is more dominant than applied wall shear stress for generating stresses in a cell body (Vaughan et al. 2013b). Another study combined in vitro live imaging of osteocytes during steady FSS stimulation with computational modelling to determine the viscoelastic material properties of osteocytes based on cell deformation

seen in vitro (Qiu et al. 2014). The work presented in Chapter 5 of this thesis predicted that oscillatory FSS with peak shear stress of 1 Pa within the in-house bioreactor alternates between generating a positive and a negative pressure (±1000 Pa) at the chamber inlet nearest to the syringe pump. This study predicted that positive pressure in the chamber puts the cell-cell contact surface into compression of -170 Pa for cells with contractility, and -315 Pa for cells without contractility. Negative pressure puts the cell-cell contact surface into tension of 480 Pa with or without contractility implemented. This fluctuation between compression and tension at the cell-cell contact surface is not seen in steady FSS, where cells remain in compression once FSS is applied. The switch from tension to compression is an important consideration for adhesion junctions as tension is required to maintain adhesion junction stability (Hong et al. 2011; Hong et al. 2013). This work provides a means of further understanding the mechanical stimulation of cells and their adhesion junctions, using different fluid flow regimes in parallel plate bioreactors.

Computational models of cells undergoing FSS stimulation have previously focused on predicting the strains generated in single cells attached to a substrate (Rydholm et al. 2010; Verbruggen et al. 2012; Vaughan et al. 2013a; Qiu et al. 2014; Vaughan et al. 2014; Khayyeri et al. 2015). These studies have provided insightful results showing that localised areas of high strain occur at mechanosensing mechanisms such as cell-substrate attachments (integrins) (Verbruggen et al. 2012; Vaughan et al. 2013b; Qiu et al. 2014; Vaughan et al. 2014) and at the base of the protruding primary cilia (Vaughan et al. 2014; Khayyeri et al. 2015). The work presented in Chapter 5 of this thesis shows that AJs experience large fluctuations in strain from 0 - 5.6%, depending on fluid flow regime and time during oscillatory FSS. In Chapter 5 of this thesis, cell thermal contractility was implemented to represent cytoskeletal contraction and resulted in 2-3% strain during the fluid oscillation. Adhesion junction mechanotransduction of mechanical stimulus into an osteogenic response is facilitated by β-catenin. β-catenin is a folded molecule and the unfolding of β-catenin gradually reveals binding sites on the β-catenin domains that interact with other proteins in the cytoplasm and lead to β-catenin translocation into the nucleus (Roura et al. 1999; Murase et al. 2002; Lilien and Balsamo 2005; Valbuena et al. 2012). Application of 5-50

pN of tensile force using an AFM system results in an increase in β-catenin length of up to 12 nm (Valbuena et al. 2012; Maki et al. 2015). The maximum length extension seen before rupture was ~25 nm, but the theoretical full length of unfolded β-catenin is ~304 nm (Maki et al. 2015). The mechanics of such protein unfolding are not simply described as a percentage strain of the molecule as the exact length of folded β-catenin at the AJ is unclear, but it could be inferred that β-catenin will rupture when experiencing small length increases relative to the maximum unfolded length. Additionally, unfolding of β-catenin increases the number of exposed binding sites up until protein rupture. The strains computed in the cell cytoplasm in Chapter 5 (0 – 5.6%) could be in the same range as the increase in β-catenin protein length, but this requires further investigation. In another computational study, Charras et al. 2002 varied Poissons ratio or Young's modulus of endothelial cells undergoing multiple stimulatory methods, including 5 Pa FSS and 5 Pa hydrostatic pressure application (Charras and Horton 2002). This study showed that an increased Young's modulus resulted in decreased linear elastic strain due to hydrostatic pressure and FSS. Additionally, increased Poisson's ratio resulted in decreased linear elastic strain during hydrostatic pressure application. This work, and the work presented in this thesis both predicted decreased cell deformation due to FSS or hydrostatic pressure with increased contractility or elastic modulus. Other computational works have shown that the contractile cytoskeletal network increases the compression resistance of cells (Ronan et al. 2012). When contractility and FSS were simulated in Chapter 5, over 90% of the cell volume experiences stimulation strain of over 1% throughout the entire fluid flow oscillation. When contractility is not implemented in the model, 90% of the cell volume was below 1% strain in the first half of the oscillation when positive pressure was applied, but above 3.5% when peak negative pressure was applied in the latter half of the oscillation.

7.3.4. Insight into the role of adhesion junctions in dictating MSC viscoelastic material properties

The studies in Chapter 6 of this thesis sought to investigate the influence of adhesion junctions on the viscoelastic material properties of MSC aggregates undergoing

osteogenic differentiation. This study builds upon previous research in the areas of cell biomechanics and mechanobiology by drawing upon a modern 3D tissue engineering technique wherein stem cells are cultured in suspended spherical aggregates. Previous experimental research has shown, using atomic force microscopy and cytochalasin D to disassemble stress fibres, that the elastic modulus of MSCs is significantly influenced by the cytoskeleton (Titushkin and Cho 2007). The cytoskeleton increases the cytoplasm elastic modulus by forming contractile stress fibres (Rotsch and Radmacher 2000) that can be observed during in vitro culture to terminate at cell-substrate or cell-cell contact points. The mechanical forces generated by cytoskeletal tension can be transmitted between adjacent cells via adhesion junctions (Ganz et al. 2006; Maruthamuthu et al. 2011). Indeed, adhesion junctions can respond to changes in their mechanical environment; application of tugging forces (20-60 nN) to the adhesion junction results in increased junction size (20-70 μm^2) (Liu et al. 2010b). This equates to tensile stress of approximately 1000 Pa at the cell-cell junction. Stresses of half magnitude were seen in the computational model, but alternated between tensile and compressive with each oscillation. Previous research into adhesion junction mechanics has shown that OB-cadherin can resist two-fold higher forces (95±20 pN) than N-cadherin adhesion junctions (44±19 pN) (Pittet et al. 2008). These works, when considered together, indicate that specific cadherin expression may be a significant factor in the MSC mechanical properties. Indeed, it was observed that silencing OB-cadherin, the stronger cadherin, resulted in significantly more stress fibres within the cell, which perhaps occurred to compensate for the loss in cell-cell tension previously transmitted through OB-cadherin. Chapter 6 of this thesis contributed to the body of work investigating the mechanical function and significance of adhesion junctions. This research showed for the first time that higher stress fibre formation, viscosity, instantaneous Young's modulus and long term Young's modulus occur when OB-cadherin expression is inhibited in mesenspheres.

The test methods used to assess viscoelastic material properties of MSCs have predominantly tested single cells using atomic force microscopy (Takai et al. 2005; Darling et al. 2008; Docheva et al. 2008; Sugawara et al. 2008; Mullen et al. 2014a), micropipette aspiration (Haider and Guilak 2002; Zhao et al. 2009; Yu et al. 2010) or

magnetic beads (Bausch et al. 1998). Mechanical testing at a single cell level will result in a high level of variability between tested samples due to the spatial variation in properties within the substructures of the cell (nucleus, cytoplasm). As such, the assumption of a homogeneous isotropic material cannot be justified when choosing a model to interpret single cell data (Reynolds and McGarry 2015; Weafer et al. 2015). The parallel plate compression testing system used in Chapter 6 was advantageous as it allowed for the measurement of the creep strain of a composite cellular aggregate consisting of >500 cells. The mesensphere long term Young's modulus measured at day 2 (1.58 ± 0.31 kPa) was approximately three-fold higher than spherical, unspread MSCs (0.47 ± 0.52 kPa) and was approximately 0.7 that of spread MSCs (2.27 ± 1.9 kPa) as measured using AFM testing of single cells (Darling et al. 2008). In contrast to unspread cells, spread cells exhibit highly developed stress fibres. Additionally, mesensphere viscosity at day 2 (1.5 x 10^5 Pa.s) was much higher than the viscosity of bone marrow (approx. 20 - 100 Pa.s) (Metzger et al. 2014; Jansen et al. 2015) where MSCs often reside in vivo.

7.3.5. Adhesion junctions in bone diseases

Almost all mammalian cells express a repertoire of cadherins that vary depending on the cell type. Altered cadherin expression has been linked to a variety of diseases including metastatic cancer (Van Roy 2014), Crohn's disease (Muise et al. 2009) and diabetes related complications (Navaratna et al. 2007). Emerging research has sought to understand whether cadherins are possible treatment targets for specific diseases. For example, P-cadherin deficiency results in skin, retinal and limb defects (Kjær et al. 2005; Shimomura et al. 2008) and M-cadherin deficiency is associated with mild to severe intellectual disability (Bhalla et al. 2008). Of particular relevance to this thesis is the role of N-cadherin in bone disease such as osteoporosis. Osteoporosis is an age-related disease of the bone that usually presents in older patients. Early studies looking at mechanosensitivity showed that osteoblasts derived from the periosteal surface responded to 3000 µstrain, while cells derived from the haversian system required higher strains of 10,000 µstrain to illicit a significant response (Jones et al. 1991). In female patients with osteoporosis, there is a significantly more bone turn-

over (both formation and resorption) at the cortico-endosteal envelope, but not the trabecular surface (Brown et al. 1987) in comparison to non-osteoporotic women. Computational studies have sought to investigate how osteoporosis might change the mechanical environment experienced by bone cells, and such studies have shown increased shear stresses (Birmingham et al. 2013) and cell strain (Vaughan et al. 2015) in the bone marrow around trabeculae for models with reduced bone mass. N-cadherin adhesion junctions are influential to the tissue development of the periosteum (Evans et al. 2013) and can be linked to osteoporosis as they control osteoblast differentiation and bone mass in vitro and in vivo via canonical Wnt signalling (Haÿ et al. 2009; Di Benedetto et al. 2010). Adhesion junctions can sequester β-catenin, an important molecule for canonical Wnt signalling, in the adhesion junction complex and genome wide association studies have identified β-catenin as a gene likely associated with osteoporosis (Haÿ et al. 2009; Di Benedetto et al. 2010; Estrada et al. 2012). Additionally, N-cadherin plays a complex role in maintaining the hematopoietic stem cell (HSC) population; HSCs are maintained in a quiescent state in the MSC niche via attachment to N-cadherin positive osteoblasts on the endosteal surface of bone (Zhang et al. 2003; Xie et al. 2009). HSCs differentiate into an array of myeloid and lymphoid cells that together make up the cells of the blood system (Barron et al. 2010; Xu et al. 2012). Over-expression of osteoblast N-cadherin inhibits the division of HSCs, while knock-down of HSC N-cadherin reduced the adhesion of HSCs onto the bone surfaces (Hosokawa et al. 2010). HSC transplants have been used as a treatment for cancer and immune system disorders (Cheng et al. 2001a; Ishihara et al. 2013), and an increased understanding of the factors influencing the maintenance of a healthy HSC population could help in the development of improved treatment options.

Alterations in cadherin expression have also been implicated in tumorigenesis (Wheelock and Johnson 2003; Nakajima et al. 2004). For example, an increase in OB-cadherin expression promotes the metastasis of prostate cancer cells in bone (Chu et al. 2008). Synthetic peptides of the His-Ala-Val (HAV) sequence bind to the first extracellular domains of classical cadherins and inhibit cell-cell adhesion (Blaschuk et al. 1990; Williams et al. 2000). Metastasis, the spread of cancer to another part of the

body not directly connected to the original cancer, greatly decreases life expectancy (Chen et al. 2016) but treatment with N-cadherin blocking peptide resulted in significant reductions in pancreatic tumour growth and lung metastasis (Shintani et al. 2008). Another study showed that when prostate cancer cells were injected into the heart of a mouse, silencing of OB-cadherin results in significantly lower metastasis to bone but not to other organs (Chu et al. 2008). In aggressive human breast cancers (MDA-MB-231) OB-cadherin is found at elevated levels (Pishvaian et al. 1999) and promotes metastases of the cancer cells to bone (Tamura et al. 2008). Furthermore, a preclinical study showed that treating highly metastatic prostate cancer cells (PC3-mm2) with anti-OB-cadherin monoclonal antibody prevented bone metastases in a mouse model (Lee et al. 2013). Metastases can also be correlated with the material properties of the cells; cell's with a higher Young's modulus result in less metastasis (Swaminathan et al. 2011; Watanabe et al. 2012). The work presented in Chapter 6 showed that siRNA silencing of OB-cadherin caused significantly higher viscoelastic material properties of MSCs in comparison to scrambled siRNA treated MSCs – thus showing that cadherins can significantly influence the material properties of a cell. The work detailed in Chapter 6 links OB-cadherin expression and the cell material properties, there-in relating the silencing of OB-cadherin with both significantly lower bone metastasis (Chu et al. 2008) with significantly higher viscoelastic material properties (Chapter 6) and supports the results of (Swaminathan et al. 2011; Watanabe et al. 2012).

7.4. Future Work

7.4.1. Adhesion Junctions and Osteogenesis

The work completed in Chapter 4 of this thesis investigated the osteogenic response of MC3T3-EI pre-osteoblasts to FSS when adhesion junctions were inhibited. The specific response investigated was the significantly higher Cox-2, Runx2 gene expression and PGE_2 production. However, there are a number of other osteogenic markers that could be investigated to further understand the role of adhesion junctions for osteogenic differentiation of bone cells, namely Osteopontin, Osteocalcin and Osterix gene expression. Osteopontin mRNA expression in osteoblasts is significantly higher with

FSS stimulation in comparison to static controls (Toma et al. 1997). In static conditions, a dominant negative cadherin in murine calvaria cells can inhibit BMP-2-induced expression of osteopontin (Cheng et al. 2000). Indeed it has also been shown that osteopontin expression increases in response to integrin attachment to fibronectin (Carvalho et al. 1998) or over-expression of αvβ3 (Cheng et al. 2001b). In control conditions, osteopontin levels increase with FSS, but this does not occur when primary cilia are inhibited (Malone et al. 2007b). Osteocalcin expression is significantly lower with over-expression of αvβ3 (Cheng et al. 2001b). Osterix is vitally important for osteogenesis (Nakashima et al. 2002; Nakashima and de Crombrugghe 2003; Ortuño et al. 2010), and the osterix expression levels in MSCs from osteoporotic bone increased when the MSCs were transfected with integrin α2 (Valbuena et al. 2012).

The work performed in Chapter 4 of this thesis used calcium chelation (EGTA) to prevent the formation of adhesion junctions. However, this treatment did not target specific cadherins. N-cadherin has been previously linked to an increase in the expression of osteoblast transcription factors Osterix, Osteomodulin and Osteoglycin (Guntur et al. 2012) and the presence of both N-cadherin and OB-cadherin results in higher ALP expression in comparison to either cadherin alone (Kii et al. 2004b). Through the use of siRNA specific to either N-cadherin or OB-cadherin, as were used in Chapter 6, the influence of these two cadherins in the MC3T3-EI osteogenic response to FSS could be investigated to see if their roles are distinctly different, or complimentary. EGTA was used in this study as it is a temporary treatment that allowed investigation of the short-term response to FSS of osteoblasts without pre-formed adhesion junctions. The use of siRNA treatment would prevent adhesion junction formation of a specific cadherin type for a longer period of time before, during and after FSS application.

7.4.2. Computational Modelling of Osteoblasts during Oscillatory FSS

In Chapter 5, a simple linear elastic material was used to model an osteoblast pair. Computational models employing complex material models to characterise the cell body, such as viscoelastic (Qiu et al. 2014), hyper-elastic (McGarry and McHugh 2008)

and “active” material models (Dowling et al. 2012; Reynolds et al. 2014; Reynolds and McGarry 2015), have predominantly been implemented in simulations of static conditions or steady FSS. A recent publication has modelled an osteocyte undergoing steady FSS as a viscoelastic material (Qiu et al. 2014). “Active” material models that predict stress fibre formation and orientation in response to mechanical environment have recently been developed (Deshpande et al. 2006; Deshpande et al. 2008). This active model has shown strong results for predicting cytoskeleton stress fibre formation and cell deformation under applied loads and in static conditions (Dowling et al. 2012; Ronan et al. 2012; Dowling et al. 2013; Weafer et al. 2013; Reynolds et al. 2014; Reynolds and McGarry 2015; Ronan et al. 2015). Implementing an active material model to cells undergoing oscillatory FSS could shed further light on the response of the cytoskeleton to the fluctuating hydrostatic pressure generated during oscillatory FSS.

7.4.3. Influence of OB-cadherin or N-cadherin on Cytoskeletal gene expression

The different influences of OB- and N-cadherin on stress fibre formation and mesensphere μ, E_0 and E_∞ could indicate that N-cadherin interacts differently with stress fibre regulatory pathways than OB-cadherin, either via biochemical or mechanosensory means. Adhesion junction formation has been associated with two pathways that influence the formation and stability of stress fibres. RhoA activity is markedly reduced by cadherin engagement (Anastasiadis et al. 2000; Noren et al. 2001; Noren et al. 2003). RhoA indirectly inhibits the depolymerisation of actin filaments (Maekawa et al. 1999), promotes actomyosin contraction (Kimura et al. 1996) and significantly increases the osteogenic differentiation of MSCs (McBeath et al. 2004). Additionally, Rac1 can be induced by cadherin engagement (Nakagawa et al. 2001; Ehrlich et al. 2002; Liu et al. 2006). Rac1 is an important protein for cytoskeleton remodelling (Castets et al. 2005) and suppresses the formation of contractile actin (Sander et al. 1999b; Burridge and Wennerberg 2004). These pathways could be responsible for the significantly higher actin stress fibre formation in response to the inhibition of OB-cadherin. Additionally, the canonical Wnt signalling pathway could also play a role in the changes in mesensphere mechanics due to the down-regulation

of N- or OB-cadherin. The ablation of either cadherin results in significantly lower β-catenin abundance (Di Benedetto et al. 2010) and the presence of OB-cadherin coincides with significantly higher binding of β-catenin to N-cadherin (Kii et al. 2004a). Canonical Wnt signalling is important because it influences both MSC renewal and differentiation. Downregulation of canonical Wnt signalling encourages MSC renewal, while an upregulation of canonical Wnt signalling encourages osteogenic differentiation of MSCs through upregulation of Runx2, Cox-2 and Osterix (Norvell et al. 2004a; Bennett et al. 2005; Gregory et al. 2005; Jackson et al. 2005; Rodda and McMahon 2006; Arnsdorf et al. 2009a). The results presented here show that in addition to previous reports of the complementary roles of cadherins in osteogenic signalling processes, N- and OB-cadherins also play different roles in influencing the mechanical environment in mesenspheres undergoing osteogenesis. However, the changes in Rhoa/ROCK signalling and canonical Wnt signalling with N- or OB-cadherin silencing in mesenspheres requires further investigation to reveal changes to these signalling pathways due to specific cadherin silencing.

7.5 Conclusion

In conclusion, this thesis has presented experimental and computation studies performed throughout the course of the authors PhD studies to investigate the importance of adhesion junctions in cell mechanobiology and mechanosensation of mechanical stimulation, in the context of osteogenic differentiation of pre-osteoblasts and mesenchymal stem cells. In vitro cell culture methods were used to investigate the importance of adhesion junctions for the osteogenic response of pre-osteoblasts to fluid shear stress (FSS) in a parallel plate bioreactor. Computational methods were used to characterise the stresses and strains transmitted to pre-osteoblasts during steady and oscillatory FSS stimulation. Together, these two studies provided evidence of the up-regulated osteogenic response (PGE_2 production, Cox-2 and Runx2 gene expression) of MC3T3-E1s exposed to oscillatory FSS in a specific parallel plate bioreactor, and then computationally predicted the mechanical stimulus and resulting cellular stresses and strains that might explain this response, using a fluid structure interaction model of an idealised, contractile pair of osteoblasts. The work in this thesis showed that the osteogenic response of MC3T3-E1s to oscillatory FSS is

inhibited when adhesion junction formation is prevented. The thesis computationally characterised the difference in the stress-state of the cell with and without cell-cell attachment at a contact surface. This thesis also showed that N-cadherin and OB-cadherin adhesion junctions have different influences on the viscoelastic material properties of MSCs undergoing osteogenic differentiation, and thus provided a novel insight into the mechanical contribution of specific cadherins. This work also showed the influence of specific cadherins on the stress fibre formation of MSCs in a 3D suspension cultured spheroid (mesensphere), wherein the confounding factor of cell-substrate interactions is removed. The results from this thesis provide a novel insight into the role of adhesion junctions in cell mechanobiology and mechanosensation of mechanical stimulation. Understanding of adhesion junction mechanobiology with respect to osteogenesis is fundamental to the development of treatments for bone disease where altered cadherin expression and adhesion junction function are implicated.

References

A-Hassan, E., W. F. Heinz, M. D. Antonik, N. P. D'Costa, S. Nageswaran, C.-A. Schoenenberger and J. H. Hoh (1998). "Relative Microelastic Mapping of Living Cells by Atomic Force Microscopy." Biophysical Journal **74**(3): 1564-1578.

Aberle, H., A. Bauer, J. Stappert, A. Kispert and R. Kemler (1997). "β-catenin is a target for the ubiquitin–proteasome pathway." The EMBO journal **16**(13): 3797-3804.

Adams, C. L., Y.-T. Chen, S. J. Smith and W. James Nelson (1998). "Mechanisms of Epithelial Cell–Cell Adhesion and Cell Compaction Revealed by High-resolution Tracking of E-Cadherin– Green Fluorescent Protein." The Journal of Cell Biology **142**(4): 1105-1119.

Al-Kilani, A., O. de Freitas, S. Dufour and F. Gallet (2011). "Negative Feedback from Integrins to Cadherins: A Micromechanical Study." Biophysical Journal **101**(2): 336-344.

Al-Rekabi, Z., K. Haase and A. E. Pelling (2014). "Microtubules mediate changes in membrane cortical elasticity during contractile activation." Experimental cell research **322**(1): 21-29.

Anastasiadis, P. Z., S. Y. Moon, M. A. Thoreson, D. J. Mariner, H. C. Crawford, Y. Zheng and A. B. Reynolds (2000). "Inhibition of RhoA by p120 catenin." Nature Cell Biology **2**(9): 637-644.

Anderson, D. W. (1960). "Studies of the lymphatic pathways of bone and bone marrow." Journal of Bone and Joint Surgery **42A**: 716-717.

Anderson, E., T. Falls, A. Sorkin and M. Tate (2006). "The imperative for controlled mechanical stresses in unraveling cellular mechanisms of mechanotransduction." BioMedical Engineering OnLine **5**(1): 27.

Anderson, E. J., S. Kaliyamoorthy, J. I. D. Alexander and M. L. K. Tate (2005). "Nano–microscale models of periosteocytic flow show differences in stresses imparted to cell body and processes." Annals of Biomedical Engineering **33**(1): 52-62.

Anderson, E. J. and M. L. K. Tate (2008). "Idealization of pericellular fluid space geometry and dimension results in a profound underprediction of nano-microscale stresses imparted by fluid drag on osteocytes." Journal of biomechanics **41**(8): 1736-1746.

Ando, J. and K. Yamamoto (2013). Flow detection and calcium signalling in vascular endothelial cells.

Arnsdorf, E. J., P. Tummala and C. R. Jacobs (2009a). "Non-Canonical Wnt Signaling and N-Cadherin Related β-Catenin Signaling Play a Role in Mechanically Induced Osteogenic Cell Fate." PLoS ONE **4**(4): e5388.

Arnsdorf, E. J., P. Tummala, R. Y. Kwon and C. R. Jacobs (2009b). "Mechanically induced osteogenic differentiation – the role of RhoA, ROCKII and cytoskeletal dynamics." Journal of Cell Science **122**(4): 546-553.

Athanasiou, K. A. and R. M. Natoli (2008). "Introduction to continuum biomechanics." Synthesis Lectures on Biomedical Engineering **3**(1): 1-206.

Aubin, J., F. Liu, L. Malaval and A. Gupta (1995). "Osteoblast and chondroblast differentiation." Bone **17**(2): S77-S83.

Aubin, J. E. (1998). "Advances in the osteoblast lineage." Biochemistry and Cell Biology **76**(6): 899-910.

Augat, P. and S. Schorlemmer (2006). "The role of cortical bone and its microstructure in bone strength." Age and ageing **35**(suppl 2): ii27-ii31.

Bacabac, R. G., T. H. Smit, S. C. Cowin, J. J. W. A. Van Loon, F. T. M. Nieuwstadt, R. Heethaar and J. Klein-Nulend (2005). "Dynamic shear stress in parallel-plate flow chambers." Journal of Biomechanics **38**(1): 159-167.

Backman, V., M. B. Wallace, L. T. Perelman, J. T. Arendt, R. Gurjar, M. G. Muller, Q. Zhang, G. Zonios, E. Kline, T. McGillican, S. Shapshay, T. Valdez, K. Badizadegan, J. M. Crawford, M. Fitzmaurice, S. Kabani, H. S. Levin, M. Seiler, R. R. Dasari, I. Itzkan, J. Van Dam and M. S. Feld (2000). "Detection of preinvasive cancer cells." Nature **406**(6791): 35-36.

Bajpai, S., J. Correia, Y. Feng, J. Figueiredo, S. X. Sun, G. D. Longmore, G. Suriano and D. Wirtz (2008). "α-Catenin mediates initial E-cadherin-dependent cell–cell recognition and subsequent bond strengthening." Proceedings of the National Academy of Sciences **105**(47): 18331-18336.

Bakker, A., J. Klein-Nulend and E. Burger (2003a). "Mechanotransduction in bone cells proceeds via activation of COX-2, but not COX-1." Biochemical and Biophysical Research Communications **305**(3): 677-683.

Bakker, A. D., M. Joldersma, J. Klein-Nulend and E. H. Burger (2003b). "Interactive effects of PTH and mechanical stress on nitric oxide and PGE2 production by primary mouse osteoblastic cells." American Journal of Physiology-Endocrinology and Metabolism **285**(3): E608-E613.

Baraniak, P. and T. McDevitt (2012). "Scaffold-free culture of mesenchymal stem cell spheroids in suspension preserves multilineage potential." Cell and Tissue Research **347**(3): 701-711.

Barron, M. J., C.-J. Tsai and S. W. Donahue (2010). "Mechanical stimulation mediates gene expression in MC3T3 osteoblastic cells differently in 2D and 3D environments." Journal of biomechanical engineering **132**(4): 041005.

Bausch, A. R., F. Ziemann, A. A. Boulbitch, K. Jacobson and E. Sackmann (1998). "Local measurements of viscoelastic parameters of adherent cell surfaces by magnetic bead microrheometry." Biophysical Journal **75**(4): 2038-2049.

Behrens, J., J. P. von Kries, M. Kühl, L. Bruhn, D. Wedlich, R. Grosschedl and W. Birchmeier (1996). "Functional interaction of β-catenin with the transcription factor LEF-1." Nature **382**(6592): 638-642.

Bellows, C., J. Aubin and J. Heersche (1987). "Physiological concentrations of glucocorticoids stimulate formation of bone nodules from isolated rat calvaria cells in vitro." Endocrinology **121**(6): 1985-1992.

Bellows, C. G., S. M. Reimers and J. N. M. Heersche (1999). "Expression of mRNAs for type-I collagen, bone sialoprotein, osteocalcin, and osteopontin at different stages of osteoblastic differentiation and their regulation by 1,25 dihydroxyvitamin D3." Cell and Tissue Research **297**(2): 249-259.

Bennett, C. N., K. A. Longo, W. S. Wright, L. J. Suva, T. F. Lane, K. D. Hankenson and O. A. MacDougald (2005). "Regulation of osteoblastogenesis and bone mass by Wnt10b." Proceedings of the National Academy of Sciences of the United States of America **102**(9): 3324-3329.

Benra, F.-K., H. J. Dohmen, J. Pei, S. Schuster and B. Wan (2011). "A comparison of one-way and two-way coupling methods for numerical analysis of fluid-structure interactions." Journal of Applied Mathematics **2011**.

Berenbaum, F. (2000). "Proinflammatory cytokines, prostaglandins, and the chondrocyte: mechanisms of intracellular activation." Joint Bone Spine **67**(6): 561-564.

Bershadsky, A. D. and J. M. Vasiliev (2012). Cytoskeleton, Springer Science & Business Media.

Besser, A. and S. A. Safran (2006). "Force-Induced Adsorption and Anisotropic Growth of Focal Adhesions." Biophysical Journal **90**(10): 3469-3484.

Besser, A. and U. S. Schwarz (2007). "Coupling biochemistry and mechanics in cell adhesion: a model for inhomogeneous stress fiber contraction." New Journal of Physics **9**(11): 425.

Bhalla, K., Y. Luo, T. Buchan, M. A. Beachem, G. F. Guzauskas, S. Ladd, S. J. Bratcher, R. J. Schroer, J. Balsamo, B. R. DuPont, J. Lilien and A. K. Srivastava (2008). "Alterations in CDH15 and KIRREL3 in Patients with Mild to Severe Intellectual Disability." The American Journal of Human Genetics **83**(6): 703-713.

Binderman, I., Z. Shimshoni and D. Somjen (1984). "Biochemical pathways involved in the translation of physical stimulus into biological message." Calcified Tissue International **36**(1): S82-S85.

Binderman, I., U. Zor, A. M. Kaye, Z. Shimshoni, A. Harell and D. Sömjen (1988). "The transduction of mechanical force into biochemical events in bone cells may involve activation of phospholipase A2." Calcified Tissue International **42**(4): 261-266.

Birmingham, E., J. Grogan, G. Niebur, L. McNamara and P. McHugh (2013). "Computational modelling of the mechanics of trabecular bone and marrow using fluid structure interaction techniques." Annals of biomedical engineering **41**(4): 814-826.

Blaschuk, O. W., R. Sullivan, S. David and Y. Pouliot (1990). "Identification of a cadherin cell adhesion recognition sequence." Developmental Biology **139**(1): 227-229.

Bongiorno, T., J. Kazlow, R. Mezencev, S. Griffiths, R. Olivares-Navarrete, J. F. McDonald, Z. Schwartz, B. D. Boyan, T. C. McDevitt and T. Sulchek (2014). "Mechanical stiffness as an improved single-cell indicator of osteoblastic human mesenchymal stem cell differentiation." Journal of Biomechanics **47**(9): 2197-2204.

Boskey, A. L. (1996). "Matrix proteins and mineralization: an overview." Connective tissue research **35**(1-4): 357-363.

Brown, J. P., P. D. Delmas and M. Arlot (1987). "Active bone turnover of the cortico-endosteal envelope in postmenopausal osteoporosis." The Journal of Clinical Endocrinology & Metabolism **64**(5): 954-959.

Brunsting, A. and P. F. Mullaney (1974). "Differential Light Scattering from Spherical Mammalian Cells." Biophysical Journal **14**(6): 439-453.

Buckley, C. D., J. Tan, K. L. Anderson, D. Hanein, N. Volkmann, W. I. Weis, W. J. Nelson and A. R. Dunn (2014). "The minimal cadherin-catenin complex binds to actin filaments under force." Science **346**(6209): 1254211.

Burger, E. H. and J. Klein-Nulend (1999). "Mechanotransduction in bone - role of the lacunocanalicular network." The FASEB Journal **13**: S101-S112.

Burger, E. H., J. Klein-Nulend and T. H. Smit (2003). "Strain-derived canalicular fluid flow regulates osteoclast activity in a remodelling osteon—a proposal." Journal of Biomechanics **36**(10): 1453-1459.

Burra, S., D. Nicolella, W. Francis, C. Freitas, N. Mueschke, K. Poole and J. Jiang (2010a). "Dendritic processes of osteocytes are mechanotransducers that induce the opening of hemichannels." Proc Natl Acad Sci U S A **107**(31): 13648-13653.

Burra, S., D. P. Nicolella, W. L. Francis, C. J. Freitas, N. J. Mueschke, K. Poole and J. X. Jiang (2010b). "Dendritic processes of osteocytes are mechanotransducers that induce the opening of hemichannels." Proceedings of the National Academy of Sciences **107**(31): 13648-13653.

Burridge, K. and K. Wennerberg (2004). "Rho and Rac take center stage." Cell **116**(2): 167-179.

Caille, N., O. Thoumine, Y. Tardy and J.-J. Meister (2002). "Contribution of the nucleus to the mechanical properties of endothelial cells." Journal of Biomechanics **35**(2): 177-187.

Carter, D. R. and W. E. Caler (1985). "A cumulative damage model for bone fracture." Journal of Orthopaedic Research **3**(1): 84-90.

Carvalho, R., J. Schaffer and L. Gerstenfeld (1998). "Osteoblasts induce osteopontin expression in response to attachment on fibronectin: demonstration of a common role for integrin receptors in the signal transduction processes of cell attachment and mechanical stimulation." Journal of Cellular Biochemistry **70**(3): 376-390.

Case, N., B. Sen, J. Thomas, M. Styner, Z. Xie, C. Jacobs and J. Rubin (2011). "Steady and oscillatory fluid flows produce a similar osteogenic phenotype." Calcified Tissue International **88**(3): 189-197.

Castets, M., C. Schaeffer, E. Bechara, A. Schenck, E. W. Khandjian, S. Luche, H. Moine, T. Rabilloud, J.-L. Mandel and B. Bardoni (2005). "FMRP interferes with the Rac1 pathway and controls actin cytoskeleton dynamics in murine fibroblasts." Human Molecular Genetics **14**(6): 835-844.

Castro, C. H., C. S. Shin, J. P. Stains, S.-L. Cheng, S. Sheikh, G. Mbalaviele, V. L. Szejnfeld and R. Civitelli (2004). "Targeted expression of a dominant-negative N-cadherin in vivo delays peak bone mass and increases adipogenesis." Journal of Cell Science **117**(13): 2853-2864.

Cavallo, R. A., R. T. Cox, M. M. Moline, J. Roose, G. A. Polevoy, H. Clevers, M. Peifer and A. Bejsovec (1998). "Drosophila Tcf and Groucho interact to repress Wingless signalling activity." Nature **395**(6702): 604-608.

Chae, H.-D., K. E. Lee, D. A. Williams and Y. Gu (2008). "Cross-talk between RhoH and Rac1 in regulation of actin cytoskeleton and chemotaxis of hematopoietic progenitor cells." Blood **111**(5): 2597-2605.

Chambers, T. J., M. Evans, T. N. Gardner, A. Turner-Smith and J. W. Chow (1993). "Induction of bone formation in rat tail vertebrae by mechanical loading." Bone and mineral **20**(2): 167-178.

Charras, G. T. and M. A. Horton (2002). "Determination of Cellular Strains by Combined Atomic Force Microscopy and Finite Element Modeling." Biophysical Journal **83**(2): 858-879.

Chen, J. C., D. A. Hoey, M. Chua, R. Bellon and C. R. Jacobs (2016). "Mechanical signals promote osteogenic fate through a primary cilia-mediated mechanism." The FASEB Journal **30**(4): 1504-1511.

Chen, N. X., K. D. Ryder, F. M. Pavalko, C. H. Turner, D. B. Burr, J. Qiu and R. L. Duncan (2000). "Ca2+ regulates fluid shear-induced cytoskeletal reorganization and gene expression in osteoblasts." American Journal of Physiology - Cell Physiology **278**(5): C989-C997.

Cheng, B., S. Zhao, J. Luo, E. Sprague, L. F. Bonewald and J. X. Jiang (2001a). "Expression of functional gap junctions and regulation by fluid flow in osteocyte-like MLO-Y4 cells." Journal of Bone and Mineral Research **16**(2): 249-259.

Cheng, S.-L., C.-F. Lai, S. D. Blystone and L. V. Avioli (2001b). "Bone Mineralization and Osteoblast Differentiation Are Negatively Modulated by Integrin αvβ3." Journal of Bone and Mineral Research **16**(2): 277-288.

Cheng, S.-L., F. Lecanda, M. K. Davidson, P. M. Warlow, S.-F. Zhang, L. Zhang, S. Suzuki, T. St. John and R. Civitelli (1998a). "Human Osteoblasts Express a Repertoire of Cadherins, Which Are Critical for BMP-2–Induced Osteogenic Differentiation." Journal of Bone and Mineral Research **13**(4): 633-644.

Cheng, S.-L., C. S. Shin, D. A. Towler and R. Civitelli (2000). "A Dominant Negative Cadherin Inhibits Osteoblast Differentiation." Journal of Bone and Mineral Research **15**(12): 2362-2370.

Cheng, S. U. L. I., F. Lecanda, M. K. Davidson, P. M. Warlow, S. F. Zhang, L. Zhang, S. Suzuki, T. S. T. John and R. Civitelli (1998b). "Human osteoblasts express a repertoire of cadherins, which are critical for BMP-2-induced osteogenic differentiation." Journal of Bone and Mineral Research **13**(4): 633-644.

Chopra, A., E. Tabdanov, H. Patel, P. A. Janmey and J. Y. Kresh (2011). "Cardiac myocyte remodeling mediated by N-cadherin-dependent mechanosensing." American Journal of Physiology-Heart and Circulatory Physiology **300**(4): H1252.

Chu, K., C.-J. Cheng, X. Ye, Y.-C. Lee, A. J. Zurita, D.-T. Chen, L.-Y. Yu-Lee, S. Zhang, E. T. Yeh and M. C. Hu (2008). "Cadherin-11 promotes the metastasis of prostate cancer cells to bone." Molecular Cancer Research **6**(8): 1259-1267.

Chung, B. J., A. M. Robertson and D. G. Peters (2003). "The numerical design of a parallel plate flow chamber for investigation of endothelial cell response to shear stress." Computers & Structures **81**(8–11): 535-546.

Collinsworth, A. M., S. Zhang, W. E. Kraus and G. A. Truskey (2002). "Apparent elastic modulus and hysteresis of skeletal muscle cells throughout differentiation." American Journal of Physiology-Cell Physiology **283**(4): C1219-C1227.

Conway, D. E., M. T. Breckenridge, E. Hinde, E. Gratton, C. S. Chen and M. A. Schwartz (2013). "Fluid shear stress on endothelial cells modulates mechanical tension across VE-cadherin and PECAM-1." Current Biology **23**(11): 1024-1030.

Cook, M. M., K. Futrega, M. Osiecki, M. Kabiri, B. Kul, A. Rice, K. Atkinson, G. Brooke and M. Doran (2012). "Micromarrows—three-dimensional coculture of hematopoietic stem cells and mesenchymal stromal cells." Tissue Engineering Part C: Methods **18**(5): 319-328.

Costa, K. D., W. J. Hucker and F. C. P. Yin (2002). "Buckling of actin stress fibers: A new wrinkle in the cytoskeletal tapestry." Cell Motility and the Cytoskeleton **52**(4): 266-274.

Cowin, S. C., L. Moss-Salentijn and M. L. Moss (1991). "Candidates for the mechanosensory system in bone." Journal of Biomechanical Engineering **113**(2): 191-197.

Crawford, R. and R. J. Crawford (1998). Plastics engineering, Butterworth-Heinemann.

Crockett, J. C., M. J. Rogers, F. P. Coxon, L. J. Hocking and M. H. Helfrich (2011). "Bone remodelling at a glance." Journal of Cell Science **124**(7): 991-998.

Cully, M., H. You, A. J. Levine and T. W. Mak (2006). "Beyond PTEN mutations: the PI3K pathway as an integrator of multiple inputs during tumorigenesis." Nat Rev Cancer **6**(3): 184-192.

Currey, J. D. (2014). The mechanical adaptations of bones, Princeton University Press.

Curties, A. (1964). "The mechanism of adhesion of cells to glass." J. Cell Biol. **20**: 199-215.

Dady, A., C. Blavet and J. L. Duband (2012). "Timing and kinetics of E-to N-cadherin switch during neurulation in the avian embryo." Developmental Dynamics **241**(8): 1333-1349.

Dailey, H. L., L. M. Ricles, H. C. Yalcin and S. N. Ghadiali (2009). "Image-based finite element modeling of alveolar epithelial cell injury during airway reopening." Journal of Applied Physiology **106**(1): 221-232.

Daneshjou, N., N. Sieracki, G. P. van Nieuw Amerongen, D. E. Conway, M. A. Schwartz, Y. A. Komarova and A. B. Malik (2015). "Rac1 functions as a reversible tension modulator to stabilize VE-cadherin trans-interaction." The Journal of Cell Biology **208**(1): 23-32.

Danowski, B. A. (1989). "Fibroblast contractility and actin organization are stimulated by microtubule inhibitors." Journal of Cell Science **93**(2): 255-266.

Darling, E. M., M. Topel, S. Zauscher, T. P. Vail and F. Guilak (2008). "Viscoelastic properties of human mesenchymally-derived stem cells and primary osteoblasts, chondrocytes, and adipocytes." Journal of Biomechanics **41**(2): 454-464.

Darling, E. M., S. Zauscher and F. Guilak (2006). "Viscoelastic properties of zonal articular chondrocytes measured by atomic force microscopy." Osteoarthritis and Cartilage **14**(6): 571-579.

Datta, H. K., W. F. Ng, J. A. Walker, S. P. Tuck and S. S. Varanasi (2008). "The cell biology of bone metabolism." Journal of Clinical Pathology **61**(5): 577-587.

Day, T. F., X. Guo, L. Garrett-Beal and Y. Yang (2005). "Wnt/β-Catenin Signaling in Mesenchymal Progenitors Controls Osteoblast and Chondrocyte Differentiation during Vertebrate Skeletogenesis." Developmental Cell **8**(5): 739-750.

de Beco, S., J.-B. Perney, S. Coscoy and F. Amblard (2015). "Mechanosensitive Adaptation of E-Cadherin Turnover across <italic>adherens</italic> Junctions." PLoS ONE **10**(6): e0128281.

de Rooij, J., A. Kerstens, G. Danuser, M. A. Schwartz and C. M. Waterman-Storer (2005). "Integrin-dependent actomyosin contraction regulates epithelial cell scattering." The Journal of Cell Biology **171**(1): 153-164.

Del Rio, A., R. Perez-Jimenez, R. Liu, P. Roca-Cusachs, J. M. Fernandez and M. P. Sheetz (2009). "Stretching single talin rod molecules activates vinculin binding." Science **323**(5914): 638-641.

Delaine-Smith, R., S. MacNeil and G. Reilly (2012). "Matrix production and collagen structure are enhanced in two types of osteogenic progenitor cells by a simple fluid shear stress stimulus." Eur Cell Mater **24**: 162-174.

Delaine-Smith, R. M., A. Sittichokechaiwut and G. C. Reilly (2014). "Primary cilia respond to fluid shear stress and mediate flow-induced calcium deposition in osteoblasts." The FASEB Journal **28**(1): 430-439.

Dennis, J. E., J.-P. Carbillet, A. Caplan and P. Charbord (2002). "The STRO-1+ marrow cell population is multipotential." Cells Tissues Organs **170**(2-3): 73-82.

Deshpande, V. S., R. M. McMeeking and A. G. Evans (2006). "A bio-chemo-mechanical model for cell contractility." Proceedings of the National Academy of Sciences **103**(38): 14015-14020.

Deshpande, V. S., M. Mrksich, R. M. McMeeking and A. G. Evans (2008). "A bio-mechanical model for coupling cell contractility with focal adhesion formation." Journal of the Mechanics and Physics of Solids **56**(4): 1484-1510.

Dey, I., M. Lejeune and K. Chadee (2006). "Prostaglandin E2 receptor distribution and function in the gastrointestinal tract." British journal of pharmacology **149**(6): 611-623.

Di Benedetto, A., M. Watkins, S. Grimston, V. Salazar, C. Donsante, G. Mbalaviele, G. L. Radice and R. Civitelli (2010). "N-cadherin and cadherin 11 modulate postnatal bone growth and osteoblast differentiation by distinct mechanisms." Journal of Cell Science **123**(15): 2640-2648.

Docheva, D., D. Padula, C. Popov, W. Mutschler, H. Clausen-Schaumann and M. Schieker (2008). "Researching into the cellular shape, volume and elasticity of mesenchymal stem cells, osteoblasts and osteosarcoma cells by atomic force microscopy." Journal of cellular and molecular medicine **12**(2): 537-552.

Dominici, M., K. Le Blanc, I. Mueller, I. Slaper-Cortenbach, F. Marini, D. Krause, R. Deans, A. Keating, D. Prockop and E. Horwitz (2006). "Minimal criteria for defining multipotent mesenchymal stromal cells. The International Society for Cellular Therapy position statement." Cytotherapy **8**(4): 315-317.

Domke, J., S. Dannöhl, W. J. Parak, O. Müller, W. K. Aicher and M. Radmacher (2000). "Substrate dependent differences in morphology and elasticity of living osteoblasts investigated by atomic force microscopy." Colloids and Surfaces B: Biointerfaces **19**(4): 367-379.

Donahue, T. L. H., T. R. Haut, C. E. Yellowley, H. J. Donahue and C. R. Jacobs (2003). "Mechanosensitivity of bone cells to oscillating fluid flow induced shear stress may be modulated by chemotransport." Journal of Biomechanics **36**(9): 1363-1371.

Dong, Y.-F., D. Y. Soung, E. M. Schwarz, R. J. O'Keefe and H. Drissi (2006). "Wnt induction of chondrocyte hypertrophy through the Runx2 transcription factor." Journal of Cellular Physiology **208**(1): 77-86.

Dos Remedios, C., D. Chhabra, M. Kekic, I. Dedova, M. Tsubakihara, D. Berry and N. Nosworthy (2003). "Actin binding proteins: regulation of cytoskeletal microfilaments." Physiological reviews **83**(2): 433-473.

Doty, S. B. (1981). "Morphological evidence of gap junctions between bone cells." Calcified Tissue International **33**(1): 509-512.

Dowling, E. P., W. Ronan and J. P. McGarry (2013). "Computational investigation of in situ chondrocyte deformation and actin cytoskeleton remodelling under physiological loading." Acta Biomaterialia **9**(4): 5943-5955.

Dowling, E. P., W. Ronan, G. Ofek, V. S. Deshpande, R. M. McMeeking, K. A. Athanasiou and J. P. McGarry (2012). "The effect of remodelling and contractility of the actin cytoskeleton on the

shear resistance of single cells: a computational and experimental investigation." Journal of The Royal Society Interface **9**(77): 3469-3479.
Ducy, P., R. Zhang, V. Geoffroy, A. L. Ridall and G. Karsenty (1997). "Osf2/Cbfa1: a transcriptional activator of osteoblast differentiation." Cell **89**(5): 747-754.
Duguay, D., R. A. Foty and M. S. Steinberg (2003). "Cadherin-mediated cell adhesion and tissue segregation: qualitative and quantitative determinants." Developmental Biology **253**(2): 309-323.
Ebihara, L., X. Liu and J. D. Pal (2003). "Effect of external magnesium and calcium on human connexin46 hemichannels." Biophysical Journal **84**(1): 277-286.
Ehrlich, J. S., M. D. Hansen and W. J. Nelson (2002). "Spatio-temporal regulation of Rac1 localization and lamellipodia dynamics during epithelial cell-cell adhesion." Developmental Cell **3**(2): 259-270.
Eibl, R., D. Eibl, R. Pörtner, G. Catapano and P. Czermak (2008). Cell and tissue reaction engineering, Springer Science & Business Media.
Ellis, R. J. and A. P. Minton (2003). "Cell biology: Join the crowd." Nature **425**(6953): 27-28.
Engler, A. J., M. A. Griffin, S. Sen, C. G. Bönnemann, H. L. Sweeney and D. E. Discher (2004). "Myotubes differentiate optimally on substrates with tissue-like stiffness pathological implications for soft or stiff microenvironments." The Journal of Cell Biology **166**(6): 877-887.
Engler, A. J., S. Sen, H. L. Sweeney and D. E. Discher (2006). "Matrix Elasticity Directs Stem Cell Lineage Specification." Cell **126**(4): 677-689.
Estrada, K., U. Styrkarsdottir, E. Evangelou, Y.-H. Hsu, E. L. Duncan, E. E. Ntzani, L. Oei, O. M. Albagha, N. Amin and J. P. Kemp (2012). "Genome-wide meta-analysis identifies 56 bone mineral density loci and reveals 14 loci associated with risk of fracture." Nature genetics **44**(5): 491-501.
Evans, S. F., D. Docheva, A. Bernecker, C. Colnot, R. P. Richter and M. L. K. Tate (2013). "Solid-supported lipid bilayers to drive stem cell fate and tissue architecture using periosteum derived progenitor cells." Biomaterials **34**(8): 1878-1887.
Ezratty, E. J., M. A. Partridge and G. G. Gundersen (2005). "Microtubule-induced focal adhesion disassembly is mediated by dynamin and focal adhesion kinase." Nat Cell Biol **7**(6): 581-590.
Fagan, M. J. (1992). Finite Element Analysis: Theory and Practice, Longman Scientific & Technical.
Fagotto, F. and B. M. Gumbiner (1994). "Beta-catenin localization during Xenopus embryogenesis: accumulation at tissue and somite boundaries." Development **120**(12): 3667-3679.
Ferrari, S. L., K. Traianedes, M. Thorne, M.-H. Lafage-Proust, P. Genever, M. G. Cecchini, V. Behar, A. Bisello, M. Chorev, M. Rosenblatt and L. J. Suva (2000). "A Role for N-Cadherin in the Development of the Differentiated Osteoblastic Phenotype." Journal of Bone and Mineral Research **15**(2): 198-208.
Ferraro, J. T., M. Daneshmand, R. Bizios and V. Rizzo (2004). Depletion of plasma membrane cholesterol dampens hydrostatic pressure and shear stress-induced mechanotransduction pathways in osteoblast cultures.
Fiedler, M., C. Mendoza-Topaz, T. J. Rutherford, J. Mieszczanek and M. Bienz (2011). "Dishevelled interacts with the DIX domain polymerization interface of Axin to interfere with its function in down-regulating β-catenin." Proceedings of the National Academy of Sciences **108**(5): 1937-1942.
Firth, A. L. and J. X.-J. Yuan (2012). "Identification of functional progenitor cells in the pulmonary vasculature." Pulmonary circulation **2**(1): 84.
Fletcher, D. A. and R. D. Mullins (2010). "Cell mechanics and the cytoskeleton." Nature **463**(7280): 485-492.
Franceschi, R. T. and B. S. Iyer (1992). "Relationship between collagen synthesis and expression of the osteoblast phenotype in MC3T3-E1 cells." Journal of Bone and Mineral Research **7**(2): 235-246.
Fratzl, P., H. Gupta, E. Paschalis and P. Roschger (2004). "Structure and mechanical quality of the collagen–mineral nano-composite in bone." Journal of materials chemistry **14**(14): 2115-2123.
Frost, H. M. (1960). "In vivo osteocyte death." The Journal of Bone & Joint Surgery **42**(1): 138-143.
Frost, H. M. (1973). Bone remodeling and its relationship to metabolic bone diseases, Charles C. Thomas Publisher.
Fujita, H., M. Yamamoto, T. Ogino, H. Kobuchi, N. Ohmoto, E. Aoyama, T. Oka, T. Nakanishi, K. Inoue and J. Sasaki (2014). "Necrotic and apoptotic cells serve as nuclei for calcification on osteoblastic differentiation of human mesenchymal stem cells in vitro." Cell Biochemistry and Function **32**(1): 77-86.

Fukunaga, Y., H. Liu, M. Shimizu, S. Komiya, M. Kawasuji and A. Nagafuchi (2005). "Defining the Roles of. BETA.-catenin and Plakoglobin in Cell-cell Adhesion: Isolation of. BETA.-catenin/plakoglobin-deficient F9 Cells." Cell structure and function **30**(2): 25-34.

Funk, C. D. (2001). "Prostaglandins and leukotrienes: advances in eicosanoid biology." Science **294**(5548): 1871-1875.

Ganz, A., M. Lambert, A. Saez, P. Silberzan, A. Buguin, R. M. Mège and B. Ladoux (2006). "Traction forces exerted through N-cadherin contacts." Biology of the Cell **98**(12): 721-730.

Gao, L., R. McBeath and C. S. Chen (2010). "Stem Cell Shape Regulates a Chondrogenic Versus Myogenic Fate Through Rac1 and N-Cadherin." STEM CELLS **28**(3): 564-572.

Gardinier, J. D., S. Majumdar, R. L. Duncan and L. Wang (2009). "Cyclic hydraulic pressure and fluid flow differentially modulate cytoskeleton re-organization in MC3T3 osteoblasts." Cellular and Molecular Bioengineering **2**(1): 133-143.

Geiger, B., K. Tokuyasu, A. H. Dutton and S. Singer (1980). "Vinculin, an intracellular protein localized at specialized sites where microfilament bundles terminate at cell membranes." Proceedings of the National Academy of Sciences **77**(7): 4127-4131.

Genda, T., M. Sakamoto, T. Ichida, H. Asakura and S. Hirohashi (2000). "Loss of cell-cell contact is induced by integrin-mediated cell-substratum adhesion in highly-motile and highly-metastatic hepatocellular carcinoma cells." Laboratory investigation **80**(3): 387-394.

Genetos, D. C., C. J. Kephart, Y. Zhang, C. E. Yellowley and H. J. Donahue (2007). "Oscillating fluid flow activation of gap junction hemichannels induces ATP release from MLO-Y4 osteocytes." Journal of Cellular Physiology **212**(1): 207-214.

Gilbert, S. F. (2000). "Osteogenesis: the development of bones."

Gilmore, A. P. and K. Burridge (1996). "Regulation of vinculin binding to talin and actin by phosphatidyl-inositol-4-5-bisphosphate." Nature **381**(6582): 531-535.

Girard, P. R. and R. M. Nerem (1995). "Shear stress modulates endothelial cell morphology and F-actin organization through the regulation of focal adhesion-associated proteins." Journal of Cellular Physiology **163**(1): 179-193.

Glass Ii, D. A., P. Bialek, J. D. Ahn, M. Starbuck, M. S. Patel, H. Clevers, M. M. Taketo, F. Long, A. P. McMahon, R. A. Lang and G. Karsenty (2005). "Canonical Wnt Signaling in Differentiated Osteoblasts Controls Osteoclast Differentiation." Developmental Cell **8**(5): 751-764.

Gnutt, D., M. Gao, O. Brylski, M. Heyden and S. Ebbinghaus (2015). "Excluded-Volume Effects in Living Cells." Angewandte Chemie International Edition **54**(8): 2548-2551.

Goddette, D. and C. Frieden (1986). "Actin polymerization. The mechanism of action of cytochalasin D." Journal of Biological Chemistry **261**(34): 15974-15980.

Goldstein, S. A., R. Goulet and D. McCubbrey (1993). "Measurement and significance of three-dimensional architecture to the mechanical integrity of trabecular bone." Calcified Tissue International **53**(1): S127-S133.

Golji, J., J. Lam and M. R. K. Mofrad (2011). "Vinculin activation is necessary for complete talin binding." Biophysical Journal **100**(2): 332-340.

Golub, E. E. and K. Boesze-Battaglia (2007). "The role of alkaline phosphatase in mineralization." Current Opinion in Orthopaedics **18**(5): 444-448.

Goomer, R., T. Maris and D. Amiel (1998). "Age-related changes in the expression of cadherin-11, the mesenchyme specific calcium-dependent cell adhesion molecule." Calcified Tissue International **62**(6): 532-537.

Gori, F., L. C. Hofbauer, C. R. Dunstan, T. C. Spelsberg, S. Khosla and B. L. Riggs (2000). "The Expression of Osteoprotegerin and RANK Ligand and the Support of Osteoclast Formation by Stromal-Osteoblast Lineage Cells Is Developmentally Regulated." Endocrinology **141**(12): 4768-4776.

Gregory, C. A., W. G. Gunn, E. Reyes, A. J. Smolarz, J. Munoz, J. L. Spees and D. J. Prockop (2005). "How Wnt Signaling Affects Bone Repair by Mesenchymal Stem Cells from the Bone Marrow." Annals of the New York Academy of Sciences **1049**(1): 97-106.

Guigas, G., C. Kalla and M. Weiss (2007). "Probing the Nanoscale Viscoelasticity of Intracellular Fluids in Living Cells." Biophysical Journal **93**(1): 316-323.

Guilak, F., J. R. Tedrow and R. Burgkart (2000). "Viscoelastic properties of the cell nucleus." Biochemical and Biophysical Research Communications **269**(3): 781-786.

Gumbiner, B. M. (1996). "Cell Adhesion: The Molecular Basis of Tissue Architecture and Morphogenesis." Cell **84**(3): 345-357.

Gumbiner, B. M. (2005). "Regulation of cadherin-mediated adhesion in morphogenesis." Nature Reviews Molecular Cell Biology **6**(8): 622-634.

Guntur, A. R., C. J. Rosen and M. C. Naski (2012). "N-cadherin adherens junctions mediate osteogenesis through PI3K signaling." Bone **50**(1): 54-62.

Guo, Y., C. Zhang, Q. Zeng, R. Li, L. Liu, Q. Hao, C. Shi, X. Zhang and Y. Yan (2012). "Mechanical strain promotes osteoblast ECM formation and improves its osteoinductive potential." Biomed Eng Online **11**(1).

Haÿ, E., E. Laplantine, V. Geoffroy, M. Frain, T. Kohler, R. Müller and P. J. Marie (2009). "N-Cadherin Interacts with Axin and LRP5 To Negatively Regulate Wnt/β-Catenin Signaling, Osteoblast Function, and Bone Formation." Molecular and Cellular Biology **29**(4): 953-964.

Haÿ, E., J. Lemonnier, D. Modrowski, A. Lomri, F. Lasmoles and P. J. Marie (2000). "N- and E-cadherin mediate early human calvaria osteoblast differentiation promoted by bone morphogenetic protein-2." Journal of Cellular Physiology **183**(1): 117-128.

Haertel-Wiesmann, M., Y. Liang, W. J. Fantl and L. T. Williams (2000). "Regulation of Cyclooxygenase-2 and Periostin by Wnt-3 in Mouse Mammary Epithelial Cells." Journal of Biological Chemistry **275**(41): 32046-32051.

Haider, M. A. and F. Guilak (2002). "An axisymmetric boundary integral model for assessing elastic cell properties in the micropipette aspiration contact problem." Journal of Biomechanical Engineering **124**(5): 586-595.

Hall, B. K. and T. Miyake (2000). "All for one and one for all: condensations and the initiation of skeletal development." Bioessays **22**(2): 138-147.

Han, Y., S. C. Cowin, M. B. Schaffler and S. Weinbaum (2004). "Mechanotransduction and strain amplification in osteocyte cell processes." Proceedings of the National Academy of Sciences of the United States of America **101**(47): 16689-16694.

Harada, H., S. Tagashira, M. Fujiwara, S. Ogawa, T. Katsumata, A. Yamaguchi, T. Komori and M. Nakatsuka (1999). "Cbfa1 Isoforms Exert Functional Differences in Osteoblast Differentiation." Journal of Biological Chemistry **274**(11): 6972-6978.

Harell, A., S. Dekel and I. Binderman (1976). "Biochemical effect of mechanical stress on cultured bone cells." Calcified Tissue International **22**: 202-207.

Hart, R. (2001). "Bone modeling and remodeling: theories and computation." Bone mechanics handbook: 1-42.

Haugh, M. G., T. J. Vaughan and L. M. McNamara (2015). "The role of integrin α V β 3 in osteocyte mechanotransduction." Journal of the Mechanical Behavior of Biomedical Materials **42**: 67-75.

He, X., M. Semenov, K. Tamai and X. Zeng (2004). "LDL receptor-related proteins 5 and 6 in Wnt/β-catenin signaling: Arrows point the way." Development **131**(8): 1663-1677.

Helmlinger, G., B. C. Berk and R. M. Nerem (1995). "Calcium responses of endothelial cell monolayers subjected to pulsatile and steady laminar flow differ." American Journal of Physiology-Cell Physiology **269**(2): C367-C375.

Higuchi, C., N. Nakamura, H. Yoshikawa and K. Itoh (2009). "Transient dynamic actin cytoskeletal change stimulates the osteoblastic differentiation." Journal of bone and mineral metabolism **27**(2): 158-167.

Hoey, D. A., J. C. Chen and C. R. Jacobs (2012a). "The primary cilium as a novel extracellular sensor in bone." Frontiers in endocrinology **3**: 75.

Hoey, D. A., S. Tormey, S. Ramcharan, F. J. O'Brien and C. R. Jacobs (2012b). "Primary cilia-mediated mechanotransduction in human mesenchymal stem cells." STEM CELLS **30**(11): 2561-2570.

Hong, S., R. B. Troyanovsky and S. M. Troyanovsky (2010). "Spontaneous assembly and active disassembly balance adherens junction homeostasis." Proceedings of the National Academy of Sciences **107**(8): 3528-3533.

Hong, S., R. B. Troyanovsky and S. M. Troyanovsky (2011). "Cadherin exits the junction by switching its adhesive bond." The Journal of Cell Biology **192**(6): 1073-1083.

Hong, S., R. B. Troyanovsky and S. M. Troyanovsky (2013). "Binding to F-actin guides cadherin cluster assembly, stability, and movement." The Journal of Cell Biology **201**(1): 131-143.

Hosokawa, K., F. Arai, H. Yoshihara, H. Iwasaki, Y. Nakamura, Y. Gomei and T. Suda (2010). "Knockdown of N-cadherin suppresses the long-term engraftment of hematopoietic stem cells." Blood **116**(4): 554-563.

Hsu, S.-h. and G.-S. Huang (2013). "Substrate-dependent Wnt signaling in MSC differentiation within biomaterial-derived 3D spheroids." Biomaterials **34**(20): 4725-4738.

Huang, L., X. Y. Teng, Y. Y. Cheng, K. M. Lee and S. M. Kumta (2004). "Expression of preosteoblast markers and Cbfa-1 and Osterix gene transcripts in stromal tumour cells of giant cell tumour of bone." Bone **34**(3): 393-401.

Huber, A. H., D. B. Stewart, D. V. Laurents, W. J. Nelson and W. I. Weis (2001). "The Cadherin Cytoplasmic Domain Is Unstructured in the Absence of β-Catenin A POSSIBLE MECHANISM FOR REGULATING CADHERIN TURNOVER." Journal of Biological Chemistry **276**(15): 12301-12309.

Huebsch, N., P. R. Arany, A. S. Mao, D. Shvartsman, O. A. Ali, S. A. Bencherif, J. Rivera-Feliciano and D. J. Mooney (2010). "Harnessing traction-mediated manipulation of the cell/matrix interface to control stem-cell fate." Nat Mater **9**(6): 518-526.

Huesa, C., M. H. Helfrich and R. M. Aspden (2010). "Parallel-plate fluid flow systems for bone cell stimulation." Journal of Biomechanics **43**(6): 1182-1189.

Hui, M., M. Hu and H. Tenenbaum (1993). "Changes in cell adhesion and cell proliferation are associated with expression of tissue non-specific alkaline phosphatase." Cell and Tissue Research **274**(3): 429-437.

Huiskes, R., R. Ruimerman, G. H. van Lenthe and J. D. Janssen (2000). "Effects of mechanical forces on maintenance and adaptation of form in trabecular bone." Nature **405**(6787): 704-706.

Huo, B., X. L. Lu, C. T. Hung, K. D. Costa, Q. Xu, G. M. Whitesides and X. E. Guo (2008). "Fluid flow induced calcium response in bone cell network." Cellular and Molecular Bioengineering **1**(1): 58-66.

Huveneers, S. and J. de Rooij (2013). "Mechanosensitive systems at the cadherin–F-actin interface." Journal of Cell Science **126**(2): 403-413.

Huveneers, S., J. Oldenburg, E. Spanjaard, G. van der Krogt, I. Grigoriev, A. Akhmanova, H. Rehmann and J. de Rooij (2012). "Vinculin associates with endothelial VE-cadherin junctions to control force-dependent remodeling." The Journal of Cell Biology **196**(5): 641-652.

Huxley, A. F. and R. Niedergerke (1954). "Structural changes in muscle during contraction." Nature **173**(4412): 971-973.

Huxley, H. and J. Hanson (1954). "Changes in the cross-striations of muscle during contraction and stretch and their structural interpretation." Nature(173): 973-976.

Hynes, R. O. (2004). "The emergence of integrins: a personal and historical perspective." Matrix Biology **23**(6): 333-340.

Igarashi, K., M. Hirafuji, H. Adachi, H. Shinoda and H. Mitani (1994). "Role of endogenous PGE 2 in osteoblastic functions of a clonal osteoblast-like cell, MC3T3-E1." Prostaglandins, leukotrienes and essential fatty acids **50**(4): 169-172.

Imai, Y., M.-Y. Youn, K. Inoue, I. Takada, A. Kouzmenko and S. Kato (2013). Nuclear Receptors in Bone Physiology and Diseases.

Ishihara, Y., Y. Sugawara, H. Kamioka, N. Kawanabe, S. Hayano, T. A. Balam, K. Naruse and T. Yamashiro (2013). "Ex vivo real-time observation of Ca 2+ signaling in living bone in response to shear stress applied on the bone surface." Bone **53**(1): 204-215.

Jaasma, M. J., W. M. Jackson, R. Y. Tang and T. M. Keaveny (2007). "Adaptation of cellular mechanical behavior to mechanical loading for osteoblastic cells." Journal of Biomechanics **40**(9): 1938-1945.

Jaasma, M. J. and F. J. O'Brien (2008). "Mechanical stimulation of osteoblasts using steady and dynamic fluid flow." Tissue Engineering Part A **14**(7): 1213-1223.

Jackson, A., B. Vayssière, T. Garcia, W. Newell, R. Baron, S. Roman-Roman and G. Rawadi (2005). "Gene array analysis of Wnt-regulated genes in C3H10T1/2 cells." Bone **36**(4): 585-598.

Jacobs, C. R., C. E. Yellowley, B. R. Davis, Z. Zhou, J. M. Cimbala and H. J. Donahue (1998). "Differential effect of steady versus oscillating flow on bone cells." Journal of Biomechanics **31**(11): 969-976.

Jafari Bidhendi, A. and R. K. Korhonen (2012). "A Finite Element Study of Micropipette Aspiration of Single Cells: Effect of Compressibility." Computational and Mathematical Methods in Medicine **2012**: 9.

Jaiswal, N., S. E. Haynesworth, A. I. Caplan and S. P. Bruder (1997). "Osteogenic differentiation of purified, culture-expanded human mesenchymal stem cells in vitro." Journal of Cellular Biochemistry **64**(2): 295-312.

Jamieson, G. A. and D. M. Robinson (2014). Mammalian Cell Membranes: Volume 2: The Diversity of Membranes, Elsevier.

Jansen, L. E., N. P. Birch, J. D. Schiffman, A. J. Crosby and S. R. Peyton (2015). "Mechanics of intact bone marrow." Journal of the Mechanical Behavior of Biomedical Materials **50**: 299-307.

Javed, A., G. L. Barnes, B. O. Jasanya, J. L. Stein, L. Gerstenfeld, J. B. Lian and G. S. Stein (2001). "runt Homology Domain Transcription Factors (Runx, Cbfa, and AML) Mediate Repression of the Bone Sialoprotein Promoter: Evidence for Promoter Context-Dependent Activity of Cbfa Proteins." Molecular and Cellular Biology **21**(8): 2891-2905.

Jean, R. P., C. S. Chen and A. A. Spector (2005). "Finite-Element Analysis of the Adhesion-Cytoskeleton-Nucleus Mechanotransduction Pathway During Endothelial Cell Rounding: Axisymmetric Model." Journal of Biomechanical Engineering **127**(4): 594-600.

Jeansonne, B. G., F. F. Feagin, R. W. McMinn, R. L. Shoemaker and W. S. Rehm (1979). "Cell-to-Cell Communication of Osteoblasts." Journal of Dental Research **58**(4): 1415-1423.

Jekir, M. G. and H. J. Donahue (2009). "Gap junctions and osteoblast-like cell gene expression in response to fluid flow." Journal of Biomechanical Engineering **131**(1).

Jones, D., H. Nolte, J. Scholübbers, E. Turner and D. Veltel (1991). "Biochemical signal transduction of mechanical strain in osteoblast-like cells." Biomaterials **12**(2): 101-110.

Jossen, V., R. Pörtner, S. C. Kaiser, M. Kraume, D. Eibl and R. Eibl (2014). Mass production of mesenchymal stem cells: impact of bioreactor design and flow conditions on proliferation and differentiation.

Joukar, A., H. Niroomand-Oscuii and F. Ghalichi (2016). "Numerical simulation of osteocyte cell in response to directional mechanical loadings and mechanotransduction analysis: considering lacunar-canalicular interstitial fluid flow." Computer Methods and Programs in Biomedicine.

Jung, G. Y., Y. J. Park and J. S. Han (2011). "Mediation of Rac1 activation by kindlin-2: An essential function in osteoblast adhesion, spreading, and proliferation." Journal of Cellular Biochemistry **112**(9): 2541-2548.

Kabiri, M., B. Kul, W. B. Lott, K. Futrega, P. Ghanavi, Z. Upton and M. R. Doran (2012). "3D mesenchymal stem/stromal cell osteogenesis and autocrine signalling." Biochemical and Biophysical Research Communications **419**(2): 142-147.

Kaiser, S., B. Hackanson, M. Follo, A. Mehlhorn, K. Geiger, G. Ihorst and U. Kapp (2007). "BM cells giving rise to MSC in culture have a heterogeneous CD34 and CD45 phenotype." Cytotherapy **9**(5): 439-450.

Kamel, M. A., J. L. Picconi, N. Lara-Castillo and M. L. Johnson (2010). "Activation of β-catenin signaling in MLO-Y4 osteocytic cells versus 2T3 osteoblastic cells by fluid flow shear stress and PGE2: Implications for the study of mechanosensation in bone." Bone **47**(5): 872-881.

Kanczler, J. and R. Oreffo (2008). "Osteogenesis and angiogenesis: the potential for engineering bone." Eur Cell Mater **15**(2): 100-114.

Kapur, S., D. J. Baylink and K. H. William Lau (2003). "Fluid flow shear stress stimulates human osteoblast proliferation and differentiation through multiple interacting and competing signal transduction pathways." Bone **32**(3): 241-251.

Karaplis, A. C. (2002). "Embryonic development of bone and the molecular regulation of intramembranous and endochondral bone formation." Principles of bone biology **1**: 33-58.

Karcher, H., J. Lammerding, H. Huang, R. T. Lee, R. D. Kamm and M. R. Kaazempur-Mofrad (2003). "A Three-Dimensional Viscoelastic Model for Cell Deformation with Experimental Verification." Biophysical Journal **85**(5): 3336-3349.

Käs, J., H. Strey, J. Tang, D. Finger, R. Ezzell, E. Sackmann and P. Janmey (1996). "F-actin, a model polymer for semiflexible chains in dilute, semidilute, and liquid crystalline solutions." Biophysical Journal **70**(2): 609.

Katz, S., R. Boland and G. Santillán (2006). "Modulation of ERK 1/2 and p38 MAPK signaling pathways by ATP in osteoblasts: Involvement of mechanical stress-activated calcium influx, PKC and Src activation." The international journal of biochemistry & cell biology **38**(12): 2082-2091.

Kaunas, R. and H.-J. Hsu (2009). "A kinematic model of stretch-induced stress fiber turnover and reorientation." Journal of theoretical biology **257**(2): 320-330.

Kawaguchi, J., I. Kii, Y. Sugiyama, S. Takeshita and A. Kudo (2001). "The Transition of Cadherin Expression in Osteoblast Differentiation from Mesenchymal Cells: Consistent Expression of Cadherin-11 in Osteoblast Lineage." Journal of Bone and Mineral Research **16**(2): 260-269.

Keller, R. (2002). "Shaping the vertebrate body plan by polarized embryonic cell movements." Science **298**(5600): 1950-1954.

Keramidas, A., L. Kuhlmann, A. J. Moorhouse and P. H. Barry (1999). "Measurement of the limiting equivalent conductivities and mobilities of the most prevalent ionic species of EGTA (EGTA2−

and EGTA3−) for use in electrophysiological experiments." Journal of Neuroscience Methods **89**(1): 41-47.
Kern, B., J. Shen, M. Starbuck and G. Karsenty (2001). "Cbfa1 Contributes to the Osteoblast-specific Expression of type I collagen Genes." Journal of Biological Chemistry **276**(10): 7101-7107.
Khayyeri, H., S. Barreto and D. Lacroix (2015). "Primary cilia mechanics affects cell mechanosensation: A computational study." Journal of Theoretical Biology **379**: 38-46.
Kii, I., N. Amizuka, J. Shimomura, Y. Saga and A. Kudo (2004a). "Cell-Cell Interaction Mediated by Cadherin-11 Directly Regulates the Differentiation of Mesenchymal Cells Into the Cells of the Osteo-Lineage and the Chondro-Lineage." Journal of Bone and Mineral Research **19**(11): 1840-1849.
Kii, I., N. Amizuka, J. Shimomura, Y. Saga and A. Kudo (2004b). "Cell-Cell Interaction Mediated by Cadherin-11 Directly Regulates the Differentiation of Mesenchymal Cells Into the Cells of the Osteo-Lineage and the Chondro-Lineage." Journal of Bone and Mineral Research **19**(11): 1840-1849.
Kim, S. H., Y. R. Choi, M. S. Park, J. W. Shin, K. D. Park, S. J. Kim and J. W. Lee (2007). "ERK 1/2 activation in enhanced osteogenesis of human mesenchymal stem cells in poly (lactic-glycolic acid) by cyclic hydrostatic pressure." Journal of Biomedical Materials Research Part A **80**(4): 826-836.
Kim, S. K., A. Shindo, T. J. Park, E. C. Oh, S. Ghosh, R. S. Gray, R. A. Lewis, C. A. Johnson, T. Attie-Bittach and N. Katsanis (2010). "Planar cell polarity acts through septins to control collective cell movement and ciliogenesis." Science **329**(5997): 1337-1340.
Kimura, K., M. Ito, M. Amano, K. Chihara, Y. Fukata, M. Nakafuku, B. Yamamori, J. Feng, T. Nakano and K. Okawa (1996). "Regulation of myosin phosphatase by Rho and Rho-associated kinase (Rho-kinase)." Science **273**(5272): 245-248.
Kinney, M. A., R. Saeed and T. C. McDevitt (2012). "Systematic analysis of embryonic stem cell differentiation in hydrodynamic environments with controlled embryoid body size." Integrative biology **4**(6): 641-650.
Kinney, M. A., R. Saeed and T. C. McDevitt (2014). "Mesenchymal morphogenesis of embryonic stem cells dynamically modulates the biophysical microtissue niche." Scientific reports **4**.
Kirkham, G. R. and S. H. Cartmell (2007). Genes and Proteins involved in the regulation of osteogenesis. Topics in Tissue Engineering. N. Ashammakhi, R. Reis and E. Chiellini. **3:** 1-22.
Kjær, K. W., L. Hansen, G. Schwabe, A. Marques-de-Faria, H. Eiberg, S. Mundlos, N. Tommerup and T. Rosenberg (2005). "Distinct CDH3 mutations cause ectodermal dysplasia, ectrodactyly, macular dystrophy (EEM syndrome)." Journal of medical genetics **42**(4): 292-298.
Klein-Nulend, J., C. M. Semeins, N. E. Ajubi, P. J. Nijweide and E. H. Burger (1995). "Pulsating Fluid Flow Increases Nitric Oxide (NO) Synthesis by Osteocytes but Not Periosteal Fibroblasts - Correlation with Prostaglandin Upregulation." Biochemical and Biophysical Research Communications **217**(2): 640-648.
Klöppel, T. and W. Wall (2011). "A novel two-layer, coupled finite element approach for modeling the nonlinear elastic and viscoelastic behavior of human erythrocytes." Biomechanics and Modeling in Mechanobiology **10**(4): 445-459.
Knothe Tate, M. L., U. Knothe and P. Niederer (1998). "Experimental Elucidation of Mechanical Load-Induced Fluid Flow and Its Potential Role in Bone Metabolism and Functional Adaptation." The American Journal of the Medical Sciences **316**(3): 189-195.
Ko, K. S., P. D. Arora and C. A. G. McCulloch (2001). "Cadherins Mediate Intercellular Mechanical Signaling in Fibroblasts by Activation of Stretch-sensitive Calcium-permeable Channels." Journal of Biological Chemistry **276**(38): 35967-35977.
Kolodney, M. S. and E. L. Elson (1995). "Contraction due to microtubule disruption is associated with increased phosphorylation of myosin regulatory light chain." Proceedings of the National Academy of Sciences **92**(22): 10252-10256.
Komori, T. (2006). "Regulation of osteoblast differentiation by transcription factors." Journal of Cellular Biochemistry **99**(5): 1233-1239.
Kwon, R. Y., S. Temiyasathit, P. Tummala, C. C. Quah and C. R. Jacobs (2010). "Primary cilium-dependent mechanosensing is mediated by adenylyl cyclase 6 and cyclic AMP in bone cells." The FASEB Journal **24**(8): 2859-2868.
Kwon, Y. T., A. Gupta, Y. Zhou, M. Nikolic and L.-H. Tsai (2000). "Regulation of N-cadherin-mediated adhesion by the p35–Cdk5 kinase." Current Biology **10**(7): 363-372.

Lacey, D., E. Timms, H.-L. Tan, M. Kelley, C. Dunstan, T. Burgess, R. Elliott, A. Colombero, G. Elliott and S. Scully (1998). "Osteoprotegerin ligand is a cytokine that regulates osteoclast differentiation and activation." Cell **93**(2): 165-176.

Ladjal, H., J.-L. Hanus, A. Pillarisetti, C. Keefer, A. Ferreira and J. P. Desai (2009). Atomic force microscopy-based single-cell indentation: Experimentation and finite element simulation. Intelligent Robots and Systems, 2009. IROS 2009. IEEE/RSJ International Conference on, IEEE.

Ladoux, B., E. Anon, M. Lambert, A. Rabodzey, P. Hersen, A. Buguin, P. Silberzan and R.-M. Mège (2010). "Strength Dependence of Cadherin-Mediated Adhesions." Biophysical Journal **98**(4): 534-542.

Lane, W. O., A. E. Jantzen, T. A. Carlon, R. M. Jamiolkowski, J. E. Grenet, M. M. Ley, J. M. Haseltine, L. J. Galinat, F.-H. Lin, J. D. Allen, G. A. Truskey and H. E. Achneck (2012). "Parallel-plate Flow Chamber and Continuous Flow Circuit to Evaluate Endothelial Progenitor Cells under Laminar Flow Shear Stress." J Vis Exp(59): e3349.

Lang, T., A. LeBlanc, H. Evans, Y. Lu, H. Genant and A. Yu (2004). "Cortical and Trabecular Bone Mineral Loss From the Spine and Hip in Long-Duration Spaceflight." Journal of Bone and Mineral Research **19**(6): 1006-1012.

Lanyon, L. (1993). "Osteocytes, strain detection, bone modeling and remodeling." Calcified Tissue International **53**(1): S102-S107.

Lanyon, L. and T. Skerry (2001). "Perspective: Postmenopausal Osteoporosis as a Failure of Bone's Adaptation to Functional Loading: A Hypothesis*." Journal of Bone and Mineral Research **16**(11): 1937-1947.

Leckband, D. E., Q. le Duc, N. Wang and J. de Rooij (2011). "Mechanotransduction at cadherin-mediated adhesions." Current Opinion in Cell Biology **23**(5): 523-530.

Lee, C.-H., C.-H. Hong, Y.-T. Chen, Y.-C. Chen and M.-R. Shen (2012). "TGF-beta1 increases cell rigidity by enhancing expression of smooth muscle actin: Keloid-derived fibroblasts as a model for cellular mechanics." Journal of Dermatological Science **67**(3): 173-180.

Lee, D.-Y., C.-R. Yeh, S.-F. Chang, P.-L. Lee, S. Chien, C.-K. Cheng and J.-J. Chiu (2008a). "Integrin-Mediated Expression of Bone Formation-Related Genes in Osteoblast-Like Cells in Response to Fluid Shear Stress: Roles of Extracellular Matrix, Shc, and Mitogen-Activated Protein Kinase." Journal of Bone and Mineral Research **23**(7): 1140-1149.

Lee, D. A., M. M. Knight, J. J. Campbell and D. L. Bader (2011). "Stem cell mechanobiology." Journal of Cellular Biochemistry **112**(1): 1-9.

Lee, D. Y., C. R. Yeh, S. F. Chang, P. L. Lee, S. Chien, C. K. Cheng and J. J. Chiu (2008b). "Integrin-Mediated Expression of Bone Formation-Related Genes in Osteoblast-Like Cells in Response to Fluid Shear Stress: Roles of Extracellular Matrix, Shc, and Mitogen-Activated Protein Kinase." Journal of Bone and Mineral Research **23**(7): 1140-1149.

Lee, K. L., M. D. Guevarra, A. M. Nguyen, M. C. Chua, Y. Wang and C. R. Jacobs (2015). "The primary cilium functions as a mechanical and calcium signaling nexus." Cilia **4**(1): 1.

Lee, M.-H., T.-G. Kwon, H.-S. Park, J. M. Wozney and H.-M. Ryoo (2003). "BMP-2-induced Osterix expression is mediated by Dlx5 but is independent of Runx2." Biochemical and Biophysical Research Communications **309**(3): 689-694.

Lee, Y.-C., M. A. Bilen, G. Yu, S.-C. Lin, C.-F. Huang, A. Ortiz, H. Cho, J. H. Song, R. L. Satcher and J. Kuang (2013). "Inhibition of cell adhesion by a cadherin-11 antibody thwarts bone metastasis." Molecular Cancer Research **11**(11): 1401-1411.

Leerberg, J. M., G. A. Gomez, S. Verma, E. J. Moussa, S. K. Wu, R. Priya, B. D. Hoffman, C. Grashoff, M. A. Schwartz and A. S. Yap (2014). "Tension-sensitive actin assembly supports contractility at the epithelial zonula adherens." Current Biology **24**(15): 1689-1699.

Lehtinen, J. T., M. J. Tingart, M. Apreleva and J. J. P. Warner (2004). "Total, trabecular, and cortical bone mineral density in different regions of the glenoid." Journal of Shoulder and Elbow Surgery **13**(3): 344-348.

Lemonnier, J., E. Haÿ, P. Delannoy, A. Lomri, D. Modrowski, J. Caverzasio and P. J. Marie (2001). "Role of N-Cadherin and Protein Kinase C in Osteoblast Gene Activation Induced by the S252W Fibroblast Growth Factor Receptor 2 Mutation in Apert Craniosynostosis." Journal of Bone and Mineral Research **16**(5): 832-845.

Leong, W. S., C. Y. Tay, H. Yu, A. Li, S. C. Wu, D.-H. Duc, C. T. Lim and L. P. Tan (2010). "Thickness sensing of hMSCs on collagen gel directs stem cell fate." Biochemical and Biophysical Research Communications **401**(2): 287-292.

Levesque, M. J. and R. M. Nerem (1985). "The Elongation and Orientation of Cultured Endothelial Cells in Response to Shear Stress." Journal of Biomechanical Engineering **107**(4): 341-347.

Lewiecki, E. M. (2011). "New targets for intervention in the treatment of postmenopausal osteoporosis." Nat Rev Rheumatol **7**(11): 631-638.

Li, L., R. Hartley, B. Reiss, Y. Sun, J. Pu, D. Wu, F. Lin, T. Hoang, S. Yamada and J. Jiang (2012a). "E-cadherin plays an essential role in collective directional migration of large epithelial sheets." Cellular and Molecular Life Sciences **69**(16): 2779-2789.

Li, P., Y. c. Ma, H. l. Shen, H. Han, J. Wang, H. j. Cheng, C. f. Wang and Y. y. Xia (2012b). "Cytoskeletal reorganization mediates fluid shear stress-induced ERK5 activation in osteoblastic cells." Cell biology international **36**(3): 229-236.

Li, Y.-P., W. Chen, Y. Liang, E. Li and P. Stashenko (1999). "Atp6i-deficient mice exhibit severe osteopetrosis due to loss of osteoclast-mediated extracellular acidification." Nature genetics **23**(4): 447-451.

Lilien, J. and J. Balsamo (2005). "The regulation of cadherin-mediated adhesion by tyrosine phosphorylation/dephosphorylation of β-catenin." Current opinion in cell biology **17**(5): 459-465.

Litzenberger, J. B., J.-B. Kim, P. Tummala and C. R. Jacobs (2010). "β1 integrins mediate mechanosensitive signaling pathways in osteocytes." Calcified Tissue International **86**(4): 325-332.

Liu, B. and J. McGrath (2007). "Freezing osteoblast cells attached to hydroxyapatite discs and glass coverslips: Mechanisms of damage." Science in China Series E: Technological Sciences **50**(2): 248-256.

Liu, D., D. C. Genetos, Y. Shao, D. J. Geist, J. Li, H. Z. Ke, C. H. Turner and R. L. Duncan (2008). "Activation of extracellular-signal regulated kinase (ERK1/2) by fluid shear is Ca2+- and ATP-dependent in MC3T3-E1 osteoblasts." Bone **42**(4): 644-652.

Liu, W., N. S. Murcia, Y. Duan, S. Weinbaum, B. K. Yoder, E. Schwiebert and L. M. Satlin (2005). "Mechanoregulation of intracellular Ca2+ concentration is attenuated in collecting duct of monocilium-impaired orpk mice." American Journal of Physiology-Renal Physiology **289**(5): F978-F988.

Liu, W. F., C. M. Nelson, D. M. Pirone and C. S. Chen (2006). "E-cadherin engagement stimulates proliferation via Rac1." The Journal of Cell Biology **173**(3): 431-441.

Liu, X., X. Zhang and I. Lee (2010a). "A quantitative study on morphological responses of osteoblastic cells to fluid shear stress." Acta Biochimica et Biophysica Sinica **42**(3): 195-201.

Liu, Z., J. L. Tan, D. M. Cohen, M. T. Yang, N. J. Sniadecki, S. A. Ruiz, C. M. Nelson and C. S. Chen (2010b). "Mechanical tugging force regulates the size of cell–cell junctions." Proceedings of the National Academy of Sciences **107**(22): 9944-9949.

Livak, K. J. and T. D. Schmittgen (2001). "Analysis of relative gene expression data using real-time quantitative PCR and the 2(-Delta Delta C(T)) Method." Methods **25**(4): 402-408.

Lodish, H., A. Berk, S. L. Zipursky, P. Matsudaira, D. Baltimore and J. Darnell (2000). "Organelles of the Eukaryotic Cell."

Logan, C. Y. and R. Nusse (2004). "The Wnt Signalling Pathway in Development and Disease." Annual Review of Cell and Developmental Biology **20**(1): 781-810.

Luegmayr, E., H. Glantschnig, F. Varga and K. Klaushofer (2000). "The organization of adherens junctions in mouse osteoblast-like cells (MC3T3-E1) and their modulation by triiodothyronine and 1,25-dihydroxyvitamin D3." Histochemistry and Cell Biology **113**(6): 467-478.

Luo, Y. and G. L. Radice (2003). "Cadherin-mediated adhesion is essential for myofibril continuity across the plasma membrane but not for assembly of the contractile apparatus." Journal of Cell Science **116**(8): 1471-1479.

Luu, H. H., W. X. Song, X. Luo, D. Manning, J. Luo, Z. L. Deng, K. A. Sharff, A. G. Montag, R. C. Haydon and T. C. He (2007). "Distinct roles of bone morphogenetic proteins in osteogenic differentiation of mesenchymal stem cells." Journal of Orthopaedic Research **25**(5): 665-677.

Lyashenko, N., M. Winter, D. Migliorini, T. Biechele, R. T. Moon and C. Hartmann (2011). "Differential requirement for the dual functions of [beta]-catenin in embryonic stem cell self-renewal and germ layer formation." Nature Cell Biology **13**(7): 753-761.

MacKelvie, K. J., K. M. Khan, M. A. Petit, P. A. Janssen and H. A. McKay (2003). "A school-based exercise intervention elicits substantial bone health benefits: a 2-year randomized controlled trial in girls." Pediatrics **112**(6): e447-e452.

Maekawa, M., T. Ishizaki, S. Boku, N. Watanabe, A. Fujita, A. Iwamatsu, T. Obinata, K. Ohashi, K. Mizuno and S. Narumiya (1999). "Signaling from Rho to the Actin Cytoskeleton Through Protein Kinases ROCK and LIM-kinase." Science **285**(5429): 895-898.

Mai, Z., Z. Peng, J. Zhang, L. Chen, H. Liang, B. Cai and H. Ai (2013). "miRNA expression profile during fluid shear stress-induced osteogenic differentiation in MC3T3-E1 cells." Chin Med J (Engl) **126**(8): 1544-1550.

Maki, K., S.-W. Han and T. Adachi (2015). "β-Catenin as a tension transmitter revealed by AFM nanomechanical testing." Cellular and Molecular Bioengineering **8**(1): 14-21.

Malek, A. M. and S. Izumo (1996). "Mechanism of endothelial cell shape change and cytoskeletal remodeling in response to fluid shear stress." Journal of Cell Science **109**(4): 713-726.

Malone, A. M., C. T. Anderson, P. Tummala, R. Y. Kwon, T. R. Johnston, T. Stearns and C. R. Jacobs (2007a). "Primary cilia mediate mechanosensing in bone cells by a calcium-independent mechanism." Proc Natl Acad Sci U S A **104**(33): 13325-13330.

Malone, A. M. D., C. T. Anderson, P. Tummala, R. Y. Kwon, T. R. Johnston, T. Stearns and C. R. Jacobs (2007b). "Primary cilia mediate mechanosensing in bone cells by a calcium-independent mechanism." Proceedings of the National Academy of Sciences **104**(33): 13325-13330.

Malone, A. M. D., N. N. Batra, G. Shivaram, R. Y. Kwon, L. You, C. H. Kim, J. Rodriguez, K. Jair and C. R. Jacobs (2007c). "The role of actin cytoskeleton in oscillatory fluid flow-induced signaling in MC3T3-E1 osteoblasts." American Journal of Physiology - Cell Physiology **292**(5): C1830-C1836.

Mani, S. A., W. Guo, M.-J. Liao, E. N. Eaton, A. Ayyanan, A. Y. Zhou, M. Brooks, F. Reinhard, C. C. Zhang and M. Shipitsin (2008). "The epithelial-mesenchymal transition generates cells with properties of stem cells." Cell **133**(4): 704-715.

Maniotis, A. J., C. S. Chen and D. E. Ingber (1997). "Demonstration of mechanical connections between integrins, cytoskeletal filaments, and nucleoplasm that stabilize nuclear structure." Proceedings of the National Academy of Sciences **94**(3): 849-854.

Martinez-Rico, C., F. Pincet, J.-P. Thiery and S. Dufour (2010). "Integrins stimulate E-cadherin-mediated intercellular adhesion by regulating Src-kinase activation and actomyosin contractility." Journal of Cell Science **123**(5): 712-722.

Maruthamuthu, V., B. Sabass, U. S. Schwarz and M. L. Gardel (2011). "Cell-ECM traction force modulates endogenous tension at cell–cell contacts." Proceedings of the National Academy of Sciences **108**(12): 4708-4713.

Matter, K. and M. S. Balda (2003). "Signalling to and from tight junctions." Nature Reviews Molecular Cell Biology **4**(3): 225-237.

McBeath, R., D. M. Pirone, C. M. Nelson, K. Bhadriraju and C. S. Chen (2004). "Cell Shape, Cytoskeletal Tension, and RhoA Regulate Stem Cell Lineage Commitment." Developmental Cell **6**(4): 483-495.

McGarry, J., J. Fu, M. Yang, C. Chen, R. McMeeking, A. Evans and V. Deshpande (2009). "Simulation of the contractile response of cells on an array of micro-posts." Philosophical Transactions of the Royal Society of London A: Mathematical, Physical and Engineering Sciences **367**(1902): 3477-3497.

McGarry, J. and P. Prendergast (2004). "A three-dimensional finite element model of an adherent eukaryotic cell." Eur Cell Mater **7**: 27-33.

McGarry, J. G., J. Klein-Nulend, M. G. Mullender and P. J. Prendergast (2005a). "A comparison of strain and fluid shear stress in stimulating bone cell responses—a computational and experimental study." The FASEB Journal **19**(3): 482-484.

McGarry, J. G., J. Klein-Nulend and P. J. Prendergast (2005b). "The effect of cytoskeletal disruption on pulsatile fluid flow-induced nitric oxide and prostaglandin E2 release in osteocytes and osteoblasts." Biochemical and Biophysical Research Communications **330**(1): 341-348.

McGarry, J. P. (2009). "Characterization of Cell Mechanical Properties by Computational Modeling of Parallel Plate Compression." Annals of Biomedical Engineering **37**(11): 2317-2325.

McGarry, J. P. and P. E. McHugh (2008). "Modelling of in vitro chondrocyte detachment." Journal of the Mechanics and Physics of Solids **56**(4): 1554-1565.

McNamara, L., P. Ducheyne, K. E. Healy and D. E. Hutmacher (2011). Bone as a Material. Comrehensive Biomaterials. D. W. Grainger and C. J. Kirkpatrick, Elsevier Science & Technology. **2:** 169-186.

McNamara, L., R. Majeska, S. Weinbaum, V. Friedrich and M. Schaffler (2009a). "Attachment of osteocyte cell processes to the bone matrix." The Anatomical Record **292**(3): 355-363.

McNamara, L. M., R. J. Majeska, S. Weinbaum, V. Friedrich and M. B. Schaffler (2009b). "Attachment of Osteocyte Cell Processes to the Bone Matrix." Anat Rec (Hoboken) **292**(3): 355-363.

Mège, R.-M., J. Gavard and M. Lambert (2006). "Regulation of cell–cell junctions by the cytoskeleton." Current Opinion in Cell Biology **18**(5): 541-548.

Mehrotra, M., M. Saegusa, O. Voznesensky and C. Pilbeam (2006). "Role of Cbfa1/Runx2 in the fluid shear stress induction of COX-2 in osteoblasts." Biochemical and Biophysical Research Communications **341**(4): 1225-1230.

Meşe, G., G. Richard and T. W. White (2007). "Gap junctions: basic structure and function." Journal of Investigative Dermatology **127**(11): 2516-2524.

Metzger, T. A., J. M. Shudick, R. Seekell, Y. Zhu and G. L. Niebur (2014). "Rheological behavior of fresh bone marrow and the effects of storage." Journal of the Mechanical Behavior of Biomedical Materials **40**: 307-313.

Mijailovich, S. M., M. Kojic, M. Zivkovic, B. Fabry and J. J. Fredberg (2002). "A finite element model of cell deformation during magnetic bead twisting." Journal of Applied Physiology **93**(4): 1429-1436.

Miller, A. and S. Parker (1984). "Collagen: the organic matrix of bone [and discussion]." Philosophical Transactions of the Royal Society B: Biological Sciences **304**(1121): 455-477.

Milner, J. S., M. W. Grol, K. L. Beaucage, S. J. Dixon and D. W. Holdsworth (2012). "Finite-element modeling of viscoelastic cells during high-frequency cyclic strain." Journal of functional biomaterials **3**(1): 209-224.

Miyake, Y., N. Inoue, K. Nishimura, N. Kinoshita, H. Hosoya and S. Yonemura (2006). "Actomyosin tension is required for correct recruitment of adherens junction components and zonula occludens formation." Experimental cell research **312**(9): 1637-1650.

Mödder, U. I., M. M. Roforth, K. Hoey, L. K. McCready, J. M. Peterson, D. G. Monroe, M. J. Oursler and S. Khosla (2011). "Effects of estrogen on osteoprogenitor cells and cytokines/bone-regulatory factors in postmenopausal women." Bone **49**(2): 202-207.

Mohrdieck, C., A. Wanner, W. Roos, A. Roth, E. Sackmann, J. P. Spatz and E. Arzt (2005). "A Theoretical Description of Elastic Pillar Substrates in Biophysical Experiments." ChemPhysChem **6**(8): 1492-1498.

Molenaar, M., M. van de Wetering, M. Oosterwegel, J. Peterson-Maduro, S. Godsave, V. Korinek, J. Roose, O. Destrée and H. Clevers (1996). "XTcf-3 transcription factor mediates β-catenin-induced axis formation in Xenopus embryos." Cell **86**(3): 391-399.

Monaghan, H., V. J. Bubb, R. Sirimujalin, S. J. Millward-Sadler and D. M. Salter (2001). "Adenomatous polyposis coli (APC), β-catenin, and cadherin are expressed in human bone and cartilage." Histopathology **39**(6): 611-619.

Moon, R. T., B. Bowerman, M. Boutros and N. Perrimon (2002). "The Promise and Perils of Wnt Signaling Through β-Catenin." Science **296**(5573): 1644-1646.

Muise, A. M., T. D. Walters, W. K. Glowacka, A. M. Griffiths, B. Ngan, H. Lan, W. Xu, M. Silverberg and D. Rotin (2009). "Polymorphisms in E-cadherin (CDH1) result in a mis-localised cytoplasmic protein that is associated with Crohn's disease." Gut **58**(8): 1121-1127.

Mullen, C., T. Vaughan, M. Voisin, M. Brennan, P. Layrolle and L. McNamara (2014a). "Cell morphology and focal adhesion location alters internal cell stress." Journal of The Royal Society Interface **11**(101): 20140885.

Mullen, C. A., M. G. Haugh, M. B. Schaffler, R. J. Majeska and L. M. McNamara (2013). "Osteocyte differentiation is regulated by extracellular matrix stiffness and intercellular separation." Journal of the Mechanical Behavior of Biomedical Materials **28**(0): 183-194.

Mullen, C. A., T. J. Vaughan, K. L. Billiar and L. M. McNamara (2015). "The Effect of Substrate Stiffness, Thickness, and Cross-Linking Density on Osteogenic Cell Behavior." Biophysical Journal **108**(7): 1604-1612.

Mullen, C. A., T. J. Vaughan, M. C. Voisin, M. A. Brennan, P. Layrolle and L. M. McNamara (2014b). "Cell morphology and focal adhesion location alters internal cell stress." Journal of The Royal Society Interface **11**(101).

Mullender, M., R. Huiskes and H. Weinans (1994). "A physiological approach to the simulation of bone remodeling as a self-organizational control process." Journal of Biomechanics **27**(11): 1389-1394.

Mullender, M. G. and R. Huiskes (1995). "Proposal for the regulatory mechanism of Wolff's law." Journal of Orthopaedic Research **13**(4): 503-512.

Mullender, M. G. and R. Huiskes (1997). "Osteocytes and bone lining cells: Which are the best candidates for mechano-sensors in cancellous bone?" Bone **20**(6): 527-532.

Murase, S., E. Mosser and E. M. Schuman (2002). "Depolarization drives β-catenin into neuronal spines promoting changes in synaptic structure and function." Neuron **35**(1): 91-105.

Nakagawa, M., M. Fukata, M. Yamaga, N. Itoh and K. Kaibuchi (2001). "Recruitment and activation of Rac1 by the formation of E-cadherin-mediated cell-cell adhesion sites." Journal of Cell Science **114**(10): 1829-1838.

Nakahama, K.-i. (2010). "Cellular communications in bone homeostasis and repair." Cellular and Molecular Life Sciences **67**(23): 4001-4009.

Nakajima, S., R. Doi, E. Toyoda, S. Tsuji, M. Wada, M. Koizumi, S. S. Tulachan, D. Ito, K. Kami and T. Mori (2004). "N-cadherin expression and epithelial-mesenchymal transition in pancreatic carcinoma." Clinical Cancer Research **10**(12): 4125-4133.

Nakashima, K. and B. de Crombrugghe (2003). "Transcriptional mechanisms in osteoblast differentiation and bone formation." Trends in Genetics **19**(8): 458-466.

Nakashima, K., X. Zhou, G. Kunkel, Z. Zhang, J. M. Deng, R. R. Behringer and B. de Crombrugghe (2002). "The Novel Zinc Finger-Containing Transcription Factor Osterix Is Required for Osteoblast Differentiation and Bone Formation." Cell **108**(1): 17-29.

Nauli, S. M., F. J. Alenghat, Y. Luo, E. Williams, P. Vassilev, X. Li, A. E. Elia, W. Lu, E. M. Brown and S. J. Quinn (2003). "Polycystins 1 and 2 mediate mechanosensation in the primary cilium of kidney cells." Nature genetics **33**(2): 129-137.

Nauman, E., R. Satcher, T. Keaveny, B. Halloran and D. Bikle (2001). "Osteoblasts respond to pulsatile fluid flow with short-term increases in PGE(2) but no change in mineralization." J Appl Physiol **90**: 1849 - 1854.

Navaratna, D., P. G. McGuire, G. Menicucci and A. Das (2007). "Proteolytic Degradation of VE-Cadherin Alters the Blood-Retinal Barrier in Diabetes." Diabetes **56**(9): 2380-2387.

Nelson, W. J. and R. Nusse (2004). "Convergence of Wnt, ß-Catenin, and Cadherin Pathways." Science **303**(5663): 1483-1487.

Ng, M. R., A. Besser, G. Danuser and J. S. Brugge (2012). "Substrate stiffness regulates cadherin-dependent collective migration through myosin-II contractility." The Journal of Cell Biology **199**(3): 545-563.

Nguyen, B. V., Q. G. Wang, N. J. Kuiper, A. J. El Haj, C. R. Thomas and Z. Zhang (2010). "Biomechanical properties of single chondrocytes and chondrons determined by micromanipulation and finite-element modelling." Journal of The Royal Society Interface **7**(53): 1723-1733.

Nicolas, A. and S. A. Safran (2006). "Limitation of Cell Adhesion by the Elasticity of the Extracellular Matrix." Biophysical Journal **91**(1): 61-73.

Niessen, C. M., D. Leckband and A. S. Yap (2011). "Tissue Organization by Cadherin Adhesion Molecules: Dynamic Molecular and Cellular Mechanisms of Morphogenetic Regulation." Physiological reviews **91**(2): 691-731.

Noguchi, K., M. Shitashige, H. Endo, H. Kondo, Y. Yotsumoto, Y. Izumi, H. Nitta and I. Ishikawa (2001). "Involvement of cyclooxygenase-2 in serum-induced prostaglandin production by human oral gingival epithelial cells." Journal of periodontal research **36**(2): 124-130.

Nollet, F., P. Kools and F. Van Roy (2000). "Phylogenetic analysis of the cadherin superfamily allows identification of six major subfamilies besides several solitary members." Journal of molecular biology **299**(3): 551-572.

Noren, N. K., W. T. Arthur and K. Burridge (2003). "Cadherin engagement inhibits RhoA via p190RhoGAP." Journal of Biological Chemistry **278**(16): 13615-13618.

Noren, N. K., C. M. Niessen, B. M. Gumbiner and K. Burridge (2001). "Cadherin engagement regulates Rho family GTPases." Journal of Biological Chemistry **276**(36): 33305-33308.

Noria, S., D. B. Cowan, A. I. Gotlieb and B. L. Langille (1999). "Transient and Steady-State Effects of Shear Stress on Endothelial Cell Adherens Junctions." Circulation Research **85**(6): 504-514.

Norvell, S. M., M. Alvarez, J. P. Bidwell and F. M. Pavalko (2004a). "Fluid Shear Stress Induces ß-Catenin Signaling in Osteoblasts." Calcified Tissue International **75**(5): 396-404.

Norvell, S. M., S. M. Ponik, D. K. Bowen, R. Gerard and F. M. Pavalko (2004b). Fluid shear stress induction of COX-2 protein and prostaglandin release in cultured MC3T3-E1 osteoblasts does not require intact microfilaments or microtubules.

Nose, A., A. Nagafuchi and M. Takeichi (1988). "Expressed recombinant cadherins mediate cell sorting in model systems." Cell **54**(7): 993-1001.

Nusse, R. (2012). "Wnt Signaling." Cold Spring Harbor Perspectives in Biology **4**(5).
Obbink-Huizer, C., C. W. Oomens, S. Loerakker, J. Foolen, C. V. Bouten and F. P. Baaijens (2014). "Computational model predicts cell orientation in response to a range of mechanical stimuli." Biomechanics and modeling in mechanobiology **13**(1): 227-236.
Oberlender, S. A. and R. S. Tuan (1994). "Spatiotemporal Profile of N-Cadherin Expression in the Developing Limb Mesenchyme." Cell Communication and Adhesion **2**(6): 521-537.
Ohashi, T., Y. Ishii, Y. Ishikawa, T. Matsumoto and M. Sato (2001). "Experimental and numerical analyses of local mechanical properties measured by atomic force microscopy for sheared endothelial cells." Bio-medical materials and engineering **12**(3): 319-327.
Ohayon, J., P. Tracqui, R. Fodil, S. Féréol, V. r. M. Laurent, E. Planus and D. Isabey (2004). "Analysis of nonlinear responses of adherent epithelial cells probed by magnetic bead twisting: A finite element model based on a homogenization approach." Journal of Biomechanical Engineering **126**(6): 685-698.
Okada, Y., O. Voznesensky, H. Herschman, J. Harrison and C. Pilbeam (2000). "Identification of multiple cis-acting elements mediating the induction of prostaglandin G/H synthase-2 by phorbol ester in murine osteoblastic cells." Journal of Cellular Biochemistry **78**(2): 197-209.
Orlandini, M. and S. Oliviero (2001). "In Fibroblasts Vegf-D Expression Is Induced by Cell-Cell Contact Mediated by Cadherin-11." Journal of Biological Chemistry **276**(9): 6576-6581.
Ortuño, M. J., S. Ruiz-Gaspà, E. Rodríguez-Carballo, A. R. Susperregui, R. Bartrons, J. L. Rosa and F. Ventura (2010). "p38 regulates expression of osteoblast-specific genes by phosphorylation of osterix." Journal of Biological Chemistry **285**(42): 31985-31994.
Otter, M., V. Palmieri and G. Cochran (1990). "Transcortical streaming potentials are generated by circulatory pressure gradients in living canine tibia." Journal of Orthopaedic Research **8**(1): 119-126.
Otto, F., M. Lübbert and M. Stock (2003). "Upstream and downstream targets of RUNX proteins." Journal of Cellular Biochemistry **89**(1): 9-18.
Overduin, M., T. S. Harvey, S. Bagby, K. I. Tong, P. Yau, M. Takeichi and M. Ikura (1995). "Solution structure of the epithelial cadherin domain responsible for selective cell adhesion." Science (New York, N.Y.) **267**(5196): 386-389.
Owan, I., D. B. Burr, C. H. Turner, J. Qiu, Y. Tu, J. E. Onyia and R. L. Duncan (1997). "Mechanotransduction in bone: osteoblasts are more responsive to fluid forces than mechanical strain." American Journal of Physiology-Cell Physiology **273**(3): C810-C815.
Owen, M. (1985). "Lineage of osteogenic cells and their relationship to the stromal system." Bone and mineral research 3: 1-25.
Pablo Rodríguez, J., M. González, S. Ríos and V. Cambiazo (2004). "Cytoskeletal organization of human mesenchymal stem cells (MSC) changes during their osteogenic differentiation." Journal of Cellular Biochemistry **93**(4): 721-731.
Pacquelet, A. and P. Rørth (2005). "Regulatory mechanisms required for DE-cadherin function in cell migration and other types of adhesion." The Journal of Cell Biology **170**(5): 803-812.
Papachroni, K. K., D. N. Karatzas, K. A. Papavassiliou, E. K. Basdra and A. G. Papavassiliou (2009). "Mechanotransduction in osteoblast regulation and bone disease." Trends in Molecular Medicine **15**(5): 208-216.
Paredes, J., A. L. Correia, A. S. Ribeiro, A. Albergaria, F. Milanezi and F. C. Schmitt (2007). "P-cadherin expression in breast cancer: a review." Breast Cancer Res **9**(5): 214.
Parfitt, A. (1994). "Osteonal and hemi-osteonal remodeling: The spatial and temporal framework for signal traffic in adult human bone." Journal of Cellular Biochemistry **55**(3): 273-286.
Pattabiraman, P. P. and P. V. Rao (2010). Mechanistic basis of Rho GTPase-induced extracellular matrix synthesis in trabecular meshwork cells.
Paul, R., P. Heil, J. P. Spatz and U. S. Schwarz (2008). "Propagation of Mechanical Stress through the Actin Cytoskeleton toward Focal Adhesions: Model and Experiment." Biophysical Journal **94**(4): 1470-1482.
Pavalko, F. M., N. X. Chen, C. H. Turner, D. B. Burr, S. Atkinson, Y.-F. Hsieh, J. Qiu and R. L. Duncan (1998). "Fluid shear-induced mechanical signaling in MC3T3-E1 osteoblasts requires cytoskeleton-integrin interactions." American Journal of Physiology - Cell Physiology **275**(6): C1591-C1601.
Pavalko, F. M., R. L. Gerard, S. M. Ponik, P. J. Gallagher, Y. Jin and S. M. Norvell (2003a). "Fluid shear stress inhibits TNF-α-induced apoptosis in osteoblasts: A role for fluid shear stress-induced

activation of PI3-kinase and inhibition of caspase-3." Journal of Cellular Physiology **194**(2): 194-205.

Pavalko, F. M., S. M. Norvell, D. B. Burr, C. H. Turner, R. L. Duncan and J. P. Bidwell (2003b). "A Model for mechanotransduction in bone cells: The load-bearing mechanosomes." Journal of Cellular Biochemistry **88**(1): 104-112.

Pece, S., M. Chiariello, C. Murga and J. S. Gutkind (1999). "Activation of the Protein Kinase Akt/PKB by the Formation of E-cadherin-mediated Cell-Cell Junctions: EVIDENCE FOR THE ASSOCIATION OF PHOSPHATIDYLINOSITOL 3-KINASE WITH THE E-CADHERIN ADHESION COMPLEX." Journal of Biological Chemistry **274**(27): 19347-19351.

Peng, X., L. E. Cuff, C. D. Lawton and K. A. DeMali (2010). "Vinculin regulates cell-surface E-cadherin expression by binding to β-catenin." Journal of Cell Science **123**(4): 567-577.

Peterson, L. J., Z. Rajfur, A. S. Maddox, C. D. Freel, Y. Chen, M. Edlund, C. Otey and K. Burridge (2004). "Simultaneous Stretching and Contraction of Stress Fibers In Vivo." Molecular Biology of the Cell **15**(7): 3497-3508.

Pishvaian, M. J., C. M. Feltes, P. Thompson, M. J. Bussemakers, J. A. Schalken and S. W. Byers (1999). "Cadherin-11 is expressed in invasive breast cancer cell lines." Cancer research **59**(4): 947-952.

Pittet, P., K. Lee, A. J. Kulik, J.-J. Meister and B. Hinz (2008). "Fibrogenic fibroblasts increase intercellular adhesion strength by reinforcing individual OB-cadherin bonds." Journal of Cell Science **121**(6): 877-886.

Ponik, S. M. and F. M. Pavalko (2004). "Formation of focal adhesions on fibronectin promotes fluid shear stress induction of COX-2 and PGE2 release in MC3T3-E1 osteoblasts." Journal of Applied Physiology **97**(1): 135-142.

Ponik, S. M., J. W. Triplett and F. M. Pavalko (2007). "Osteoblasts and osteocytes respond differently to oscillatory and unidirectional fluid flow profiles." Journal of Cellular Biochemistry **100**(3): 794-807.

Portanova, J. P., Y. Zhang, G. D. Anderson, S. D. Hauser, J. L. Masferrer, K. Seibert, S. A. Gregory and P. C. Isakson (1996). "Selective neutralization of prostaglandin E2 blocks inflammation, hyperalgesia, and interleukin 6 production in vivo." The Journal of experimental medicine **184**(3): 883-891.

Praetorius, H. and K. R. Spring (2001). "Bending the MDCK cell primary cilium increases intracellular calcium." The Journal of membrane biology **184**(1): 71-79.

Praetorius, H. and K. R. Spring (2003). "Removal of the MDCK cell primary cilium abolishes flow sensing." The Journal of membrane biology **191**(1): 69-76.

Pravincumar, P., D. L. Bader and M. M. Knight (2012). "Viscoelastic cell mechanics and actin remodelling are dependent on the rate of applied pressure."

Prendergast, P. J. and R. Huiskes (1996). "Microdamage and osteocyte-lacuna strain in bone: a microstructural finite element analysis." Journal of Biomechanical Engineering **118**(2): 240-246.

Qiu, J., A. D. Baik, X. L. Lu, E. M. C. Hillman, Z. Zhuang, C. Dong and X. E. Guo (2014). "A noninvasive approach to determine viscoelastic properties of an individual adherent cell under fluid flow." Journal of Biomechanics **47**(6): 1537-1541.

Quist, A. P., S. K. Rhee, H. Lin and R. Lal (2000). "Physiological Role of Gap-Junctional Hemichannels Extracellular Calcium-Dependent Isosmotic Volume Regulation." The Journal of Cell Biology **148**(5): 1063-1074.

Rape, A., W.-h. Guo and Y.-l. Wang (2011). "Microtubule depolymerization induces traction force increase through two distinct pathways." Journal of Cell Science **124**(24): 4233-4240.

Reynolds, N. and J. McGarry (2015). "Single cell active force generation under dynamic loading–Part II: Active modelling insights." Acta Biomaterialia **27**: 251-263.

Reynolds, N. H., W. Ronan, E. P. Dowling, P. Owens, R. M. McMeeking and J. P. McGarry (2014). "On the role of the actin cytoskeleton and nucleus in the biomechanical response of spread cells." Biomaterials **35**(13): 4015-4025.

Rico, H., J. Gonzalez-Riola, M. Revilla, L. Villa, F. Gomez-Castresana and J. Escribano (1994). "Cortical versus trabecular bone mass: influence of activity on both bone components." Calcified Tissue International **54**(6): 470-472.

Rodda, S. J. and A. P. McMahon (2006). "Distinct roles for Hedgehog and canonical Wnt signaling in specification, differentiation and maintenance of osteoblast progenitors." Development **133**(16): 3231-3244.

Ronan, W., V. S. Deshpande, R. M. McMeeking and J. P. McGarry (2012). "Numerical investigation of the active role of the actin cytoskeleton in the compression resistance of cells." Journal of the Mechanical Behavior of Biomedical Materials **14**: 143-157.

Ronan, W., V. S. Deshpande, R. M. McMeeking and J. P. McGarry (2014). "Cellular contractility and substrate elasticity: a numerical investigation of the actin cytoskeleton and cell adhesion." Biomechanics and Modeling in Mechanobiology **13**(2): 417-435.

Ronan, W., R. M. McMeeking, C. S. Chen, J. P. McGarry and V. S. Deshpande (2015). "Cooperative contractility: The role of stress fibres in the regulation of cell-cell junctions." Journal of Biomechanics **48**(3): 520-528.

Roose, J., M. Molenaar, J. Peterson, J. Hurenkamp, H. Brantjes, P. Moerer, M. van de Wetering, O. Destrée and H. Clevers (1998). "The Xenopus Wnt effector XTcf-3 interacts with Groucho-related transcriptional repressors." Nature **395**(6702): 608-612.

Rotsch, C. and M. Radmacher (2000). "Drug-Induced Changes of Cytoskeletal Structure and Mechanics in Fibroblasts: An Atomic Force Microscopy Study." Biophysical Journal **78**(1): 520-535.

Roura, S., S. Miravet, J. Piedra, A. G. a. de Herreros and M. Duñach (1999). "Regulation of E-cadherin/Catenin association by tyrosine phosphorylation." Journal of Biological Chemistry **274**(51): 36734-36740.

Roy, B., T. Das, D. Mishra, T. K. Maiti and S. Chakraborty (2014). "Oscillatory shear stress induced calcium flickers in osteoblast cells." Integrative Biology **6**(3): 289-299.

Rüedi, T. P., R. E. Buckley and C. G. Moran (2007). AO Principles of Fracture Management, AO Publishing - Thieme Verlag.

Rydholm, S., G. Zwartz, J. M. Kowalewski, P. Kamali-Zare, T. Frisk and H. Brismar (2010). Mechanical properties of primary cilia regulate the response to fluid flow.

Sachlos, E. and D. T. Auguste (2008). "Embryoid body morphology influences diffusive transport of inductive biochemicals: A strategy for stem cell differentiation." Biomaterials **29**(34): 4471-4480.

Saito, A., K. Ochiai, S. Kondo, K. Tsumagari, T. Murakami, D. R. Cavener and K. Imaizumi (2011). "Endoplasmic reticulum stress response mediated by the PERK-eIF2α-ATF4 pathway is involved in osteoblast differentiation induced by BMP2." Journal of Biological Chemistry **286**(6): 4809-4818.

Salameh, A. and S. Dhein (2013). "Effects of mechanical forces and stretch on intercellular gap junction coupling." Biochimica et Biophysica Acta (BBA) - Biomembranes **1828**(1): 147-156.

Samir, J., J. Echaabi and M. Hattabi (2012). Control Volume Finite Element Methods for Flow in Porous Media: Resin Transfer Molding, INTECH Open Access Publisher.

Sander, E. E., P. Jean, S. van Delft, R. A. van der Kammen and J. G. Collard (1999a). "Rac downregulates rho activity reciprocal balance between both gtpases determines cellular morphology and migratory behavior." The Journal of Cell Biology **147**(5): 1009-1022.

Sander, E. E., J. P. ten Klooster, S. van Delft, R. A. van der Kammen and J. G. Collard (1999b). "Rac Downregulates Rho Activity: Reciprocal Balance between Both Gtpases Determines Cellular Morphology and Migratory Behavior." The Journal of Cell Biology **147**(5): 1009-1022.

Sanui, H. and N. Pace (1967). "Effect of ATP, EDTA and EGTA on the simultaneous binding of Na, K, Mg and Ca by rat liver microsomes." Journal of Cellular Physiology **69**(1): 11-19.

Sarugaser, R., L. Hanoun, A. Keating, W. L. Stanford and J. E. Davies (2009). "Human mesenchymal stem cells self-renew and differentiate according to a deterministic hierarchy." PLoS ONE **4**(8): e6498.

Sato, K., T. Adachi, Y. Shirai, N. Saito and Y. Tomita (2006). "Local Disassembly of Actin Stress Fibers Induced by Selected Release of Intracellular Tension in Osteoblastic Cell." Journal of Biomechanical Science and Engineering **1**(1): 204-214.

Saunders, M., J. You, J. Trosko, H. Yamasaki, Z. Li, H. Donahue and C. Jacobs (2001). "Gap junctions and fluid flow response in MC3T3-E1 cells." American Journal of Physiology-Cell Physiology **281**(6): C1917-C1925.

Saunders, M. M., J. You, Z. Zhou, Z. Li, C. E. Yellowley, E. L. Kunze, C. R. Jacobs and H. J. Donahue (2003). "Fluid flow-induced prostaglandin E2 response of osteoblastic ROS 17/2.8 cells is gap junction-mediated and independent of cytosolic calcium." Bone **32**(4): 350-356.

Sawada, Y., M. Tamada, B. J. Dubin-Thaler, O. Cherniavskaya, R. Sakai, S. Tanaka and M. P. Sheetz (2006). "Force Sensing by Mechanical Extension of the Src Family Kinase Substrate p130Cas." Cell **127**(5): 1015-1026.

Schäfer, G., M. Narasimha, E. Vogelsang and M. Leptin (2014). "Cadherin switching during the formation and differentiation of the Drosophila mesoderm–implications for epithelial-to-mesenchymal transitions." Journal of Cell Science **127**(7): 1511-1522.

Schnittler, H.-J., B. Püschel and D. Drenckhahn (1997). "Role of cadherins and plakoglobin in interendothelial adhesion under resting conditions and shear stress." American Journal of Physiology - Heart and Circulatory Physiology **273**(5): H2396-H2405.

Schürmann, M., J. Scholze, P. Müller, J. Guck and C. J. Chan (2016). "Cell nuclei have lower refractive index and mass density than cytoplasm." Journal of biophotonics.

Seliger, W. G. (1970). "Tissue fluid movement in compact bone." The Anatomical Record **166**(2): 247-255.

Sen, S., A. Engler and D. Discher (2009). "Matrix Strains Induced by Cells: Computing How Far Cells Can Feel." Cellular and Molecular Bioengineering **2**(1): 39-48.

Sfeir, C., L. Ho, B. A. Doll, K. Azari and J. O. Hollinger (2005). Fracture repair. Bone Regeneration and Repair, Springer**:** 21-44.

Shapiro, L., A. M. Fannon, P. D. Kwong, A. Thompson, M. S. Lehmann, G. Grubel, J.-F. Legrand, J. Als-Nielsen, D. R. Colman and W. A. Hendrickson (1995). "Structural basis of cell-cell adhesion by cadherins." Nature **374**(6520): 327-337.

Shimomura, Y., M. Wajid, L. Shapiro and A. M. Christiano (2008). "P-cadherin is a p63 target gene with a crucial role in the developing human limb bud and hair follicle." Development **135**(4): 743-753.

Shin, C. S., F. Lecanda, S. Sheikh, L. Weitzmann, S.-L. Cheng and R. Civitelli (2000). "Relative abundance of different cadherins defines differentiation of mesenchymal precursors into osteogenic, myogenic, or adipogenic pathways." Journal of Cellular Biochemistry **78**(4): 566-577.

Shintani, Y., Y. Fukumoto, N. Chaika, P. M. Grandgenett, M. A. Hollingsworth, M. J. Wheelock and K. R. Johnson (2008). "ADH-1 suppresses N-cadherin-dependent pancreatic cancer progression." International Journal of Cancer **122**(1): 71-77.

Silver, I. A., R. J. Murrills and D. J. Etherington (1988). "Microelectrode studies on the acid microenvironment beneath adherent macrophages and osteoclasts." Experimental Cell Research **175**(2): 266-276.

Simmons, C. A., S. Matlis, A. J. Thornton, S. Chen, C.-Y. Wang and D. J. Mooney (2003). "Cyclic strain enhances matrix mineralization by adult human mesenchymal stem cells via the extracellular signal-regulated kinase (ERK1/2) signaling pathway." Journal of Biomechanics **36**(8): 1087-1096.

Slomka, N. and A. Gefen (2010). "Confocal microscopy-based three-dimensional cell-specific modeling for large deformation analyses in cellular mechanics." Journal of Biomechanics **43**(9): 1806-1816.

Smalt, R., F. T. Mitchell, R. L. Howard and T. J. Chambers (1997). "Induction of NO and prostaglandin E2 in osteoblasts by wall-shear stress but not mechanical strain." American Journal of Physiology - Endocrinology And Metabolism **273**(4): E751-E758.

Smit, T. H. and E. H. Burger (2000). "Is BMU-coupling a strain-regulated phenomenon? A finite element analysis." Journal of Bone and Mineral Research **15**(2): 301-307.

Somjen, D., I. Binderman, E. Berger and A. Harell (1980). "Bone remodelling induced by physical stress is prostaglandin E 2 mediated." Biochimica et Biophysica Acta (BBA)-General Subjects **627**(1): 91-100.

Spencer, G. J., J. C. Utting, S. L. Etheridge, T. R. Arnett and P. G. Genever (2006). "Wnt signalling in osteoblasts regulates expression of the receptor activator of NFκB ligand and inhibits osteoclastogenesis in vitro." Journal of Cell Science **119**(7): 1283-1296.

Stains, J. P. and R. Civitelli (2005). "Cell-to-cell interactions in bone." Biochemical and Biophysical Research Communications **328**(3): 721-727.

Standal, T., M. Borset and A. Sundan (2004). "Role of osteopontin in adhesion, migration, cell survival and bone remodeling." Exp Oncol **26**(3): 179-184.

Steck, R., P. Niederer and M. L. Knothe Tate (2000). "A finite difference model of load-induced fluid displacements within bone under mechanical loading." Medical Engineering & Physics **22**(2): 117-125.

Steinberg, M. S. and M. Takeichi (1994). "Experimental specification of cell sorting, tissue spreading, and specific spatial patterning by quantitative differences in cadherin expression." Proceedings of the National Academy of Sciences **91**(1): 206-209.

Steward, R., D. Tambe, C. C. Hardin, R. Krishnan and J. J. Fredberg (2015). "Fluid shear, intercellular stress, and endothelial cell alignment." American Journal of Physiology - Cell Physiology **308**(8).

Stops, A., L. McMahon, D. O'Mahoney, P. Prendergast and P. McHugh (2008). "A finite element prediction of strain on cells in a highly porous collagen-glycosaminoglycan scaffold." Journal of Biomechanical Engineering **130**(6): 061001.

Stroka, K. and H. Aranda-Espinoza (2011). "Effects of Morphology vs. Cell–Cell Interactions on Endothelial Cell Stiffness." Cellular and Molecular Bioengineering **4**(1): 9-27.

Suda, T., N. Takahashi and T. J. Martin (1992). "Modulation of osteoclast differentiation." Endocrine reviews **13**(1): 66-80.

Sudo, H., H.-A. Kodama, Y. Amagai, S. Yamamoto and S. Kasai (1983). "In vitro differentiation and calcification in a new clonal osteogenic cell line derived from newborn mouse calvaria." The Journal of Cell Biology **96**(1): 191-198.

Sugawara, Y., R. Ando, H. Kamioka, Y. Ishihara, S. A. Murshid, K. Hashimoto, N. Kataoka, K. Tsujioka, F. Kajiya, T. Yamashiro and T. Takano-Yamamoto (2008). "The alteration of a mechanical property of bone cells during the process of changing from osteoblasts to osteocytes." Bone **43**(1): 19-24.

Suzuki, S., K. Sano and H. Tanihara (1991). "Diversity of the cadherin family: evidence for eight new cadherins in nervous tissue." Cell Regulation **2**(3): 261-270.

Swaminathan, V., K. Mythreye, E. T. O'Brien, A. Berchuck, G. C. Blobe and R. Superfine (2011). "Mechanical stiffness grades metastatic potential in patient tumor cells and in cancer cell lines." Cancer research **71**(15): 5075-5080.

Swope, D., L. Cheng, E. Gao, J. Li and G. L. Radice (2012). "Loss of cadherin-binding proteins β-catenin and plakoglobin in the heart leads to gap junction remodeling and arrhythmogenesis." Molecular and Cellular Biology **32**(6): 1056-1067.

Taddei, A., C. Giampietro, A. Conti, F. Orsenigo, F. Breviario, V. Pirazzoli, M. Potente, C. Daly, S. Dimmeler and E. Dejana (2008). "Endothelial adherens junctions control tight junctions by VE-cadherin-mediated upregulation of claudin-5." Nature Cell Biology **10**(8): 923-934.

Takai, E., K. Costa, A. Shaheen, C. Hung and X. E. Guo (2005). "Osteoblast Elastic Modulus Measured by Atomic Force Microscopy Is Substrate Dependent." Annals of Biomedical Engineering **33**(7): 963-971.

Takeichi, M. (1990). "Cadherins: a molecular family important in selective cell-cell adhesion." Annual Review of Biochemistry **59**(1): 237-252.

Takeichi, M. (1995). "Morphogenetic roles of classic cadherins." Current Opinion in Cell Biology **7**(5): 619-627.

Tamura, D., T. Hiraga, A. Myoui, H. Yoshikawa and T. Yoneda (2008). "Cadherin-11-mediated interactions with bone marrow stromal/osteoblastic cells support selective colonization of breast cancer cells in bone." International journal of oncology **33**(1): 17.

Tan, S., J. Y. Fang, Z. Yang, M. E. Nimni and B. Han (2014). "The synergetic effect of hydrogel stiffness and growth factor on osteogenic differentiation." Biomaterials **35**(20): 5294-5306.

Tanaka, K.-i., E. Matsumoto, Y. Higashimaki, T. Katagiri, T. Sugimoto, S. Seino and H. Kaji (2012). "Role of Osteoglycin in the Linkage between Muscle and Bone." Journal of Biological Chemistry **287**(15): 11616-11628.

Tanihara, H., K. Sano, R. L. Heimark, T. St. John and S. Suzuki (1994). "Cloning of Five Human Cadherins Clarifies Characteristic Features of Cadherin Extracellular Domain and Provides Further Evidence for Two Structurally Different Types of Cadherin." Cell Communication and Adhesion **2**(1): 15-26.

Tao, Q., S. Nandadasa, P. D. McCrea, J. Heasman and C. Wylie (2007). "G-protein-coupled signals control cortical actin assembly by controlling cadherin expression in the early Xenopus embryo." Development **134**(14): 2651-2661.

Tarbell, J. M., S. Weinbaum and R. D. Kamm (2005). "Cellular fluid mechanics and mechanotransduction." Annals of Biomedical Engineering **33**(12): 1719-1723.

Tashima, T., S. Nagatoishi, H. Sagara, S.-i. Ohnuma and K. Tsumoto (2015). "Osteomodulin regulates diameter and alters shape of collagen fibrils." Biochemical and Biophysical Research Communications **463**(3): 292-296.

Tate, M. L. K., J. R. Adamson, A. E. Tami and T. W. Bauer (2004). "The osteocyte." The international journal of biochemistry & cell biology **36**(1): 1-8.

Thi, M., T. Kojima, S. Cowin, S. Weinbaum and D. Spray (2003). "Fluid shear stress remodels expression and function of junctional proteins in cultured bone cells." Am J Physiol Cell Physiol **284**(2): C389-403.

Thompson, T., P. Owens and D. Wilson (1989). "Intramembranous osteogenesis and angiogenesis in the chick embryo." Journal of anatomy **166**: 55.

Thorsen, K., A. O. Kristoffersson, U. H. Lerner and R. P. Lorentzon "In situ microdialysis in bone tissue. Stimulation of prostaglandin E2 release by weight-bearing mechanical loading." The Journal of Clinical Investigation **98**(11): 2446-2449.

Thorsen, K., A. O. Kristoffersson, U. H. Lerner and R. P. Lorentzon (1996). "In situ microdialysis in bone tissue. Stimulation of prostaglandin E2 release by weight-bearing mechanical loading." Journal of Clinical Investigation **98**(11): 2446.

Thoumine, O., M. Lambert, R.-M. Mège and D. Choquet (2006). "Regulation of N-Cadherin Dynamics at Neuronal Contacts by Ligand Binding and Cytoskeletal Coupling." Molecular Biology of the Cell **17**(2): 862-875.

Tian, X., Z. Liu, B. Niu, J. Zhang, T. K. Tan, S. R. Lee, Y. Zhao, D. C. Harris and G. Zheng (2011). "E-cadherin/β-catenin complex and the epithelial barrier." BioMed Research International **2011**.

Ting, L. H., J. R. Jahn, J. I. Jung, B. R. Shuman, S. Feghhi, S. J. Han, M. L. Rodriguez and N. J. Sniadecki (2012). "Flow mechanotransduction regulates traction forces, intercellular forces, and adherens junctions." American Journal of Physiology - Heart and Circulatory Physiology **302**(11): H2220-H2229.

Titushkin, I. and M. Cho (2007). "Modulation of Cellular Mechanics during Osteogenic Differentiation of Human Mesenchymal Stem Cells." Biophysical Journal **93**(10): 3693-3702.

Toma, C., S. Ashkar, M. Gray, J. Schaffer and L. Gerstenfeld (1997). "Signal transduction of mechanical stimuli is dependent on microfilament integrity: identification of osteopontin as a mechanically induced gene in osteoblasts." Journal of Bone and Mineral Research **12**(10): 1626-1636.

Townes, P. L. and J. Holtfreter (1955). "Directed movements and selective adhesion of embryonic amphibian cells." Journal of experimental zoology **128**(1): 53-120.

Troyanovsky, R. B., O. Laur and S. M. Troyanovsky (2007). "Stable and unstable cadherin dimers: mechanisms of formation and roles in cell adhesion." Molecular Biology of the Cell **18**(11): 4343-4352.

Tseng, P.-C., T.-H. Young, T.-M. Wang, H.-W. Peng, S.-M. Hou and M.-L. Yen (2012). "Spontaneous osteogenesis of MSCs cultured on 3D microcarriers through alteration of cytoskeletal tension." Biomaterials **33**(2): 556-564.

Tseng, Y., J. S. H. Lee, T. P. Kole, I. Jiang and D. Wirtz (2004). "Micro-organization and visco-elasticity of the interphase nucleus revealed by particle nanotracking." Journal of Cell Science **117**(10): 2159-2167.

Tsutsumimoto, T., S. Kawasaki, S. Ebara and K. Takaoka (1999). "TNF-α and IL-1β Suppress N-Cadherin Expression in MC3T3-E1 Cells." Journal of Bone and Mineral Research **14**(10): 1751-1760.

Tucker, R. P., P. Henningsson, S. L. Franklin, D. Chen, Y. Ventikos, R. J. Bomphrey and M. S. Thompson (2014). "See-saw rocking: an in vitro model for mechanotransduction research." Journal of The Royal Society Interface **11**(97).

Tufan, A. C. and R. S. Tuan (2001). "Wnt regulation of limb mesenchymal chondrogenesis is accompanied by altered N-cadherin-related functions." The FASEB Journal **15**(8): 1436-1438.

Tunggal, J. A., I. Helfrich, A. Schmitz, H. Schwarz, D. Günzel, M. Fromm, R. Kemler, T. Krieg and C. M. Niessen (2005). "E-cadherin is essential for in vivo epidermal barrier function by regulating tight junctions." The EMBO journal **24**(6): 1146-1156.

Turner, C., M. Forwood and M. Otter (1994). "Mechanotransduction in bone: do bone cells act as sensors of fluid flow?" The FASEB Journal **8**(11): 875-878.

Tzima, E., M. Irani-Tehrani, W. B. Kiosses, E. Dejana, D. A. Schultz, B. Engelhardt, G. Cao, H. DeLisser and M. A. Schwartz (2005). "A mechanosensory complex that mediates the endothelial cell response to fluid shear stress." Nature **437**(7057): 426-431.

Udagawa, N., N. Takahashi, T. Akatsu, H. Tanaka, T. Sasaki, T. Nishihara, T. Koga, T. J. Martin and T. Suda (1990). "Origin of osteoclasts: mature monocytes and macrophages are capable of differentiating into osteoclasts under a suitable microenvironment prepared by bone marrow-derived stromal cells." Proceedings of the National Academy of Sciences **87**(18): 7260-7264.

Udagawa, N., N. Takahashi, H. Yasuda, A. Mizuno, K. Itoh, Y. Ueno, T. Shinki, M. T. Gillespie, T. J. Martin and K. Higashio (2000). "Osteoprotegerin Produced by Osteoblasts Is an Important Regulator in Osteoclast Development and Function 1." Endocrinology **141**(9): 3478-3484.

Vaez Ghaemi, R., B. Vahidi, M. H. Sabour, N. Haghighipour and Z. Alihemmati (2015). "Fluid–Structure Interactions Analysis of Shear-Induced Modulation of a Mesenchymal Stem Cell: An Image-Based Study." Artificial Organs: n/a-n/a.

Vaezi, A., C. Bauer, V. Vasioukhin and E. Fuchs (2002). "Actin cable dynamics and Rho/Rock orchestrate a polarized cytoskeletal architecture in the early steps of assembling a stratified epithelium." Developmental Cell **3**(3): 367-381.

Valbuena, A., A. M. Vera, J. Oroz, M. Menéndez and M. Carrión-Vázquez (2012). "Mechanical properties of β-catenin revealed by single-molecule experiments." Biophysical journal **103**(8): 1744-1752.

Vale, R. and T. Kreis (1999). Guidebook to the cytoskeletal and motor proteins, Oxford University Press.

Van Lommel, A. T. (2003). From cells to organs: a histology textbook and atlas, Springer Science & Business Media.

Van Roy, F. (2014). "Beyond E-cadherin: roles of other cadherin superfamily members in cancer." Nature Reviews Cancer **14**(2): 121-134.

Vance, J., S. Galley, D. F. Liu and S. W. Donahue (2005). "Mechanical stimulation of MC3T3 osteoblastic cells in a bone tissue-engineering bioreactor enhances prostaglandin E2 release." Tissue Engineering **11**(11-12): 1832-1839.

Vasioukhin, V., C. Bauer, M. Yin and E. Fuchs (2000). "Directed actin polymerization is the driving force for epithelial cell–cell adhesion." Cell **100**(2): 209-219.

Vaughan, T., M. Haugh and L. McNamara (2013a). Fluid-Structure Interaction Modelling Predicts That Strain Transfer Through Focal Attachments of Osteoblast Cells are the Primary Mediators of Mechanical Stimulation Under Fluid Flow. ASME 2013 Summer Bioengineering Conference, American Society of Mechanical Engineers.

Vaughan, T., C. McCarthy and L. McNamara (2012). "A three-scale finite element investigation into the effects of tissue mineralisation and lamellar organisation in human cortical and trabecular bone." Journal of the Mechanical Behavior of Biomedical Materials **12**: 50-62.

Vaughan, T., C. Mullen, S. Verbruggen and L. McNamara (2014). "Bone cell mechanosensation of fluid flow stimulation: a fluid–structure interaction model characterising the role integrin attachments and primary cilia." Biomechanics and Modeling in Mechanobiology: 1-16.

Vaughan, T., M. Voisin, G. Niebur and L. McNamara (2015). "Multiscale modeling of trabecular bone marrow: understanding the micromechanical environment of mesenchymal stem cells during osteoporosis." Journal of biomechanical engineering **137**(1): 011003.

Vaughan, T. J., M. G. Haugh and L. M. McNamara (2013b). "A fluid–structure interaction model to characterize bone cell stimulation in parallel-plate flow chamber systems." Journal of The Royal Society Interface **10**(81).

Verbruggen, S. W., T. J. Vaughan and L. M. McNamara (2012). "Strain amplification in bone mechanobiology: a computational investigation of the in vivo mechanics of osteocytes." Journal of The Royal Society Interface **9**(75): 2735-2744.

Verbruggen, S. W., T. J. Vaughan and L. M. McNamara (2014). "Fluid flow in the osteocyte mechanical environment: a fluid–structure interaction approach." Biomechanics and Modeling in Mechanobiology **13**(1): 85-97.

Vernerey, F. J. and M. Farsad (2011). "A constrained mixture approach to mechano-sensing and force generation in contractile cells." Journal of the mechanical behavior of biomedical materials **4**(8): 1683-1699.

Versteeg, H. K. and W. Malalasekera (2007). An introduction to computational fluid dynamics: the finite volume method, Pearson Education.

Vichare, S., M. M. Inamdar and S. Sen (2012). "Influence of cell spreading and contractility on stiffness measurements using AFM." Soft Matter **8**(40): 10464-10471.

Vico, L., P. Collet, A. Guignandon, M. H. Lafage-Proust, T. Thomas, M. Rehailia and C. Alexandre (2000). "Effects of long-term microgravity exposure on cancellous and cortical weight-bearing bones of cosmonauts." Lancet **355**(9215): 1607-1611.

Waarsing, J. H., J. S. Day, J. A. N. Verhaar, A. G. H. Ederveen and H. Weinans (2006). "Bone loss dynamics result in trabecular alignment in aging and ovariectomized rats." Journal of Orthopaedic Research **24**(5): 926-935.

Wadhwa, S., S. Choudhary, M. Voznesensky, M. Epstein, L. Raisz and C. Pilbeam (2002). "Fluid flow induces COX-2 expression in MC3T3-E1 osteoblasts via a PKA signaling pathway." Biochemical and Biophysical Research Communications **297**(1): 46-51.

Wang, L., H. Fan, Z.-Y. Zhang, A.-J. Lou, G.-X. Pei, S. Jiang, T.-W. Mu, J.-J. Qin, S.-Y. Chen and D. Jin (2010). "Osteogenesis and angiogenesis of tissue-engineered bone constructed by prevascularized β-tricalcium phosphate scaffold and mesenchymal stem cells." Biomaterials **31**(36): 9452-9461.

Wang, N., J. P. Butler and D. E. Ingber (1993). "Mechanotransduction across the cell surface and through the cytoskeleton." Science **260**(5111): 1124-1127.

Wang, W., K. Itaka, S. Ohba, N. Nishiyama, U.-i. Chung, Y. Yamasaki and K. Kataoka (2009). "3D spheroid culture system on micropatterned substrates for improved differentiation efficiency of multipotent mesenchymal stem cells." Biomaterials **30**(14): 2705-2715.

Wang, Y., L. McNamara, M. Schaffler and S. Weinbaum (2008). "Strain amplification and integrin based signaling in osteocytes." Journal of musculoskeletal & neuronal interactions **8**(4): 332.

Wang, Y., L. M. McNamara, M. B. Schaffler and S. Weinbaum (2007). "A model for the role of integrins in flow induced mechanotransduction in osteocytes." Proc Natl Acad Sci U S A **104**(40): 15941-15946.

Watanabe, T., H. Kuramochi, A. Takahashi, K. Imai, N. Katsuta, T. Nakayama, H. Fujiki and M. Suganuma (2012). "Higher cell stiffness indicating lower metastatic potential in B16 melanoma cell variants and in (−)-epigallocatechin gallate-treated cells." Journal of cancer research and clinical oncology **138**(5): 859-866.

Watt, F. M. and B. L. M. Hogan (2000). "Out of eden: Stem cells and their niches." Science **287**(5457): 1427-1430.

Weafer, P., N. Reynolds, S. Jarvis and J. McGarry (2015). "Single cell active force generation under dynamic loading–Part I: AFM experiments." Acta Biomaterialia **27**: 236-250.

Weafer, P., W. Ronan, S. Jarvis and J. McGarry (2013). "Experimental and computational investigation of the role of stress fiber contractility in the resistance of osteoblasts to compression." Bulletin of mathematical biology **75**(8): 1284-1303.

Weber, G. F., M. A. Bjerke and D. W. DeSimone (2011). "Integrins and cadherins join forces to form adhesive networks." Journal of Cell Science **124**(8): 1183-1193.

Wei, C.-J., R. Francis, X. Xu and C. W. Lo (2005). "Connexin43 Associated with an N-cadherin-containing Multiprotein Complex Is Required for Gap Junction Formation in NIH3T3 Cells." Journal of Biological Chemistry **280**(20): 19925-19936.

Weinbaum, S., S. C. Cowin and Y. Zeng (1994). "A model for the excitation of osteocytes by mechanical loading-induced bone fluid shear stresses." Journal of Biomechanics **27**(3): 339-360.

Westendorf, J. J., R. A. Kahler and T. M. Schroeder (2004). "Wnt signaling in osteoblasts and bone diseases." Gene **341**(0): 19-39.

Wheatley, D. N., A. M. Wang and G. E. Strugnell (1996). "Expression of primary cilia in mammalian cells." Cell Biology International **20**(1): 73-81.

Wheelock, M. J. and K. R. Johnson (2003). "Cadherins as modulators of cellular phenotype." Annual Review of Cell and Developmental Biology **19**(1): 207-235.

White, F. M. (2008). Fluid Mechanics. New York, McGraw Hill.

Wikipedia. from https://en.wikisource.org/wiki/Popular_Science_Monthly/Volume_42/April_1893/The_Correlation_of_Structure,_Action,_and_Thought#/media/File:PSM_V42_D775_Femur_fibre_arrangement_for_strength.jpg.

Williams, E., G. Williams, B. J. Gour, O. W. Blaschuk and P. Doherty (2000). "A Novel Family of Cyclic Peptide Antagonists Suggests That N-cadherin Specificity Is Determined by Amino Acids That Flank the HAV Motif." Journal of Biological Chemistry **275**(6): 4007-4012.

Woo, S., S. C. Kuei, D. Amiel, M. Gomez, W. Hayes, F. White and W. Akeson (1981). "The effect of prolonged physical training on the properties of long bone: a study of Wolff's Law." The Journal of Bone & Joint Surgery **63**(5): 780-787.

Wozniak, M. A., R. Desai, P. A. Solski, C. J. Der and P. J. Keely (2003). "ROCK-generated contractility regulates breast epithelial cell differentiation in response to the physical properties of a three-dimensional collagen matrix." The Journal of Cell Biology **163**(3): 583-595.

Xie, Y., T. Yin, W. Wiegraebe, X. C. He, D. Miller, D. Stark, K. Perko, R. Alexander, J. Schwartz and J. C. Grindley (2009). "Detection of functional haematopoietic stem cell niche using real-time imaging." Nature **457**(7225): 97-101.

Xu, H., J. Zhang, J. Wu, Y. Guan, Y. Weng and P. Shang (2012). "Oscillatory fluid flow elicits changes in morphology, cytoskeleton and integrin-associated molecules in MLO-Y4 cells, but not in MC3T3-E1 cells." Biological research **45**(2): 163-169.

Xu, L., F. Meng, M. Ni, Y. Lee and G. Li (2013). "N-cadherin regulates osteogenesis and migration of bone marrow-derived mesenchymal stem cells." Molecular biology reports **40**(3): 2533-2539.

Yagi, T. and M. Takeichi (2000). "Cadherin superfamily genes: functions, genomic organization, and neurologic diversity." Genes & Development **14**(10): 1169-1180.

Yamada, S. and W. J. Nelson (2007). "Localized zones of Rho and Rac activities drive initiation and expansion of epithelial cell–cell adhesion." The Journal of Cell Biology **178**(3): 517-527.

Yang, Z., J. P. Bidwell, S. R. Young, R. Gerard-O'Riley, H. Wang and F. M. Pavalko (2010). "Nmp4/CIZ inhibits mechanically induced β-catenin signaling activity in osteoblasts." Journal of cellular physiology **223**(2): 435-441.

Yao, C., D. Sakata, Y. Esaki, Y. Li, T. Matsuoka, K. Kuroiwa, Y. Sugimoto and S. Narumiya (2009). "Prostaglandin E2-EP4 signaling promotes immune inflammation through TH1 cell differentiation and TH17 cell expansion." Nat Med **15**(6): 633-640.

Yin, T. and L. Li (2006). "The stem cell niches in bone." Journal of Clinical Investigation **116**(5): 1195-1201.

Yonemura, S., Y. Wada, T. Watanabe, A. Nagafuchi and M. Shibata (2010). "α-Catenin as a tension transducer that induces adherens junction development." Nature Cell Biology **12**(6): 533-542.

You, J., G. C. Reilly, X. Zhen, C. E. Yellowley, Q. Chen, H. J. Donahue and C. R. Jacobs (2001). "Osteopontin Gene Regulation by Oscillatory Fluid Flow via Intracellular Calcium Mobilization and Activation of Mitogen-activated Protein Kinase in MC3T3–E1 Osteoblasts." Journal of Biological Chemistry **276**(16): 13365-13371.

You, J., C. E. Yellowley, H. J. Donahue, Y. Zhang, Q. Chen and C. R. Jacobs (2000). "Substrate Deformation Levels Associated With Routine Physical Activity Are Less Stimulatory to Bone Cells Relative to Loading-Induced Oscillatory Fluid Flow." Journal of Biomechanical Engineering **122**(4): 387-393.

Young, S. R., R. Gerard-O'Riley, J. B. Kim and F. M. Pavalko (2009). "Focal adhesion kinase is important for fluid shear stress-induced mechanotransduction in osteoblasts." Journal of Bone and Mineral Research **24**(3): 411-424.

Yourek, G., S. M. McCormick, J. J. Mao and G. C. Reilly (2010). "Shear stress induces osteogenic differentiation of human mesenchymal stem cells." Regenerative medicine **5**(5): 713-724.

Yu, H., C. Y. Tay, W. S. Leong, S. C. W. Tan, K. Liao and L. P. Tan (2010). "Mechanical behavior of human mesenchymal stem cells during adipogenic and osteogenic differentiation." Biochemical and Biophysical Research Communications **393**(1): 150-155.

Zeng, Q., Y. Guo, Y. Liu, R. Li, X. Zhang, L. Liu, Y. Wang, X. Zhang and X. Zou (2015). "Integrin-β1, not integrin-β5, mediates osteoblastic differentiation and ECM formation promoted by mechanical tensile strain." Biological research **48**(1): 25.

Zeng, X., K. Tamai, B. Doble, S. Li, H. Huang, R. Habas, H. Okamura, J. Woodgett and X. He (2005). "A dual-kinase mechanism for Wnt co-receptor phosphorylation and activation." Nature **438**(7069): 873-877.

Zeng, Y., S. Cowin and S. Weinbaum (1994). "A fiber matrix model for fluid flow and streaming potentials in the canaliculi of an osteon." Annals of biomedical engineering **22**(3): 280-292.

Zhang, D., S. C. Cowin and S. Weinbaum (1997). "Electrical signal transmission and gap junction regulation in a bone cell network: a cable model for an osteon." Annals of Biomedical Engineering **25**(2): 357-374.

Zhang, J., C. Niu, L. Ye, H. Huang, X. He, W.-G. Tong, J. Ross, J. Haug, T. Johnson and J. Q. Feng (2003). "Identification of the haematopoietic stem cell niche and control of the niche size." Nature **425**(6960): 836-841.

Zhang, X., E. M. Schwarz, D. A. Young, J. E. Puzas, R. N. Rosier and R. J. O'Keefe (2002). "Cyclooxygenase-2 regulates mesenchymal cell differentiation into the osteoblast lineage and is critically involved in bone repair." The Journal of Clinical Investigation **109**(109 (11)): 1405-1415.

Zhao, R., K. Wyss and C. A. Simmons (2009). "Comparison of analytical and inverse finite element approaches to estimate cell viscoelastic properties by micropipette aspiration." Journal of Biomechanics **42**(16): 2768-2773.

Zheng, L. and H. M. Kim (2013). "Low-Rac1 activity downregulates MC3T3-E1 osteoblastic cell motility on a nanoscale topography prepared on polystyrene substrates in vitro." Journal of Biomedical Materials Research Part A **101**(6): 1629-1636.

Zhu, B., S. Chappuis-Flament, E. Wong, I. E. Jensen, B. M. Gumbiner and D. Leckband (2003). "Functional Analysis of the Structural Basis of Homophilic Cadherin Adhesion." Biophysical Journal **84**(6): 4033-4042.

Zimmermann, J. A. and T. C. McDevitt (2014). "Pre-conditioning mesenchymal stromal cell spheroids for immunomodulatory paracrine factor secretion." Cytotherapy **16**(3): 331-345.

Zreiqat, H., C. Howlett, A. Zannettino, P. Evans, G. Schulze-Tanzil, C. Knabe and M. Shakibaei (2002). "Mechanisms of magnesium-stimulated adhesion of osteoblastic cells to commonly used orthopaedic implants." Journal of biomedical materials research **62**(2): 175-184.

Appendix 1:

Parallel Plate Bioreactor

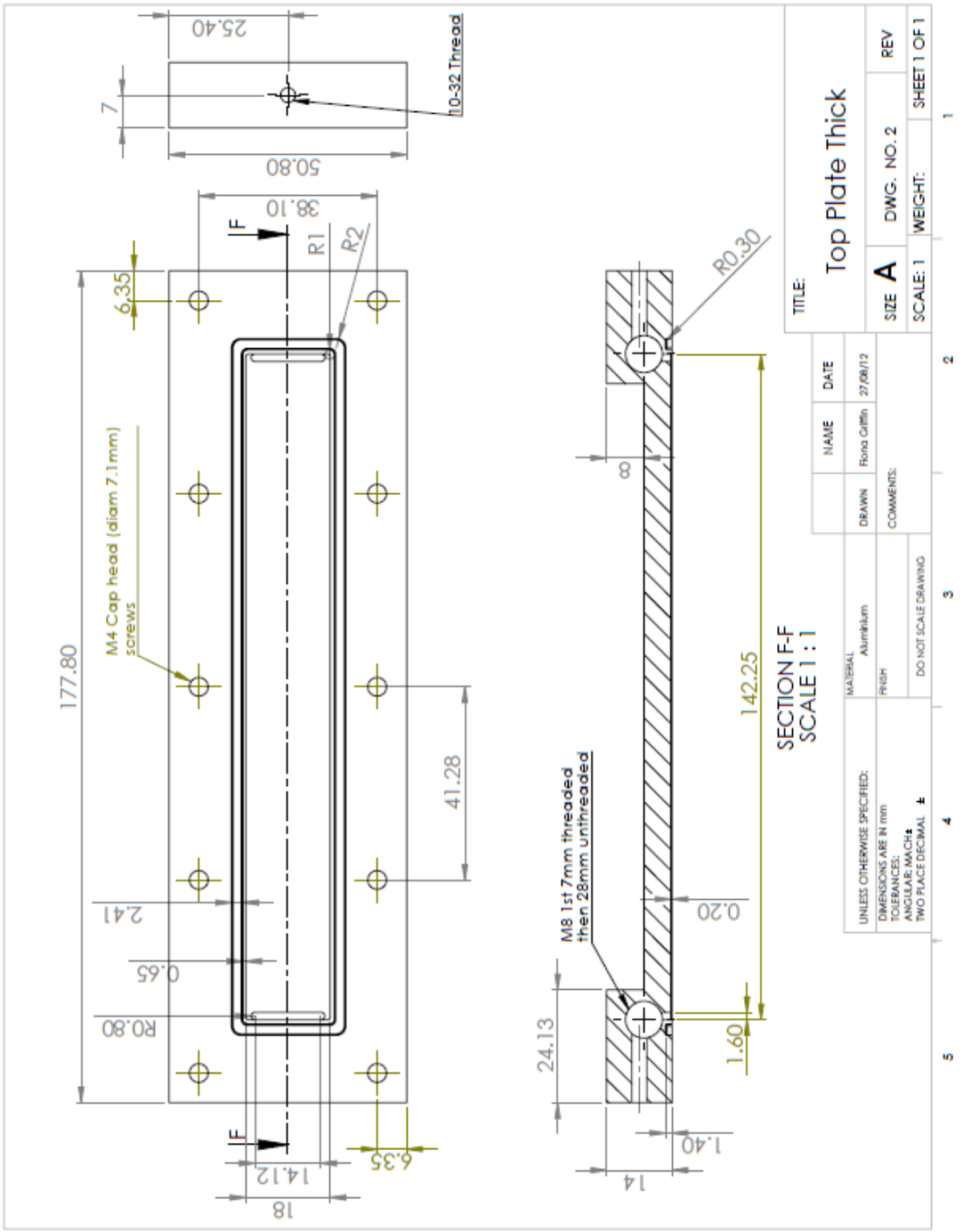

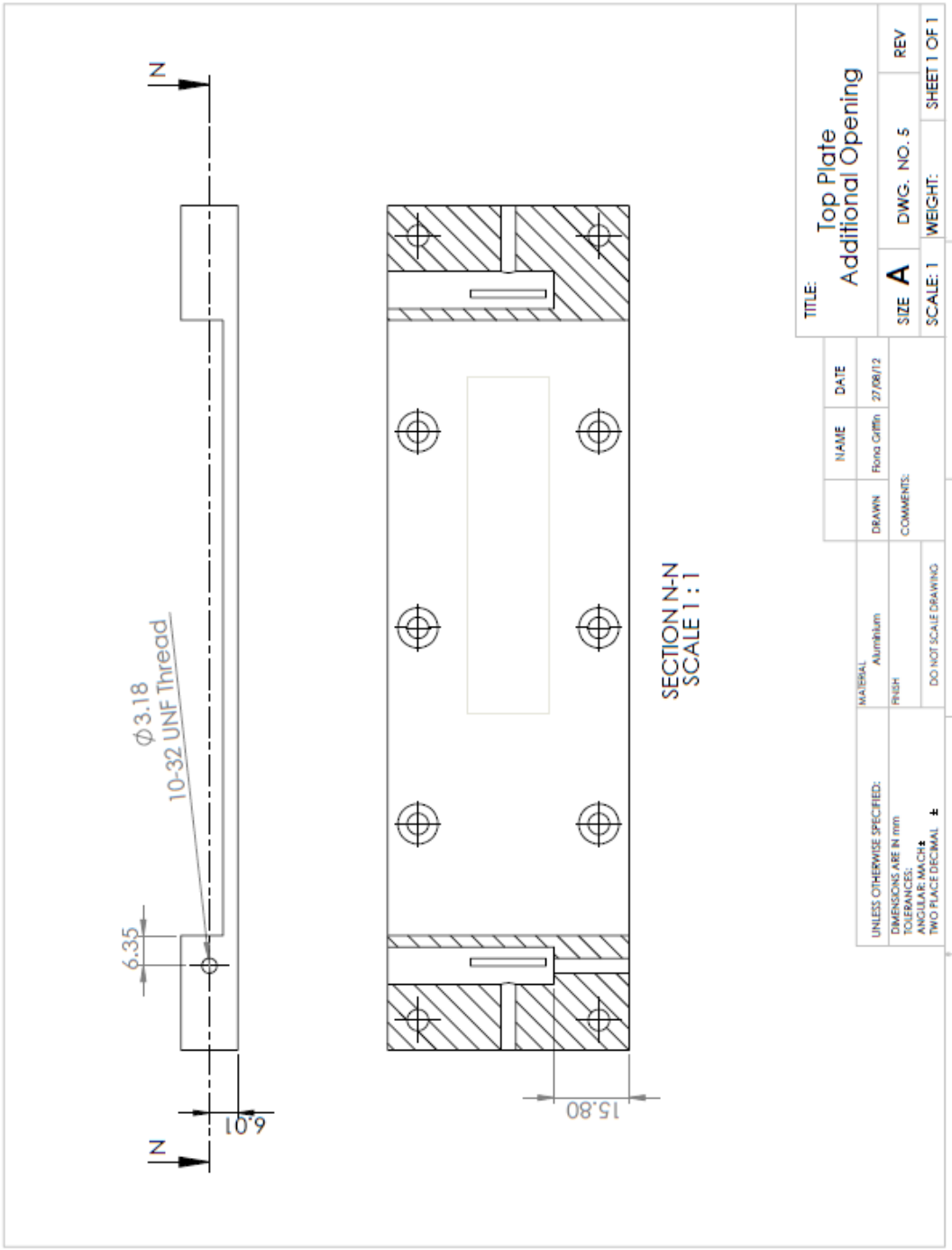
N
N
Ø3.18
10-32 UNF Thread
6.35
6.01
15.80
SECTION N-N
SCALE 1 : 1
TITLE:
Top Plate
Additional Opening
SIZE A
DWG. NO. 5
REV
SCALE: 1
WEIGHT:
SHEET 1 OF 1
NAME
DATE
DRAWN
Fiona Griffin
27/08/12
COMMENTS:
MATERIAL
Aluminium
FINISH
DO NOT SCALE DRAWING
UNLESS OTHERWISE SPECIFIED:
DIMENSIONS ARE IN mm
TOLERANCES:
ANGULAR: MACH ±
TWO PLACE DECIMAL ±

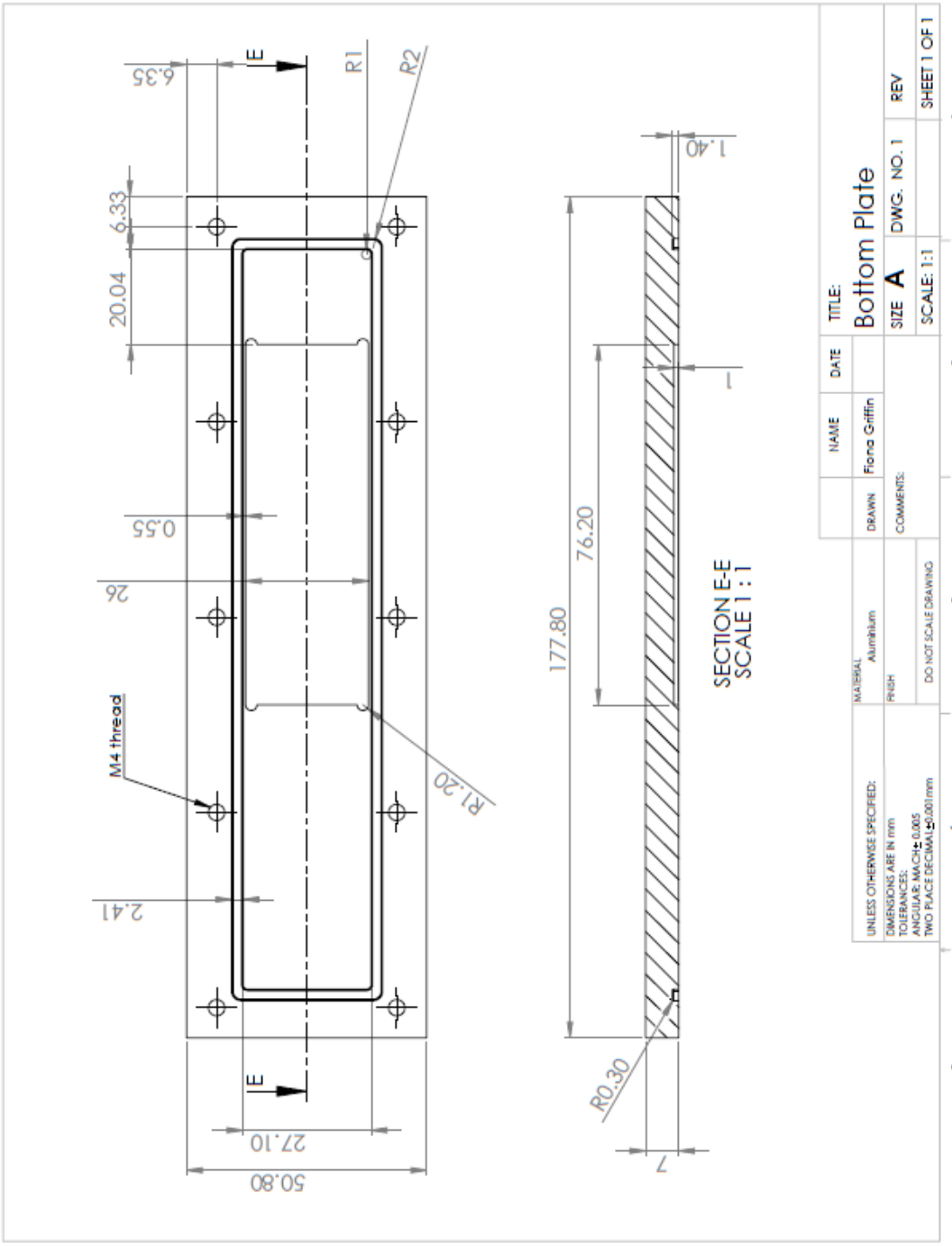
6.35
E
R1
R2
6.33
20.04
0.55
26
M4 thread
R1.20
2.41
E
27.10
50.80
1.40
1
76.20
177.80
SECTION E-E
SCALE 1 : 1
R0.30
7
TITLE:
Bottom Plate
NAME
DATE
DRAWN
Fiona Griffin
COMMENTS:
SIZE A
DWG. NO. 1
REV
SCALE: 1:1
SHEET 1 OF 1
MATERIAL
Aluminium
FINISH
DO NOT SCALE DRAWING
UNLESS OTHERWISE SPECIFIED:
DIMENSIONS ARE IN mm
TOLERANCES:
ANGULAR: MACH ± 0.005
TWO PLACE DECIMAL ± 0.001mm